PETROLEUM RESEARCH JOURNAL

The Use of Complex Wells for Reserves Optimization in the Mabruk Field .....
A. Gaaim, Y. Bigno and A. Al-Faia 1

A Method for an Efficient Fast Track Evaluation and the Assessment of Re-engineering Potential of Mature Fields .....
Claude Mouret, Jean Chastang and Jean-Paul Valois 9

Re-Development of a Mature Field for Production Acceleration, Intisar 103E Field .....
E. Senturk, M. Lahwel, B. Bzezi and M. Elghmari 17

Nakhla Oil Field, Concession 97, Libya Development Strategy and Improved Oil Recovery
Thomas Franzen 27

Hydraulic Frac Stimulation of the Sarir Sandstone in Nakhla Oilfield .....
Bernd Leonhardt 35

Re-establishing Reservoir Performance by Revaporization of Condensate in the Nubian Sandstone Reservoir .....
R.T. Bujnowicz and K. Jerbi 43

2-D Geological Modeling in the Vicinity of Horizontal Wells – Case Study Integrating Borehole Images and Openhole logs .....
Aimen Amer 51

CO_2 Gas Flooding in Sandstone and Limestone Reservoirs in Hungary .....
Z. Biró and L. Cziczlavicz 59

Naturally Fractured Reservoirs – Modeling and Simulation Methods .....
Leonhard Ganzer and Diethard Kratzer 69

New Parallelized Adaptive Implicit Methods for Large Compositional Reservoir Simulations .....
Y. Caillabet, J.F. Magras and O. Ricois 81

Could WAG be the Right EOR Process for Libyan Carbonate Reservoirs? .....
Rafa Labedi, Omar Abdulkarim, Karlo Krizmanic and Saleh El-Fakhri 91

Application of Downhole Oil-Water Separation: A Feasibility Study .....
Mohamed A. Alhoni 105

Water Shutoff Polymer/Gel Treatments for Oil or Gas Production Wells .....
A. Zaitoun, R. Tabary and N. Kohler 115

Field Applications of a Productivity Tool for Improved Oil Recovery (IOR) .....
M. B. Amish, M. B. Oyeneyin and M. H. Hodder 123

Depressurization as an Effective IOR Strategy .....
M. Babs Oyeneyin 133

Evaluation and Ranking of Scenarios for Redeveloping Mature Fields: A Need for Improved Methodologies .....
François Kalaydjian, Isabelle Zabalza-Mezghani, Emmanuel Manceau, Mathieu Feraille and Paul van Lingen 137

Consequences of Asphaltene Adsorption on Flow Phenomena in Porous Media .....
B. Rayes, I. Lakatos and J. Toth 149

VOLUME 18 - (2005)

Petroleum Research Centre
P.O. Box 6431, Tripoli
Great Socialist People's Libyan Arab Jamahiriya

Petroleum Res. J. Vol. 18 (2005); P. 1–8, 7 Figs.

The Use of Complex Wells for Reserves Optimization in the Mabruk Field

A. Gaaim*, Y. Bigno** and A. Al-Faia**

استخدام الآبار المعقدة لتحسين الاحتياطي في حقل المبروك

أ. قعيم، ي. بينو وأ. الفايا

يقع حقل المبروك الضخم في حوض سرت ويتكون من عدد 4 تجمعات للزيت، هي شمال المبروك – شرق المبروك– وسط المبروك وغرب المبروك ، لقد تم تطوير غرب المبروك تطويرا شاملا نظرا لوجود ميزات مكمنية واضحة به.

يتصف مكمن المبروك الجيري الواقع على عمق 3500 قدم بتغير شديد في السحنات مع تصنيف معقد نتج عنه عدم تجانس كبير للمكمن.

لقد بذلت محاولات عدة من قبل شركات متعددة منذ الخمسينيات لتطوير الحقل باستخدام الآبار العمودية ، ولكن بسبب السمك القليل الذي لا يتعدى 45 قدم ولقلة النفاذية كان أداء الآبار العمودية ضعيفا.

منذ سنة 1995 نجحت شركة توتال (CPTL) في استحداث طريقة لتطوير الحقل وزيادة الاحتياطي في حقل المبروك الغربي وذلك باستخدام تقنية حفر متطورة . إن استخدام الآبار الأفقية والجانبية سمحت بالتغلب على الإنتاجية الضعيفة وخففت من أثر عدم التجانس المكمني – عملية المحاكاة المكمنية استخدمت أيضا للتنبؤ بالمساحات التي قد تكون مسحت بضعف وذلك لغرض التخطيط للحفر البيني. ونتج من استخدام هذه الطريقة ازدياد تدريجي في تقدير الاحتياطي من 19% سنة 1995 إلى 28% اليوم.

المرحلة القادمة لتطوير المبروك هي استغلال الدروس المستفادة من غرب المبروك وتكييفها للأجزاء الأخرى من حقل المبروك وعلى الأخص شرق ووسط المبروك أيضا. إن مراجعة أداء الآبار والتحسن في الفهم الجيولوجي ستقود إلى تطورات أكبر في تصميم الآبار مستقبلا متضمنا هندسة الآبار والمسافات البينية واستراتيجية تحسين الإنتاجية وبرنامج حقن المياه.

هذه الورقة تناقش فلسفة التطوير المتبعة إلى حد الآن والتحسينات المستقبلية التي هي الآن تحت الدراسة لزيادة تحسين معامل المسترد النهائي في الحقل، كما تم تقديم نتائج أولية من هذه الدراسة المستمرة.

Abstract: *The Mabruk field, located in the Sirt Basin, is made up of four oil accumulations, namely North Mabruk, East Mabruk, Central Mabruk, and West Mabruk. The latter one, where fair reservoir characteristics were encountered, is the most extensively developed. The Mabruk carbonate reservoir, located at a depth of 3500 ft, is characterized by steep variations of facies together with a complex compartmentalization, resulting in massive reservoir heterogeneity.*

Several attempts were made by various companies since the late fifties to develop the field with vertical wells. But due to the small thickness (45 ft) and low reservoir permeability, the performance of vertical wells is generally poor.

* National Oil Corporation, Libya
** Compagnie des Petroles Total Libye (CPTL), Libya

Since 1995, the approach used by Compagnie des Petroles Total Libye (CPTL) succeeded in developing and increasing the reserves in the West Mabruk field by using sophisticated drilling techniques. The use of horizontal and multi-lateral wells allowed coping with the low productivity and alleviated the impact of heterogeneities. Reservoir simulation was also utilized to predict the areas that will be poorly swept, and plan infill drilling. A gradual increase of forecasted recovery from 19% in 1995 to 28% today resulted from this approach.

The next stage of the Mabruk development will be to capitalize on the knowledge gained in West Mabruk, to adapt in the other parts of the Mabruk field (particularly the East and Central areas). Also, a review of the well performance and the improvement in geological understanding should lead to further improvements in future well design, including: well geometry, spacing, simulation and intervention strategy, and water injection scheme.

This paper discusses the development philosophy followed so far, and the foreseen improvements currently under study to further improve the ultimate recovery factor in the field. Preliminary results from the ongoing investigations are also presented.

INTRODUCTION: MABRUK FIELD HISTORY

The Mabruk field is located in Block NC 17 in the Sirt Basin (Fig. 1). The most sizeable oil volumes are located in the West and East panels of the Mabruk reservoir (Fig. 2), a carbonate member of the Heira marine shales, in the Paleocene. The West Mabruk (Fig. 3) has been so far the most extensively developed, due to its relatively fair reservoir properties (porosity of 15 to 25%, and permeability of 1 to 100 md). It is characterised by compartmentalisation of the structure, induced by heavy faulting. Large and unpredictable property variations were however, the main drawback in the field preventing a full-field development until the mid 1990's.

The history of West Mabruk started in 1959 when the field was discovered by Exxon, with well A01, encountering oil in the Mabruk and Garian reservoirs. Between 1959 and 1961, Exxon drilled 26 wells and implemented a five spot water injection pilot test (250m spacing) in West Mabruk. However, following

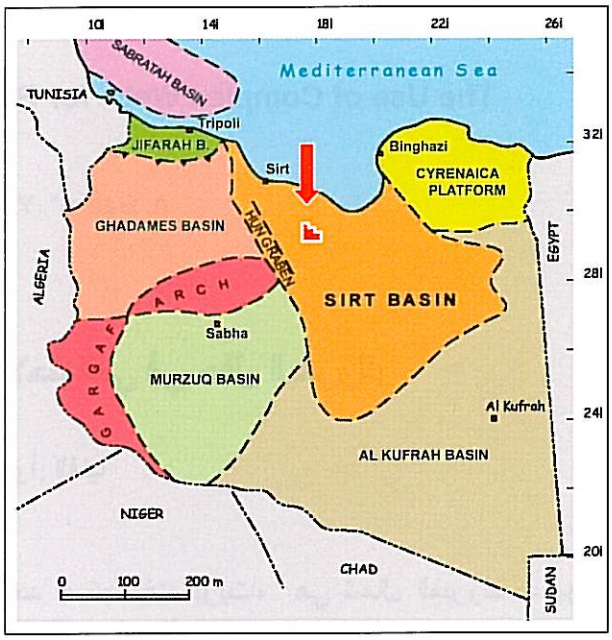


Fig. 1. Mabruk Block NC17 location.

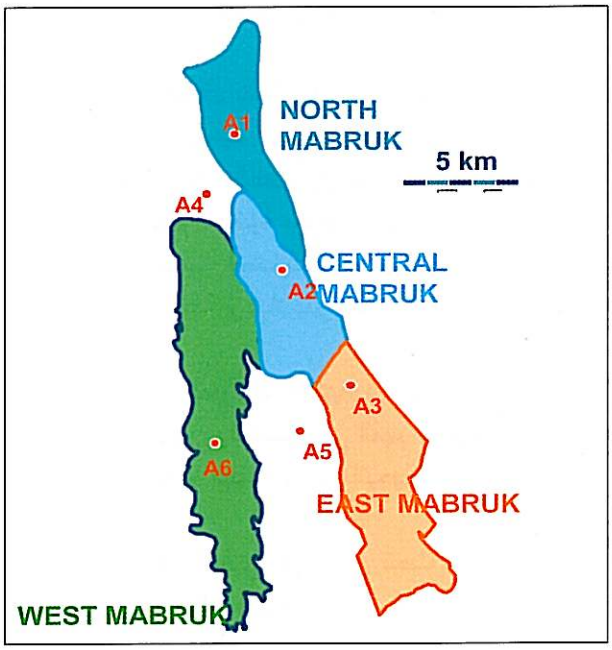


Fig. 2. Panel location and corresponding discovery/appraisal wells.

corrosion problems and early water breakthrough, the idea of a full development was given up. Sirte Oil Company resumed the development in 1982, shot a 3-D seismic, drilled 4 wells but, also abandoned due to the poor performance of vertical wells. Subsequently, Lasmo took over but gave up as well. Since the beginning, the IOIP estimate has decreased from 1 BSTB to about half this value. The real development of the field only started in 1995 with CPTL as an operator, and the use of horizontal and multi-lateral wells. The development included a two-year pilot phase prior to finalizing the

development scheme. Water injection was implemented, first at peripheral locations, then in pattern, over the entire panel.

To date, almost 35 million STB of oil have been recovered from West Mabruk, and the current rate is around 15,500 BOPD from 35 producers, the reservoir pressure being maintained by 28 injectors. Of the 63 active wells, 26 are vertical (dating from the early development attempts), 26 are horizontal and 11 are multi-lateral. Horizontal and multi-lateral wells are drilled with 6" open-hole drains in the reservoir. Regular 3D model updates are carried out, with reservoir history-matches, in order to identify remaining opportunities (well interventions, re-entries or infill wells). Reservoir management is an integral part of the development, and the field is closely monitored with regards to well performance, water injection at voidage replacement, etc. The ultimate recovery factor for West Mabruk has progressed from 5% in 1988 to 28% today.

In the 7 years of development history by CPTL, a more precise knowledge of the Mabruk reservoir has been acquired. This will particularly help in the full development of the other panels, starting with the East and Central areas, planned this year (2004). Also, the influence of the reservoir characteristics on the wells completed in Mabruk is better understood, as presented in the next section.

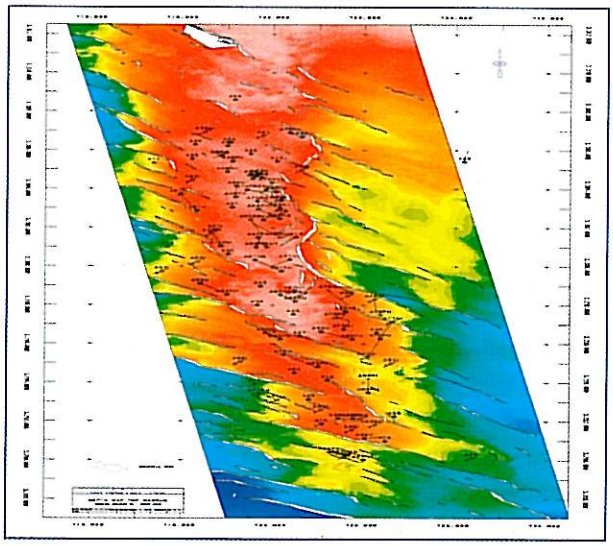


Fig. 3. West Mabruk structure showing the extent of fault panels.

THE MABRUK RESERVOIR: CURRENT KNOWLEDGE

The Mabruk reservoir is heterogeneous in both lateral and vertical directions. Rapid changes of facies and fracture networks are combined with a complex structural context, characterised by faulted blocks that are not necessarily recognisable from seismic data. The reservoir characteristics are degraded towards the flanks of the reservoir, which translates into a lack of natural (aquifer) support. The Mabruk oil is practically free of dissolved gas and provides no significant energy. This has motivated the decision to perform water injection at a very early stage in the field.

The lateral and vertical heterogeneity has influenced the chosen well design. By adopting horizontal and multi-lateral wells geometries, the chance of intercepting good facies or fracture networks was increased. See Figure 4 for a schematic of the current well design. Horizontal and multi-lateral wells, of open-hole design, have been used extensively since 1995 and contributed to the success of Mabruk so far. The benefit from fully open-hole horizontal and multi-lateral wells should not however, hide their drawbacks which are being recognised:

- The higher cost and drilling risks,
- The absence of stimulation in most of them (because of cost and feasibility considerations),
- The lack of future down-hole monitoring and well intervention capabilities (isolation or stimulation of specific drains or parts of drains), due to the open-hole nature of these wells.

The behaviour of horizontal and multi-lateral wells has actually not been as good as one could have expected in terms of productivity and developed reserves, especially in some parts of the field. Looking

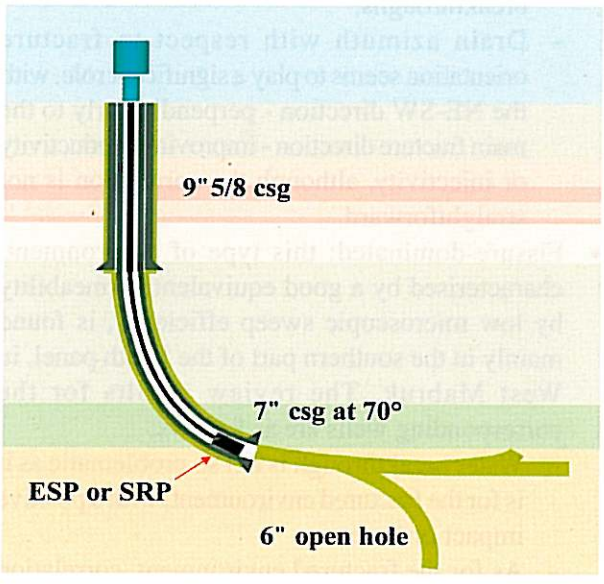


Fig. 4. Typical current well design used in the Mabruk reservoir.

at the historical performance of the West Mabruk wells, it is indeed possible to relate productivity, water-cut development and pressure support to the local reservoir characteristics. For this, a systematic review of all Mabruk wells was recently performed, which aimed at improving the understanding of the field, while also identifying possible data gathering and intervention opportunities. The review strongly suggested that the Mabruk wells performance depends on the prevailing fracture environment, as follows:

- Fracture-dominated: this type of environment characterises the production in the Northern panel of West Mabruk, where large fracture corridors have been recognised by fracture characterization studies. The effects on well performance and its link to well design, confirmed by the well review, are as follows:
  - Rapid water breakthrough is observed, due to the interception of open fractures. This affects the ultimate recovery, generally lower than for other environments,
  - There is no clear correlation between drilled length and well performance. The longer multi-lateral drains seem to actually perform worse, in terms of productivity and reserves, possibly due to the fact that a limited number of fractures are contributing to production. Productivity of vertical wells can be as good as for horizontal ones (when they intercept fractures). Reserves developed by multi-lateral and even horizontal wells is disappointing compared to vertical wells, due to the impossibility to isolate fracture-related water breakthroughs,
  - Drain azimuth with respect to fracture orientation seems to play a significant role, with the NE-SW direction - perpendicularly to the main fracture direction - improving productivity or injectivity, although the correlation is not straightforward.
- Fissure-dominated: this type of environment, characterised by a good equivalent permeability by low microscopic sweep efficiency, is found mainly in the southern part of the South panel, in West Mabruk. The review results for the corresponding wells are as follows:
  - Water breakthrough is not so problematic as it is for the fractured environment, with a positive impact on reserves,
  - As for the fractured environment, correlation between drilled length and productivity is not straightforward, and some vertical wells perform better than horizontal and multi-lateral wells. The poorer wells (in terms of productivity and reserves) are however vertical so horizontal geometry seems to increase the chance of intercepting good facies and fissure networks,
  - Productivity/injectivity is, again, possibly improved by NE-SW azimuth directions.
- Matrix-dominated: this environment, where no significant fracture of fissure network is encountered, is found mainly in the Central panel and the northern part of the South panel, in West Mabruk. The results of the well review for the concerned wells shows that:
  - As expected, water production is not yet a problem in this environment, and there is even an acceleration potential with infill drilling at tight spacing,
  - There is a much clearer correlation of liquid rate and productivity with the drilled length. Productivity is generally lower than for the fractured/fissured environment, but is clearly improved by drain length. Reserves are also well correlated with the drilled length,
  - Drain azimuth is not seen as an influencing parameter.

This improved knowledge led to the belief that well design should be adapted to the fracture environment, which resulted into a specific investigation: the Well Concept Study.

THE WAY FORWARD: STUDIES OF NEW WELL DESIGNS

A Well Concept Study was initiated in 2003, in order to optimise the design of future wells for the Mabruk further development (both on the East and Central undeveloped areas, and at infill locations in West Mabruk). The outcome will be a set of recommendations affecting not only future drilling practices but also completion and stimulation methods. The ability to effectively stimulate wells is seen as a major contributor to the success of the future designs. The methodology was to first define the reservoir requirements needed in each fracture environment:

- High productivity: as confirmed by the well review, for the fractured and fissured environments, efficient connection of the fracture/fissure network is needed, but does not necessarily require long drain length. On the other hand, long

lengths are needed in matrix environments, as they provide larger productivity and reserves. Fracture plugging and matrix damage should be avoided or cured, through appropriate stimulation, avoiding large sections of the drain not producing, which would explain the poor performance of some of the longest existing wells,

- Efficient pressure support: well design should be optimised to allow pressure support while avoiding early water breakthrough. The currently low water-cut in the matrix environment points at the opportunity for smaller spacing. The distance should be optimised (larger in higher permeability or fractured/fissured environments than in poor permeability or matrix formations), but also a balanced production and injection between the reservoir layers needs to be obtained,
- Practical well intervention: the current 'fully open-hole' well design does not allow practical down-hole monitoring and water shut-off, despite the need for such interventions in many existing wells. The drawback has been lower developed reserves. Future well design should offer the possibility of such interventions so that reserves are maximised.

Based on the above analysis, the investigation of the following well concepts was proposed, the objective of the Well Concept Study was then to fine-tune the design parameters and determine their technical and economical viability:

- For a fractured medium: see Figure 5. The proposed design is that of a lined, cemented, perforated and stimulated single-horizontal well, oriented perpendicular to the fracture direction, with large spacing and line-drive. A large length would ensure that a maximum of conductive fractures would be intercepted, and save on the number of wells. Such large length would however require that each fractured zone is individually perforated and stimulated, so that production and injection is not affected by uneven damage. The cemented liner would also ensure selective water shut-off. The large spacing avoids early breakthrough.
- For a fissured medium: see Figure 6. The proposed design is a lined and cemented short trunk, possibly with one or two short open-hole laterals targeting each main pay zone, with large spacing and 5-spot injection. Large open-hole length is not necessarily required, but more than one drain would improve the chance of intercepting the fissure network. The cemented liner in the trunk would ensure future water shut-off (of a whole leg at a time, no isolation required within each leg), isolation of legs while drilling (to prevent differential damage between legs) and also a selective light stimulation program (acid or bleach circulation at TD). The 5-spot ensures optimum volumetric sweep for these relatively small wells.

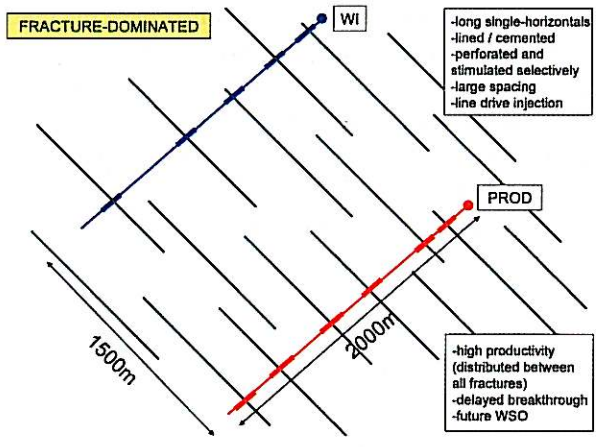


Fig. 5. Proposed well design adapted to a fractured-dominated environment.

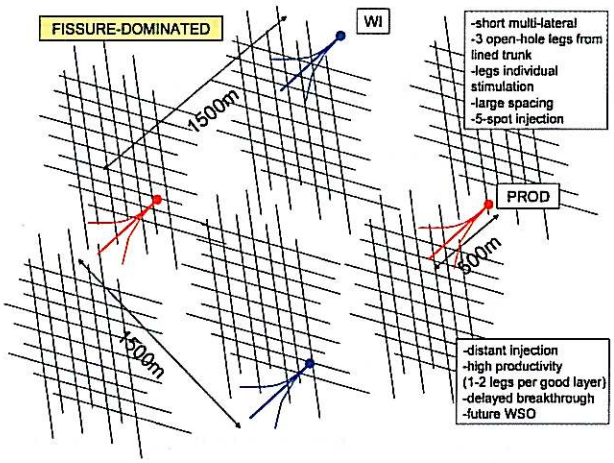


Fig. 6. Proposed well design adapted to a fissured-dominated environment.

- For a matrix medium: see Figure 7. The proposed design would be a lined, cemented horizontal backbone with open-hole lateral legs, drilled at small spacing, with line drive. Productivity would be ensured by the very large open-hole length, the spacing would be small enough to provide pressure support. The lined and cemented backbone ensures the same functions as the trunk of the fissured medium design, with possibility of leg isolation and selective stimulation.

Note that the Figures 5-7 are proposed designs and the quoted lengths/distances are qualitative

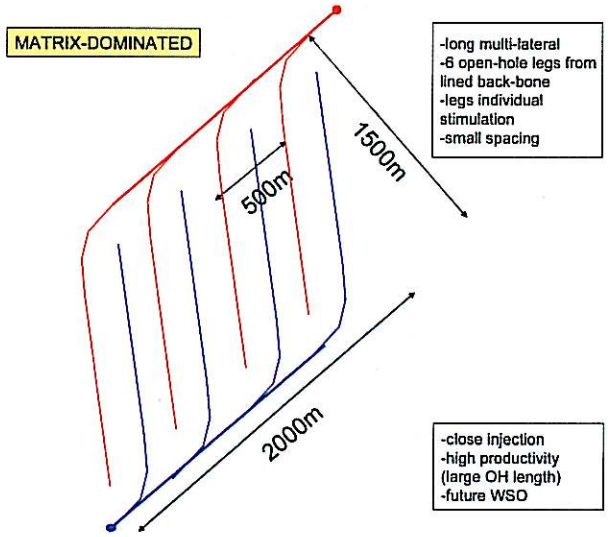


Fig. 7. Proposed well designs adapted to a matrix-dominated environment.

indications only, and were fine-tuned during the study. The technical feasibility of the 3 designs is also being investigated, with answers to the following questions:

- Technical and cost impact of drilling a sufficiently large diameter in the reservoir (8.5"), subsequently lined and cemented (7" liner), common to all three designs. This represents a major change compared to the current well design, for which the 7" liner is set at the top-reservoir, with an impact on costs,
- Feasibility of proposed geometrical parameters (lengths, angles, etc.), of completion and stimulation requirements, and cost impact,

The preliminary results of the study show that the proposed well concepts are technically achievable. Although they will cost more, the associated gain in productivity and reserves should largely compensate for the incremental CAPEX. The increase in productivity estimated by the study was very large, due to the adapted geometry but also the assumed effectiveness of stimulation methods. The gain in reserves was extremely encouraging. Recovery factors ranging between 40 and more than 50% were indeed obtained by sector model simulations. While lower recoveries are expected in full-field situations, figures in the range of 35 to 40% could still be expected in West Mabruk, compared to about 28% currently booked. This represents a gain of 7 to 12% recovery. The gain will be even superior in East-Central Mabruk, where only 16% recovery is currently expected. These results are however, subject to more in-depth studies, such as:

- Further sensitivities on reservoir parameters and uncertainties,
- A more detailed review of the technical feasibility of the new wells, with cost estimates, that will help fine-tune the economical evaluation,

However, nothing will better confirm the encouraging results than some field trials. As the success of the new designs will largely depend on the effectiveness of stimulation, it is proposed to test innovative stimulation methods in one or several existing horizontal or multi-lateral wells. Then, several pilots could be drilled in the field within a few months following the completion of the study.

CONCLUSIONS: REACHING 40% RECOVERY IN MABRUK?

The early years in the Mabruk development have been characterised by a lack of reservoir knowledge, in a field where lateral and vertical heterogeneities have a major effect on well performance. This lack of knowledge meant that reservoir properties could only be assessed as wells were being drilled. This, and other difficulties such as the presence of seismic 'blind' zones, made Mabruk a very challenging development. Since 1995, however, a lot of ground has been covered in the recognition of properties, their mapping, and the reduction of seismic risks, through data acquired in new wells but also by performing subsurface characterization studies. A better understanding of the fracture network, and its influence on well performance, was in particular a very valuable knowledge, which could subsequently be translated into improved well concepts, currently under evaluation.

The principles behind the choice of new well designs were motivated by the fulfilment of the main reservoir requirements ensuring efficient development of the Mabruk reservoir: the need for productivity (and injectivity), the need for effective pressure support (through water injection), and the benefit from an appropriate well life-cycle. This last point relates to the ability to perform data gathering and water shut-off activities in order to maximise reserves.

From the preliminary results of the study, the foreseen improvement in productivity from the new well concepts could be very significant, and is to be confirmed by field trials and pilots. It will certainly alleviate the need for large number of wells in the undeveloped parts of Mabruk (East and Central).

Even more importantly, the improvement in reserves is very encouraging. It shows that recovery factors from even difficult reservoirs such as Mabruk can match the highest levels obtained in the oil industry, reaching in this case the 40% level, possibly more. The application of such analysis and studies, and possibly the adoption of similar well concepts in other difficult fields could prove very attractive to the long-term development of resources in Libya.

Simple open-hole multilateral wells have been commonly drilled in the 1990s in different worldwide locations[1-7], some of them using similar "fishbone" geometries[4, 5]. The application of multi-lateral well technology has been particularly extensive in the Middle East, especially in Oman[5-7]. However, the Mabruk field in Libya has benefited from multi-lateral wells since the end of the 1990s, with an overall success[3].

REFERENCES

[1] Aubert, W.G., 1998. Variations in multilateral well design and execution in the Prudhoe Bay Unit. Paper SPE 39388 prepared for presentation at the 1998 IADC/SPE Drilling Conference, Dallas, 3–6 March.

[2] Vullinghs, P. and Dech, J.A., 1999. Multilateral well utilization on the increase. Paper SPE 56954 presented at the 1999 SPE Offshore Europe Conference, Aberdeen, 7–9 September.

[3] Chaussumier, D. and Ludot, B., 2002. The History of Libya's Mabruk field: How to develop a challenging field. *Petrol. Res. J.*, **14**, 83-92.

[4] Stalder, J.L. et al., 2001. Multilateral-horizontal wells increase rate and lower cost Per barrel in the Zuata field, Faja, Venezuela. Paper SPE 69700 presented at the 2001 SPE International Thermal Operations and Heavy Oil Symposium, Porlamar, Margarita Island, Venezuela, 12–14 March.

[5] Bigno, Y., Al-Bahry, A., Melanson, D. D., Al-Hasani, S., Senger, J. Ch. and Henning, R., 2001. Multilateral waterflood development of a low-permeability carbonate reservoir. Paper SPE 71609 prepared for presentation at the 2001 SPE Annual Technical Conference and Exhibition held in New Orleans, Louisiana, 30 September–3 October.

[6] Al-Khodhori, S., 2001. The challenges and way forward of horizontal dual lateral wells in Fahud matrix reservoir. Paper SPE 68204 presented at the 2001 SPE Middle East Oil Show, Bahrain, 17–20 March.

[7] Al Salhi, M., Al Maimani, A., and Mäkel, G.H., 2001. A switch from verticals to dual lateral producers accelerate oil production and reduces UTC for Natih field. Paper SPE 68127 presented at the 2001 SPE Middle East Oil Show, Bahrain, 17–20 March.

Petroleum Res. J. Vol. 18 (2005); P. 9–16, 10 Figs.

A Method for an Efficient Fast Track Evaluation and the Assessment of Re-engineering Potential of Mature Fields

Claude Mouret, Jean Chastang and Jean-Paul Valois*

طريقة كفأة سريعة لتقييم إمكانية إعادة هندسة الحقول المعمّرة

كلود موريه، جان شستانج وجون بول فالوا

يواجه رفع كفاءة إنتاجية الحقول المعمرة تحديات عديدة منها مشاكل التآكل المتعلقة بالعلوم الجيولوجية وهي ذات أهمية قصوى.

طريقة ولفير التي طورتها شركة توتال لمواجهة الكثير من هذه المشاكل تستهدف توصيف سلوك المكمن والكشف عن مناطق الاستنزاف وتقترح سيناريوهات لإعادة هندسته.

تستخدم هذه الطريقة منظومة برمجة تم تطويرها محليا مبينة على تحليل بيانات إنتاجية أحادية ومتعددة التغير، أساسية، بالإضافة إلى بيانات عددية مكمنية وجيولوجية كما تشمل تكامل، إعادة كمية وكيفية لجميع البيانات الجيولوجية والإنتاجية، مع نتائج الحاسوب الإحصائية. لقد تم تلخيص تاريخ إنتاجية كل بئر على حدة بخصائص مختارة تسمى بمؤشرات الإنتاج، والتي تحسب وتخرط للمساحة الكلية للمكمن. وبهذه الطريقة تبدو إنتاجية أقسام وقطاعات الحقل المختلفة واضحة يمكن تفسيرها بمساعدة بيانات الموائع والمواد الساكنة.

تظهر غالبا معالم غير معروفة مثل انسداد الفجوات المنتجة (انسداد السطوح وتصدع الأروقة واختراقات محاور الماء والغاز... إلخ) وزيادة مساحات اتصالات المكمن العمودية والتوزيع المكاني للانسداد غير المتجانس، أو قطاعات الحقل ذات إنتاجية مختلفة. إن انتظام الإنتاج أو العكس في المدى الكبير لسلوك إنتاجية البئر على طول مساحة المكمن، يدل على درجة استمرارية الإنتاج التي تعكس مميزات المكمن. إن معرفة هذه المعلومات وتفسيرها تقود إلى تشخيص المكمن وإلى التكهن بدرجة كفاءة إنتاجية الآبار مستقبلا. كما تستعمل هذه النتائج فيما بعد لتحديد مواقع المساحات غير المنتجة. يمكن بعد ذلك اختبار فرضيات إعادة هندسة الحقل وحساب الإنتاج المتوقع، وقد تم اختبار عينات منتقاة لتوضيح هذه الأوجه، تتعلق الأولى بمكامن ذات ترسبات نهرية رملية تبين كيف تم تقسيم الحقل إلى مناطق مختلفة الجودة، أما الحقل الآخر المكون من ترسبات الدلتا الرملية متكررة عموديا والتي يمكن تقسيمها إلى مناطق واضحة مميزة بسلوك حركي، وتم على أساس هذه المعرفة اقتراح إعادة هندسة الحقول. وتتعلق الأخرى بطبقة كلسية تكونت فوق حفريات قديمة. أثبتت الحسابات التي أجريت بطريقة ولفير زيادة الاتصالات العمودية بالقرب من الجزء العلوي للمركب المتوافق مع الترسيب والتكوينات الصخرية وقادت هذه إلى اقتراح تطويرات إضافية للحفر أثبتت جدواها.

أظهرت الخبرة المكتسبة من بعض عشرات الحقول أن معظم الحقول يمكن معاملتها بطريقة ولفير ومنظومة البرمجة ويمكن معالجة الحقول ذات التاريخ الإنتاجي الطويل المكونة من عدة آبار (أكثر من 40 عاما ومن 500 بئراً) بالطريقة الموضحة في المثال الأول.

لقد اكتسبنا خبرة من مكامن ذات ترسبات بيئية وأنواع من التكوينات التركيبية وخصائص المواقع المختلفة، يمكن تطبيقها إيجابياً على حقول منتجة لمدة طويلة دون الحاجة إلى بيانات عديدة.

إن طريقة ولفير التي تمكن من الكشف على وجود الهيدروكربونات وبالتالي زيادة الاحتياطي القابل للاستخراج، تعتبر طريقة هامة لزيادة إنتاجية الحقول النفطية.

* TOTAL, France

Abstract: *Mature-fields production optimisation faces many challenges, among which geoscience-related problems are of paramount importance.*

The Welfare method developed by TOTAL addresses many of these problems, as it is aimed at characterising reservoir behaviour and detecting insufficiently drained areas, as well as proposing and testing of re-engineering scenarios.

The method uses an in-house developed software that is based on mono-variant and multi-variant statistical analyses of mainly production data, as well as geological, reservoir and fluids data. It includes an iterative integration of all, quantitative or qualitative, geoscience and production data with the statistical computation results.

Each well production history is summarised by selected characteristic values, called Production Indicators that are calculated and mapped all over the reservoir area. In this way, field compartments and sectors with different production characteristics clearly appear and are interpreted with the help of static and fluids data.

Previously unknown features often appear, such as production-impacting fractures (sealing surfaces, fracture corridors, axes of water or gas breakthroughs, etc.), areas with increased vertical reservoir connection, spatial distribution of impacting heterogeneity, or field sectors of different value. The uniformity, or to the contrary, a large variation range, of well production behaviours throughout the reservoir area indicates the degree of lateral continuity that characterises reservoir properties. The knowledge of this, and related interpretations, led to a reservoir diagnosis, and to a qualification of the degree of predictability of production behaviour of future infill wells. These results are subsequently used to determine the location of under-produced areas, and a new scenario of future field re-engineering can then be tested and future production calculated.

Selected examples illustrate these aspects. Variable field heterogeneity and linear trends impacting production are presented.

An example of fluvial-deposited silici-clastic reservoirs shows why the field had to be divided into separate areas for water injection. A second field, made up of vertically repeated deltaic sandstone reservoirs, could be split into significant areas with a clearly distinct dynamic behaviour. Re-engineering proposals were based directly on their knowledge.

Another example concerns a platform carbonate reservoir that developed on a paleo-high. Calculations with Welfare proved, in a very fast way, an increased vertical connectivity near the top part of the structure that is fully compatible with the sedimentary and diagenetic settings. This knowledge and the distribution of, for instance, produced water salinity led us to proposing a modification of the water injection pattern and additional development drilling that proved very productive.

The experience acquired over a few tens of fields demonstrates that most of the fields can be processed with the Welfare method and software. Fields with long production history and many wells (say more than 40 years of production and more than 1500 wells) can be easily processed, as demonstrated by one of our examples.

Our experience was gained from reservoirs covering most of the silici-clastic and carbonate depositional environments, and a variety of structural settings and fluids characteristics.

Welfare is a key tool to IOR as it allows spotting un-drained hydrocarbons and thus increasing the quantity of recoverable reserves, and as it facilitates the optimisation of field re-engineering,

INTRODUCTION

Oil and gas field exploitation classically faces many difficulties. Mature fields bring their own lot of additional challenges that need to be thoroughly addressed, in order to extract, in the most economical way, barrels of oil that remain to be produced. Mature fields often started producing long ago, when techniques for extracting information from the reservoir were not as developed as they are nowadays; consequently, the quantity and quality of data may be rather variable throughout the reservoir history. This might drastically impact future field development and economics, if we were not in the position to investigate field behaviour and reservoir characteristics with the necessary accuracy. What we want is clearly to maximise hydrocarbon recovery, optimise economics and exploit natural resources in the best way.

In order to master the recovery of remaining and bypassed hydrocarbons we must maximise the amount and the quality of information that can be

extracted from any available data. Therefore, processing all data as thoroughly as possible and integrating them is of great importance. For instance, production rates highly depend on field geological characteristics, reservoir properties and fluids properties; the knowledge of these three allows the understanding of reservoirs for which production history files are available.

In order to obtain the most and the best from the available data, TOTAL has developed an in-house computer-assisted method, called Welfare, dedicated to an efficient fast track processing and interpretation of reservoir-related numerical and qualitative data.

THE WELFARE METHOD

Welfare does not use the classical history matching required by numerical reservoir simulation models, which can last several months or more. Instead, it organises and integrates all dynamic and static data at the same scale, with the spirit of data mining [1,2,3]. It is powerful and fast: a study lasts a few weeks only, sometimes less.

The method includes a data processing and a related, iterative, synthesis that takes into account both static and dynamic results. It can be described as a "computer-assisted brainstorming", in which the software is the tool to answer questions that arise during the study. Nevertheless, there are several steps, ranging from a validation of numerical data and a first synthesis of qualitative data, computations and interpretations that lead to a field diagnosis for each reservoir for which production data are available, breaking the field into sectors, proposing field re-engineering, and testing of scenarios and previsions. Some of the steps may be used in different ways, to further enforce results with other methods.

The numerical data processing primarily uses the production history record, known per completion (one branch of a well equals a completion, in this sense) and, preferably, per reservoir[4]. Numerical geological data (such as hydrocarbon pore volume, net-to-gross, porosity, permeability) and/ or seismic characteristics (such as attributes or interval velocities) can also be included, according to the needs. The numerical processing is based on mono-variant and multi-variant statistical data analyses[5] which can include all numerical data together, at the same scale. The processing options and the necessary control are derived, at every step of the work, from the synthesis of all aspects of reservoir characteristics. Iterations between processing and interpretation improve the results until they are considered satisfactory.

Production history files are numeric tables of varying parameters (such as oil flow rate, water flow rate, cumulative values, water cut, gas-oil ratio) *vs.* time or each other After an adequate preparation (with a homogeneous presentation that will enable a proper use of the tables), the data validation is implemented, through cross-checking and, if necessary, cross-correlation. Production data are smoothed or modelled for each well and each reservoir. Time-related drifts are corrected and readings recorded at different dates, hence at different degrees of reservoir depletion, can then be compared. Key values, called Production Indicators that correspond with singular evolution points (hinge points, maximums, slopes of selected parts of curves) are calculated and filed.

The dedicated software generates histograms, cross-plots and maps all connected by dynamic links[6]. In this way, all production characteristics, including apparent ''anomalies'', can be duly investigated. For each mapped Production Indicator, areas showing a given behaviour are selected and their whole distribution is interpreted. Then, deterministic synthesis maps are built to gather the useful information. They summarise reservoir behaviour, and show ranked areas with high or low production, water inflow, breakthroughs, etc. Classes, obtained from a multivariant statistical clustering of production parameters, are ranked and interpreted, in order to cross-check deterministic results.

All along, syntheses of geological and geophysical data, available at the same scale as dynamic data, are used to calibrate observed dynamic behaviours, and their apparent "anomalies". There is an iterative work to explain dynamic facts from reservoir geology and to evaluate how salient geological features impact production.

Reservoir Diagnosis

The Welfare method is aimed at visualising the salient aspects of a reservoir, evidencing previously unknown features, finding out what heterogeneity impacts production the most, defining compartments and/or sectors with a homogeneous or nearly homogeneous reservoir behaviour, i.e. at highlighting features important to a good understanding of the reservoir area. This field diagnosis is needed to propose adequate solutions for field re-engineering. It must evidence the variable size and location of

areas with a given dynamic behaviour and characterise the boundaries between them.

Compartments are defined from different data, which include pressure patterns, Productivity Index maps, Production Indicators distribution and linear features. Sectors are defined as areas with comparable production behaviours. One or several sectors may correspond to a compartment. When compartments cannot be defined, then sectors become predominant. There is a characteristic behaviour pattern for every reservoir in every field.

Evidencing a Degree of Heterogeneity

Some fields are very simple, with a sub-regular pattern of dynamic behaviours: in Figure 1 below, ranked classes 1 (poorest) to 4 (best) follow a nearly radial pattern. Class 1 produces a lot of water and it clearly indicates a water influx from the west, which is related to a stronger aquifer support. Class 4 is located in two central areas and has a lower water cut and a higher oil flow rate Qo; it is located further away from water influx areas and it probably corresponds to higher hydrocarbon pore volume values.

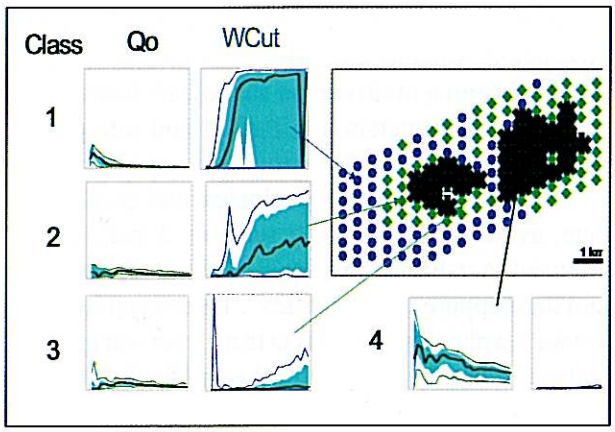


Fig. 1. Reservoir with a simple behaviour pattern.

In this carbonate field, re-engineering is relatively simple to define, and it is based on a choice of the less produced parts or less water-invaded areas.

On the contrary, other fields may show a high degree of variation of dynamic properties. For example, the silici-clastic field of Figures 2 and 3 shows a highly varying pattern, which is clearly visible on Production Indicators maps (as shown in the oil decline rate, Fig. 2) and on classes of production behaviour (Fig. 3).

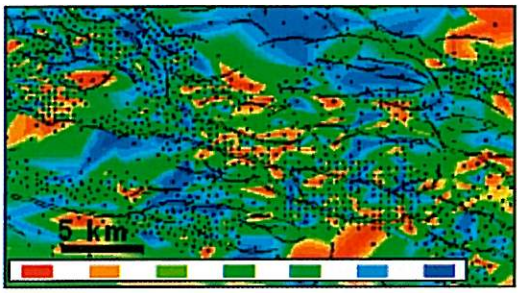


Fig. 2. Reservoir showing a large degree of variation of the Qo decline (larger declines in blue).

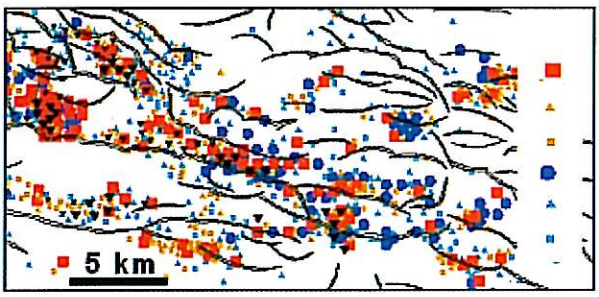


Fig. 3. The same reservoir, seen at the light of a six-class visualisation; it is highly heterogeneous, as some regions are largely different from others, and as large variations occur in every area (best classes in red, worst ones in blue).

Examples of Production-Impacting Linear Features

Previously unknown boundaries are commonly evidenced. This is very important, because it obviously has direct implications on the reservoir behaviour understanding and on re-engineering. Very often, the newly evidenced boundaries are faults at a sub-seismic scale, but they can also correspond to facies variations or diagenetic patterns. Boundaries may be tight, or simply tighter than the surrounding areas, or behave as drains facilitating the propagation of water from the aquifer or from injectors, or gas from the gas cap or from injectors (Figs. 4 and 5).

These cases involve linear axes that can be associated with structural discontinuities. Calibration on seismic and/ or on regional tectonic trends is necessary to finally interpret and refine the patterns.

The impact of evidencing such preferential axes of dynamic behaviour may be very high on a re-engineering project. Not all redevelopment patterns are suitable. The individual injection arrays must be adapted to real constraints that were previously unknown.

Evidencing Compartments Through Dynamic Lineaments Mapping

In a South American silici-clastic field with more than 1500 wells and a production period over 40

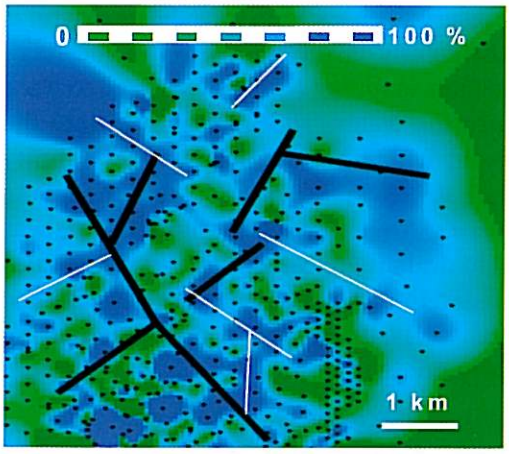


Fig. 4. In this silici-clastic reservoir from South America, the water cut distribution follows trends which can be calibrated on previously mapped faults (in black). Many more faults may be suggested (in white), and their mapping needs to be refined according to the structural knowledge.

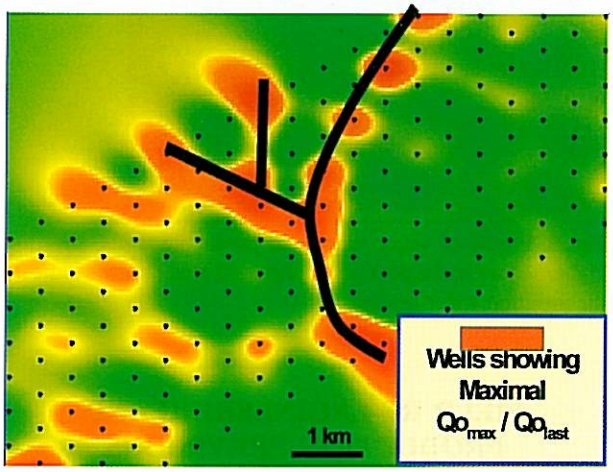


Fig. 5. In this carbonate reservoir from the Middle East, the ratio between the maximum and final oil flow rate indicates trends with a larger decrease, themselves indicating a tighter formation ; the alignments suggest structural patterns.

years, production indicators mapping revealed previously unknown features[7]. These are visible as alignments of wells showing distinct production behaviour from nearby wells (Fig. 6). Overall, well production was poorer in aligned wells, as it could be demonstrated with a mono-variant statistical analysis of several Production Indicators, confirmed by a multi-variant statistical analysis generating ranked classes of well behaviour.

The structural study showed that a first trend of lineaments was parallel to the main trend of normal faults in the field. A second trend was almost perpendicular to it, and was not corresponding with previously mapped faults from 2D seismic. It could be demonstrated that it was the direction of another group of normal faults, present at a sub-seismic scale.

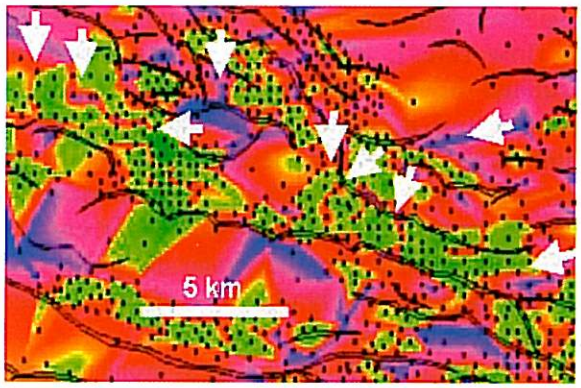


Fig. 6. Dynamic lineaments (shown by arrows) are evidenced from contrasting values of production indicators in aligned wells.

This indicated the need for a seismic reprocessing and the acquisition of 3D seismic, and that (re)processing had to be designed to highlight subtle faults.

The major consequence of the presence of lineaments that behave as trends of much lower permeability is that the field bears many more compartments than those initially thought to exist. Lineaments are partial barriers to water flows and to oil sweep and are potentially detrimental to the efficiency of water injection. Therefore, the design of new injection patterns must be adapted to this new constraint, in order to maximise their efficiency.

Such results are critical for field re-development, as well patterns can be adjusted to heterogeneity.

Evidencing Sectors, Including Natural Water Input Areas

In a West African field (Fig. 7), oil-bearing deltaic to coastal sandstones below a primary gas cap were produced through natural depletion and solution gas drive, with nearly 30 wells. After data validation and

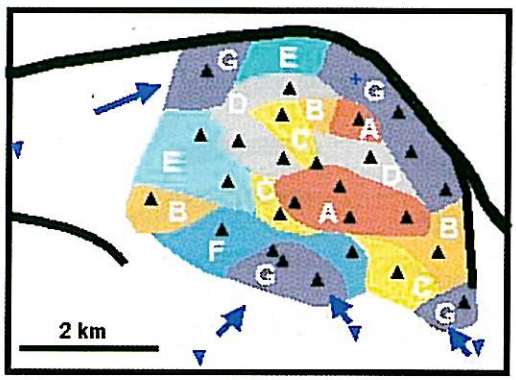


Fig. 7. Sectors definition in deltaic sandstones. A peripheral ring is more water-invaded (areas F and G), while best area A is located atop the structure (blue triangles = water injectors; others= producers).

curve smoothing (water cuts, GOR) or modelling (oil flow rates), Production Indicators were calculated for each well. Around 20 of them were selected and mapped. This led to generate synthesis maps showing the areas with better (A area) and worse (G areas) reservoir behaviour (from larger oil flows and lower water cuts to smaller oil flows and higher water cuts). Several ranked areas with clearly identified characteristics were defined in this way.

This work clearly highlights areas prone to water influx. Based on well density in every area and on the corresponding dynamic and geological characteristics, sectors prone to receive infill wells were selected. This selection can be refined afterwards, through grid reservoir models. It greatly helps in drastically reducing the size and the complexity of these models.

Evidencing an Area with a High Vertical Transmissibility

In a West African carbonate field with nearly 50 producing wells and 7 water injectors, an area with a better vertical transmissibility was evidenced by mapping the "b" value of the 1/b exponent of oil rate decline curves (Arp's Equation). Significantly lower "b" values, below 0.3, are encountered around the structure apex. It was demonstrated that this upper area corresponds with interruptions of three intervening beds of anhydrite and tight dolomite (Fig. 8). This is due to non deposition and dissolution during relative sea level falls that occurred on the salt-related paleo-high where sedimentation took place. Carbonate spread dissolution during the falls, increased porosity and permeability in the same area.

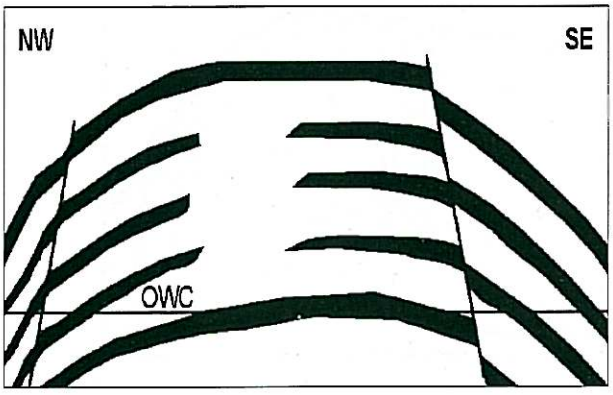


Fig. 8. Simplified reservoir geometry, with a central area of better vertical transmissibility related to interrupted internal barriers and carbonate reservoir dissolution.

These reservoir characteristics indicate that oil is drained differently in different parts of the field. Salinity values mapping (Fig. 9) was used to trace where injection water (at 35 g/l) moved into the oil reservoir, which has a connate water salinity of 250 g/l areas less drained were near the structure apex. An increase of production rate was proposed to drain it and water injection flow rates were adjusted to direct the water front toward the concerned wells. Proposed additional drilling proved very productive.

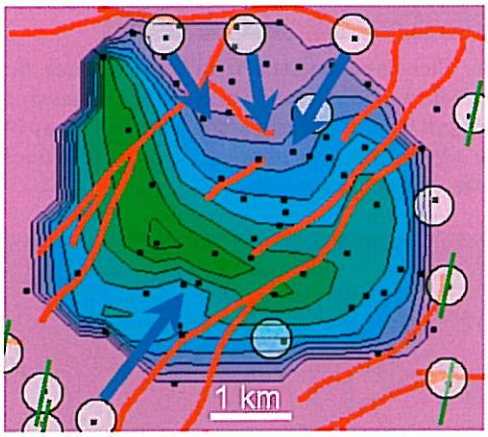


Fig. 9. Produced water salinity in producing wells, showing higher values in the poorly swept central area ; arrows indicate the injection water motion.

FIELD RE-ENGINEERING AND PRODUCTION PREVISIONS

Once the reservoir diagnosis is completed, i.e. once its characteristics and behaviour during production have been duly investigated and understood, and whenever necessary for each production mechanism or EOR/ IOR step, proposals for field re-engineering can be made. They take into account the distribution and density of already existing wells in each of the sectors ranked according to their quality (with reference to oil flow rate, water cut, GOR) and the prevailing production mechanism. Newly acquired knowledge on barriers and drains is largely used to define the re-engineering scheme.

Additional wells may be proposed, or simply redistribute injectors and producers in order to focus the sweeping fluid toward the best producers. Workovers or stimulations can also be proposed. Each scenario can be tested with Welfare, in order to evidence its impact on hydrocarbon recovery.

Production prevision curves can be generated for each sector, compartment or group of wells. They may take into account successive scenarios and production mechanisms (Fig. 10). In this way, the benefits from each scenario can be evaluated and compared, which leads to select the optimum solution.

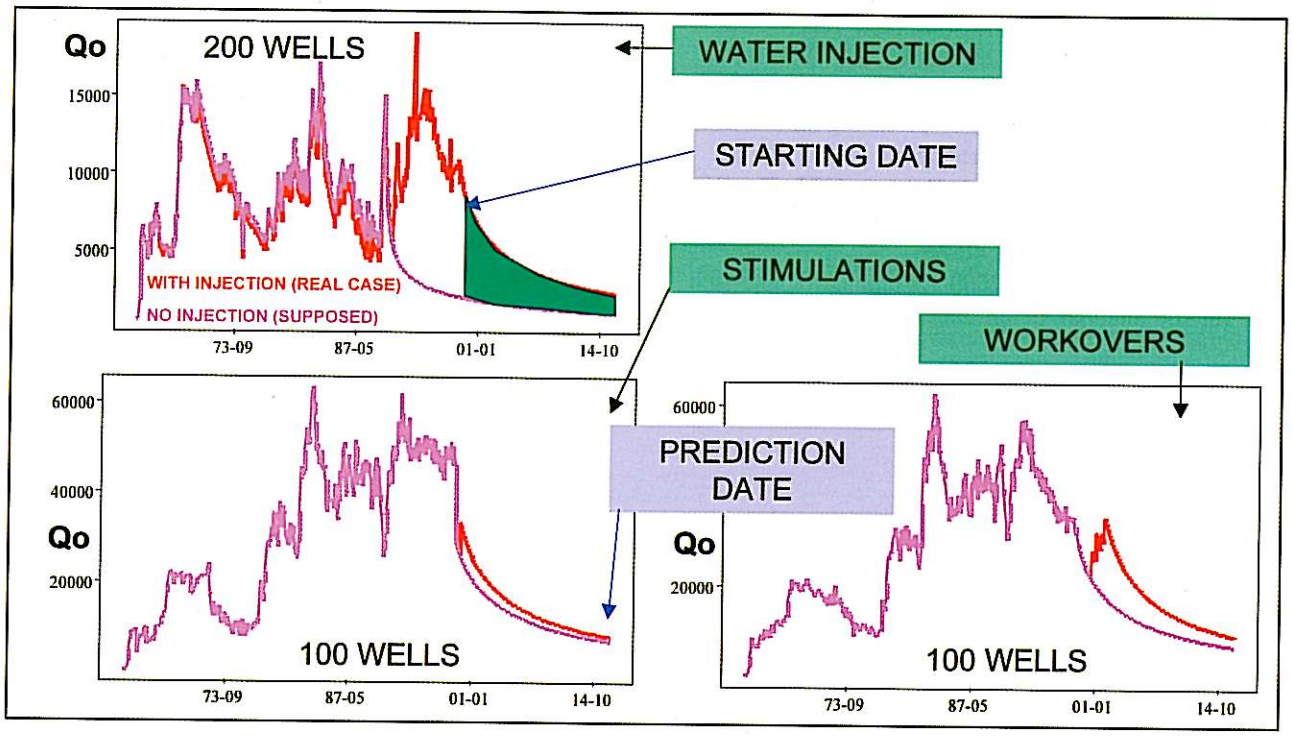


Fig. 10. Examples of curves for different group of wells and re-engineering scenarios. The graphs show the situation at the starting date (Year 2000) and forecasted production.

CONCLUSIONS

The use of production and static data, with the spirit of data mining, and the interpretation of Production Indicators, is an efficient and fast way to map reservoir performance, provided necessary precautions are taken. These precautions noticeably include the consideration of what production mechanism is involved, its degree of continuity through time, the distribution of well activation methods and the distribution of well completions. They also relate to the many uncertainties which usually exist in a mature field.

Production Indicators study is well adapted to find out what major production behaviour patterns occur in the reservoir (inversion approach). After their calibration with geological and geophysical knowledge, and the identification of geological features impacting production, the zones with remaining potential are selected and proposals for reservoir re-engineering are made. Recommended areas or solutions largely take into account the new information provided by the Welfare study. Field re-engineering is, therefore, much more relevant to existing reservoir complexity, and therefore more efficient.

The Welfare method is extremely powerful for both reservoir diagnosis and efficient proposals of re-engineering. By spotting un-produced or bypassed hydrocarbons, and by testing re-engineering scenarios, this method allows large improvements of production. It helps to maximise hydrocarbon recovery, producing natural resources in the most efficient way. It is a key tool to add value to producing fields.

The experience currently acquired by TOTAL concerns a few tens of fields. They correspond to most of the depositional environments, reservoir geometry patterns, and a variety of structural settings and fluid characteristics. Welfare can be applied to most of the fields, but it is particularly efficient for mature fields with long production histories, a large number of wells, with an irregular data array.

The use of Welfare studies may largely contribute to a good field understanding before EOR/ IOR programmes are implemented.

REFERENCES

[1] Berry M.J.A., Linoff, G., 1997. *Data Mining Techniques for Marketing, Sales and Customer Support.* John Wiley and Sons, New York, 378 p.

[2] Coste J.F., Valois J.P., Mouret C., and Guittard M., Baleix J.M., Larrouquet F., Mastin E., Daniel O., 2002. Data mining techniques for optimizing fast track re-engineering of mature fields. *SPE* 78333, Europec

[3] Ehrlich R.E., Dropkin M.J., Broussard N.J., Gay P.S. (2001). Data mining is a key strategy. *Oil and Gas Journal*, Aug. 20, 2001, 40-46.

[4] Coste J.F., Valois J.P., 2000. An innovative approach for the analysis of production history in mature fields: a key stage for field re-engineering. *SPE* 62880, presented at the *SPE ATCE*, Dallas, Oct. 2000

[5] Valois J.P., 2000. *A Robust Approach in Hierarchical Clustering: Application to the Sectorisation of Oil Fields.* Proceedings 7th IFCS, 11-14 Juil. 2000, Namur (Belgique), Springer Verlag ed., 95-100.

[6] Cleveland W.S., 1993. *Visualizing Data.* Hobart Press, 369p.

[7] Mouret C., Coste J.F., Valois J.P., 2003. *Optimized Inversion of Production Data for Reservoir Characterization. EAGE 65th* Conference and Exhibition, Stavanger, Norway, 2-5 June 2003, Paper D44.

Petroleum Res. J. Vol. 18 (2005); P. 17–26, 16 Figs.

Re-Development of a Mature Field For Production Acceleration, Intisar 103E Field

E. Senturk, M. Lahwel, B. Bzezi and M. Elghmari*

إعادة تطوير حقل معمر لتعجيل الإنتاج - حقل انتصار 103 E

إ. سنترك، م. الاحول، ب. بزيزي، م. الغماري

تعرض هذه الورقة إعادة تطوير وتعجيل إنتاج ناجحة لحقل انتصار E مكامن تكوين الجير العليا A,B,C لشركة الزويتينة . بدأ تنفيذ هذا المشروع منذ سنة 1999-2002 على أساس دراسة نموذج محاكاة بحفر 6 آبار حقن إضافية عمودية وعدد 6 آبار إنتاج أفقية واستكمال ثمانية آبار موجودة أصلا بالحقل للمزج أو الإنتاج المزدوج. ونتيجة لهذا المشروع بلغ إنتاج الزيت الكامن لمكمن الجير العلوي زيادة تقدر بعدد 3 أضعاف بمتوسط قدره 6,400 برميل/لليوم سنة 1999 إلى 20,600 برميل/لليوم في سبتمبر 2002.
ومن المتوقع أن تكون الزيادة في احتياطي الزيت في هذا المشروع 33.4 مليون برميل حتى العام 2022.

Abstract: *This paper presents a successful re-development and production acceleration project of Intisar E Field, Upper Girs A, B and C reservoirs of the Zueitina Oil Company. The project was implemented from 1999 to 2002 on the bases of a reservoir simulation study. The re-development plan comprised drilling 6 vertical injectors and 6 horizontal producers, and re-completion of existing 8 wells as commingled and/or dual producers. As a result of this project, the oil production potential of Upper Gir reservoirs has been increased almost by three folds from an average of 6,400 STB/D in 1999 to 20,000 STB/D in September 2002. The incremental reserves are predicted at 33.4 MMSTB until the year 2022.*

INTRODUCTION

Intisar 103E Field is located approximately 260 km to the South of Benghazi in the Sirt Basin, Concession 103. The field was discovered in 1968 by drilling well E1-103 down to a total depth of 10,890 ft in Upper Sabil. The well was drilled on a structure similar to the giant reef fields at 103A and 103D. In 103E field, however, the reef proved to be wet. Figure 1 shows the location of the field in Concession 103 of the Zueitina Oil Company.

As of December 2002, a total of 40 wells have been drilled in the field. Among these wells, 23 are vertical producers, 6 horizontal producers and 11 water injectors. The well location map is shown in Figure 2.

The Intisar 103E Field comprises seven separate producing reservoirs, designated from top to bottom as Elgiza A and B, Upper Girs A, B and C, Lower Girs and Shoal. The reservoir structures are four way-dipping anticlines with varying closures from 50 ft to 150 ft. All reservoirs are carbonates, mainly limestone, stacking on top of each other. The cross-section shown in Figure 3

* Zueitina Oil Company, Libya

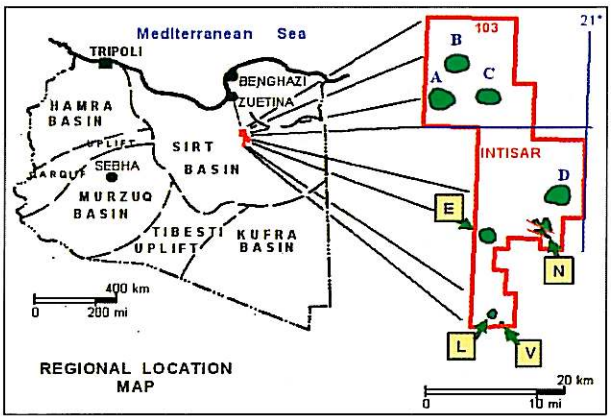


Fig. 1. 103E field location.

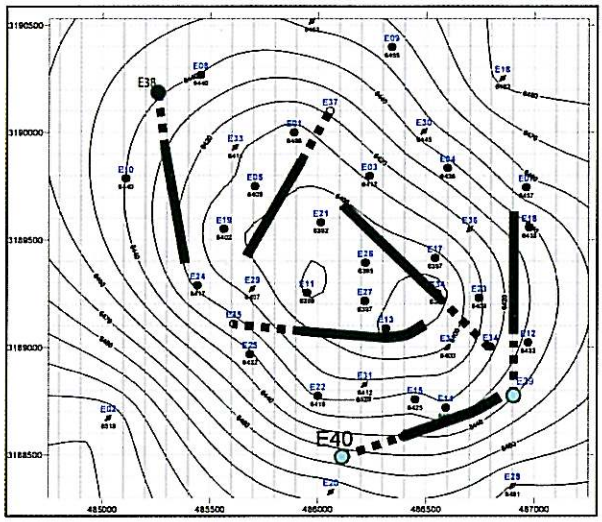


Fig. 2. 103E field well locations.

depicts all reservoir units from Elgiza down to Shoal (Upper Sabil).

Among the seven reservoir pools in the field, the Upper Girs are the largest reservoirs with respect to original oil in place and reserves. Table 1 presents the original oil in place and reserves distribution among the pools.

The Upper Gir A, B and C reservoirs comprise an OOIP (original oil in place) of 264 MMSTB, which constitute about 70% of the total field initial oil in place of 391 MMSTB and 89% of the field total initial reserves of 121.7 MMSTB.

The Gir A reservoir, with an OOIP of 168.4 MMSTB, is the largest compared to Gir B and C reservoirs having OOIPs of 79 MMSTB and 17 MMSTB respectively.

The reservoir rock is limestone with a rather high porosity of 23-28%, but low permeability of 10 – 20 md. These reservoirs are not in communication and stacking on top of each other. They are separated by non-communicating tight layers. Figure 4 illustrates the cross-section indicating the thickness, porosity and relative vertical layout of the subject reservoirs, which were subdivided into several layers for the simulation modeling. Gir A was subdivided into 5 layers designated as A1, A2, A3, A4, A5; Gir B into 3 layers as B1, B2 and B3 and; Gir C into 2 layers as C1 and C2. The accumulation of the oil in these separate reservoir pools has taken place due to presence of

Table 1. 103E Field OOIP and reserves distribution.

	OOIP MMSTB	Oil Reserves MMSTB
Elgiza A & B	28.5	2.3
Upper Girs, A, B & C	264.2	108
Lower Girs	91.2	9.4
Shoal	7.1	2
Total	391	121.7

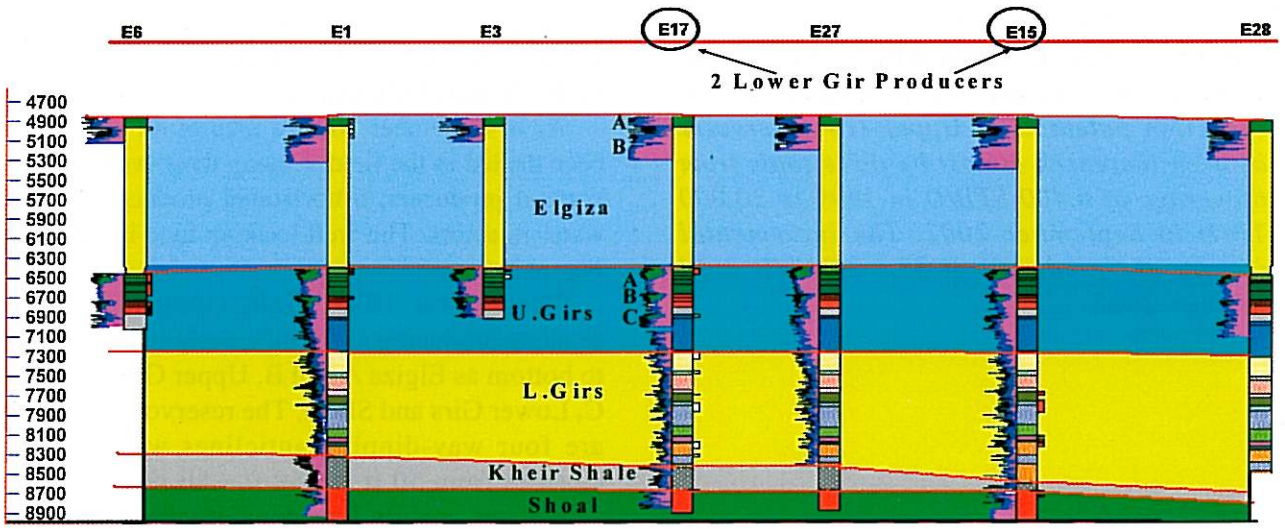


Fig. 3. Cross-section along the field (E6 to E28).

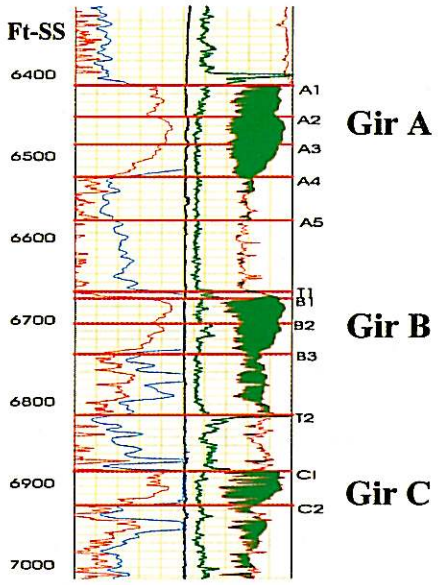


Fig. 4. E23 open hole log interpretation in Gir A, B and C.

tight formations (cap rocks) at the reservoir tops designated here as T1 for Gir B and T2 for Gir C.

STRATIGRAPHY AND TRAPPING MECHANISM

The general stratigraphy and structure has been controlled in the 103 area by its presence in the area of the shelf edge in Upper Palaeocene times between the Marsa Brega trough and the Gialo/Amal high. Reefal bioherms developed on this shelf edge through the Upper Palaeocene after which there was a transgression or subsidence in the very late Palaeocene resulting in the deposition of the Kheir marls and shale. During the Eocene, there was predominantly shelf carbonate deposition with the grain size being determined by provenance and water depth. Locally the sedimentation has been influenced by drape over the reef resulting in locally shallow water depths in the immediate area of the reef resulting in rather gentle homoclines providing up to 150 feet of closure. The oil accumulated in 103E in the Shoals, Gir and Elgiza formations being trapped by the above homoclines. Figure 5 illustrates the generalized stratigraphic section of 103E area.

GEOLOGY OF THE GIR 'A', 'B' AND 'C' IN THE 103E AREA

Several cross-sections in the area indicate that the geology of the Upper Girs in the 103E area is

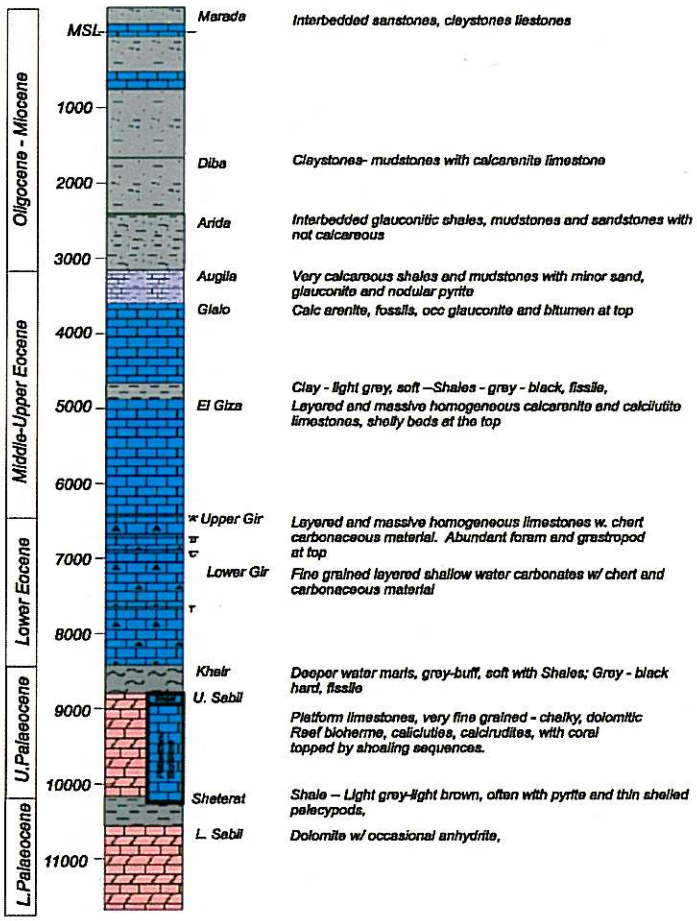


Fig. 5. Generalized stratigraphic section, 103 E area.

quite monotonous. The same sequence exists at other fields in the area, however, the thickness varies. Table 2 compares the relative thickness of Upper Girs in the 103E and 103D fields, which are about 15 km apart.

Table 2. Thickness of Upper Girs in the area.

Zone	103E Field Thickness at E13	103D Field Thickness at D4
Gir 'A'	268	134
Tight Zone '1'	10	15
Gir 'B'	135	220
Tight Zone '2'	82	95
Gir 'C'	Not defined	Not defined

In the area of interest, there appears to be little faulting above the Palaeocene. The traps that have been found in the Gir and El Giza at 103A, 103D, and 103E are formed by gentle domes draped over an underlying reef with up to 150 feet of closures. The sedimentation, however, was influenced mainly by underlying old structure on the shelf edge and by the overall deformation of the Sirt Basin.

PETROPHYSICAL PROPERTIES OF THE RESERVOIR LAYERS

The gross thickness of Gir 'A' at 103E averages 270 feet and thickens to the west towards E2. The net oil pay of Gir A is estimated at 80 feet. The average gross and net oil pay thickness of Gir B are 135 feet and 60 feet respectively. The net oil pay in Gir C is estimated at 25 feet.

The petrophysical properties of the sub divided layers in each reservoir are shown in Table 3.

Table 3. Petrophysical properties of sub-layers.

Gir A					
Layer	A1	A2	A3	A4	A5
Thickness. ft	44.7	34.4	32.5	62.3	96.3
Porosity (log%)	23.8	28	25.8	21.7	21.4
Sw (log%)	34.3	26.1	54.2	100	100
Core Kh (mD)	0.2-3.1	7.7-10.7	7.2-7.7	4.8	N/A
Core Ky (mD)	1.1-3.8	5.8-8.4	6.2-7.5	3.7	N/A
Gir B & C					
Layer	B1	B2	B3	C1	
Thickness.ft	27.9	28.2	75.3	31.7	
Porosity (log %)	25.2	23.2	21	24.6	
Sw (log%)	32.2	42.8	78.7	49.9	
Core Kh(mD)	6.4-17.2	3.9-9.6	11.3	N/A	
Core Ky (mD)	0.9-16.2	0-5.6	2.3	N/A	

The C2 zone in the Gir C reservoir is considered the top of the shallow water carbonates, which extends toward the Kheir Formation and has been termed the Lower Gir.

RESERVOIR DRIVING MECHANISM

The porosity is, in general, high, above 20%, in all reservoirs but contrary to that, the permeability is relatively low, particularly in Gir A at a neighborhood of 3 md to 8 md. The range of permeability of Gir B and Gir C are relatively higher than Gir A at ranges of 10-15 md. Due to the low reservoir and aquifer permeability, the strength and response of the aquifer to the production is not significant. Therefore, particularly at early production stages, the reservoir pressures in each reservoir declined significantly and, consequently, a peripheral water injection scheme was initiated after 1980 to arrest the declining pressure. Figures 6 and 7 show the history and decline trends of reservoir pressures in the Gir A and Gir B reservoirs. In spite of low early production rates, the reservoir pressures declined by 40% percent from around 3000 psia to 1800 psia in the centre of the reservoir. It is obvious that initial peripheral water injection did not help too much in arresting the pressure

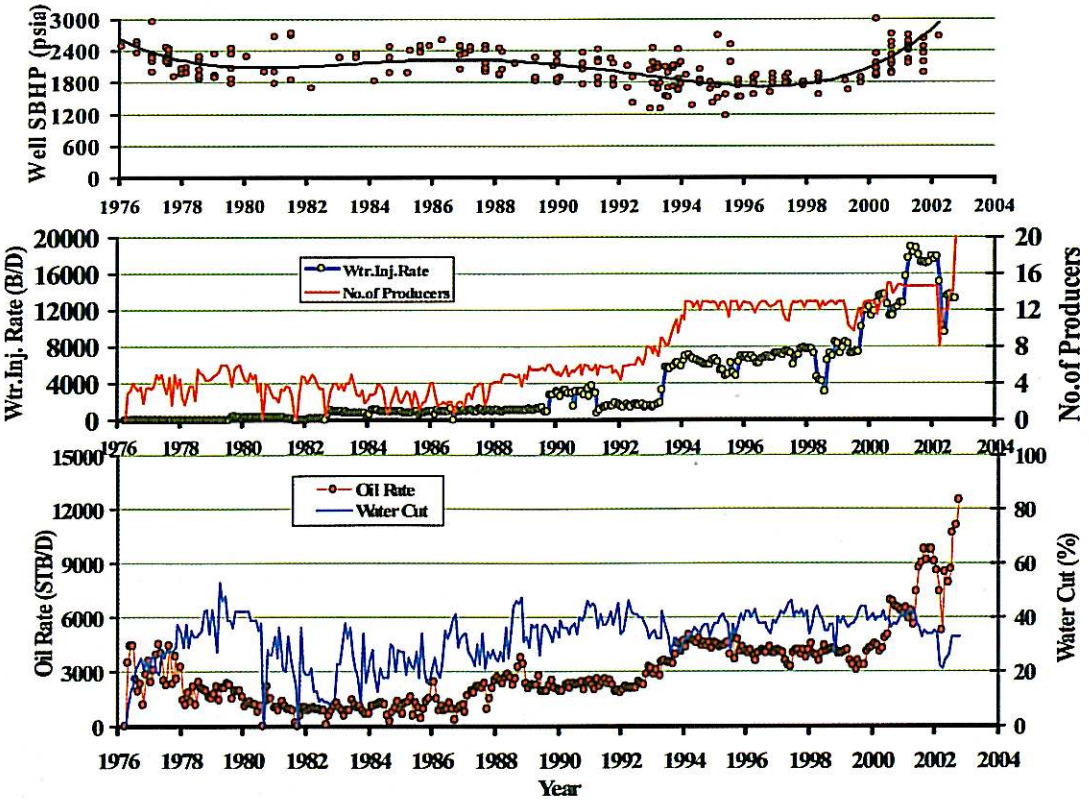


Fig. 6. Gir A production/injection/pressure performance history.

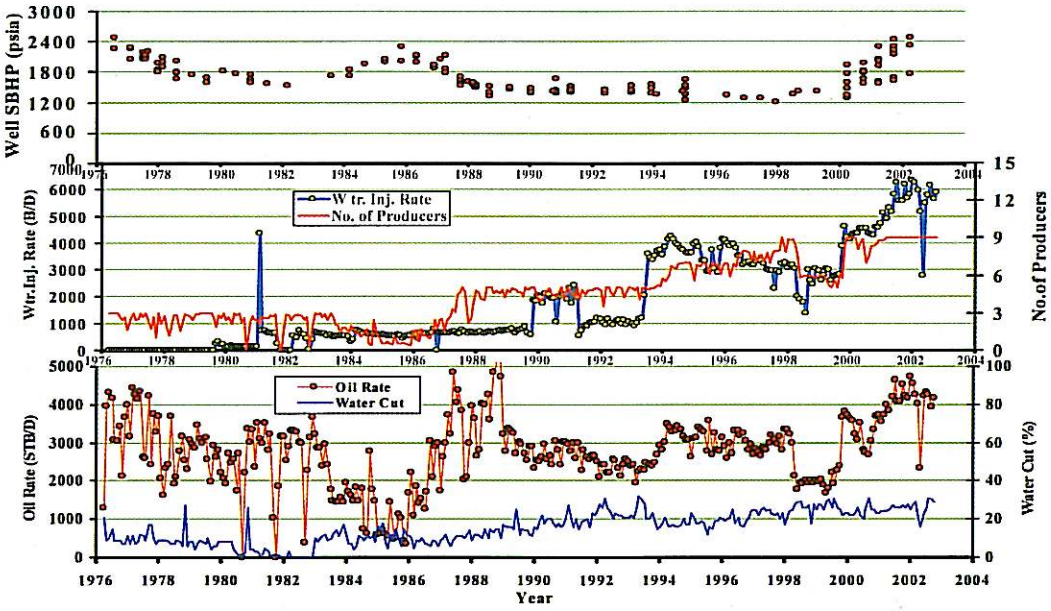


Fig. 7. Gir B production/injection/pressure performance history.

decline or in improving the production rate of the field. This was mainly due to; 1) poor injectivity due to low permeability and 2) distant proximity of the injectors to the main producers in the centre of the reservoir.

OIL PROPERTIES

The following table (Table 4) shows the range of PVT properties in the Gir A, B, and C:

Table 4. Reservoir oil properties.

	Deg. API	Pb psia	GOR SCF/STB
Gir A	35	390	185
Gir B	36	560	282
Gir C	39	460	346

FIELD DEVELOPMENT HISTORY

The field development is comprised of three phases as follows:

Phase 1 – 1968 to 1976. A total of 12 wells were drilled during this period. The first 2 wells, E1 and E2, were drilled deep down to the Lower Sabil and the other 10 wells were drilled shallow, down to Upper Girs. Initially, Upper Gir reservoirs were developed with 4 producers in Gir A and 3 producers in Gir B. Due to lack of aquifer strength and the consequent depletion of reservoir pressures, two peripheral wells, E2 and E6 were completed in 1980 as commingled injectors in Gir A and B to arrest the declining pressures. The production from Upper Girs utilized artificial Gas Lift. The gas was provided by the associated gas produced from the nearby giant fields, 103D and 103A.

During this period, Elgiza A and B reservoirs were also produced from three wells with electrical submersible pumps for a short time between 1976 to 1978. Figure 8 presents the field well lay out during this phase.

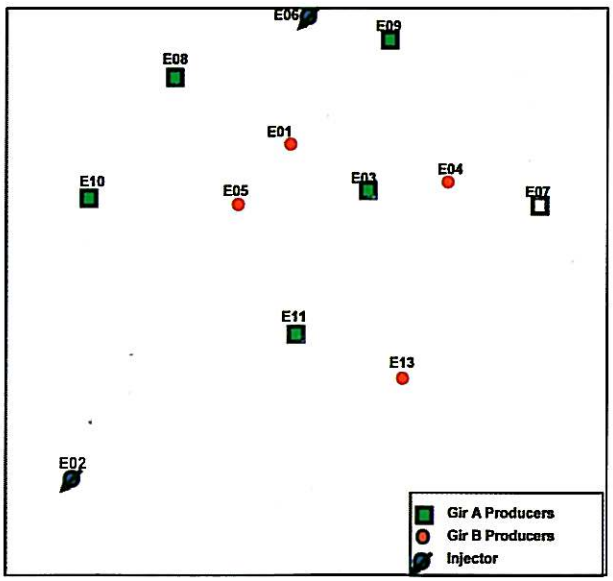


Fig. 8. Well lay out from 1968 up to 1985.

Phase 2: 1985 to 1995. The field was further developed by drilling additional 16 vertical wells of which 6 were drilled deep to the Upper Sabil Shoal reservoir. Due to continuing decline of reservoir pressure in Upper Girs, particularly towards the

centre, an additional three wells, E16, E20 and E28, were completed as peripheral commingled water injectors.

During this period, the deeper reservoirs, Lower Girs and Shoal were tested extensively. The Shoal reservoir was completed and produced from the wells E15 and E27. The potential of Shoal proved to be limited with about 2 MMSTB of reserves, however, Lower Girs proved to contain around 10 MMSTB of reserves. Lower Gir was developed after 1996 with two wells, E15 and E17. Figure 9 presents the field well lay out during this phase.

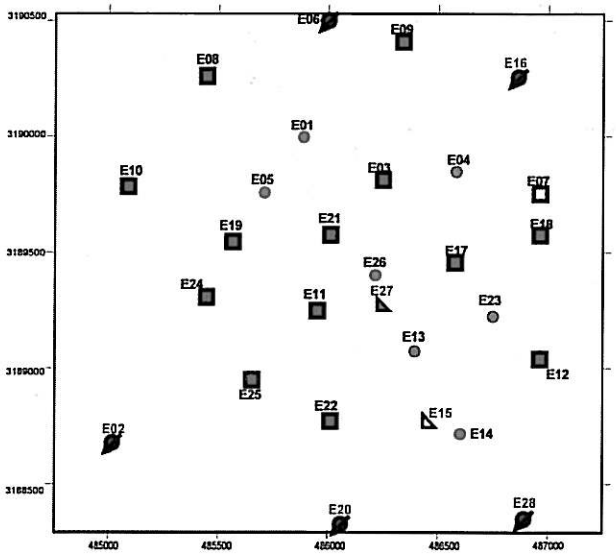


Fig. 9. Well lay out from 1985 up to 1995.

Phase 3: Production Acceleration Phase from Upper Girs, 1999 to 2002. In 1998, a simulation study was performed for Upper Girs, A, B and C in order to better define the remaining reserves, reservoir production mechanisms, aquifer responses, effect of peripheral water injection and investigate better production scenarios including horizontal wells for further developments. On the basis of this study, additional 6 vertical injectors and 6 horizontal producers were drilled and 8 existing wells were re-completed as multiple zone producers from 1999 until 2002. Figure 2 presents the field well lay out during this latest phase, which is referred to as 'Production Acceleration Project'.

UPPER GIRS A,B,C SIMULATION STUDY

A reservoir simulation study for Upper Girs was performed by HOT Engineering using their SURE simulator in 1998. The simulation model covered the three Upper Gir reservoirs A, B and C with three separate aquifers as shown in Figure 10. Prior to full field implementation of the study recommendations, the simulation model was set up, further modified and updated in-house. The orientations of the horizontal wells were optimized using the new in-house model, which included the later SURE version with PEBI gridding technique. The model proposed to drill horizontal wells for an optimum and accelerated production scenario.

During this study, the model indicated that the peripheral injection from five wells, E2, E6, E16, E20 and E28, was not effective in pressure maintenance and displacement of oil towards the producers in the centre. In order to establish an effective recovery efficiency, and accelerate the production from the field it was necessary to; 1) drill infill injectors to support the pressure in all three reservoir units 2) drill horizontal wells in Gir A to sweep significant oil remaining and, 3) re-complete some single zone producers as multiple zone producers (commingled and/or dual completions). The model indicated that the Gir A sill retains the major remaining oil reserves in the field. Therefore, the study proposed that all horizontal wells should be drilled in the Gir A.

RE-DEVELOPMENT (PRODUCTION ACCELERATION) PLAN *VS.* ACHIEVEMENTS

The re-development plan (or Production Acceleration Project) was based on the optimum depletion scenarios of the Simulation Study and its in-house updates. The plan involved; (1) Re-completion of some single zone producing wells either commingled or dual, and (2) Drilling 12 new wells as explained below.

1. Well Re-completions

This plan was comprised of:

a) Re-completion of 7 Upper Gir single zone producers (E1, E3, E4, E13, E14, E19 and E26) as multiple zone (dual zone) producers. Among these wells; E1, E4, E13 and E26 were completed in 2000 and the remaining in 2001 and 2002.

b) Re-completion of the Upper Gir A producer, E17, in Lower Gir as a producer. This well was re-completed in 2001.

c) Re-completion of the Shoal low oil producer, E27, as a dual zone injector in Upper and Lower

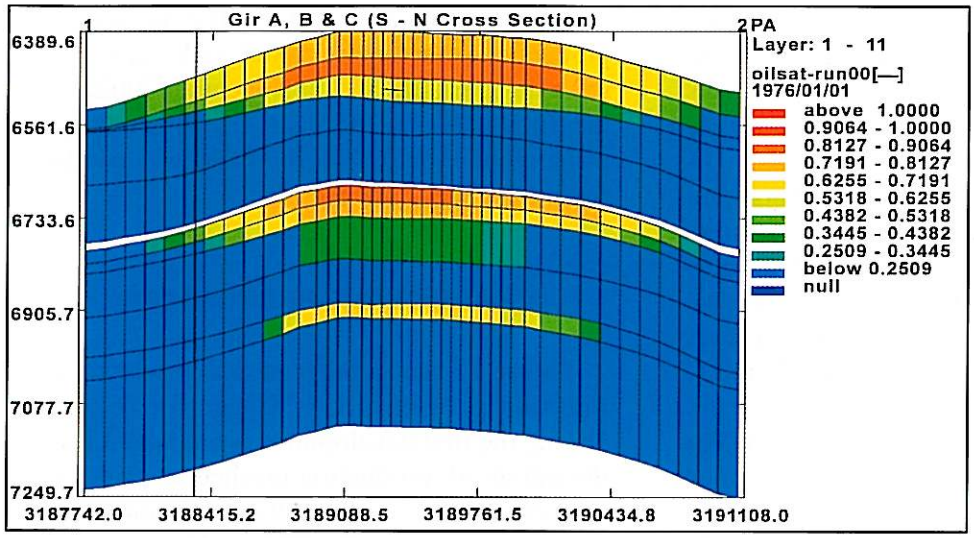


Fig. 10. Upper Gir ABC simulation model.

Girs. This job was also completed in 2001 and injection started in both reservoirs.

It is important to note that two wells, E21 (dual) and E23 (co-mingled) had been re-completed before the re-development plan.

The re-completions increased the production capacities in the subject wells significantly. Figure 11 indicates the increased production trend from well E21, which was converted from Gir A producer to a dual (multiple) zone producer in Gir A and Gir B.

In addition to the effect of re-completions, the oil production of the existing wells increased significantly after 1999 due to the good response to the new infill injection system. The following Figure 12 indicates the production performance of well E19, which shows a steady increase of the oil rate after 1999 mainly due to the effect of the nearby new injectors, E29 in the south-east and E33 in the north.

2. Development Drilling

Prior to the re-development phase there were 28 wells drilled up to E28. The re-development drilling

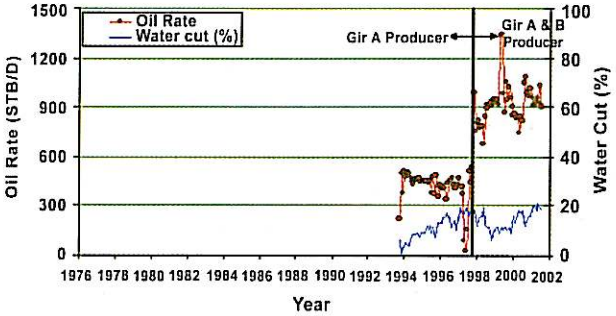


Fig. 11. Well, E21, production performance.

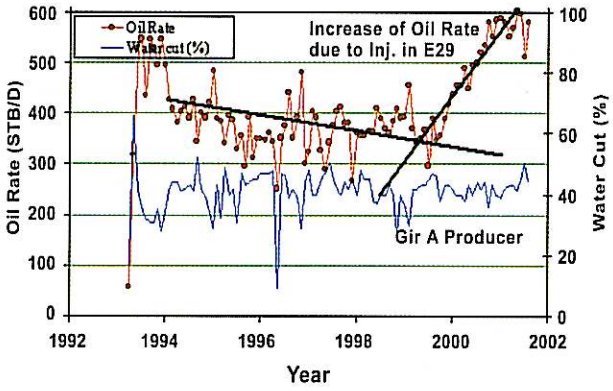


Fig. 12. Well, E19, production performance (103E, Gir ABC, well E19).

plan included the drilling of 12 new wells (6 infill water injectors, 6 horizontal producers) as shown on the map in Figure 2. The drilling of these 12 wells was completed at the end of September 2002 as shown in Table 5.

Table 5 – Actual drilling schedule.

Well	Type	Drilled
E29	Injector	05/1999
E30	Injector	06/1999
E31	Injector	07/1999
E32	Injector	12/2000
E33	Injector	02/2001
E34	Hor.Producer	03/2001
E35	Hor.Producer	05/2001
E36	Injector	04/2001
E37	Hor.Producer	06/2002
E38	Hor.Producer	07/2002
E39	Hor Producer	08/2002
E40	Hor.Producer	09/2002

Wells E39 and E40 were initially planned to be drilled as vertical wells. However, as per the latest in-house updates of the simulation study, and successful results from the previous horizontal wells, the subject two wells were re-planned and drilled as horizontals.

New Water Injectors: Six water injectors were drilled as vertical infill wells in the three reservoirs Gir A, B and C. They were completed in all three reservoirs dually with two tubing strings and dual packers in such a way that water is injected in Gir A separately from one string and in Gir B and C commingled from the other string. Figure 13 illustrates a typical dual injection completion in the field. The injection proration between Gir B and C is verified with periodic spinner surveys.

Horizontal Wells: A total of six horizontal wells were drilled in the Gir A reservoir. The horizontal lengths of the wells ranged between 1800 ft and 2100 ft depending on wells locations. They were completed all in Gir A as 8.5" open holes in the upper most 15 – 20 ft of the reservoir, which has about 80-90 ft of net pay in the centre of the field. Figure 14 shows a cross section and layout of the horizontal well, E37.

The oil production rates from the horizontal wells ranged between 1750 STB/D to 2500 STB/D, which confirmed the simulation predictions. Compared to the existing vertical producers with average oil rates of about 350-450 STB/D, the incremental production from the horizontal wells is considered to be quite significant. In November 2002, out of the total 429,730 STB of Gir A monthly oil production, 310,290 STB (72%) was produced from the 6 horizontal wells.

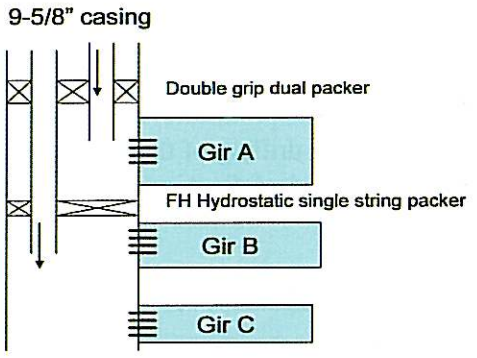


Fig. 13. Typical dual injection completions in Upper Girs.

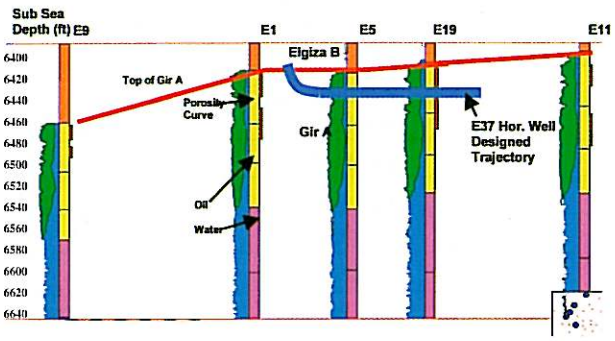


Fig. 14. Cross section around E37 trajectory.

PRODUCTION PERFORMANCE

Figure 15 shows the historical production and injection performance of Upper Gir reservoirs. During the first development phase with 12 wells, the initial oil production reached its peak rate at around 8000 STB/D in 1976 and consequently declined down to 2000 STB/D in 1986, mainly due to lack of pressure support. As new wells were further drilled after 1985 and put on stream during the second development phase, the oil rate gradually increased to its highest level of 8000 B/D in 1994 when a total of 28 wells were drilled in the field. From then on, the decline trend continued down to around 6000 STB/D until 1999. The Upper Girs average oil production rate from 1976 to 1999 is around 5000 STB/D.

Incremental Oil Production: The Upper Girs production potential has been increased from an average of 6400 STB/D in 1999 to 20,000 at the end of September 2002. The major incremental production has been achieved mostly from the 6 Gir A horizontal wells (10,500 STB/D), which constitute about 52% of the total field production. Table 6 compares the production potential before and after the production acceleration implementation.

Table 6. Comparison of production potential.

	Oil Production rate (STB/D)		
	In 1999	09/2002	Increment
Gir A	3.712	14.324	10.612
Gir B	2.497	3.576	1.079
Gir C	200	1.862	1.662
Total	6.409	19.762	13.353

Figure 16 demonstrates the actual *vs* production forecasts from the simulation study. It is obvious that the actual field production confirmed the simulation prediction to a very high degree.

After the pick oil rate at around 20,000 STB/D is reached, it would not be possible to maintain the high plateau rate and the decline will start immediately. In spite of this decline, the incremental reserves and economics are quite substantial from this project.

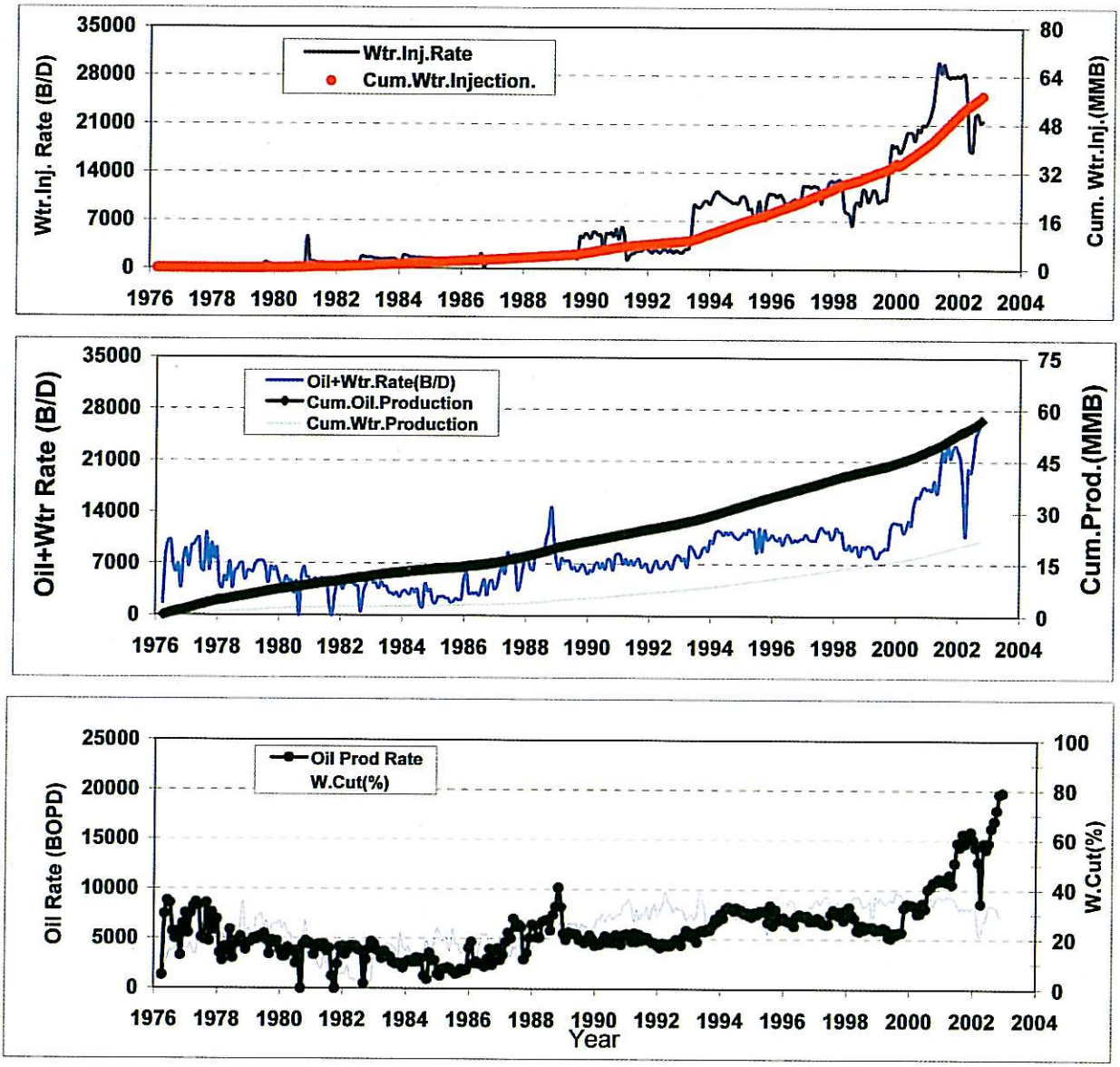


Fig. 15. Gir ABC production performance history.

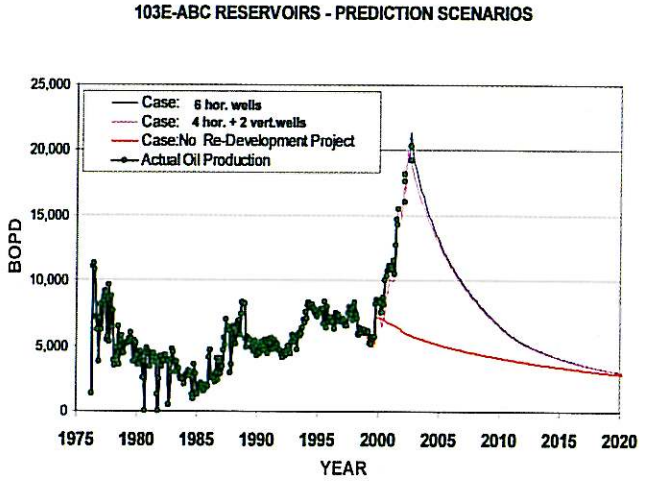


Fig. 16. Gir ABC simulation study oil rate predictions.

INCREMENTAL RESERVES AND ECONOMICS

The incremental oil reserves have been estimated at 33.4 MMSTB (*i.e.* from 74.6 MMSTB in the 'No Development Case' to 108 MMSTB in this re-development project).

The re-development project is quite attractive economically. Assuming an oil price of 20 US$/bbl at 2% escalation per year, the incremental economic returns are estimated at NPVs of MMUS$247 and MMUS$314 with 10% and 5% discount rates respectively until 2020.

CONCLUSIONS

1) The field performance after implementation of the re-development project confirmed the reservoir simulation study results and recommendations.

2) The project was implemented very successfully as the oil production potential has been increased from 6400 STB/D to 20,000 STB/D by;

- drilling 6 vertical water injectors, and 6 horizontal producers, and,
- converting 8 existing single zone producers to dual zone producers.

3) Re-completion of wells using the co-mingle/ dual completion has saved significant cost from drilling additional wells, thus improving the NPV.

4) The oil reserves increased by 33.4 MMSTB from 74.6 MMSTB to 108 MMSTB.

5) The incremental economic return is estimated at NPVs of MMUS$247 with 10% discount and MMUS$314 with 5% discount rates at an oil price of 20 US$/bbl.

ACKNOWLEDGEMENT

We are grateful to the Management of the Zueitina Oil Company for permission to publish this paper.

REFERENCES

[1] HOT Engineering, 1998. *103E Gir A, B and C Reservoir Simulation Study*, unpublished report, Zuetina Oil Company.

[2] Don Twadle, 1995. *103E Upper Gir Reservoir Description Study*. Unpublished report. Zueitina Oil Company.

[3] Servipetrol Ltd, 1991 (March), *Simulation of Gir A and Gir B Reservoirs, Intisar 103E Field, Sirte Basin, Libya, G.S.P.L.A.J.* Unpublished report, Zuetina Oil Company.

Petroleum Res. J. Vol. 18 (2005); P. 27–34, 12 Figs.

Nakhla Oil Field, Concession 97, Libya
Development Strategy and Improved Oil Recovery

Thomas Franzen*

حقل النخلة النفطي بعقد الامتياز 97 بليبيا:
إستراتيجية التطوير وتحسين المسترد الإضافي

طوماس فرانزن

حقل النخلة النفطي عبارة عن كتلة متصدعة مائلة باتجاه شمال غرب-جنوب شرق يدار من قبل شركة فينترسال ليبيا.
ترسبت الصخور المنتجة بهذا الحقل – إبان العصر الكريتاسي في بيئة نهرية ويتكون الجزأين السفلي والعلوي من هذا التكوين من صخور رملية تفصلهما عند الوسط طبقات من صخور الطفلة.
ويقتصر تواجد النفط الخام بالطبقة العلوية من هذا التكوين وبشكل عام فإن المكمن غير متجانس ومجزّء إلى سحنات.
يجري استخراج النفط من حقل النخلة منذ 28 مايو 1995 حيث أنتج حوالي 22 مليون برميل من النفط الخام حتى تاريخ 2002/12/31، وبناء على طريقة محاكاة المكمن يقدر المسترد الأقصى في الوقت الحالي بحوالي 6.5% (يوليو 2002)، كما تم استخدام هذه الطريقة في التنبؤ بالمناطق ضئيلة الإنتاج والتخطيط للحفر بين الآبار المنتجة.
لقد تم حفر ثمانية آبار عمودية وبئر أفقي وبالنظر إلى صعوبة التنبؤ بالصخور البركانية فقد كانت ثلاثة آبار منها جافة، وعلى أية حال فإن المرحلة التالية لتطوير حقل النخلة ستتم بحفر ستة آبار إضافية أخرى. وعندما يتم هذا التطوير فإن الحد الأقصى للاسترداد الإضافي سيصل إلى حوالي 114 مليون برميل (12.3 الاسترداد النهائي). وكذلك تم التخطيط لمزيد من التطوير ولكن يستلزم الأمر تطبيق ما قبل SDM والتفسير السيزمي لإعادة تقييم نموذج المكمن الديناميكي والجيولوجي.
تناقش هذه الورقة إستراتيجية تطوير الاسترداد الإضافي المتبعة حاليا والمتوقعة في المستقبل المنظور مثل:

- دراسة تحسين المسترد النفطي (صيانة الضغط).
- دراسة الاسترداد الإضافي (مثل حقن الغاز).

كما تم عرض النتائج الأولية للدراسات الجارية.

Abstract: *This paper presents the development strategy and the improved oil recovery potential of the Nakhla field. The Nakhla oil field is located in Concession 97 (G.S.P.L.A.J.) and is producing from the heterogeneous and compartmentalized Upper Sarir Sandstone since June 1995. Total production of the existing eight (8) vertical wells and one (1) horizontal well is approx. 22 MMSTB as of year end 2002. Seven vertical wells are hydraulic fractured and three wells are dry holes due to volcanics or technical problems.*

Within the next development phase (II) six (6) additional producers are planned. Based on the good experience all new wells will be drilled vertically and post hydraulic fractured. Updated static and dynamic simulation models have been used to optimize the development concept. Through natural depletion ultimate recovery

* Wintershall, Libya.

estimates currently stand at 12.0% or 112 MMSTB.

Further development (Phase III) is planned, but ongoing PreSDM and seismic interpretation has to be implemented to re-evaluate the geological and dynamic reservoir model. Ultimate recovery including Phase III estimates stand at 152 MMSTB or 16.3% of oil initially in place (OIIP).

To increase the ultimate recovery even further the 'Improved Oil Recovery (IOR)' potential is currently under investigation. Available input data was reviewed and new SCAL and PVT including special IOR/EOR data was requested. Laboratory results will be available by end of year 2003 and will be implemented into a new compositional reservoir simulation. In the meantime a preliminary analytical screening was performed to identify viable IOR/EOR techniques and to estimate 'Performance Indicators' of the West and East field regions.

Estimated 'Performance Indicators' vary between 13% - 19% for immiscible injection gas and 17% - 19% in case of miscible injection gas. In addition to improving oil recovery, the re-injection of produced gas would avoid gas flaring and confirm Wintershall's policy to protect the environment. Water flooding is predicted to give good recoveries, too. However, low permeabilities may prevent or restrict injectivity into the reservoir. Further investigations are necessary and will be performed on a full-field compositional model.

INTRODUCTION

The Nakhla oil field is situated in the south-eastern part of the Sirt Basin in Concession 97, (Fig. 1). The field is a NW-SE fault bounded horst structure operated by Wintershall Libya.

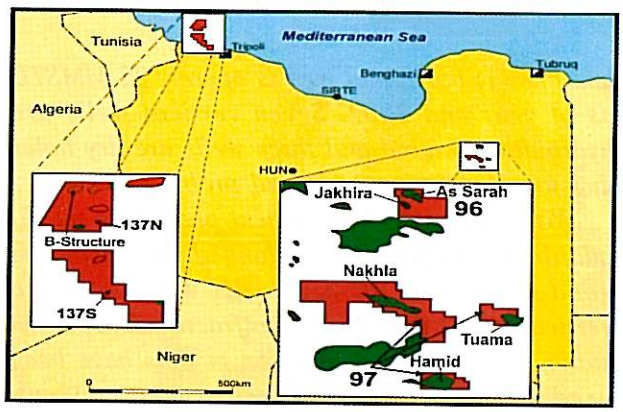


Fig. 1. Concession overview of Nakhla oilfield.

The field's reservoir is a Sarir Sandstone of the Lower Cretaceous age consisting of three subdivisions. A lower Sarir Sandstone is covered by The Middle Shale section which is overlain by The Upper Sarir Sandstone. The individual thickness of all three members vary throughout the trough, and only the upper sandstone is oil bearing.

The current knowledge of the Nakhla oil field proved the heterogeneity of the Sarir Sandstone and in some areas volcanics have replaced the sandstone entirely. The existing wells have penetrated regions of poor reservoir quality in the west and moderate to good in the east. The seismic coverage indicates a complex tectonics.

Since June 1995 Nakhla is on stream and has produced approx. 22 MMSTB from eight vertical wells and one horizontal well till year end 2002. Based on natural depletion ultimate recovery estimates currently stand at 62.0 MMSTB; i.e. 6.6% of OIIP (Status: Dec. 2002).

Within the field development so far (Phase I) seven of the eight vertical wells are hydraulic fractured. The horizontal well is an open-hole completion.

Currently, the Nakhla oil field can be classified as immature and further development of the structure is planned within development phases II and III.

Objectives of this paper are to present briefly the actual field status and the development strategy followed so far to accelerate the oil recovery by natural depletion. The development concept of the planned phase II and phase III will be presented.

Further this paper discusses oil recovery improvements scheduled or currently under investigation on:

- Improved Oil Recovery
  and
- Enhanced Oil Recovery.

Preliminary results from a first look analytical screening will show viable IOR/EOR techniques and how a 'Performance Indicator Screening' has been performed to estimate recovery factors for the West and East regions of the Nakhla field.

CURRENT NAKHLA DEVELOPMENT

The current Nakhla Development is based on a static/geological model which incorporates structural, facies and petrophysical evaluations. The structure has been shaped by various tectonic events and can be described as an extensional north-tilted horst block in the Hameimat Trough (Fig. 2).

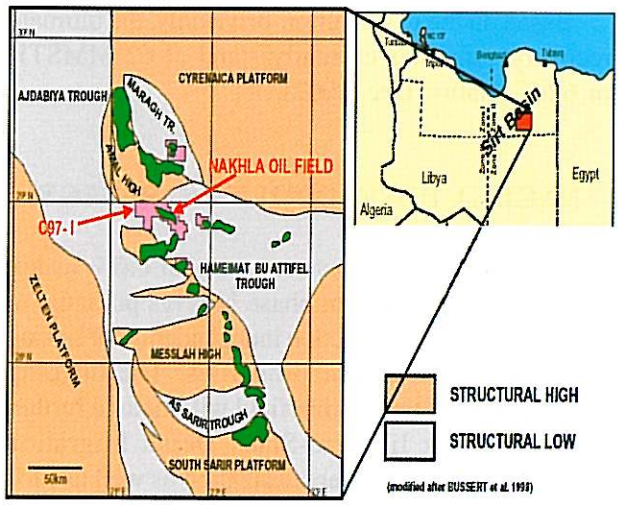


Fig. 2. Structural setting of Nakhla oilfield.

In accordance to Robertson Research studies[1] and using GR-curves the facies breakdown was evaluated. Channels have been assigned below 22 API, sandflat facies type between 22 - 45 API and above 45 API as floodplain facies type (Figs. 3 and 4). The following volumetric ratios have been evaluated:

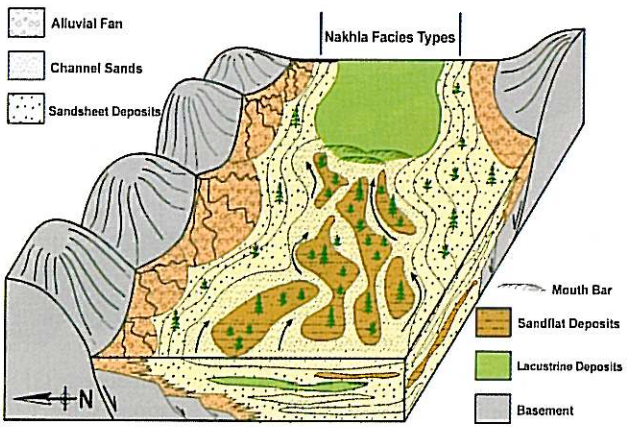


Fig. 3. Depositional model of Sarir Sandstone.

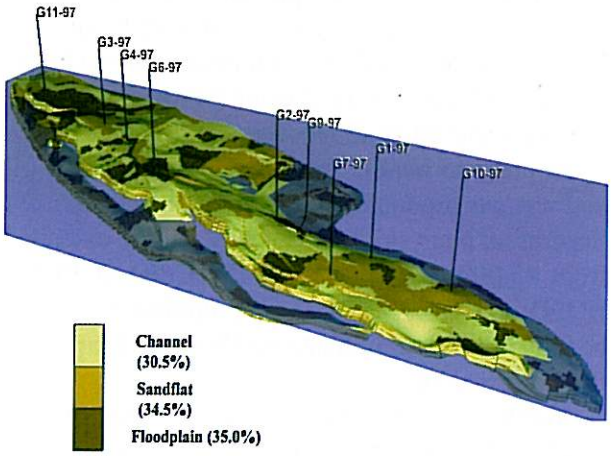


Fig. 4. Facies model of Sarir Sandstone.

Channel	30.5%
Sandflat	34.5%
Floodplain	35.0%

The petrophysical model is based on well results and on log data. Interpretations confirmed poor to relative good reservoir properties, *e.g.* permeabilities in the western region vary between 0.25 – 10 md and in the east region between 5 – 12 md. Overall, the reservoir is very heterogeneous and compartmentalized.

Based on available G and G data including a 3D seismic interpretation update a new integrated geological model has been created in May-June 2002 (Fig. 5). The high resolution of the static model with 3.75 million grid cells (250 columns * 150 rows * 150 layers) honours the complex tectonic framework and the heterogeneity in horizontal and vertical direction (Figs. 5 and 6).

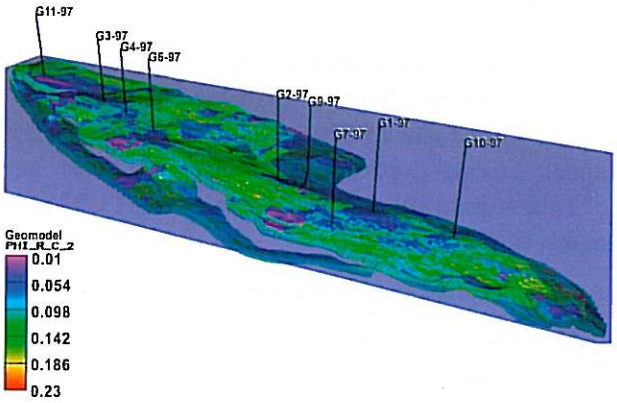


Fig. 5. Porosity distribution of Sarir Sandstone.

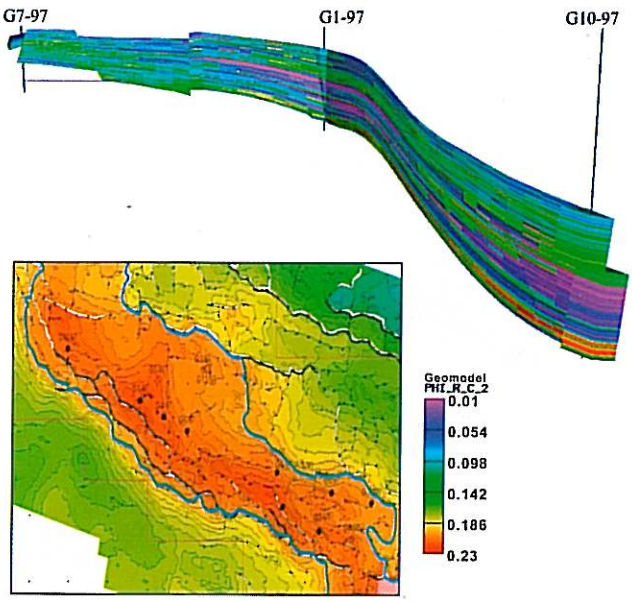


Fig. 6. Fence diagram along G7-, G1- and G10-97 showing blocked well data and possible porosity distribution.

Further volcanics spots had to be considered in the model due to drilling results of wells G5-97, G12-97 and G13-97. A conceptual assumption volcanic occurrence is presented in Figure 7, but volcanic sills and dykes are often below seismic resolution.

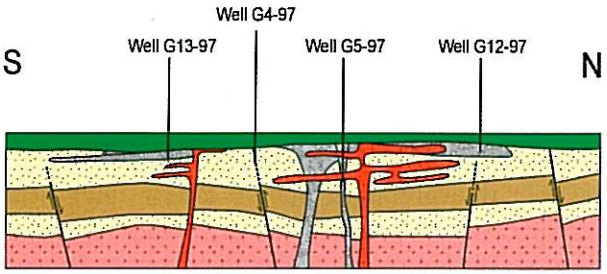


Fig. 7. Volcanic sills and dykes (conceptual).

Finally, the geological model and the evaluated porosity distribution were upscaled to 250*150*18 layers to be used in the dynamic reservoir simulation model.

A full-field simulation model was performed in July 2002 and initialized on available PVT[2] and core/SCAL data (Table 1). The geological model was not updated by the dry hole results of well G13-97, but of course pre-evaluated production of G13-97 was removed (Fig. 8).

Table 1. Simulation model parameters, post G13-97.

Grid size:	250 x 150 x 18 (T/A 675/216 M
PVT model:	cells)
k/Pc model:	PERA, March, 2000
2000/200	Wintershall Lab and ETL,
Prod. start:	June 29th, 1995
Producers, vert.:	G1, G2, G3, G4, G6, G7, G10, G11
Producers, hor.:	G9
dry holes	G5, G8, G12, G13
hydr. fracs:	G1, G3, G4, G6, G7, G11

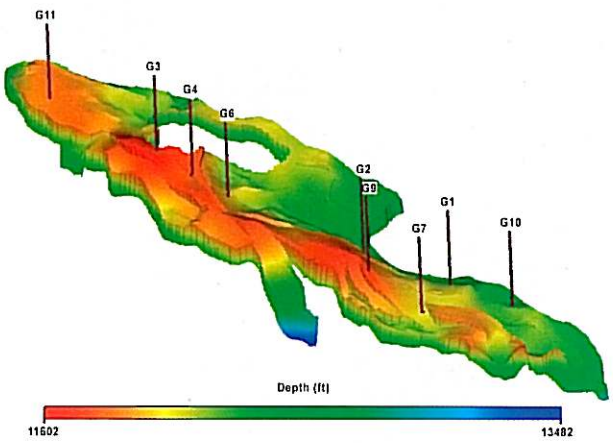


Fig. 8. Simulation model – phase I, existing producers: G1-G11.

Based on the gas-solution-drive only, the ultimate recovery estimates currently stand at 62 MMSTB or 6.6% (status: Dec. 2002).

NAKHLA DEVELOPMENT STRATEGY

The estimated ultimate recovery of 6.6% within the Nakhla development phase I leaves potential to increasing the oil production independently of having good or poor reservoir properties. The ongoing development of the Nakhla field will include further appraisal work like Pre-Stack Depth Migration (PSDM), Reservoir Characterization as well as FMI Interpretation.

Within the phase II development, the drilling of six (6) additional producers is planned in the proven area of the field (Fig. 9). Established on the geological model as of July 2002, plus considering a sealing fault to the southern compartment, the existing reservoir simulation model was modified to predict the field performance.

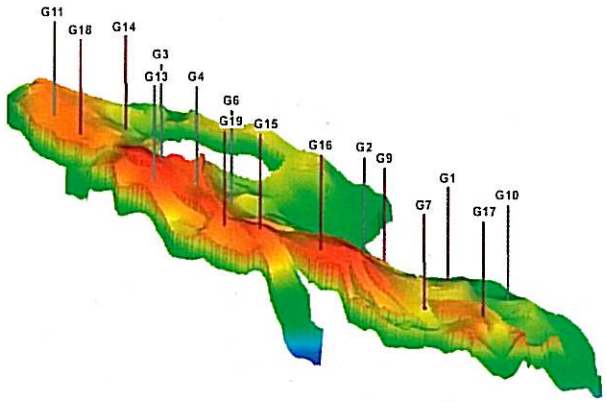


Fig. 9. Simulation model – phase II, existing producers: G1 – G11, phase II wells: G14 – G19 (well locations subject to revision).

The simulated reservoir pressure after a production period of almost 33 years is shown in Figure 10. Furthermore the final oil saturation is presented in Figure 11. Cumulative production is predicted at 111.9 MMSTB and ultimate recovery stands at 12.0%.

In order to handle the projected increase of oil and wet gas production the current Nakhla Gas Oil Separation plant (GOSP) capacity will be extended from 15,000 BOPD and 15 MMSCF/D to 30,000 BOPD and 40 MMSCF/D. The produced gas will be fully utilized to eliminate gas flaring and to protect the environment.

To increase the Nakhla production, further additional development well locations have been identified in the reservoir model as of July 2002.

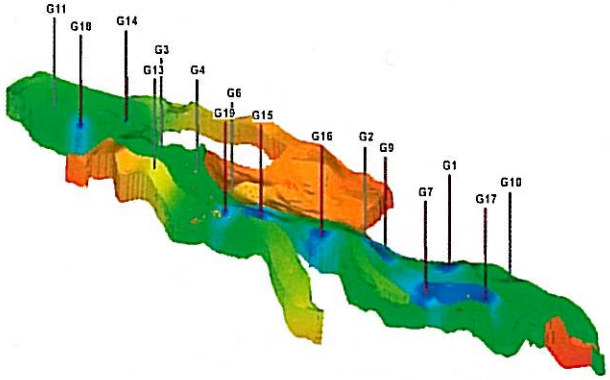


Fig. 10. Final pressure map – phase II, existing producers: G1 – G11, phase II wells: G14 – G19 (well locations subject to revision).

Based on economic evaluations, additional seven (7) development wells could be drilled. Of course, the ongoing field development and studies will provide further feedback to confirm the proposed phase III well locations, but the proposed well spacing would leave opportunities for further wells.

Seven (7) additional development wells of Nakhla phase III have been investigated using the dynamic reservoir simulation of July 2002. Considering the dry hole results of wells G5-97, G12-97 and G13-97 an incremental production of 40.5 MMSTB can be produced within the Nakhla development phase III.

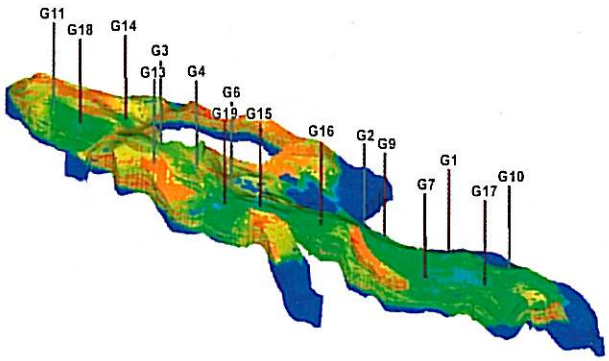


Fig. 11. Final oil saturation map – phase II, existing producers: G1 – G11, phase II wells: G14 – G19 (well locations subject to revision).

IMPROVED OIL RECOVERY

To avoid flaring of produced gas and to maintain reservoir pressure in the Nakhla oil field an 'Improved Oil Recovery (IOR)' feasibility study was performed in year 2000[3]. The scope of investigation was the western region with relatively good reservoir properties.

In general, the feasibility study proved an increased oil recovery by gas injection, but due to missing lab experiments some uncertainties on major input data are still existing. Therefore, the following recommendations were made:

- develop a new geological model.
- verify the injection gas comp.
- perform PVT laboratory experiments, including minimum miscibility pressure.
- update relative permeabilities.
- re-evaluate capillary pressure relationships.

Currently, all recommended studies are in progress and will be compiled in a new full-field reservoir simulation compositional model. However, in the meantime, analytical screening was performed to identify viable IOR/EOR processes and to estimate 'Performance Indicators' of the West and East Nakhla regions.

Performance Indicators

Developed by ECL Technology (formerly Subsurface Engineering Unit of AEA Technology) 'Performance Indicators'[4] is a preliminary screening tool based on analytical models to estimate the balance of viscous or gravity forces, sweep efficiencies *etc.* Parallel sensitivity runs can be performed to assess the impact of uncertainty on the flow mechanism and the viability of each IOR/EOR process.

A reservoir study on 'Performance Indicators' provides a qualitative understanding of expected displacements for single IOR/EOR processes and allows the elimination of unviable techniques in the case of a particular field.

Analytical Models

Two analytical models have been created based on log porosities from well G3-97 to represent the western region and well G7-97 for the eastern region of the Nakhla field. Permeability distributions are generated from evaluated laboratory porosity/ permeability correlations (Fig. 12). Accordingly to the Ö/k correlations, high permeability streaks have been included in the analytical model. Unfortunately, the model assumes connectivity of these streaks between wells and does not present the heterogeneity of the Nakhla geology.

IOR/EOR CASE STUDIES

Reference to the estimated 'Performance Indicators' is the Nakhla development phase II as

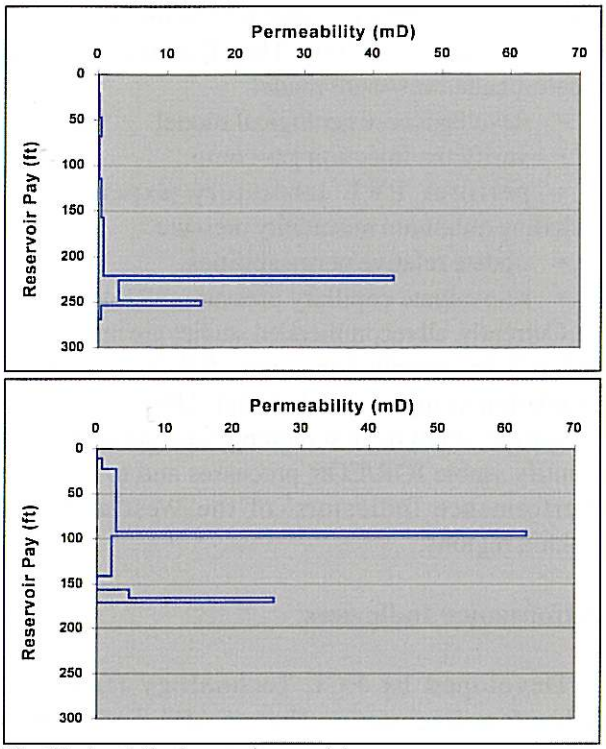


Fig. 12. Analytical screening models.

currently the most likely case (Table 2). The starting conditions used for the IOR/EOR screening and for all recovery factor calculations include: assuming an IOR/EOR start in the year 2006, approximately 29 MMSTB to be produced until year 2005, in addition to reducing the OOIP from 933 MMSTB to 904 MMSTB.

Table 2. Nakla C97/1 - development strategy and IOR/EOR case studies.

IOR/EOR	Oil recovery	
Start in 2006	West	East
Depletion	12.0 %	
Lean gas	13.3%	19.1%
Separator gas	13.3%	19.1%
Enriched gas	17.6%	25.2%
Waterflood	14.0%	14.6%
CO_2	No source	No source
Nitrogen	15.6%	22.4%

Gas Injection

Hydrocarbon gas injection was investigated in a pattern flood mode, because of the complex field compartmentalization. Three different gas compositions were used to consider miscible and immiscible conditions:

- Separator gas
- Lean hydrocarbon gas
- Enriched hydrocarbon gas.

In general, the low vertical permeability caused by claystone layers or lenses mean that gas can segregate slowly in the reservoir. This can be beneficial for gas injection and further claystone layers are probably not continuous between wells and may provide a tourtous route for the gas to move upwards. This improves the gas sweep. However, the areal heterogeneity cannot be adequately modelled using an analytical model.

In case of re-injection of 'Lean gas' (Table 2) the secondary recovery is predicted as 13.3% in the west and 19.1% in the eastern field region. The same results have been estimated for 'Separator Gas Injection', because of unchanged immiscible conditions (Table 2). To get a miscible flood a 10%- 15% NGL enrichment is required and recoveries by 'Enriched Hydrocarbon Gas' increase to 17.6% and 25.2% for west and east regions respectively (Table 2).

Water Flooding

A viscous dominated pattern water flood was performed to predict secondary recovery by pressure maintenance. The analytical model assumes good connectivity and no lateral heterogeneity between wells. The model, therefore, will predict no unswept reservoir regions and the actual sweep efficiency will be over-predicted. A risk factor has been introduced to compensate for the analytical model disadvantages.

The risked water flood secondary recovery is predicted at 14.0% and 14.5% for west and east regions respectively (Table 2). In addition the analytical method does not assess any injectivity issues, which would prohibit any water flooding in the first place.

CO_2 Flooding

Technically CO_2 flooding is an attractive EOR process, because it is naturally miscible with reservoir fluids. Enhanced recovery factors in the range of enriched hydrocarbon gas injection has been predicted. However, there is no source of CO_2 known in the vicinity of the field (Table 2).

Nitrogen Flooding

Nitrogen has to be generated in the field which will have an additional impact on economics. However, in the analytical study, the 'Minimum Miscible Pressure (MMP)' for the nitrogen case has

been predicted to be lower than the MMP of hydrocarbon gas.

Based on a partial miscible flood the enhanced recovery is estimated at 15.6% and 22.4% for west and east regions respectively (Table 2).

Chemical Processes

The Nakhla reservoir temperature of 288°F would be too high for a Xanthan polymer to be stable. Further, the injectivity into the low permeability reservoir would be a problem.

Surfactant without a co-deployed polymer does not have a sufficient natural viscosity to provide a stable flood and will not be an option.

UNCERTAINTIES

To prove the quality of the analytical models major input parameters ranges have been used to examine the impact of uncertainties (Table 3).

The results of this uncertainty study shows no effects on the water flood efficiencies as the flood is viscous dominated.

Table 3. Uncertainty parameters.

Minimum	Minimum	Most likely	Maximum
Kv/Kh multiplier	0.1	1.0	10
Production rate @ west [BOPD]	300	500	800
Production rate @ east [BOPD]	300	1.500	2.700
Reservoir dip angle (deg.)	5.0	7.0	10
Well drainage area (width/length)	0.5	1.0	2.0
Reservoir pressure (psia)	3.000	4.200	4.500

The pattern gas flood is evaluated to be stable, too, but the uncertainties do affect the gas segregation in both field regions and reduce the vertical sweep in the west region of Nakhla.

Assuming higher permeabilities and formation net pay as represented around well G3-97 an additional sensitivity run was conducted. The results show slightly higher recovery factors of 14.1% in case of water flooding and 14.5% for hydrocarbon gas injection.

CONCLUSIONS

The Sarir Sandstone in the Nakhla oil field is very heterogeneous, tectonically complex, and the current development has proved regions of poor as well as relatively good reservoir qualities. In addition some sandstone areas have been completely replaced by volcanics.

Since production start mid 1995 till year end 2002 cumulative 22 MMSTB have been produced from eight (hydr fractured) vertical wells and one horizontal. The current ultimate recovery estimates stand at 6.6%. Further development requires a fully integrated approach of a multi-disciplinary team to manage geological and engineering uncertainties.

The results of G and G and reservoir studies as well as drilling results will be evaluated and implemented into the existing geological and dynamic models. This will serve as a means of enhancing the placement of future drilling locations and will help to reduce imminent risks for the complex Nakhla oil field reservoir.

Following this approach, Nakhla development phase II was designed and will be optimized continuously. Based on the good drilling and production experience of vertical hydraulic fractured wells it is planned to drill six (6) additional development wells in the same manner. The full-field simulation model adjusted by the G13-97 well results was used to perform a production forecast. Total production of 112 MMSTB was predicted and ultimate recovery estimates stand at 12.0%.

To extend the productive drainage area it is planned to continue the development with phase III. Additional seven (7) development wells were investigated in the existing reservoir simulation model (geol. model as of July 2002). Ultimate recovery estimates stand at 16% and cumulative production is predicted to be 152 MMSTB.

Considering the heterogeneity and low permeabilities of the Nakhla reservoir, hydrocarbon gas injection is predicted to have secondary recoveries of 13% and 19% for west and east regions respectively. Enrichment of the injection gas can increase the recoveries by 17%- 25%.

Water flooding is predicted to have good recoveries too, but major disadvantages of the simplified analytical model makes it difficult to extrapolate the results onto the real Nakhla reservoir. Furthermore, a CO_2 source is not known in the vicinity of Nakhla. Nitrogen flooding requires cost intensive generation plants and chemical processes can be denied due to the high reservoir temperature.

Based on these results and recommendations, a new full-field reservoir study based on compositional simulation will be performed incorporating 1) a new geological model post PSDM, 2) updated SCAL and

relative permeability measurements as well as 3) accurate laboratory experiments on MMP and swelling test.

REFERENCES

[1] McDougall, *et. al.*, (Robertson Research). *Geological Modelling of the Nakhla Field, Phase II*, Internal Report Wintershall, Libya

[2] Curtis H. Whitson, Tao Yang and Øivind Fevang, PERA, 2000 (March) *Nakhla Oilfield – Reservoir Fluid Characterization,* Trondheim/Norway

[3] W. Dewenter and Lötsch, Wintershall AG/Libya, 2000 (December). *Feasibility of Gas Injection in a Pilot Project of the Nakhla Oilfield,* Internal Report Wintershall.

[4] M. Thompson, 2003 (March). *Investigation of EOR Options in the Nakhla Field – Phase I,* Winfrith (UK).

Petroleum Res. J. Vol. 18 (2005); P. 35–42, 13 Figs.

Hydraulic Frac Stimulation of the Sarir Sandstone in Nakhla Oilfield

Bernd Leonhardt*

التنشيط بطريقة التكسير الهيدروليكي لحجر السرير الرملي بحقل النخلة

برند ليونهاردت

يقع حقل النخلة النفطي بعقد الامتياز رقم97 داخل حوض سرت حوالي 60 كيلومتر جنوبي عقد الامتياز 96 . تم اكتشاف الحقل بحفر البئر G1-97 سنة 1970. تم إلى اليوم حفر 13 بئرا تسعة منها تنتج بالدفق الطبيعي – ثلاثة وصلت صخورا بركانية أو ترسبات بركانية حلت كليا أو على الأقل الجزء العلوي من المكمن المحتوي على الزيت، وبئرا واحدا خفق فنيا بتكوين زلطن.

تنتج جميع الآبار من حجر السرير الرملي التابع للكريتاسي السفلي، وسمحت المسامية المتدنية (10 – 14%) والنفاذية الفقيرة ذات المدى من 0.1 – 20 مللي دارس بإنتاج متوسط (معتدل). تم التنشيط بطريقة التكسير الهيدروليكي لسبعة آبار عمودية ما بين 1995 – 2002. كما تم إجراء تقنيات حديثة تعتمد على التحليل الفعلي للوقت في تنشيط التكسير الهيدروليكي لتقييم أنسب عملية التكسير خلال الطبقات.

النتائج المتحصل عليها من طريقة التنشيط بالتكسير الهيدروليكي تم مقارنتها بنتائج إختبار البئر بعد التكسير والمتحصل عليها من تحليل تزايد الضغط . تعد مقادير التكسير داخل حدود الدقة (نصف طول الكسر) على سبيل المثال والمتحصل عليها بكلتا الطريقتين متطابقة وبشكل حسن .

تلخص هذه الورقة الدروس المستفادة في العلاج المنفذ وتأثيره على العمليات المستقبلية وتطوير الحقل.

سلوك الإنتاج للآبار المتكسرة وغير المتكسرة والنتيجة الإضافية لسعة الإنتاج تم عرضها ومناقشتها: إلى حد اليوم حوالي 45% من الإنتاج الكلي للزيت في حقل النخلة يمكن تخصيصه (تحديده) كعلاج بطريقة التكسير الهيدروليكي ، وفي السنتين الأخيرتين تم بذل مجهودات كبيرة تم تسخيرها لفهم ووصف المكمن ومتغيرات ميكانيكية الصخر أفضل من قبل. المحصلة تم تطبيقها لتحسين الطريق لتخطيط وإيجاد الأفضل من عمليات التنشيط الهيدروليكي مستقبلا.

في النهاية الخبرات الجيدة بطريقة المعالجة بالتكسير الهيدروليكي بحقل النخلة النفطي كان لها القرار الدافع لتطبيق هذه التقنية في آبار أخرى والتي تنتج من الحجر الرملي للسرير في المستقبل اعتمادا على ميكانيكية الدفع.

Abstract: *The Nakhla Oilfield is located in concession 97 within the Sirt Basin about 60 km south of concession 96. The field was discovered by drilling well G1-97 in 1970. 13 wells were drilled to date: nine of them are producing on natural flow, three found volcanics or volcanoclastic sediments replacing the entire or at least the oil-bearing, upper part of the reservoir, one technically failed in the Zelten Formation.*

All wells are producing from the Lower Cretaceous Sarir Sandstone. Low porosities of 10 to 14% and poor permeability ranging from 0.1 to 20 md only allow a moderate production. Therefore, hydraulic frac stimulation of seven vertical wells was performed between 1995 and 2002.

* Wintershall, Libya.

State-of-the-art real-time analysis was performed in all hydraulic frac stimulations to evaluate and optimize the frac operation on-the-fly. Hydraulic frac simulation findings were compared to post-frac well test results obtained from pressure buildup analysis. Within their limits of accuracy the frac parameters (e.g. frac half-length) obtained by both methods match reasonably well.

This paper also summarizes the lessons learned from the treatment executed and their impact on future operations and field development.

The production behavior of fractured and unfractured wells and the resulting additional production capacity is presented and discussed. To date, about 45% of the cumulative oil produced from Nakhla oilfield can be assigned to the hydraulic frac treatments.

Especially during the last two years, a lot of effort was made to understand and describe the reservoir and its rock mechanical parameters better than before. The outcome was also implemented to improve the approach to plan and optimize future hydraulic frac stimulations.

Finally, the good experiences with hydraulic frac treatments in the Nakhla oilfield, were driving the decision to apply this technology also in other wells producing from the Sarir Sandstone in the future, dependent on their drive mechanism.

OVERVIEW

Geology. Located in the Hameimat trough in the south-east of the Sirt Basin in Concession 97 (Fig. 1), the Nakhla Oilfield was found by drilling well G1-97 in 1970. The development of the field started in 1993.

The main productive formation is the so-called Upper Sarir Sandstone, which is forming the uppermost layer of the Sarir Group. The Sarir Group consists of two sandstones (Upper and Lower Sarir Sandstone), which are separated by the Sarir Shale Member. The Upper Sarir Sandstone is a well consolidated sandstone, which can be described as deposits of an ephemeral fluvial system, with channels, sheet flood and inter-channel sand flats (Fig. 2). Thus, clean sandstone layers alternate with shale streaks. It was deposited in the Early Cretaceous (eventually Late Jurassic) age.

The Nakhla structure is a WNW – ESE trending Sarir arm (Fig. 3). Its northwestern end is in contact with the Amal/Nafoora-Augila Basement High via a broad saddle. In the Southeast the field is bordered by the so-called "B-High" where the basement has been reached by well B1-97.

Reservoir Parameters. The Upper Sarir Sandstone in the Nakhla oilfield is at a depth of 11,700 to 12,500 ft. The net pay is in the range of 130 to 400 ft. and the porosity is 10% to 14%. Reservoir

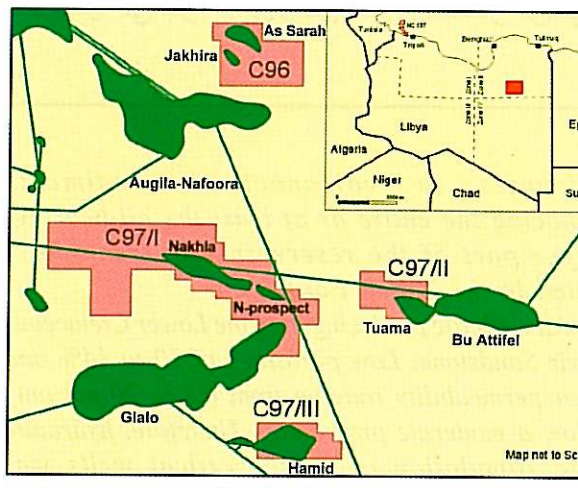


Fig 1. Location map of Nakhla Oilfield.

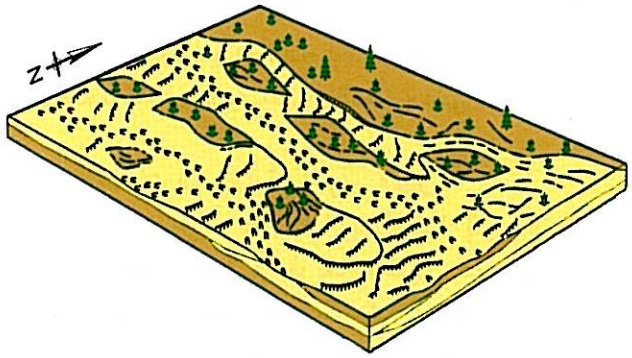


Fig. 2. Fluvial facies model, sheetflood dominated sand bed river (changed after Miall 1996).

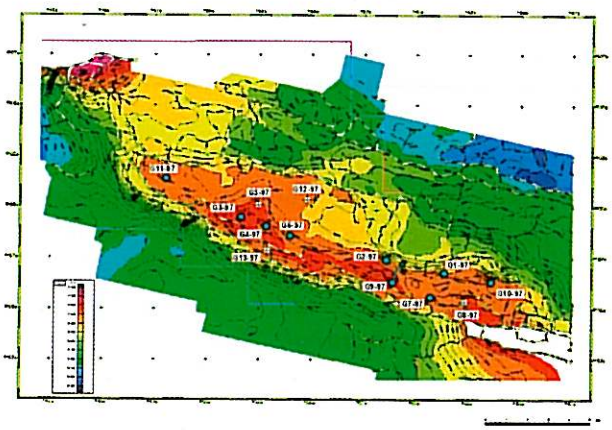


Fig. 3. Structure map Nakhla Oilfield – top upper Sarir Sandstone.

parameters and especially average permeability are improving from NW to SE, while higher pay heights have been drilled in the Northwest compared to Southeast. The permeability range is from tight (0.1 md) to fair (20 md). The main reservoir parameters are summarized in Table 1.

Table 1. Reservoir parameters of Upper Sarir Sandstone (Nakhla Oilfield).

Age	Lower Cretaceous (or Late Jurassic)	
Depth	3565 – 3760 m ss	11,700 to 12,330 ft ss
Area above OWC	60 km²	14,700 acres
Net pay	40 – 125 m	130 – 400 ft
Porosity	10 – 14 %	0.10 – 0.30
Permeability	0.1 – 12 md	0.1 – 12 md
Initial water saturation	30 – 55 %	0.30 – 0.55
Initial reservoir temperature	140 °C @ 3703 m ss	284 °F @ 12,150 ft ss
Initial reservoir pressure	414 bar @ 3703 m ss	6000 psi @ 12,150 ft ss
Initial oil in place[1]	148 MM m³	933 MMstb

[1] Status July 2002.

Oil Properties. The oil is a light oil API gravity of about 42°. Due to paraffins and waxes, pour point is high, about 100°F. Live oil viscosity is low, 0.35 cp at initial reservoir conditions. The oil properties are summarized in Table 2.

Table 2. Oil properties (Nakhla Oilfield).

Oil gravity	0.810 – 0.816 g/cm³	42 – 43 °API
Pour point	+40 °C	+104 °F
Viscosity @ *in situ* conditions	0.35 mPa · s	0.35 cp
Gas-oil-ratio	223 m³ (V_n)/m³	1250 scf/stb
Formation volume factor	1.65 m³/m³	1.65 rb/stb

FIELD HISTORY AND STATUS

Early Development Phase. The first two wells (G1-97 and G2-97) were drilled in 1970 and 1982, respectively. Initial production rates from the early wells drilled were found to be 1200 to about 2000 bopd. To improve production, Wintershall Libya decided to carry out hydraulic prop frac treatments in the existing and future wells.

The first development phase started 1993 and went through 1997. During this period six additional wells (G3- to G8-97) were drilled, of these wells G5-97 encountered volcanics, while G8-97 technically failed in the Zelten Limestone.

Since in the mid 1990's there was no provider for hydraulic frac stimulation services in the country, Wintershall Libya negotiated with three companies in order to make this service available in Libya. Finally, the jobs were awarded to Dowell Eastern (now Schlumberger Well Services).

Between 1995 and 1997, the six producing wells were successfully stimulated by hydraulic prop frac treatments. Comparison of the post-frac versus the pre-frac productivity index reveals an average productivity improvement (fold-of-increase) in excess of 3 (Fig. 4).

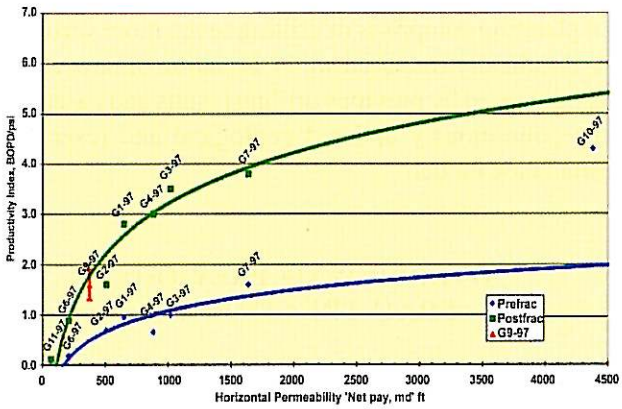


Fig. 4. Pre and post-frac productivity indices (pls) Nakhla Oilfield.

Recent Status of Field Development. After G8-97, five additional wells were drilled to date. While G9-97 is a barefoot completed horizontal well with a 3000 ft section in the Upper Sarir Sandstone, the subsequent wells were again planned vertical to delineate the extent of Nakhla oilfield to the East, West, North and South.

G10-97 in the East encountered as the first Nakhla well the initial oil water contact within the Upper Sarir Sandstone. Well G11-97 in the west, struck oil, but found extremely low permeability of 0.1 md. on average. G12-97 in the north and G13-97 in the south hit volcanoclastic sediments replacing the entire, or at least, the oil-bearing, upper part of the reservoir. Well G11-97 was hydraulically fractured in November 2002. (Fig. 5)

Future Field Development. The recent development concept foresees two more phases called Nakhla Phase II and Phase III. Phase II consists of a significant investment in surface facilities, such as upgrading of the existing Gas Oil Separation Plant (GOSP) and utilizing the gas via pipeline to the

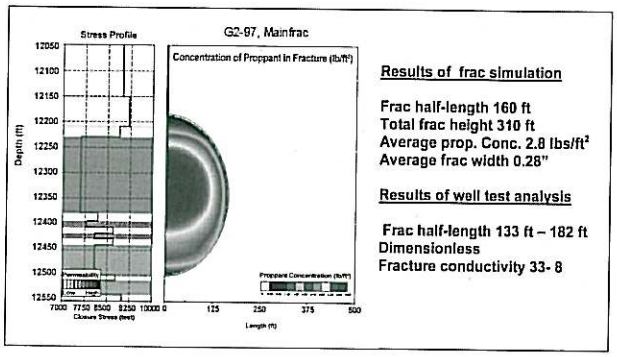


Fig. 5. Example of comparison of frac simulation and well test analysis results.

existing Jakhira GUP, furthermore drilling of six additional vertical wells including hydraulic frac treatments. The next Phase III at the current stage of planning comprises of drilling seven more vertical, hydraulically fractured wells. Location of new wells is influenced by previous drilling results and based on the continuously updated geological and reservoir simulation model.

OVERVIEW OF PREVIOUS FRAC TREATMENTS

Review of Previous Frac Jobs. To date seven wells have been hydraulically fractured in the Nakhla Oilfield: G1-, G2-, G3-, G4-, G6-, G7- and G11-97. All of these jobs have been pre-designed and optimized during execution by using a state-of-the-art, commercially available software package. This allows real-time analysis (RTA) and 3D frac simulation.

To allow RTA, job data like pressures, temperatures, pump rates and proppant concentrations were online transmitted to a laptop computer and fed into the program. Before performing the main frac, a data frac was carried out to provide specific data like the actual friction in the well and the leak-off coefficients for the different frac fluids used. In order to achieve this, bottomhole gauges were used during the frac.

Comparison of the actual data versus the expected data from designs allows changes in the pump program on-the-fly to permit an optimization of the treatment at any time during job execution. Post-job analysis and results obtained from the frac simulation, especially the frac half-length Xf and the dimensionless fracture conductivity FCD, can later be compared with information from other sources like pressure buildup (well test) analysis.

The frac-half length can directly be compared, while the frac conductivity can be crosschecked qualitatively. The following rule of thumb applies: in order to achieve a good conductivity (FCD>10-20), the proppant concentration in the frac should exceed 2 lbs/ft² in reservoirs having permeability like in the Nakhla Oilfield. An example is given in Figure 5 and the complete comparison can be obtained from Table 3. It can be seen that the data from both methods agree quite well within their limits of accuracy.

Table 3. Comparison of frac parameters from simulation and well test.

Well name	Frac half-length		Proppant concentrate	Dimensionless frac conduct.
	Frac simulation	Well test analysis	Frac simulation	Well test analysis
G1-97	240 ft	218-267 ft	1.4 lbs/ft²	>14
G2-97	160 ft	133-182 ft	2.8 lbs/ft²	>33
G3-97	260 ft	282 ft	1.5 lbs/ft²	16
G4-97	200 ft	190-212 ft	2.1 lbs/ft²	>23
G6-97	280 ft	283-302 ft	1.4 lbs/ft²	>15
G7-97	210 ft	217-224 ft	3.8 lbs/ft²	>50
G11-97	170 ft	N/A	3.6 lbs/ft²	"

Lessons Learned from Previous Frac Jobs. All job parameters like pad volume, total fluid and proppant pumped were reviewed and compared to the post job evaluation. This resulted in a significant reduction of pad volume compared to total fluid pumped (Fig. 6a), while the average proppant concentration pumped was increased (Fig. 6b).

Overall, the lessons learned so far can be summarized as follows:

- A pad volume of 20% to 25% of the total fluid volume pumped is sufficient to complete the frac job successfully.

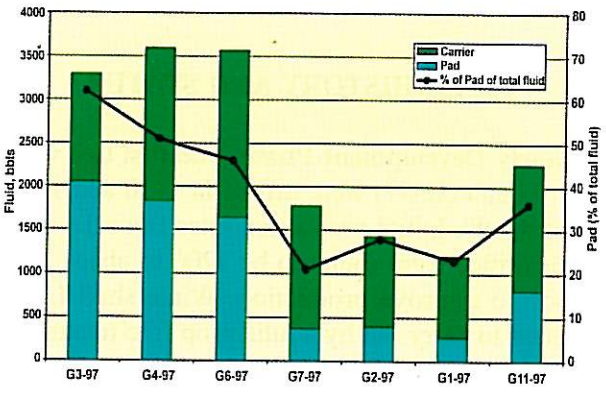


Fig. 6a. Fluid volumes pumped and percentage of pad of total fluid volume (Nakhla Oilfield).

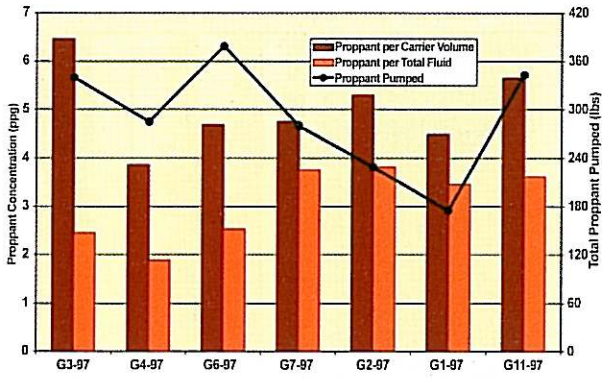


Fig. 6b. Proppant amounts pumped and average proppant concentration in frac fluids (Nakhla Oilfield).

- An average proppant concentration of 5.0 to 5.5 ppg in the carrier fluid over the whole job is anticipated to give optimal results.
- Technical procedures have been optimized to minimize risk of equipment failures during frac job execution.

Production Enhancement by Hydraulic Fracturing. To evaluate the production gain by the prop frac stimulations, decline curve analysis (DCA) was used on a well-by-well basis (Fig. 7a). Integration of the monthly production over time gave the two cumulative production figures, i.e. with and without hydraulic frac treatment (Fig. 7b).

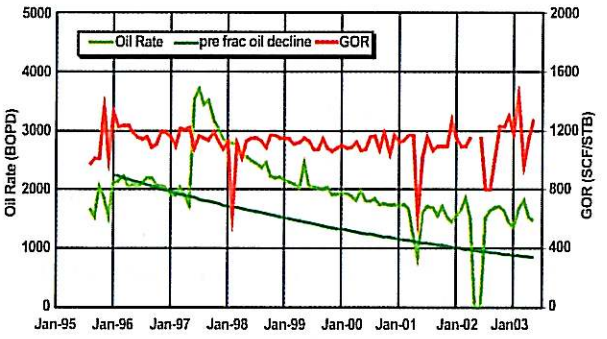


Fig. 7a. Oil rates G1-97 with and without hydraulic frac treatment, pre-frac oil decline obtained from decline curve analysis (DCA).

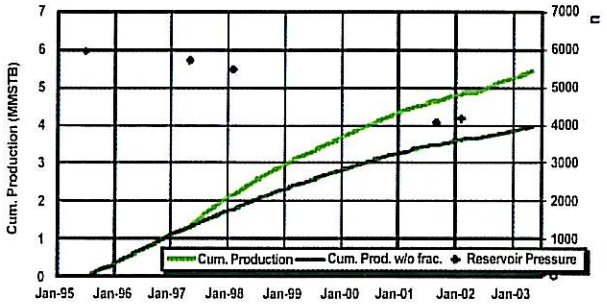


Fig. 7b. Cumulative oil production G1-97 with and without hydraulic frac treatment. Cumulative production without frac from DCA.

The same method was applied to each of the hydraulically fractured wells to obtain the cumulative production for both cases for total Nakhla Oilfield (Fig. 8). To date (status as of May 2003) 23.4 MMSTB of oil have been produced. The estimated cumulative production without frac treatments amounts to 12.8 MMSTB. Thus, the additional cumulative oil production gained to date by the fracturing project is about 45% of the actual total production.

It has to be stated clearly that part of the oil recovered is just production acceleration. However, part of it is also actually additional recovery, since the hydraulic frac treatments extend the time on how long the well can be economically produced and defers the point in time when the bottomhole flowing pressures will drop below bubble point.

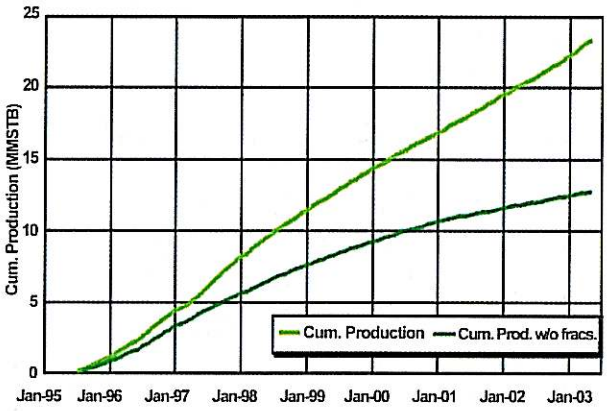


Fig. 8. Cumulative oil production Nakhla Oilfield with and without hydraulic fracs. Cumulative production without fracs obtained from well-by-well DCA.

PREPARING FOR THE FUTURE

Nakhla Stress Field. To improve our understanding of the field, a lot of effort was made especially during the last two years by carrying out a number of measurements and studies. To a large extent, these have been geological and sedimentological studies. Nevertheless, they contain extremely valuable rock mechanical information, which was used to optimize hydraulic frac planning. On the other hand, rock mechanical measurements carried out on Nakhla core material provide additional input to geological modeling.

Combining interpretations from FMI logs (Formation Micro Imager) with core measurement results provided a complete picture of the in situ stress directions of Nakhla Oilfield (Fig. 9). The maximum horizontal stresses run NE-SW, i.e. perpendicular to

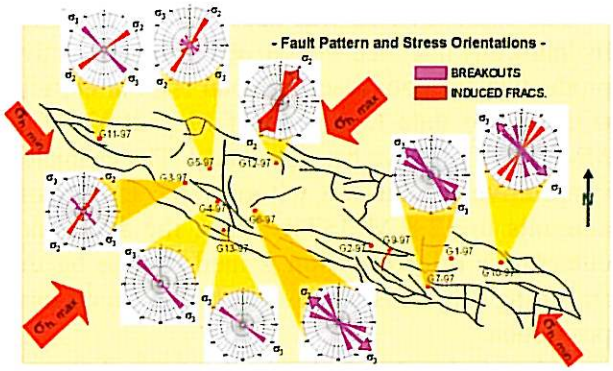


Fig. 9. Fault pattern of Nakhla Oilfield and directions of principal horizontal stresses.

the main faults of the field. The stress trend is similar to the regional trend in the Cyrenaica area (Fig. 10).

Rock Mechanics. One of the main input parameters for frac simulation programs are in-situ rock mechanical parameters such as Poisson's Ratio, Young's Modulus and formation closure stress lumped over certain intervals.

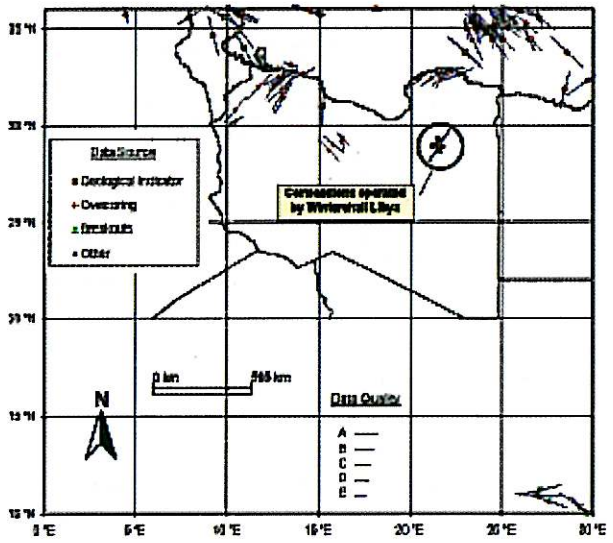


Fig. 10. Regional stresses (taken from World Stress Map, release 1997).

Usually, measurement of these in-situ values in the lab is cost intensive. Fortunately, reasonably good data can be obtained from open hole logs (Fig. 11). However, since some correlations are included in this process, laboratory measurements are required to verify or calibrate the calculations (Fig. 12).

Using these input data, the frac simulator predicts the vertical and lateral propagation of the frac and the resulting bottom hole net pressure for the whole frac operation. During job execution this pressure is compared to the actually observed net pressure (Fig. 13).

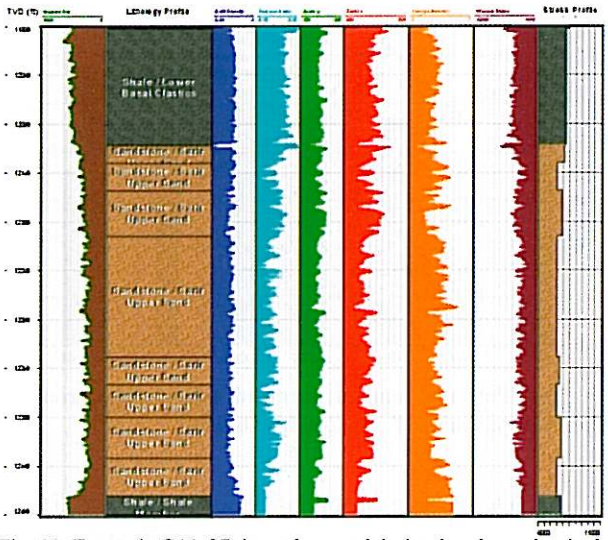


Fig. 11. Example G11-97: input logs and derived rock mechanical model for frac simulation.

Thermal Decay Time (TDT) Logging. To examine the aquifer influx in Nakhla Oilfield, TDT logging was carried out in well G10-97 one year after the well had been put into production. No change in water saturation behind pipe and especially at the oil-water-contact was observed. Thus, it could be verified that the aquifer in Nakhla Oilfield is very weak or inactive.

OUTLOOK

Nakhla Oilfield. The next step in future field development is the so-called Nakhla Phase II, which has already been started: drilling of the first well and construction of a 12" pipeline to Jakhira GUP is already ongoing, upgrading of existing surface facilities will be completed by the end of 2004.

A major frac campaign will be executed as well in 2004. Due to the broad database gained from the previous frac jobs and all the work carried out, a general main frac design can already be done and has only to be slightly adjusted to the actual drilling results of the Nakhla Phase II wells.

Adjacent Oilfields. The Upper Sarir Sandstone is also target formation of other exploration and appraisal drilling in Concession 97, which is ongoing or planned for the coming years. In these wells generally, hydraulic frac treatments costs involved are integral part of the drilling and well completion budget.

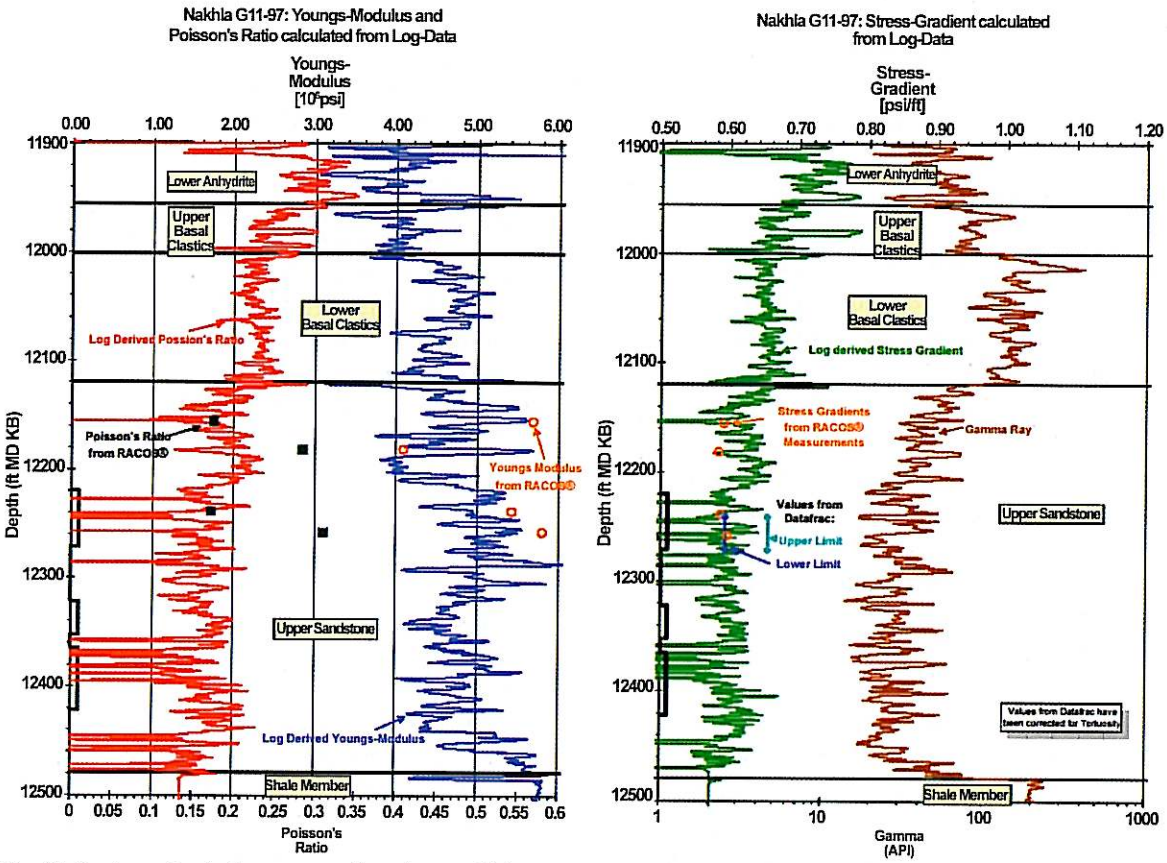


Fig. 12. Rock mechanical parameters from logs and lab measurements (RACOS®).

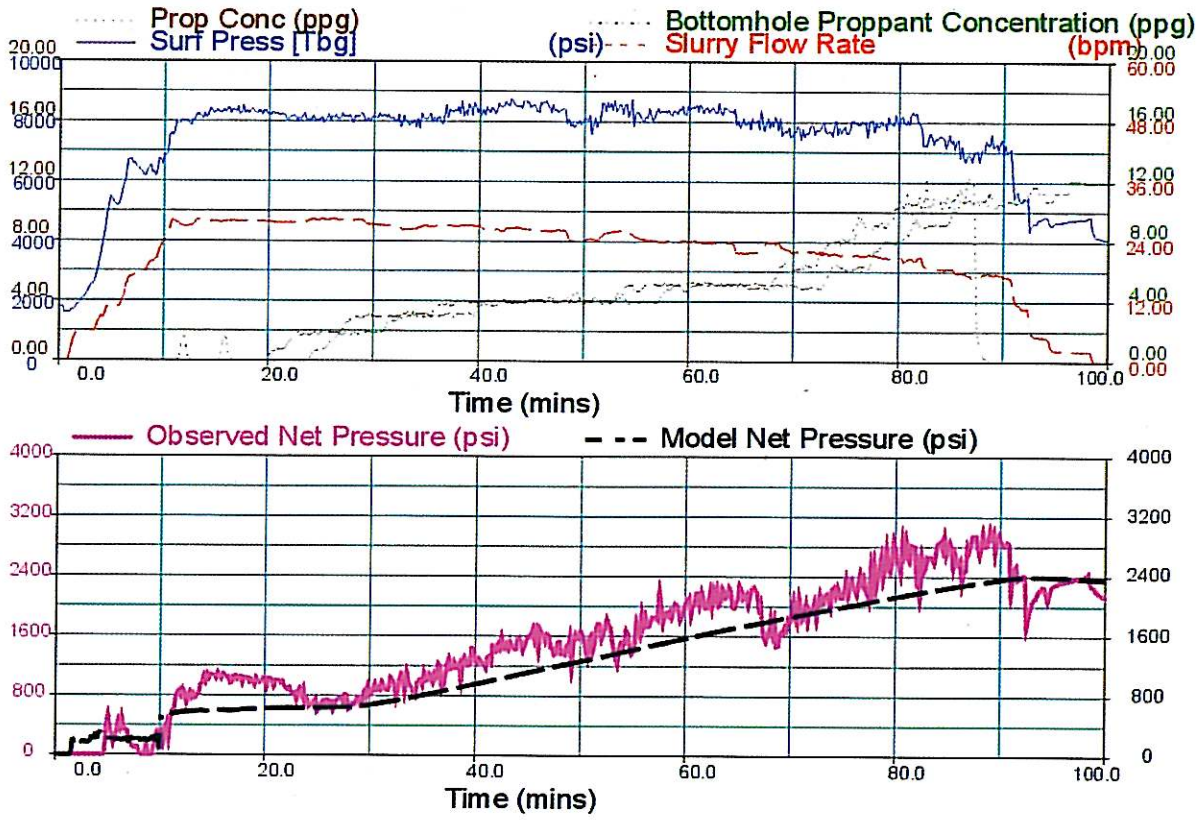


Fig. 13. Actual job data Mainfrac G7-97 and net pressure match.

CONCLUSIONS AND RECOMMENDATIONS

Five important lessons have been learned from the work carried out to date:

1. The Upper Sarir Sandstone is generally a good candidate for hydraulic frac treatments.

2. Productivity improvement achievable by prop fracs is significant. The frac treatment improves the economics of field development, and also enhances the recoverable oil reserves.

3. Best results can be expected from more aggressive frac designs.

4. Thorough frac planning is required in order to fulfill this target and get decent frac coverage over the entire pay.

5. Hydraulic fracturing should be applied early in the lifetime of a well.

However, hydraulic frac stimulation is not the solution to everything and not advisable for all applications. Oilfield wells with a strong underlying aquifer and/or existing gas cap are, in most cases, not optimal candidates for hydraulic frac treatments, since changing (oil-water or gas-oil) fluid levels will at a point in time cone into the frac. If this occurs, the unwanted phase might preferentially be produced instead of the oil.

ACKNOWLEDGEMENTS

The author wishes to thank NOC, PRC and Wintershall Libya for the opportunity to publish this material. Also, the author would like to thank his colleagues for their helpful comments and suggestions.

REFERENCES CONSULTED

[1] Ambrose G., 2000. The geology and hydrocarbon habitat of the Sarir Sandstone, SE Sirt Basin, Libya. *J. Petrol. Geol.*, **23** (2), 165-192.

[2] Bale, A. et al., 1994. Post-frac productivity calculation for complex reservoir/fracture geometry. *SPE* 28919, European Petroleum Conference, London, U.K.

[3] Crockett, A.R. *et al*, 1986. A complete integrated model for design and real-time analysis of hydraulic fracturing operations. *SPE* 15069, 56th California Regional Meeting, Oakland, CA.

[4] El-Hawat, A.S. et al., 1996. The Nubian Sandstone in the Sirt Basin and its correlatives. In: Salem *et al*, (eds), *The Geology of Sirt Basin*, Vol. **II**., Elsevier, 3-30.

[5] Gringarten, A.C. *et al*, 1975 (July). Applied pressure analysis for fractured wells. J. Petrol. Tech., 887-892.

[6] Gringarten, A.C. *et al*, 1974 (August). Unsteady-state pressure distribution created by a well with a single infinite-conductive vertical fracture. *J. Petrol. Tech.*, 346-360.

[7] Hopkins, C.W., 1997 (September). The importance of in-situ-stress profiles in hydraulic-fracturing applications. *J. Petrol. Tech.*, 944-948.

[8] Johnson, D.E. et al, 1993. On-site real-time analysis allows optimal propped fracture stimulation of a complex gas reservoir. *SPE* 25414, Production Operation Symposium, Oklahoma, USA.

[9] Sabet, M.A., 1991. Well Test Analysis. Golf Publishing Company, 175-182.

[10] World Stress Map Release 1997. New release 2004 published by Reinecker, J., Heidback, O., Tingay, M., Connolly P. and Müller, B., The 2004 release of the World Stress Map.

Petroleum Res. J. Vol. 18 (2005); P. 43–50, 11 Figs.

Re-establishing Reservoir Performance by Revaporization of Condensate in the Nubian Sandstone Reservoir

R.T. Bujnowicz* and K. Jerbi**

إعادة تقييم أداء المكمن بإعادة تبخير ناتج التكثيف في مكمن الحجر الرملي النوبي

ر. ت. بوجنويكز وخالد الجربي

يعتبر تكوين الحجر النوبي مكمنا هاما للمركبات العضوية بمنطقة عقد الامتياز 98 بليبيا، ويتكون هذا التكوين من حجر رملي دقيق الحجم يتمتع بنفاذية قليلة إلى متوسطة، ويحتوي على سوائل مكمنية تميل أن تكون مكثفة غنية بالغاز أو زيت متطاير. وفي كل حالة يكون ضغط المكمن يساوي أو أعلى بقليل من ضغط التشبع. ونظرا لأن الغاز بالمكمن غنيا بالمكثفات فإن أي انخفاض بسيط في الضغط ينتج عنه عادة كميات كبيرة من تجمع المتكثف. وفي حالة الزيت المتطاير في وقت مماثل فإن الانخفاض البسيط في الضغط ينجم عنه انتقال أجزاء كبيرة من الزيت المتطاير إلى طور متكثف. وينتج من هذه الظواهر تأثيرات مغايرة في النفاذية النسبية تستطيع الإقلال من نفاذية المركبات العضوية الأولية المستغلة.

أجريت تجارب معملية لوصف حالة سلوك سوائل المكمن وقد أعطت تحاليل لب البئر المألوفة تغطية جيدة للوصف البتروفيزيائي لصخر المكمن. وحددت تجارب السريان اللبي لاحقا السريان الأساسي لغاز المكمن تبعه تلف في النفاذية عند سلسلة من التناقص التدريجي في الضغط.

تم أجراء نماذج الضغوط في المعمل لتكون قريبة جدا من المتوقع حدوثها في الحقل والنتائج المعملية دلت على وجود تأثير على النفاذية من متوسط إلى عال بسبب درجة التشبع العالي للمكثف اللازم لحدوث سريان المكثف . ولتلطيف تأثير المكثف على النفاذية تم بناء نماذج معملية لتحديد إزالة حيوية المكثف من خلال إعادة التبخير بالحقن بالغاز.

Abstract: *The Nubian Formation is a significant hydrocarbon reservoir in the NC 98 Concession of Libya. It consists of a low to medium permeability, fine grained, sandstone. Reservoir fluids in the Nubian are either very rich retrograde condensate gas or volatile oil. In either case, the reservoir pressure is at or slightly above the saturation pressure. Because the gas-containing reservoirs are very rich in condensate, small decreases in pressure often result in high volumes of condensate accumulation. Similarly for the volatile oil case, small decrease in pressure result in large fractions of the volatile oil turning into the vapor phase. Both of these phenomenon can result in adverse relative permeability effects which can reduce the permeability to the primary hydrocarbon being exploited.*

Laboratory experiments were conducted to characterize the phase behavior of the reservoir fluids. Conventional core analysis provided good coverage of the petrophysical description of the reservoir rock. Subsequent core flow experiments determined base line flow to reservoir gas followed by the

* Hycal Energy Research Laboratories Ltd.
** Waha Oil Company.

impairment to permeability at a series of pressure decrements. The pressures modeled in the laboratory were chosen to closely approximate anticipated field conditions. Laboratory results indicate a moderate to severe effect on permeability, caused primarily by the high critical saturation of condensate necessary for flow of condensate to occur. To mitigate the effect of condensate on permeability, laboratory experiments were performed to determine the viability of condensate removal through revaporization by gas injection.

INTRODUCTION

The NC 98 concession, operated by Waha Oil Company, consists of low to medium permeability sandstone. The reservoir fluids occupying the pores of the rock tend to be volatile oils or very rich condensate bearing gas. In either case, the pressure drawdown required to cause economic production of gas or oil would require the flowing bottom hole pressure to be below the fluid saturation pressure. When the flowing bottom hole pressure drops below the dew point of the gas, large quantities of condensate will form in the pores affected by the pressure drop. The resultant condensate will not flow through the rock until critical condensate saturation is established. The critical condensate saturation is controlled by pore geometry and to a lesser extent by fluid distribution in the pores. Similarly, as the flowing bottom hole pressure drops below the bubble point of the volatile oil, large quantities of gas will form; the gas will not flow until critical gas saturation is established. In both cases, the formation of separate phases causes flow restrictions (relative permeability effect) that can be a severe detriment to economics and to ultimate recovery by primary depletion. Laboratory experiments were designed to evaluate and quantify the effect of flow impairment to the primary phase and to evaluate the remedial course of action required to regain flow to gas in the subject reservoir.

The objective of this paper is to illustrate the effect of pressure on the impairment of permeability as a result of liquid accumulation from a gas-bearing reservoir. Following the establishment of a given pore volume condensate saturation, dry gas was injected to determine the mass transfer into the gas phase and subsequent enhancement of permeability. Core samples were assembled into multiple plug stacks at reservoir conditions of saturation, pressure and temperature to model the reservoir as will be explained later.

GEOLOGY

The NC 98 concession currently consists of 4 distinct pools that have somewhat different reservoir character. The pools, A, F, C and B are listed in order of current and anticipated economic importance. The "A" is a rich gas condensate-bearing pool while the other three contain volatile oil. The "A" pool will be the focus of this paper.

The pool is comprised of the Nubian Formation - fine grained, well-cemented, occasionally shaley, sandstone. The Nubian itself is constructed of 3 members: the Upper Nubian, Middle Shale and Lower Nubian. Figure 1 illustrates the average rock quality of the Upper Nubian. Structurally, the unit is a Graben of about 600 feet thickness. Most of the pay is gas overlying water. Average gas / water contact is at 14,670 feet depth. Initial reservoir pressure is 7,100 psig and initial temperature is 318 F. Volumetric initial estimates of the reserves are 3.4 trillion cubic feet (Tcf) and 550 million barrels (MMB).

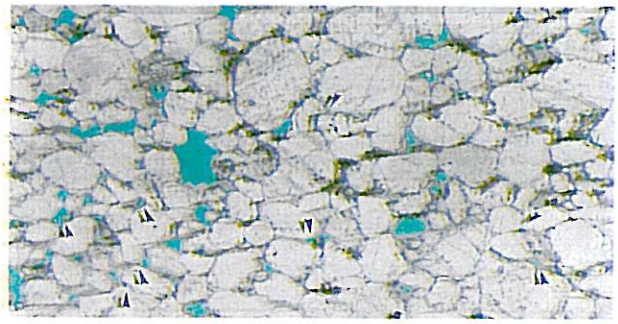


Fig. 1. Microphotograph of a typical Nubian Sandstone from Waha NC98.

RESERVOIR FLUID CHARACTER

A series of bottom hole samples were collected from the A pool. The bottom hole samples were supported by separator samples of gas and condensate that were subsequently recombined to reservoir parameters in the laboratory. Comparisons of the samples resulted in three bottom hole samples chosen to represent the reservoir. Table 1 is a compositional analysis of the reservoir gas from Well A3, DST 4. Due to the large volume of live reservoir gas necessary for the core flood experiments, the

Table 1. Waha NC98 PVT routine and special core study, vaporization of condensate by dry gas at pressure below dew point recombined composition for surface separator samples from "A" reservoir.

Composition (mole %)	Well A3 DST#4 Sample #8B Gas bottle #147 Liquid bottle #862
N_2	1.24
CO_2	5.25
H_2S	0.00
C_1	72.34
C_2	7.85
C_3	2.46
IC_4	0.65
C_4	1.10
IC_5	0.46
C_5	0.45
C_6	0.72
C_{7+}	7.48
Total	100.00
GOR	6030 SCF/bbl
Dew Point Pressure (psia)	6597

recombination of separator fluids was used. Common bottom hole cylinder volumes contain approximately 600 cc of fluid for use in lab testing versus the use of separator fluid recombination to yield "unlimited" amounts of live reservoir gas. Bottom hole sample volumes are also limited, due to cost, while separator fluid recombinations are relatively inexpensive.

Rich gas condensate systems result in high accumulations of liquid drop out over small pressure ranges. This effect is typical of fluids where conditions are near the critical point on the phase diagram. Figure 2 shows the conditions of pressure and temperature of the well A3 bottom hole sample relative to the critical point. The phase envelope was

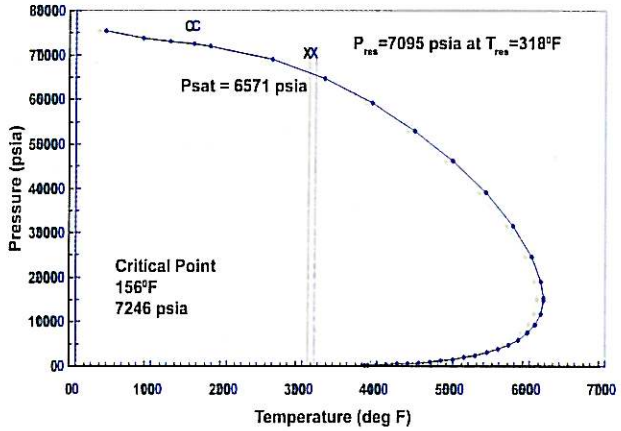


Fig. 2. Phase envelope of recombined composition for Waha A3 DST#4 sample 8B.

calculated using the Peng Robinson equation of state and was tuned by laboratory data.

The laboratory exercise known as the constant volume depletion (CVD) experiment results in a close approximation of the dynamics of gas / condensate equilibrium during pressure depletion and subsequent production. The lab data describes the almost instantaneous formation of condensate (occupying up to 15% pore volume) when the pressure drops from 6,597 psig (dew point) to 6,000 psig. Maximum condensate accumulation occurs at 3,900 psig, after which further pressure drop results in the more volatile components of the condensate revaporizing back into the gas phase. Figure 3 graphically illustrates the rates of condensate formation and revaporization.

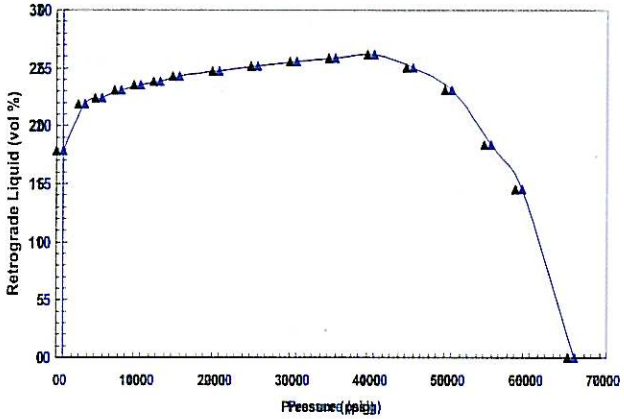


Fig. 3. Retrograde liquid volume percent during constant volume depletion.

PETROPHYSICAL PROPERTIES OF THE RESERVOIR ROCK

Initial petrophysical description of the reservoir rock was a function of statistical sampling. At intervals of approximately 1 foot, 1.5 inch diameter plug samples were cut from the full diameter core. Every 10th sample was cut as a full diameter size so as to develop the relationship between the two horizontal direction permeability values and the vertical permeability. Rock homogeneity was ultimately not a concern; permeability porosity cross plots of full diameter were indistinguishable from the small plug data plots.

The cross plot of permeability to air versus porosity is illustrated in Figure 4. Application of net overburden stress and Klinkenberg corrections to permeability resulted in a tighter grouping of the permeability porosity data. Final sample selections for the lengthy and more expensive special core

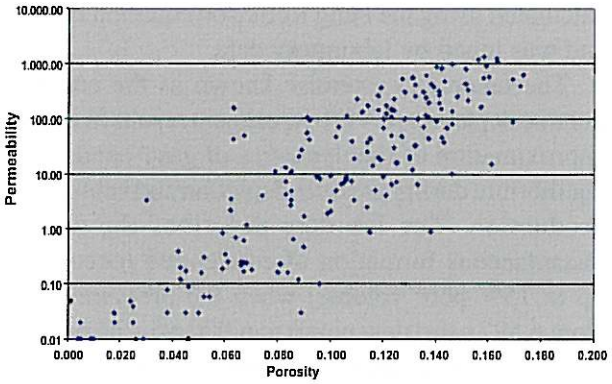


Fig. 4. Well A1-NC98 K/Phi x plot.

experiments were based on the stressed and Klinkenberg corrected measurements. In addition to the measured rock properties, extensive rock characterization was done by petrology. Thin section interpretation, x-ray diffraction and scanning electron microscopy aided in understanding rock types, reservoir layers and reservoir quality and participated in the methodology of choosing acceptable special core analysis samples.

CORE FLOOD EXPERIMENTS

Prior to the construction of the core stacks from the chosen core plugs, the question of reservoir wettability was addressed. Traditionally, oil-bearing formations have a variety of wettability conditions ranging from strongly water wet to strongly oil wet. Wettability controls include water chemistry, oil composition, reservoir rock composition and pore geometry. Gas reservoirs typically are water wet; gas being the non-wetting phase. Given the high condensate concentration, the possibility of pyrobitumen types of pore lining material and rapid condensate drop out due to pressure depletion, the core samples were allowed to come to equilibrium with the reservoir water and gas according to the Anderson method for oil water systems as described in the literature. Synthesized reservoir brine and live (from recombination of separator fluids) gas were the core filling fluids. The core restoration was conducted at reservoir conditions for a duration of 4 weeks. The results of the restoration indicated that the reservoir is a water wet system at reservoir conditions.

In order to model the impairment of permeability to live gas, as caused by condensate drop out over a reasonable depth of investigation, core stacks rather than core plugs were used. Calculations of volume and pressure versus depth suggested 10 to 12 inch core stacks would not cause unreasonable pressure differentials while allowing good volumetric control. Four core plugs of very similar porosity / permeability were assembled for each core stack. Permeability to live reservoir gas was measured at reservoir conditions (*i.e.* pressure above dew point) and at reservoir initial saturations (*i.e.* pores saturated with live gas and with irreducible water). This initial permeability served as the base line permeability.

At least six pressure decrements were believed to be sufficient to model the production pressure response around the well bore and a short distance into the reservoir. Most damage or impairment to production occurs in the near well bore region so, given the stack length and pressure ranges, we believe the lab model to be a reasonable and reliable indicator of field performance. Following each pressure decrement, the stack was allowed to come to equilibrium by flowing live gas stripped of the condensate to the same pressure as the stack. This allows the condensate at each decrement to accumulate in the porosity without additional condensate accumulation from "upstream" portions of the reservoir.

During field production, upstream gas will be stripped of some condensate in the near well bore region as affected by the pressure transient from initial reservoir pressure deep in the reservoir to the flowing draw down pressure in the well bore. Accumulation of condensate will occur until the condensate saturation eventually reaches a critical and thereafter moveable saturation. Careful data gathering in the field will yield evidence of this effect when gas liquid ratio (GLR) is plotted versus time: GLR will increase as the condensate accumulates in the pores while the leaner stripped gas is produced. Upon establishment of critical condensate saturation, the condensate becomes mobile and any further condensate will be produced with the gas stream resulting in a decrease in the GLR to some steady GLR rate at that specific production rate.

In order to control the impairment of permeability due to condensate formation in the pores and to determine the magnitude of the critical condensate saturation, decline pressure equilibrium gas was injected into the core stack.

Eight core stacks were used to model the permeability impairment as a function of pore pressure (resulting in condensate drop out). Follow

up experiments were designed to evaluate the mitigation of the condensate caused impairment by dry gas injection.

To ensure adequate volumes existed in the core for the sensitive revaporization experiments, full diameter core stacks were assembled – by much the same technique as for the core plugs. Two stacks were prepared – one to model low permeability (5 mD) rock and the other to model medium quality rock (50 mD). After establishing equilibrium condensate saturation, methane gas was reinjected for five pore volumes through the core stack. Methane gas will be the least efficient hydrocarbon based gas that would be considered for revaporization; separator A Pool gas would be the most likely "dry" gas that might be used in the field. If methane were to be successful then A Pool separator gas would be even more so due to the heavier component concentration typical of the gas produced out of the high stage separator relative to pure methane. Again, test conditions were at reservoir pressure and temperature. The composition of the effluent gas as well as gas liquid ratio were measured and added much value to the resulting permeability measurements across the core stack.

RESULTS AND DISCUSSIONS

The severity of the impairment of permeability due to condensate formation was measured for the two core samples: low permeability and high permeability core stacks described in Tables 2a and 2b. The results are shown in Figures 5a and 5b.

Rock of medium-low quality is described in Table 2a while a better quality rock is the content of Table 2b. Permeability reduction was severe in both cases i.e. from the initial 6500 psi start point where permeability was 55 mD to 1 mD at a pore pressure

Table 2a. Permeability reduction as a function of pore pressure.

Test parameters	
Core stack I.D.:	Stack #5
Formation:	Upper Nubian
Well I.D.:	A3
Core stack configuration (from inlet):	227, 192, 52, 117
Average reservoir depth (ft):	14392.75 ft
Core stack average porosity (%):	12.5 %
Core stack average permeability(mD):	5.65 mD
Test temperature (°F):	315
Net overburden pressure (psig):	4850

Table 2b. Permeability reduction as a function of pore pressure.

Test parameters	
Core stack I.D.:	Stack #8
Formation:	Upper Nubian
Well I.D.:	A1
Core stack configuration (from inlet):	17, 69, 41, 38
Average reservoir depth (ft):	14433.3 ft
Core stack average porosity (%):	12.8 %
Core stack average permeability(mD):	99.5 mD
Test temperature (°F):	315
Net overburden pressure (psig):	4850

of 100 psig for the better quality rock. The lower quality rock had initial permeability to live gas of almost 4 mD at the start condition of 6500 psi pore pressure declining down to 0.09 mD at a pore pressure of 100 psig. The impairment is due to the very high critical volume of condensate required prior to the flow of the condensate through the pore throats and the low relative permeability to gas. Though a critical condensate saturation experiment was beyond the scope of the original lab study design, anecdotal observations of the volume of condensate exiting in the core suggest a very high retained condensate volume in the rock pores hence impairing the flow of gas. Mobility and fluid dispersion in the pore environment is much more favourable towards gas rather than condensate.

Figures 5a and 5b illustrate the relationship between gas permeability at reservoir conditions as a function of pore pressure for the high and low perm quality core stacks. In both high and lower quality rock, permeability declines rapidly as pressure decreases. This can be attributed to both the large volume of condensate dropping out at pressures a

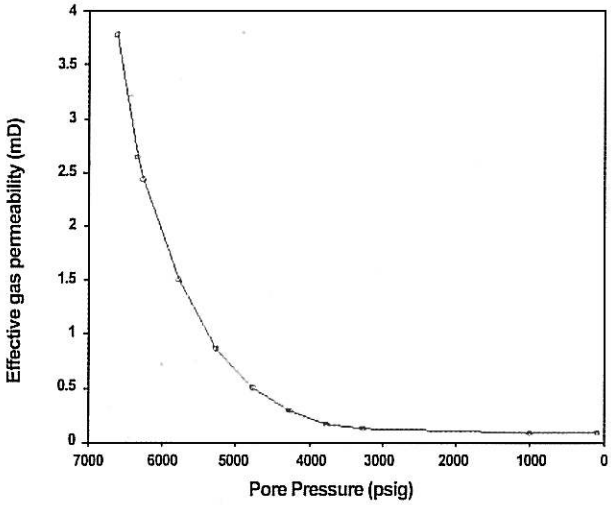


Fig. 5a. Stack #5 perm reduction.

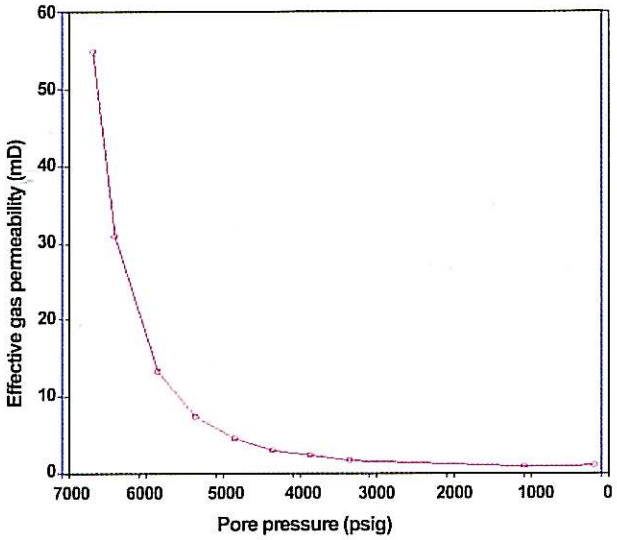


Fig. 5b. Perm reduction stack #8.

little below saturation pressure and to the pore geometry (*i.e.* little evidence of high permeability streaks and appearance of a homogeneous pore network with small pore throats).

Figure 6 is a plot of cumulative condensate production (% of initial condensate in place) versus the cumulative volume of methane gas injection, for the low permeability stack (3 mD) at pressures of 6320 and 5700 psig. At the higher pressure, most of the condensate is recovered after one pore volume of dry gas is injected. At the lower pressure, the recovery of the condensate continues increasing with continuing injection. At 3 Pore Volumes the condensate recovery is more than 80%. The high cumulative recovery of the condensate for both pressure runs is a result of two mechanisms: displacement by gas flood and vaporization of the heavier hydrocarbon components by contact with methane gas.

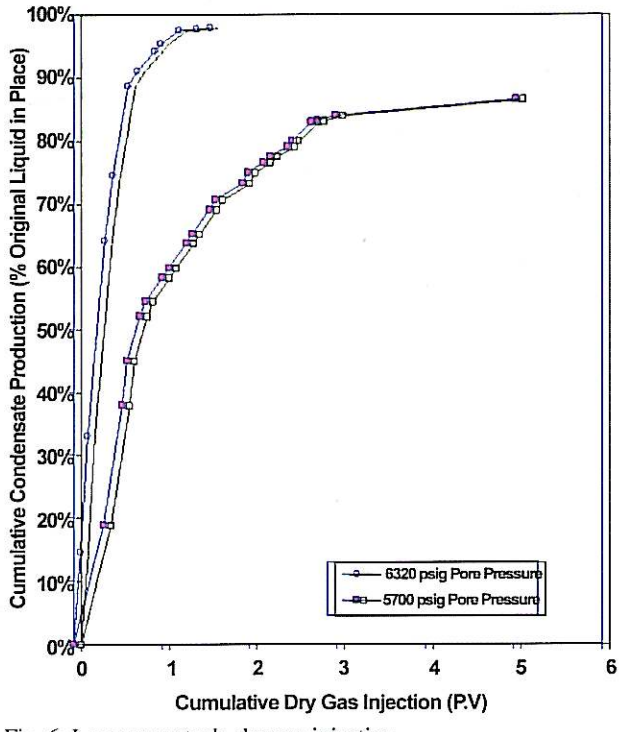


Fig. 6. Low perm stack, dry gas injection.

Figure 7 shows the molecular weight of the produced condensate liquid as a function of methane injection. The data show two different trends:

1 - at the high pressure, gas cycling appears to displace the condensate in a piston like manner i.e. very little change of the molecular weight versus gas injection but a lower molecular weight of displaced condensate than that as exists in the live gas, indicating heavier ends are remaining in the core stack.

2 - at the lower pressure, an increasing trend in the molecular weight of the produced condensate liquid which is a good indication of vaporization of the heavy hydrocarbon components by multi contact miscibility with the methane gas.

After breakthrough both the rate of condensate production and the molecular weight of the produced liquid stabilize very quickly.

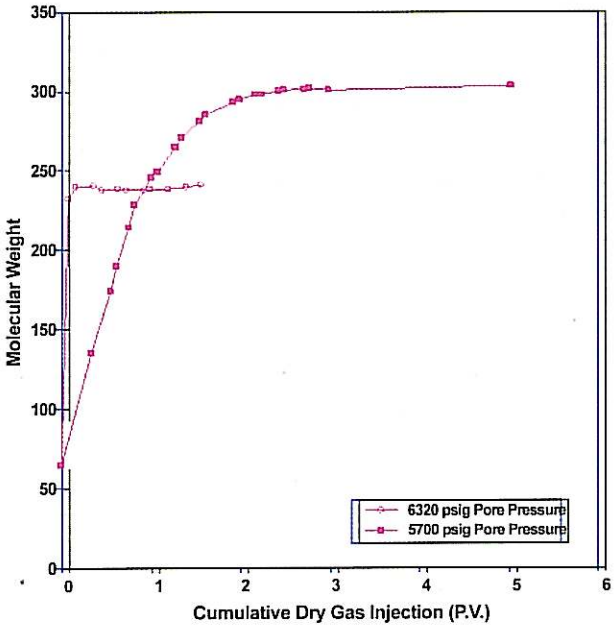


Fig. 7. Low perm stack mole weight of produced condensate.

Figure 8 is a plot of the cumulative production of the retrograde condensate liquid as a function of methane gas injection in terms of percentage of condensate in place using a stack of relatively high permeability (*i.e.*50 mD). These results show that breakthrough of the injected methane gas occurs after about 1/2 pore volume of methane injection while significant amount of condensate continues to be

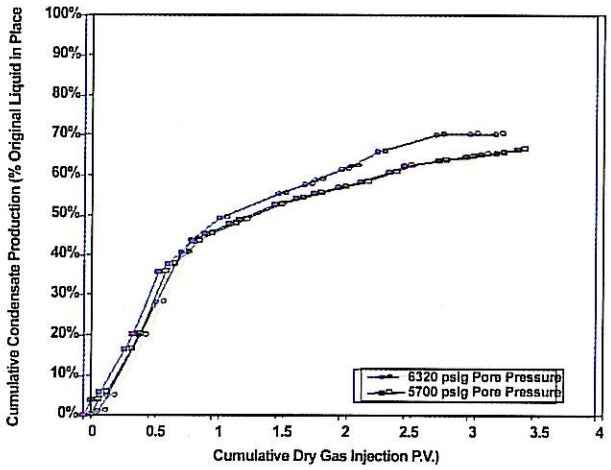


Fig. 8. High perm stack, dry gas injection.

produced after breakthrough. The overall recovery of the condensate (about 70%) is not as efficient as that in the low permeability stack probably due to the higher permeability of the core (50 mD) which causes early breakthrough and the resulting poorer sweep efficiency.

Figure 9 illustrates the relationship between the molecular weight of the produced condensate versus pore volumes of dry gas injection. The molecular weights for both pressure regimes are somewhat similar; vaporization of heavier ends after gas breakthrough occurs more for the lower pressure injection than for the higher pressure. As with the low permeability stack, the composition of the condensate changes due to the pressure at which the condensate is created hence the composition of the swept condensate reflects this phenomenon.

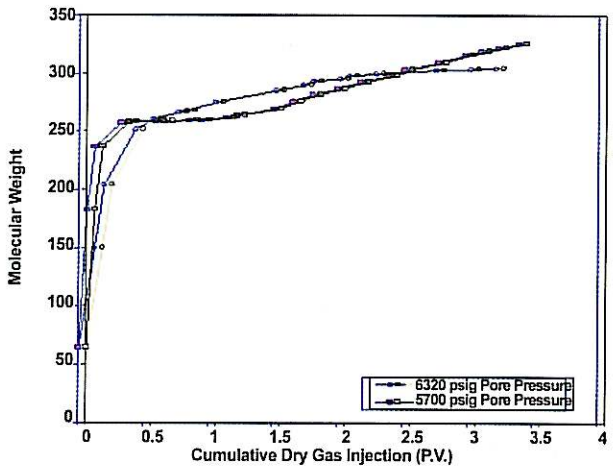


Fig. 9. High perm stack mole weight of produced condensate.

Another set of tests was conducted to investigate the regain in permeability due to condensate revaporization by dry gas injection. Starting at 6320 psi and 5700 psi (as separate tests), dry gas was injected and permeability was measured as a function of pore volumes injected of dry gas. Figure 10 shows the regain in permeability during the vaporization of condensate tests using methane injection for the low permeability stack while Figure 11 illustrates the high permeability stack behaviour. The results show that as methane gas is injected the effective permeability to gas increases from about 6 percent before the start of methane injection to about 50 percent after 3 pore volumes of methane gas has been injected for the high permeability stack. The regain in permeability never brings it back to near original values for the low permeability stack. In our experience this phenomenon may be caused by the effect of very small pore throats clogged by even small amounts of condensate.

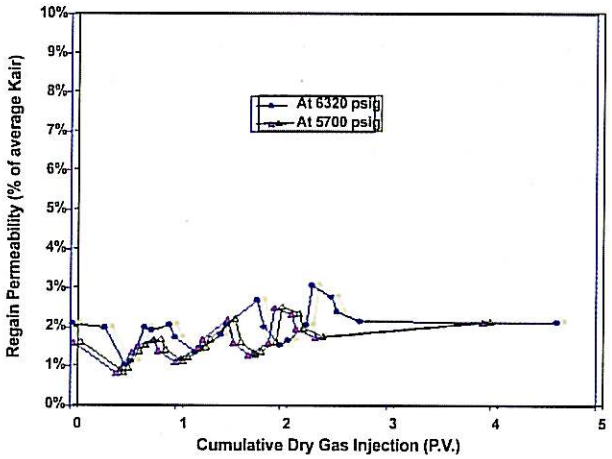


Fig. 10. Low perm stack, regain permeability.

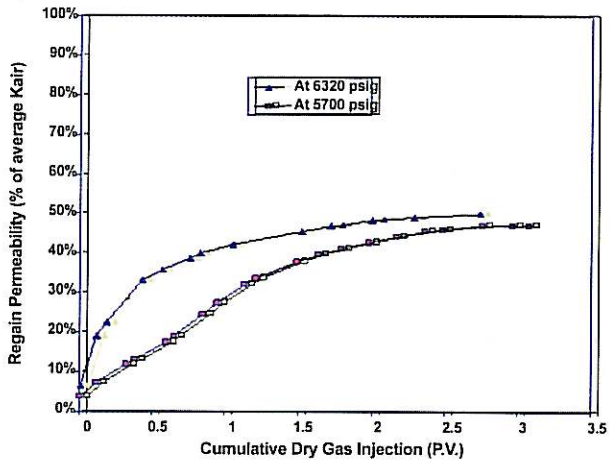


Fig. 11. High perm stack, regain permeability.

CONCLUSIONS

(1) Reservoir performance in terms of flow to gas is very dependant on flowing bottom hole pressure. Formation of condensate at flowing bottom hole pressures below dew point will significantly

impede the flow of gas. Both low and medium quality rock types will be affected significantly.

(2) Investigation of the vaporization of condensate by methane gas at pressures below the dew point pressure was conducted by displacement testing of the gas and the retrograde condensate in the presence of connate water in horizontal core stacks. All of the testing was conducted at reservoir temperature, and at different pore pressures.

The recovery of the gas condensate by laboratory displacement test with methane gas varies from about 50 to 80 percent of the original condensate in place depending on the rock permeability and the resulting sweep efficiency. Theoretically, a high percentage of the condensate should be expected to be vaporised by the methane gas given the high pressure and temperature of the system and light nature of the pore filling liquid. In practice, the recovery by the laboratory displacement test would be lower than the theoretical recovery due to poor sweep efficiency.

The displacement of gas condensate by methane gas is characterised by poor mobility ratio and viscous fingering resulting in early breakthrough of the injected methane gas and very high gas/oil ratios during the test. The volume of methane gas injection required to completely recover the condensate liquid in the core is a function of temperature, pressure, composition of the gas and especially the permeability of the core sample. For the reservoir conditions investigated in this study (*i.e.* 7082 psig and 315 °F) the methane gas requirement varies from 3 to 4 pore volumes at a permeability of 5 mD but will increase significantly at higher permeabilities (e.g. 50 mD) due to early breakthrough and poor sweep efficiencies.

(3) It is evident from the laboratory data that heavy hydrocarbon components from condensate can be vaporised by multi contact miscibility with methane gas (as evidenced by the mole weight behaviour of the produced condensate) which is believed to be the major factor in providing such high recovery of the condensate liquids from certain kinds of pore systems

(4) Re-establishing permeability to reservoir gas by dry gas injection appears to be a function of the rock quality. Poor quality rock – though well suited to high condensate recovery – appears significantly impaired and does not respond well to dry gas injection. An interpretation of the persistence of the impairment is that even small quantities of condensate cause liquid blocking effects. High quality rock seems better suited for permeability regain after dry gas injection.

A future exercise will compare field data with the laboratory derived model. The comparison will be presented as a case study.

ACKNOWLEDGEMENT

We wish to thank Waha Oil Company of Libya and Hycal Energy Research Labs for the support necessary for writing this paper.

Petroleum Res. J. Vol. 18 (2005); P. 51–58, 11 Figs.

2-D Geological Modeling in the Vicinity of Horizontal Wells – Case Study Integrating Borehole Images and Openhole logs

Aimen Amer*

نمذجة جيولوجية ثنائية الأبعاد بجوار آبار أفقية - دراسة حالة دمج صور وسرود البئر

أيمن عامر

معلومات ميل الطبقات المستنبطة من جهاز قياس ميل الطبقات ومعدات التصوير لا يتم عادة دمجها مع سرود البئر، وبالتالي فإن العلاقة بينهما سؤال يجب الإجابة عليه. ستوضح هذه الورقة أساليب جديدة لاستحداث نمذجة جيولوجية ثنائية الأبعاد ترتكز أساسا على صور سرود البئر ووصفه، وذلك باستخدام مثال حقلي في آبار أفقية.

تزود تفسيرات صور السرود والعينات بمعلومات قيّمة عند جدار البئر وبالإمكان إسقاطها على المنطقة المجاورة له عن طريق إنشاء قطاع تركيبي باستخدام الحاسوب (شكل تركيبي). إن الصورة الحالية للشكل التركيبي مخصصة إلى معلومات الميل ولا يمكن دمج معلومات سرود الآبار في القطاع التركيبي المعد ومع ذلك فإن وصف البئر يمكن دمجه في القطاع التركيبي عن طريق أجزاء من السحنات الصخرية المتحصل عليها من السرود على طول حدود الطبقة المتعرف عليها مسبقا بالقطاع التركيبي باستخدام برمجة الحاسوب.

إن النموذج العام لا يعكس دائما البنية الحقيقية المحيطة بالبئر وهذا بالطبع يعتمد على اتجاه المقطع باعتباره غير عمودي على بنية التكاوين الجيولوجية. ولقد بين تفسير الدراسة السيزمية ثنائية الأبعاد، من دراسة الحالة للبئر الأفقي، وجود منخسفات ومرتفعات، وأن هذا النظام البنيوي يتجه ناحية شمال شرق – جنوب غرب فقط. ورغم ذلك فإن المعلومات السيزمية ثلاثية الأبعاد قد تم جمعها أثناء عملية وصف العينات.

تم حفر قطاع أفقي يصل إلى 1820 قدم بواسطة "LWD-"GR، ووجد أن هذا المقطع الأفقي الطويل نسبيا قد اخترق 260 قدما من صخور سميكة من الطفلة الجيرية المانعة لهجرة النفط تلته صخور جيرية تشكل صخور المكمن.

ومن أجل حل مشكلة الحفر عبر طبقة صخور الطفلة الجيرية وتفهّم بنية وجيولوجية صخور المكمن تم الحصول على (صور وسرود الآبار).

يوضح النموذج الناتج أن للبئر ست نطاقات بنيوية مختلفة وبه سبعة صدوع معكوسة وتحت سيزمية، كما بين هذا النموذج مصيدة بنيوية للتطوير المستقبلي. وبعد الانتهاء من وضع النموذج ثنائي الأبعاد أوضح النموذج السيزمي ثلاثي الأبعاد وجود صدوع عكسية بالإضافة إلى المصيدة التركيبية.

لقد بينت دراسة الحالة هذه أن إنتاج النموذج الجيولوجي ثنائي الأبعاد ضروري لتقدير دقيق للوضع البنيوي والجيولوجي للبئر خاصة خلال المراحل الأولى من الاستكشاف وعندما تكون المعلومات محددة وغير مؤكدة ولا يقتصر تطبيق هذه الطريقة المطورة والمطبقة في هذه الورقة على الآبار الأفقية بل يمكن تطبيقها على الآبار العمودية والمائلة.

Abstract: *Dip data obtained from dipmeters and imaging tools are not usually integrated with openhole logs. This paper addresses the relationship between these two types of data and uses a horizontal well to illustrate a new methodology that produces a two-dimensional (2-*

* Schlumberger Overseas, Oman.

D) geological model based on borehole images and openhole logs.

Images provide valuable information about the borehole wall and can be easily extended to the borehole vicinity by using softwares to construct a structural cross-section. Although the software used in this study is devoted for dip data and cannot integrate openhole logs into the constructed cross-section, the log data were integrated by populating the lithofacies obtained from the logs along the bed boundaries previously identified using other software programs.

The generated model did not always reflect the true structures surrounding the well. Accuracy depended on the direction of the cross-section, and the section was not always perpendicular to the structure. However, computing and displaying the different structural zones resolved this issue.

In the case study, 2-D seismic data showed a graben and horst system with only one structural trend, oriented NE-SW. Three-dimensional (3-D) seismic data were being processed at the time of logging and were used later to validate the model. During drilling of the 1,820-ft horizontal section, which included 260 ft of cap rock, a logging-while-drilling (LWD) gamma ray log was obtained. The Cretaceous carbonate reservoir section was directly beneath the cap rock, which was composed of a thick layer of calcareous shales.

To resolve the issue of drilling through the calcareous shales and to understand the structure and geology of the reservoir, borehole images and openhole logs were acquired.

The model constructed from the images and logs identified six different structural zones (including a fold) and seven reverse faults. It also defined a structural trap with potential for further development. The newly processed 3-D seismic survey showed four reverse faults in addition to the trap, confirming the 2-D model.

This case study illustrates that a 2-D geological model is critical for accurate structural and geological definition of the wellbore environment, especially during the early exploration stages when data are limited and uncertainties are high. The procedures developed and applied in this paper are not restricted to horizontal wells; they can also be applied to vertical and deviated wells.

INTRODUCTION

High-resolution imaging tools deliver huge amounts of data, and much of this data is not convenient to use or is not fully used. The main goal of this paper is to illustrate a methodology to summarize borehole image data and lithological evaluation derived from openhole logs in one geological model (cross-section). In analogy with problems in structural geology, one might first think of cross-sections in terms of assessing a geological model (Anxionnaz and Delhomme, 1998).

The model in this article is presented as a workbench on which to refine and interpret all available well data. Nevertheless, producing such a model from raw dip data provides the geologist with insights for reservoir analysis, especially during early field appraisal. An example of these insights is illustrated in Figure 1 and leads to a better understanding of the reservoir structure.

From a geological point of view, two types of information can be used to define the reservoir geometry: seismic data and borehole images/logs. The resolution of seismic data is improving, but if structures are too small (less than 50 m), the average dip is too high, or the velocity contrast is too low, significant structures may be missed on seismic sections. In each of these cases, seismic techniques are insufficient to achieve an accurate structural description of the reservoir (Etchecopar and Bonnetain, 1992). Meanwhile, geologists, petrophysicists, and geophysicists use borehole images, dipmeters and log data in a wide range of applications to reduce the uncertainties.

The model in this paper follows the technique of Etchecopar and Bonnetain (1992), in which they introduced a computer method to produce structural cross-sections from dipmeter and imaging data. The

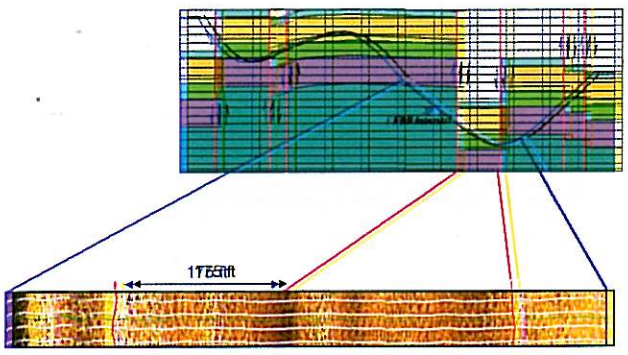


Fig. 1. The faults on this model were interpreted before acquisition of borehole images. The images confirm the fault but clearly show a 175-ft offset from one of the previous (seismic) interpretation.

constructed cross-section is based on a similar fold model (Ramsay, 1967) used to describe folds, faults, and even rollovers.

The interpretation of dipmeter data is not new. Authors such as Busk (1929), Gilreath and Maricelli (1964), Vincent *et al.* (1979), and Suppe (1985) have proposed methods to extract the information by pattern recognition. Others, such as Bengston (1981), proposed new projection methods to make the interpretation of dipmeter results easier.

Although the referenced techniques have greatly improved the structural and geological interpretation of dip data, they do not address the main goal of the geologist, which is integrating all openhole log data into one model in a short time frame.

METHODOLOGY

Our modeling is based on the technique introduced by Etchecopar and Bonnetain (1992), who based their method on two fundamental behaviors of strata during deformation: similar folding and parallel folding. There is a main constraint on the produced model, where they have to be strictly consistent with the dips measured in the well. Even with this constraint, it is often possible to interpret a single dataset as a fold or as a fault, with consistent results in both cases. The final decision about which type of structure is to be used, depends on regional knowledge.

The technique has now evolved into a software that converts a bunch of loose tadpoles into a meaningful structural cross-section. Because of its applicability to different types of structures, it is based on two hypotheses: similarity and cylindricity. These hypotheses imply that the position in space of layer boundaries can be derived from each other by a simple translation along a translation plane.

The current version of the software is devoted to dip data and cannot integrate openhole logs into the constructed cross-section. However, the openhole logs can be integrated into the structural cross-section by populating the lithofacies obtained from the logs along the software-identified bed boundaries using other computer methods (Figs. 2 and 3).

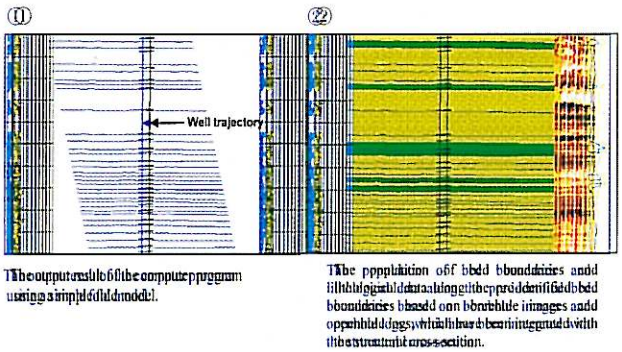


Fig. 2. Steps leading to a 2-D geological model in a vertical well.

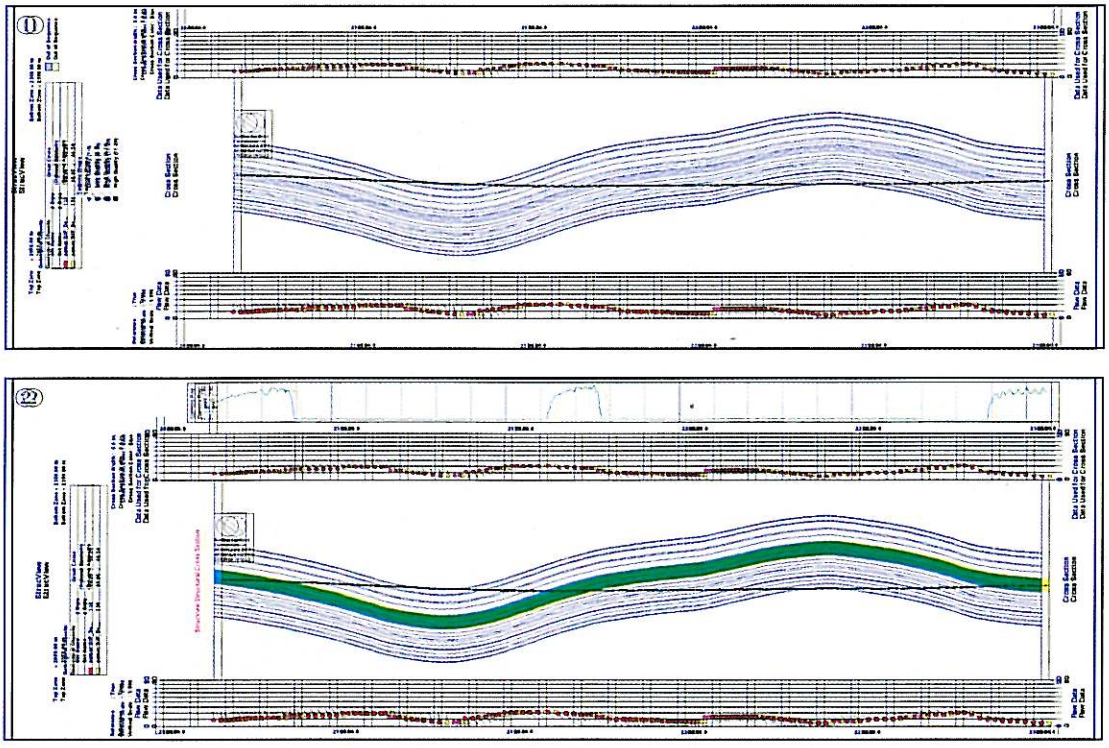


Fig. 3. A simple horizontal well structural model. (1) The output result of the computer program. (2) Using other computer programs we can populate the lithological data on the basis of openhole gamma ray log.

The field example presented in this paper has two types of input data: dips (beddings and faults) obtained from the imaging data (structural model) and the openhole logs (lithology). These two inputs are used simultaneously in a computer method to generate a 2-D geological model, which shows the structural and geological setting of the well.

The ability of the generated model to reflect true structural dip depends on the orientation of the cross-section and the complexity of the structure, because the model is not always perpendicular to the structure. To avoid this situation, different structural zones are computed and plotted beside the cross-section to reflect the real structural dip magnitude and azimuth direction in conjunction with the well trajectory.

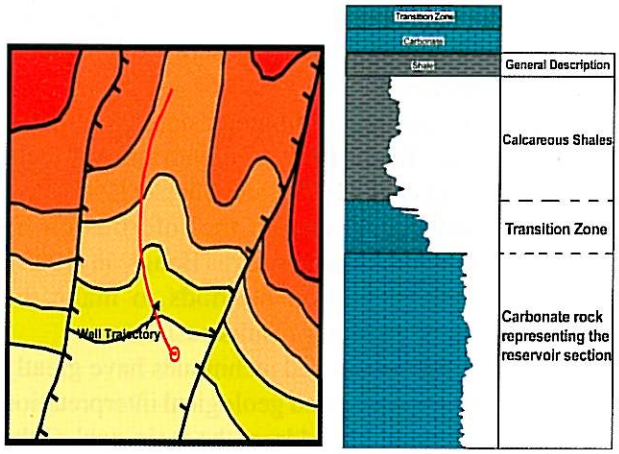


Fig. 4. Schematic drawing of the structural setting of the well before modeling and the stratigraphic summary of the drilled section.

HORIZONTAL WELL CASE STUDY

The number of horizontal wells is increasing, and identifying the geological and structural characterization of the reservoirs targeted by these wells is critical, because of the drastic lateral and vertical changes that occur both in facies or structure. It was not so long ago that reservoir studies were based mainly on cores, openhole logs, outcrop measurements, and, most importantly, seismic data.

Seismic surveys give accurate information in low and simple dip zones, whereas imaging data are more useful in identifying highly variable, steeply dipping zones and viewing sub-seismic features. However, local experience demonstrates that many important structural features cannot be interpreted from seismic data, especially at great depths.

In this case study, 2-D seismic data, interpreted prior to drilling the well, showed a graben and horst system, and no faults were interpreted along the well trajectory (Fig. 4). The structural system, as illustrated, trends to the NE-SW, and there are no other structural trends. During drilling of the 1,820-ft horizontal section, which included 260 ft of the cap rock, a gamma ray log was recorded. After drilling through the cap rock, composed of a thick layer of calcareous shales, the Cretaceous carbonate reservoir section was reached for the second time (Fig. 4).

Borehole imaging data and openhole logs were acquired to resolve the issue of drilling through the calcareous shales and to understand the structure and geology of the reservoir.

BOREHOLE IMAGE INTERPRETATION

The goal of image interpretation is to characterize formation properties. This information assists geologists in their studies and assists petroleum engineers in determining permeability paths and barriers, calculating net pay, and planning of well completions such as perforations and hydraulic fracturing. The interpretation itself is a multi-step process of observation, description, interpretation, and implementation or exploitation (Serra, 1989).

There are different types of imaging tools, and the principle of measurement changes from one tool to the other. The two main types of measurements are resistivity and acoustic (Fig. 5). The imaging tool used in this case study is an acoustic imaging tool. Acoustic images do not normally give sufficient resolution for detailed sedimentological studies, because they are very sensitive to borehole conditions (Hansen and Fett, 2000). However, in this case the

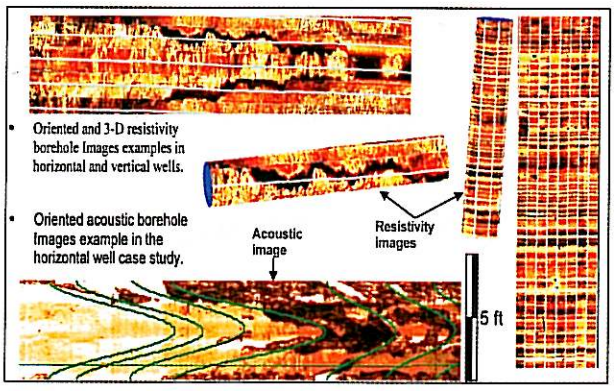


Fig. 5. Resistivity and acoustic images, horizontal and vertical, showing bedding planes.

images fulfill the objective, which is identifying the structural and geological setting of the well.

The high-quality image obtained allowed confident interpretation of bedding, fractures, borehole breakouts, faults, and vugs. Fractures and bedding dips are defined, shown as low- and high-amplitude sinusoidal patterns, respectively. Borehole breakouts are also recognized, seen as axial low-amplitude (dark) bands running along the axis of the image. Vugs are seen as dark spots, randomly distributed or sometimes aligned with bedding planes, with variable shape and size. The fault interpretation is based on the observed termination of bedding planes against the fault plane. This interpretation also includes the sharp changes in the image texture across the fault planes. Seven faults were interpreted on the acoustic images; no faults were interpreted previously from seismic data (Fig. 6). The structural dip is computed using the local curvature technique (Etchecopar and Dubas, 1992).

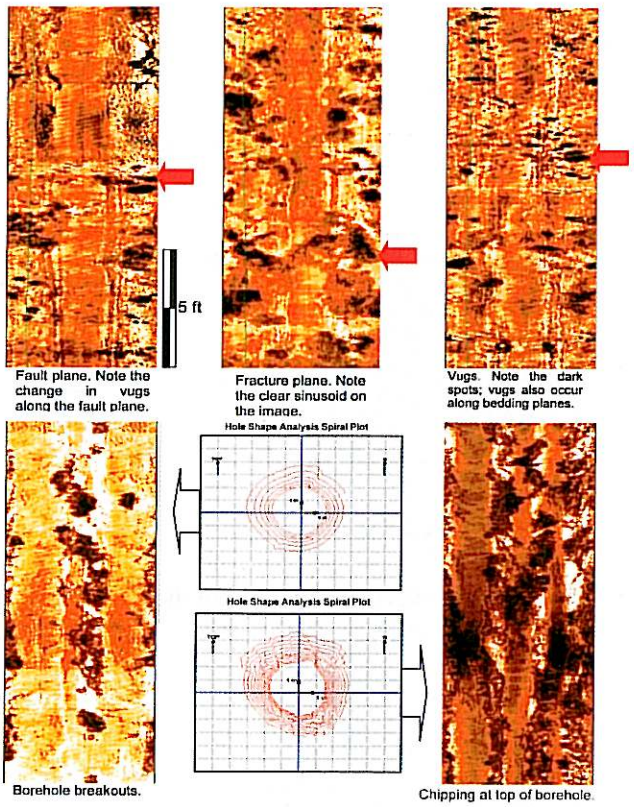


Fig. 6. Acoustic image examples along the horizontal section. All images are oriented top of hole. (After Amer and Abushaala, 2002).

This technique allows the user to subdivide the study interval into different structural zones or sub zones based on major changes in the structural dip magnitude and/or azimuth (Fig. 7). The bedding azimuthal vector plot shows the intra-formation variations of bedding orientation in the uphole

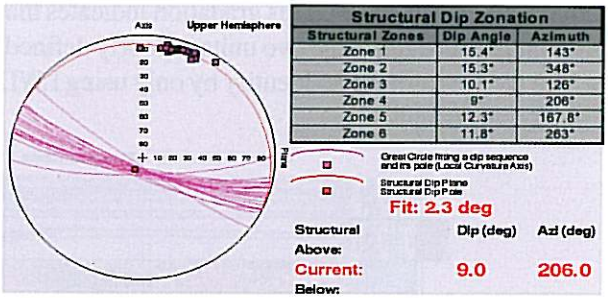


Fig. 7. Structural zonation and a Schmidt plot illustrating the local curvature axis computed over Zone 4.

direction. The bedding azimuth on the vector plot shows SW, S, and SE azimuthal trends (arc shape). These directions coincide oppositely with the well azimuth, indicating the well was drilled in the up dip direction for most of the section (Fig. 8). This up dip drilling is also observed on the geological cross-section, which is discussed in the following section. The vector plot also shows a zone of disturbance where the azimuths are changing drastically. This change outlines a fold, which is confirmed by the acoustic image and the structural dip zonation. These changes in the vector plot are due to the fact that we moved through the axis of the fold, from one limb of the fold to the other.

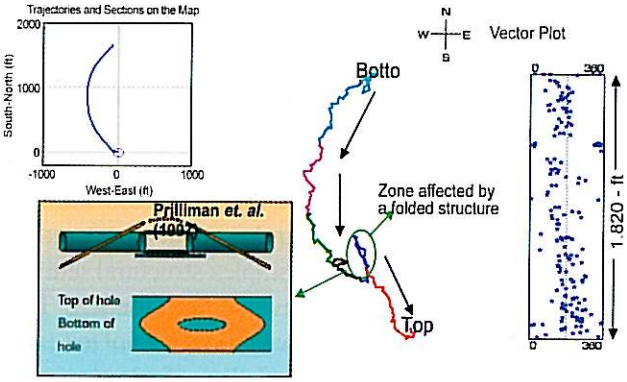


Fig. 8. Well trajectory map view and total bedding vector plot, showing the relationship between the drilling direction and beddings.

2-D MODELING

The integration of borehole images with all other available formation evaluation data is critical for accurate structural and geological assessment, especially during early exploration stages. The integration of this dataset clearly illustrates that the first entry of the well trajectory into the calcareous shales is marked by a vertical gradational change in

lithology (Figs. 4 and 9). This gradation indicates that the contact between these two units is poorly defined, which made it difficult to identify by only using LWD gamma ray data. This transition zone is marked on the ultrasonic images (Fig. 10). The presence of ENE-WSW trending fault resulted in the well trajectory

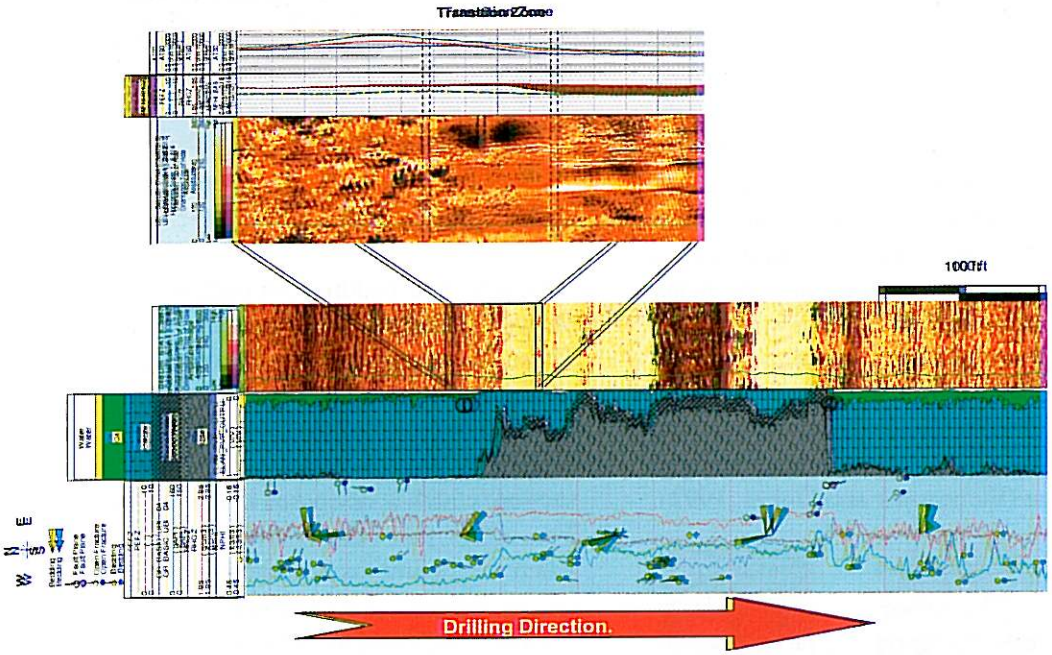


Fig. 9. A part of the well interval that crosses the cap rock. Note the smooth transition in the shale content at Point (1) resulting from the gradational change in facies and the sharp break at Point (2) caused by a fault.

reentering the reservoir zone for a second time. This reentry is very clear on both the acoustic image and openhole logs (Fig. 10).

After analyzing both the borehole images and openhole logs, the cross-section can be computed along a SE-NW, S-N, and a SW-NE line to fit the arc-shaped well trajectory. During cross-section generation, different structural models were used to determine the best fit to the complex structural setting: monocline, anticline, and reverse fault models. The fault displacements on the final model are not to scale, and the relative movement of these faults (reverse movement) are based only on the relationship between the borehole images and openhole logs.

The reverse faulting was unexpected, because this field is known to have a normal fault system. An interpretation of the processed 3-D seismic data confirmed the model with four reverse faults and a structural trap between Zones 3 and 4 (Fig. 10).

The structural dip computed using the local curvature axis technique was plotted beside the cross-section to give the true structural picture. The display revealed a domal structure (fold), a NE-SW striking axis between the two structural zones, Zones 1 and 2. Although this fold is not

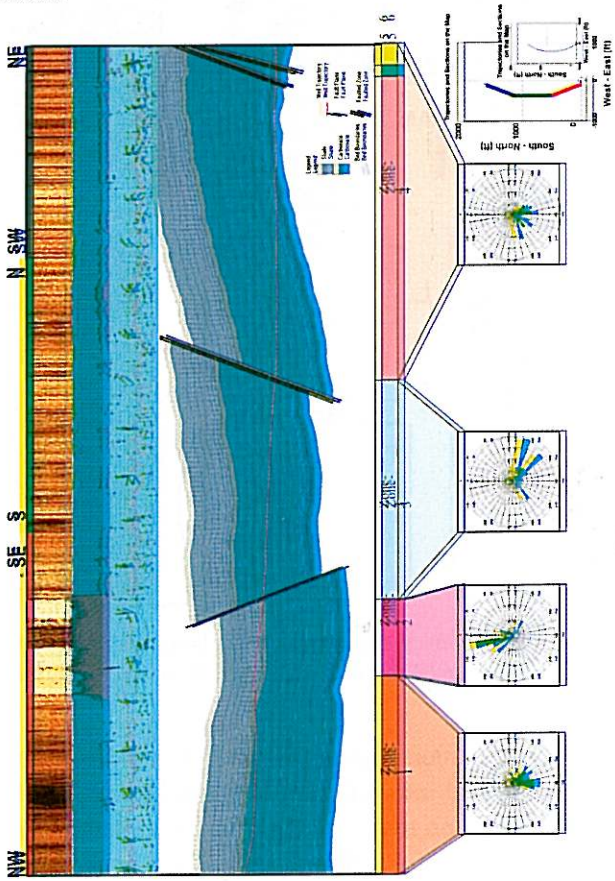


Fig. 10. 2-D geological model and structural zonation and azimuthal plots. The map view shows the direction of the cross-section.

observed on the model because the cross-section direction is not perpendicular to the structure, it is clear from the structural zones, bedding azimuth, and vector plots.

DISCUSSION

The high-quality acoustic image allowed confident interpretation of different geological features (e.g., bedding, fractures, borehole breakouts, faults, and vugs). These interpreted structural and/or sedimentological features added value to the reservoir characterization and increased the resolution of the geological, petrophysical, and seismic models.

The interpreted bed boundaries and fault planes gave a clear picture of the well's surrounding structure and fault systems (Fig. 10). The fractures and vugs were used to calculate the secondary porosity, which has a direct impact on production. The breakouts and borehole chipping analysis will be used to alleviate or avoid future drilling problems (Fig. 6). The fault identification has been used to update the available seismic maps and increase their resolution and accuracy (Fig. 11).



Fig. 11. Schematic drawing of the structural setting of the well before and after updating the map with the modeling data.

CONCLUSIONS

The 2-D geological model, based essentially on borehole images, illustrated a high degree of resolution when the images were integrated with available openhole log data.

The bedding analysis subdivided the logged interval into six structural zones. These zones mark the major changes within the structural dips and include a fold with a NE-SW striking axis. The interpretation also revealed seven reverse faults, and indicates that drilling was in the up dip direction.

The 2-D geological model, which has the same 0.2-in. resolution as the imaging tools, shows a great level of detail and accuracy. The production of such a model from dip data computed from borehole images provides the geologist with insights for reservoir analysis, especially during early field appraisal, when data are limited and uncertainties are high. In addition, this model can be integrated with seismic data for static modeling purposes. The technique is not restricted to horizontal wells; it can also be applied to vertical and deviated wells.

REFERENCES

[1] Amer A. and Abushaala S., 2002. *Fullbore Formation MicroImager and ELAN* Processing and Interpretation,* (Schlumberger internal report).

[2] Anxionnaz, H. and Delhomme, J.P., 1998. Near-wellbore 3-D reconstruction of sedimentary bodies from borehole electrical images. SPWLA Annual Logging Symposium.

[3] Bengston, C. A., 1981. Statistical curvature analysis techniques for structural interpretation of dipmeter data. *Bul. Am. Assoc. Petrol. Geol.*, **65**, 2, 312-332.

[4] Busk, H.G., 1929. *Earth Flexures*. Cambridge University Press, p. 106.

[5] Etchecopar, A. and Bonnetain, J.L., 1992. Cross-sections from dipmeter data. *Bul. Am. Assoc. Petrol. Geol.*, **76**, 5, 621-637.

[6] Etchecopar, A. and Dubas, M.O., 1992. Methods for geological interpretation of dips. SPWLA Annual Logging Symposium proceedings, Paper J.

[7] Gilreath J. A. and Maricelli, J.J., 1964. Detailed statigraphic control through dip computation. *Bul. Am. Assoc. Petrol. Geol.*, **48**, 12, 1902-1910.

[8] Hansen, S.M and Fett, T., 2000. Identification and evaluation of turbidite and other deepwater sands using open hole logs and borehole images, *in* A.H.

[9] Prilliman, Jeff, Bratton, Tom, Fredette, Mark. A, Lovell, John R., Bean, Clarke L., and Hashem, Mohamed, 1997. A Comparison of Wireline and LWD Resistivity Images in the Gulf of Mexico. First published on the *I²S*, November 1997.

[10] Ramsay, J. G., 1967. *Folding and Fracturing Rocks*. New York McGraw-Hill, 568 p.

[11] Serra, O., 1989. *Formation MicroScanner Image Interpretation*. Schlumberger Educational Services, Houston, Texas.

[12] Vincent, P., Gartner J., and Attali, G., 1979. GEODIP—an approach to detailed dip determination using correlation by pattern recognition. *J.Petro. Tech.*, **31**, 232-240.

Petroleum Res. J. Vol. 18 (2005); P. 59-68, 9 Figs.

CO_2 Gas Flooding in Sandstone and Limestone Reservoirs in Hungary

Z. Biró and L. Cziczlavicz*

الغمر بغاز ثاني أكسيد الكربون في مكامن الحجر الرملي والحجر الجيري بالمجر

ز. بيرو، ل. كزيكزلافيكز

أحرزت طريقة الغمر بغاز ثاني أكسيد الكربون بالمجر تطبيقات حقلية واسعة معتمدة على موارد ثاني أكسيد الكربون الطبيعية، وكان أقدم تطبيق على مستوى الحقل بالجزء الغربي من المجر بمكامن الحجر الرملي في حقول بودافا ولوفاسزي، وكذلك بمكامن أحجار الدولوميت والأحجار الجيرية المتشققة والمتكهفة بحقل ناجي لينجيل.

بدأ أقدم تطبيق على مستوى الحقل بعد إجراء بعض التجارب المعملية بالتكاوين الرملية من حقل بودافا عام 1972. وكان الخام المنتج من النوع البارافيني المتوسط وبمتوسط كثافة قدرها 820 كلغ/م^3 (API=41^0).

تم استعمال طريقة الغمر بغاز ثاني أكسيد الكربون في الاسترداد الثلاثي بعد طريقة الغمر بغاز الميثان أو الماء. وأحدثت هذه الطريقة زيادة 1.450.000 م^3 (9.120.000bbl) اليوم نجم عنها استخراج إضافي يصل ما بين 6 – 10% من النفط الخام بالمكمن.

تم استعمال غاز ثاني أكسيد الكربون في التكاوين المتكهفة بحقل ناجي لينجيل المحتوي على نفط ثقيل وغير مشبع، كما تم إنتاج نفط مخلوط بكميات كبيرة من الماء في السبعينيات. وفي عام 1980 بدأت التجارب المعملية بحقن غاز يحتوي على نسبة عالية من غاز ثاني أكسيد الكربون بالمكمن محدثة غطاء صناعي من الغاز. ثم أدخلت التطبيقات على مستوى الحقل عام 1988 ووصل حجم الإضافة اليوم إلى 2.260.000 م^3 (14.215.000bbl). وأثناء مشروع تطبيق الغمر بغاز ثاني أكسيد الكربون تم تطوير عدة ابتكارات في مجال كل من تقنية البئر والتجهيزات السطحية، ويقدم المؤلفون نبذة عن النتائج وتطور تقنيات جديدة في مشروع الغمر بغاز ثاني أكسيد الكربون.

Abstract: *CO_2 gas flooding in Hungary has achieved a wide range of field application based on natural carbon dioxide resources. The oldest field scale application has been applied in the western part of Hungary in sandstone reservoirs of Budafa and Lovászi fields, as well as in the fractured, karstic limestone and dolomite reservoirs of Nagylengyel field.*

After some pilot tests, the first field-scale application started in the sandstone formations of Budafa field in 1972. The produced crude is of an intermediate-paraffin character, its average density is 820 kg/m^3 (41 degrees API). CO_2 gas flooding has been used as a tertiary recovery following the CH-gas or water flooding. 1,450,000 m^3 (9,120,000 bbl) incremental oil has been produced to date, resulting in 6-10 % of original oil in place (OOIP) additional recovery.

Carbon dioxide was also applied in the karstic formations of Nagylengyel field containing under-saturated heavy oil. Crude oil was produced with high water cut in the 70's. In 1980, a pilot test was started injecting high CO_2 content gas into the reservoir, creating an artificial gas cap. The field-scale application was introduced in 1988. Incremental oil volume to date is 2,260,000 m^3 (14,215,000 bbl).

*MOL, Plc., Hungary.

During the implementation of the carbon dioxide flooding project, several innovations had been developed both in well-technology and in surface facilities. The authors give summary of the results and development of new technologies at the carbon dioxide flooding project.

INTRODUCTION

Hungary, located in the central part of the Carpathian Basin, has got two petroleum super systems:

- the older one is discovered and exploited oil and gas from pre-Tertiary reservoir rocks (predominantly fractured limestone, dolomite and metamorphites)
- the younger one is found in Tertiary clastic reservoir rocks.

The country was able to meet the oil demand in the late thirties and early forties with a modest surplus for export to Western Europe.

The strong industrialization in the fifties and sixties and the growing demand for the petroleum as energy source, in general, and growing appetite of the industry, in particular, changed the situation and Hungary became an oil importer. In this context, it was a necessity to be able to enhance the oil output of the domestic fields.

As a consequence, the simplest secondary methods to maintain the reservoir pressure (re-injection of the associated gas produced or water injection) have been intensively applied since the early forties.

Laboratory and pilot tests allowed full scale field application of different in-situ combustion methods which were applied to a low API gravity oil in an Oligocene sandstone reservoir in the northern part of the country. The experience accumulated during the design and implementation phase of this method allowed exporting this knowledge in the form of a joint pilot project to countries such as Canada, India and the Soviet Union.

With the commissioning and continuing depletion of the multi-layer Algyõ field with a number of oil pools both with saturated and under-saturated oil deposits, laboratory and pilot projects applying tertiary recovery methods (such as polymer injection and micellar solutions) were started and successfully implemented

The most successful method, however, was CO_2 injection in both sandstone and limestone reservoirs. The application of the principles of the subsurface displacement processes were introduced first in the sandstone reservoirs of Bázakerettye, Lovászi fields in Western Hungary. This method in young (Miocene and Pliocene) strongly stratified reservoirs after a reasonably long period of successful water flooding is the first item of this presentation. The second half of this paper outlines the history, results and lessons learned from the application of the CO_2 injection method in a karstic limestone reservoir.

The CO_2 source was available from high-pressure/high-rate wells producing from natural reservoirs. High-pressure pipelines were built to transport the gas to the fields where it was injected, so pressure boost was required only for re-injection. An extensive workover program was required to re-complete the existing old wells. New wells were also drilled as infill wells and as replacement of old wells having critical conditions. Material selection of downhole equipment was of critical importance. Corrosion monitoring and mitigation have been a critical issue throughout the project.

Location of above-mentioned fields is shown in Figure 1.

CO_2 GAS SOURCE

In the region of Budafa field a carbon dioxide natural gas reservoir had been developed in 1968 which had more than 10 billions m^3 of original gas in place (OGIP). The gas exists in the Miocene coarse clastic rock at 3200 m depth. Initial reservoir pressure was 33 400 kPa, and the reservoir temperature is 165 °C. Characteristic composition of the produced gas is as follows: 80 to 81 mole % CO_2, 16-17 mole % HC, 2 mole % N_2 and 0.3 to 0.4 mole % H_2S.

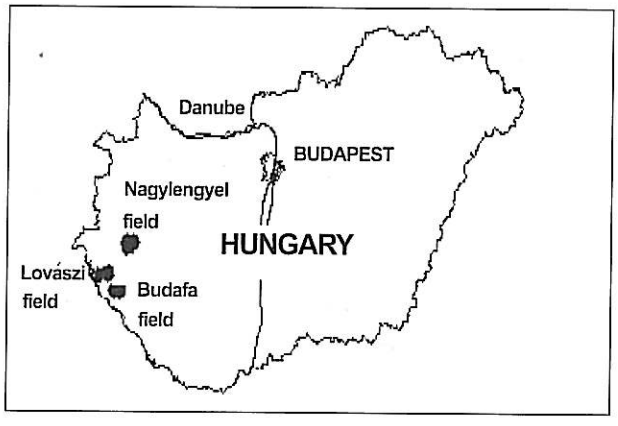


Fig. 1. Location of Budafa, Lovaszi and Nagylengyel fields.

The reservoir has very strong water drive and good hydraulic characteristics. The reservoir was exploited by three wells, with maximum production capacity of one million m^3/d at 16000 kPa well-head pressure. Thus, the gas can be injected into the crude oil reservoirs without using any compressors.

CO_2 Gas Flooding in Sandstone Reservoirs

In Budafa and Lovászi fields the oil is found in layers between 1000 and 1500 m below the surface. The reservoir rock is sandstone. Average porosity of the formations varies between 17 – 22 % and the average permeability varies between 30 – 100 mD.

The reservoir oil is of intermediate-paraffin character, its density is 820 – 830 kg/m^3 (40-38°API) at standard conditions. In the initial phase of recovery, the oil was saturated with hydrocarbon gas. Most of the reservoirs possessed initial gas cap. The initial pressures ranged from 10,000 to 15,000 kPa, and the reservoir temperature is between 60-80 °C.

Hydrocarbon production began in Budafa field in 1937 and in Lovászi in 1940. By the 1st of January 2003, cumulative oil production from Budafa field was 6.8 million m^3 and the recovery factor was 33.5 %, whereas from Lovászi field the total oil produced was 8.1 million m^3 and the recovery factor was 30.9 %. The natural edge water inflow was very weak and the reservoir pressure decreased significantly during production. Hydrocarbon gas re-injection was started in 1939 and 1944 in Budafa and Lovászi, respectively. This method resulted in 2.4 million m^3 incremental oil which implied a recovery increase of 5.27 % with respect to the area recovered by that method. In an advanced stage of production, water injection was initiated in 1953 and 1954 in Lovászi and Budafa, respectively. The water flooding was not successful as the incremental recovery factor was only 1.46 % of the OOIP.

After running the necessary laboratory tests, a pilot test was started in the Upper Lispe formation in 1969 using natural CO_2 gas. Before starting the experiment, CH gas and water–injection were performed. The oil recovery factor was 35.2 % OOIP. The pilot experiment was completed in 1980. The produced incremental oil was 67,600 m^3, and the incremental oil recovery factor was 10.13 %.

Field-scale application was started in the Budafa-West formation of the Budafa field in 1972 and in the Kiscsehi layers in 1974. Figure 2 shows a typical cross-section and Figure 3 the annual oil production rate of Budafa-West. Following the favorable

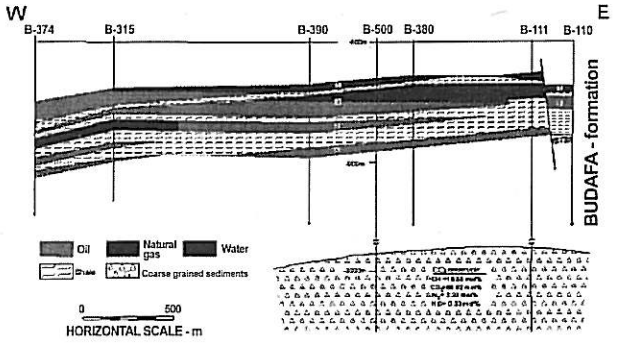


Fig. 2. Cross-section in Budafa west unit.

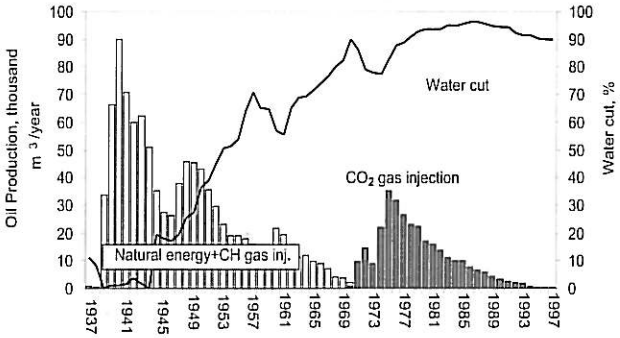


Fig. 3. Production history of Budafa-west unit.

experiences, the CO_2 natural gas was transported in pipeline to Lovászi field, where the EOR applications were begun in 1975-77. Thereafter the exploitation was continued in the Zala and Kerettye formations of Budafa field in 1981. The basic data is summarized in Table 1.

Due to the high reservoir temperature, miscible displacement could not be reached but a partial miscibility could be achieved. The carbon dioxide exerts its favorable effect, first of all, through the swelling of the oil. In the first phase of recovery, the natural CO_2 gas was injected into the reservoir through injection wells in order to increase the reservoir pressure which has declined in the primary recovery stage to its initial value. During this process, a controlled production was being performed to ensure the high (60-70 mole %) carbon dioxide concentration of the solution gas of oil. It was a fundamental condition for the success. After that, water was injected into the reservoir through the same injection wells. At those reservoirs where the produced fluid became poorer in CO_2 or in order to achieve favorable volumetric sweep efficiency, a cyclic gas-water (WAG) injection was performed.

The results of CO_2 gas flooding in Budafa and Lovászi fields have been presented in the literature. [1] Nowadays, these fields are entering a more mature phase of development. Up to date, 1,457,000 m^3 incremental oil has been produced,

Table 1. CO_2 gas flooding in sandstone reservoirs of Budafa and Lovászi fields.

Field Discovered	Budafa 1937	Budafa 1937	Budafa 1937	Budafa 1937	Budafa 1937	Lovászi 1940	Lovászi 1940
Pay zone	Upper-Lispe	Budafa-West	Kiscsehi	Zala	Kerettye	Lovászi-East	Lovászi-West
Productive area, km^2	0,7	3,5	0,9	4,1		1,4	2,3
Average depth, m (subsea level)	980	848	842	870	970	1285	1285
Mean porosity, %	21,5	21,0	20,0	21,0	20,0	17,2	17,2
Mean permeability, D	0,022	0,100	0,050	0,132	0,096	0,030	0,030
Initial pressure, kPa	10 100	9 800	9 400	10 000	11 080	15 250	15 250
Pressure at the end of primary production, kPa	3 600	2 900	5 660	3 580	6 430	9 200	5 920
Reservoir temperature, °C	68	64	64	63	69	83	83
Oil density at 20°C, g/cm^3	0,834	0,817	0,817	0,819	0,835	0,823	0,823
Oil viscosity at reservoir temperature, mPa.s	1,16	1,15	1,15	0,80	1,04	0,40	0,40
Formation volume factor	1,224	1,225	1,225	1,192	1,257	1,245	1,245
Primary recovery efficiency, %(OOIP)	35,20	22,57	29,14	31,87	34,30	31,02	38,78
Start date of CO_2 inj.	1969	1972	1974	1981		1975	1977
Producing wells	19	71	17	77		27	40
Injection wells	5	42	14	60		34	44
Oil saturation at start, %	40	50	45	42	41	44	40
Inj. CO_2gas up to 1st January 2002, million m^3	92	719	158	1168		372	784
Incremental oil recovery up to 1st January 2002 10^3m^3	67,582	310,906	60,244	540,480		163,176	304,730
Tertiary recovery, %(OOIP) 1st January 2002	10,1	7,0	13,3	6,54		6,7	10,1

resulting in an incremental recovery of 6-10 % of original oil in place.

CO_2 Gas Cap Applications in Limestone Reservoirs

Another type of reservoir can be found in the Nagylengyel field discovered in 1951. The crude is a heavy oil with high density (950-980 kg/m^3 i.e. 17-12° API) and high viscosity. The fluid contains practically no dissolved gas. The fractured, cavernous formations were created by karstic corrosion. There is practically no oil in the matrix of the rock. Most of the oil accumulated in the Upper Cretaceous limestone and Triassic dolomite formations, which contain hydro-dynamically separated blocks as a result of the structural movements. Most reservoirs have very strong water inflow, so natural water drive served as the primary source of energy during primary recovery.

Until the 1st of January 2003, some 21.5 million m^3 oil was produced and the average recovery factor was 47.9 % OOIP. During the primary recovery period, the water influx became more and more extensive and the water cut stabilized at about 95-98 % by the end of 1970s. In the 1960s, some pilot tests for enhanced oil recovery (EOR) had already began. Tests using surface active agents and ammonium hydroxide were not successful for field scale applications.

Analysis of the reservoir structure and performance indicated that creating an artificial gas cap would be the most effective recovery method. Figure 4 shows the basic forms of the driving mechanism.

Complicated physical, chemical and hydrodynamic conditions are taking place during this special recovery so the process could not be modeled in the laboratory. That was the reason why it was absolutely necessary to carry out pilot test before the field scale applications. The gas cap can be established theoretically by any gas, however, economic considerations supported the utilization of impure carbon dioxide natural gas discovered in the Budafa field.

The pilot test of forming a CO_2 gas cap started in 1980 in the Southern Triassic block of the field which

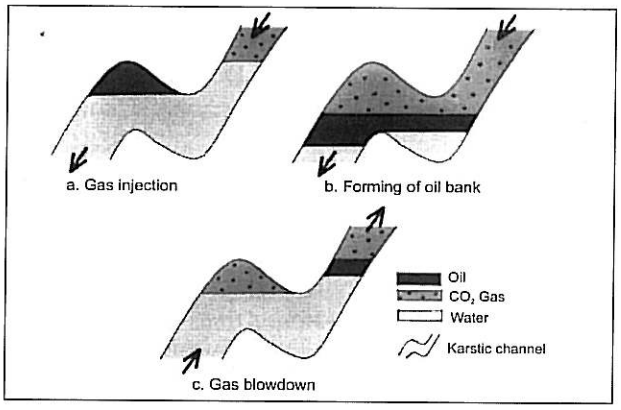


Fig. 4. Driving mechanism of CO_2 gas cap flooding.

has minor oil reserves and ended in late 1996. The characteristics of the reservoir are summarized in Table 2. Approximately 100.2 million m^3 gas were injected and 122,000 m^3 incremental oil was produced up to September 1996, which equals 10.4 % incremental recovery factor. More details of the pilot test are described in reference 2.

Based on the initial results of the pilot test it was decided to extend this technique to the whole Nagylengyel field in three stages. The annual oil production rate of the field is illustrated in Figure 5. The first stage was realized in the Block I-IV.

Table 2. CO_2 gas cap recovery of Nagylengyel field.

Reservoir properties	Pilot	Phase I.		Phase II.		
	South-Triassic block	I-IV rudistic block	VII.rudistic block	VIII rudistic block	X. North rudistic block	X. South rudistic block
Block area, km^2	0,8	11,7	3,1	5,5	2,3	2,7
Height of oil column, m	163	340	135	212	159	152
Depth at original water-oil contact, m (subsea level)	2290	2040	2010	2200	2200	2200
Initial pressure at OWOC, kPa	23 100	20 700	20 600	22 400	22 360	22 300
Reservoir temperature, °C	124	114	124	84	94	94
Mean porosity, %	2,5	1,2	3,4	1,8	0,8	1,9
Mean permeability, D	3,6	3,8	5,0	5,0	1,0	5,0
OOIP, million m^3	1,171	16,258	5,589	8,320	1,280	2,963
Stock-tank-oil gravity, g/cm^3	0,960	0,947	0,974	0,972	0,983	0,980
Oil viscosity at reservoir condition, mPa.s	92	18	49	137	125	137
Primary recovery, million m^3	0,493	6,880	2,804	4,194	0,447	1,699
% (OOIP)	42,1	42,3	50,2	50,4	34,9	57,3
Start of CO_2gas cap recovery	Sept., 1980	Oct., 1988	Jan., 1993	Aug., 1994	Nov.,1996	Apr., 1995
Producing wells	7	105	35	44	9	22
Injection wells	1	11	2	4	-	2
CO_2 gas injection, million m^3	100,0	1851,8	470,6	1094,9		560,2
Start of blown down gas	Marc., 1985	Aug., 1994	Oct., 1997	Oct., 2000		Febr., 1999
End of project	Sept., 1996	Sept., 2000	Cont.	Cont.		Cont.
CO_2 gas production through to 1 Jan. 2003, million m^3	55,5	1214,3	320,6	426,2		291,6
Incremental oil recovery through to 1 Jan. 2003 million m^3	0,122	1,732	0,145	0,133	0,032	0,169
%(OOIP)	10,42	10,65	2,58	1,59	2,50	5,70

Block I-IV has the greatest reserves in the field. The OOIP was 16.3 million m^3. The Upper Cretaceous reservoir rock is biogenic limestone of shoreline origin. Reservoir space was formed on the impact of the authigenic (uncovered) karstification during a subaerial period before Miocene. The 0.5 % original porosity of the rock increased to 4 to 6 % in the erosion zone as a result of karstic corrosion. The crude oil is of paraffin-intermediate base, its density at 20°C is 947 kg/m^3 (17°API), and the viscosity at reservoir conditions is 18 mPas. Oil-water contact was originally at 2040 m below surface. The initial reservoir pressure and temperature were 20,700 kPa and 114°C, respectively.

Production from Block I-IV started in 1951. The peak production was reached in 1955 with 1.1 million m^3/year. By the end of 1967, most wells were producing at >90 % water. Oil produced during the primary recovery stage was 6,880,000 m^3, corresponding to 42.3 % of the original oil in place.

The EOR application was carried out using 11 gas injectors and 105 producers. The gas injection was started in October 1988 and terminated in August 1994. The cumulative gas injected was 1.852 billion m^3. Thereafter, the blow-down of the gas started and it was placed into the blocks of the second stage without compressors. The project was terminated in September 2000. By that time, 1,732,000 m^3 incremental oil was recovered corresponding to an additional recovery factor of 10.65 % of the original oil in place.

Blocks # VII, VIII, and X were used for stage II of the CO_2 gas cap flooding. Reservoir rock is Upper

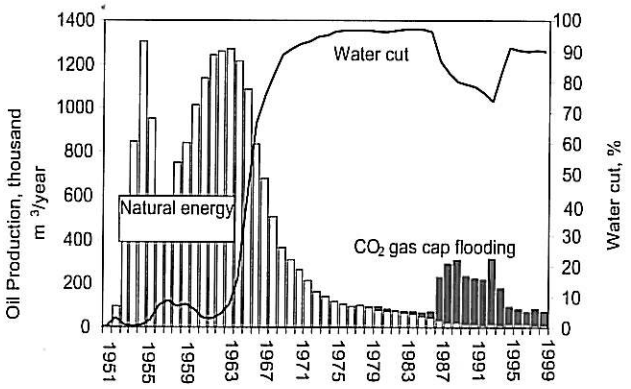


Fig. 5. Production history of Nagylengyel field.

Cretaceous biogenic limestone similar to Block I-IV. But the karstification can be characterized mainly by allogenic (covered, so called "B" type) processes. Principal geologic and reservoir engineering data are given in Table 2.

CO_2 gas injection into the blocks started at different dates between January 1993 and April 1995 and was terminated between October 1997 and October 2000. Approximately 2.126 billion m^3 of cumulative gas was injected into the reservoirs. The gas blow-down is still continuing now. The incremental oil was 477,800 m^3. Stage III is under discussion and preliminary design.

To date, 2,381,000 m^3 incremental oil has been produced from the blocks of Nagylengyel field. More information about this project is written in the literature [3].

WELL COMPLETIONS

The CO_2 producers are completed with 4 ½" gas-tight tubing. A typical HP/HT completion was selected because of the high bottom-hole temperature and the corrosive environment. Permanent drillable packers are used with Seal Bore Extension. Storm Choke is installed to prevent gas leak to the air in case of a wellhead failure. It was noted that corrosion is a problem in the upper section only (where water condensates). To reduce completion cost, it was decided to use carbon steel tubing. To mitigate corrosion, batch type inhibition treatment was applied. To eliminate elastomer problems, metal-to-metal seals were used on the wellhead installation.

The wells used for CO_2 recovery were typically 20-40 years old at the time when the CO_2 gas injection was initiated. An extensive recompletion program was required to modify the original completion and to keep the wells in proper condition to minimize operational problems.

Typical operations carried out were as follows:

- drilling deeper (where it was required)
- logging to evaluate cement bond and base log for evaluating gas migration during the CO_2 recovery
- squeeze cementing to repair cement sheath
- squeeze cementing to shut-off perforations
- re-perforate
- acid stimulation
- casing integrity test
- repair damaged casing (inside or outside casing patch)
- remove old wellhead and install new wellhead and Xmas tree to fit to the special requirements
- run completion equipment
- test the integrity of the final completion with gas (air or nitrogen).

It was of critical importance to check and repair every well (even the plugged wells) which were found within the area of CO_2 recovery, because a seal above the reservoir was necessary to prevent gas migration from the reservoir.

In some cases new wells were drilled. In sandstone reservoirs the new wells were drilled as infill wells to improve sweep efficiency. In Nagylengyel field, new wells were used generally for injection purposes because of safety reason, to replace old wells with poor casing condition.

The CO_2 injectors were completed with permanent drillable packers and gas-tight tubing. In the case of sandstone reservoirs, 2 7/8" J-55 EU tubing with Teflon ring was installed, while in Nagylengyel field metal/metal seal gas-tight connections were used to improve well safety.

Downhole Injection Safety wells and Storm Chokes were used in Nagylengyel field to avoid leakage to the air in case of a wellhead failure. Elastomers were selected carefully to meet the requirements. Viton and Teflon were used successfully in the field.

Sucker Rod Pumping is the general means of mechanical production. 13 Cr alloyed steel with controlled hardness is used widely to reduce corrosion/erosion of pump parts. Pumping wells were converted to flowing well with packer type completion when gas production was high enough to keep the well flowing.

NACE MR01-75 was taken into consideration in all completion and live well operations. Law-alloy carbon steel with controlled hardness was selected where appropriate, but in critical areas 9Cr1Mo materials were selected (*e.g.* wet parts of the packer and completion equipment below packer).

To design reliable and economical completions, a detailed analysis of the conditions and requirements was essential. A typical example illustrating the logic of completion design of the CO_2 injection well in Nagylengyel field is shown in Figure 6. A typical completion used in Nagylengyel field is shown in Figure 7. The Single String Two Zone Alternate Completion is suitable to isolate the zone which is producing with high GOR. The upper zone can be produced through a choke to lift the fluid produced from below.

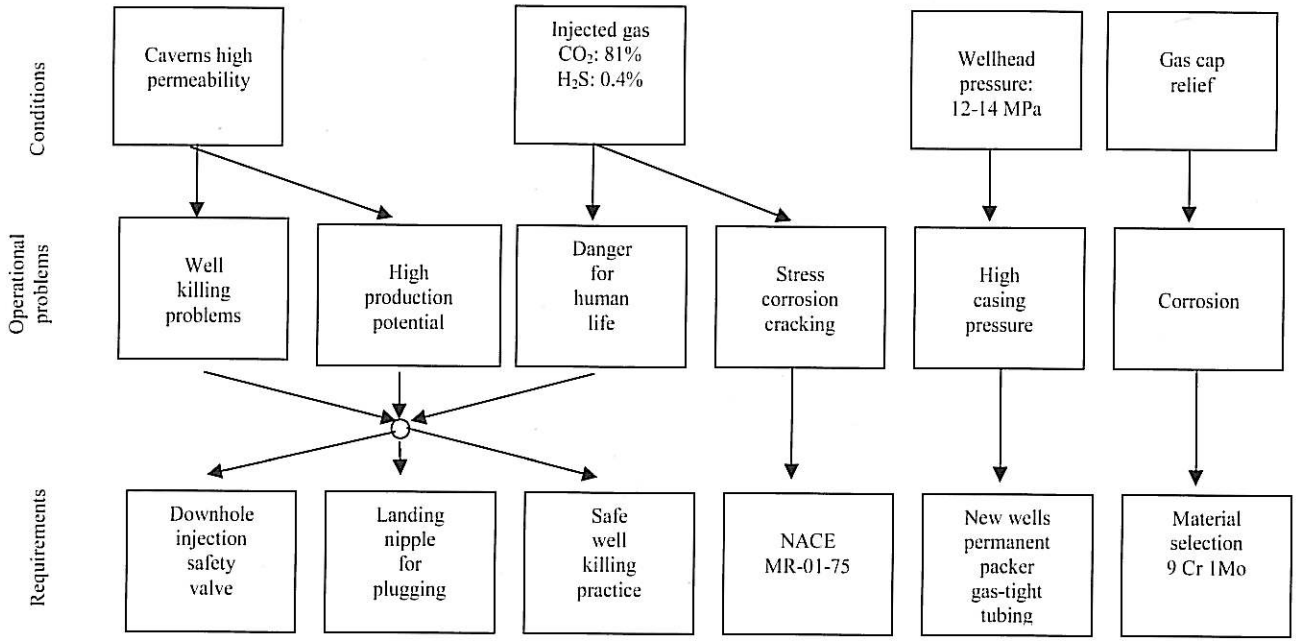


Fig. 6. Completion requirements of CO_2 injection wells in Nagylengyel field.

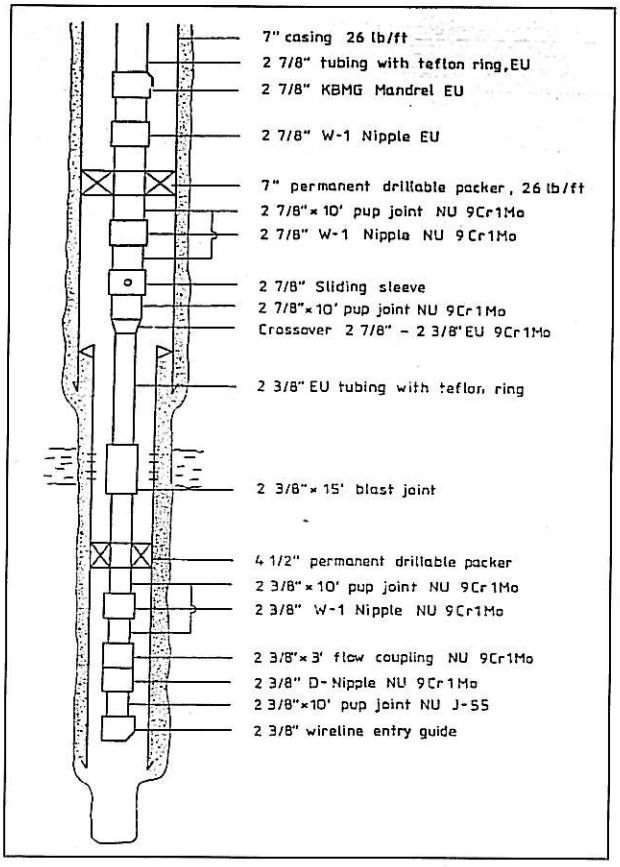


Fig. 7. Completion of selective production well in Nagylengyel field.

SURFACE FACILITIES

Two levels of technical advancement were accomplished in the design of surface facilities. At the beginning, all the facilities were simple and traditional. However, with more and more field experience and study of international literature, more sophisticated processes, methods, equipment and accessories were designed and applied.

Production, Transportation and Injection of CO_2 Gas

CO_2 gas was produced in Budafa Field from deep wells. Initially 3 production wells were used, then increased to 5 in the final stage. At the early stage the well site facilities of the CO_2 production wells were equipped with stainless steel, but for the piping system carbon steel was used. Concerning the gas treatment, it was decided not to remove the H_2S contamination, because of economical reasons. Figure 8 shows a schematic of the surface system at the early stage.

Initially the aim of gas treatment was to achieve a dehydration level necessary to avoid hydrate forming in the transportation and injection systems. The temperature of the produced gas at the wellhead was about 100°C. The gas was cooled to 45-75°C in a gas-gas and a water-gas heat exchanger. Free water was knocked out then the gas was reheated to 60-75°C by gas-gas heat exchanger. This simple treatment was good enough for short distance transportation (the distance between Budafa and Lovászi fields is about 11.3 km). Because of the very low soil temperature, methanol injection was used to

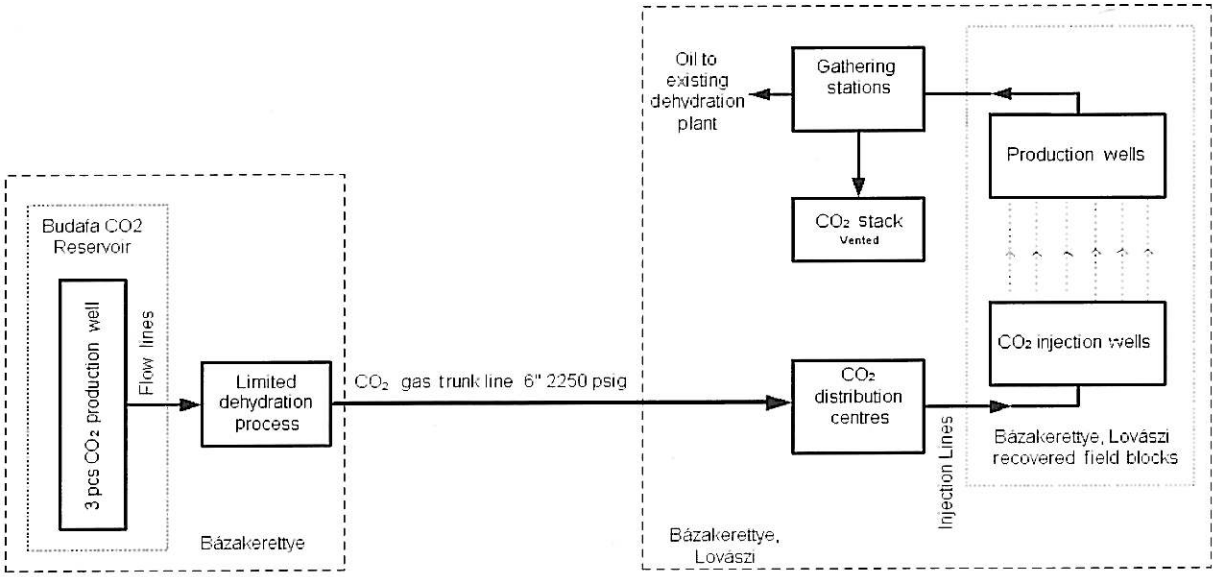


Fig. 8. Schematic of early surface system of CO_2 recovery.

prevent hydrate formation. There was no substantial pressure drop during the process so no compression was required to inject the CO_2 gas.

A higher technical level was accomplished in Nagylengyel field. The schematic of surface facilities at this stage is shown in Figure 9. The well site of CO_2 production was redesigned. Surface section of piping and all the accessories were replaced by stainless steel ones with 316 L material. The distance between Budafa and Nagylengyel field is about 34 km. The previous simple gas treatment was not acceptable for this range of transportation. A high-pressure, glycerol gas treatment plant was built, so the natural energy of the CO_2 source reservoir can be utilized to eliminate the need of compression to inject the gas in Nagylengyel field. The usual glycol as an absorbent for dehydration was not acceptable because it dissolves in the high pressure CO_2 gas stream causing a significant glycol loss. For high-pressure CO_2 stream, the glycerol proved optimal absorbent medium for dehydration. All the materials of the dehydration process on the wet gas side, piping and vessels were made of 316 L stainless steel. There were no transportation problems as the result of -5°C dew point of the treated gas. Individual injection lines were built to each injection well. The CO_2 gas was injected into the wells through distribution stations in the field.

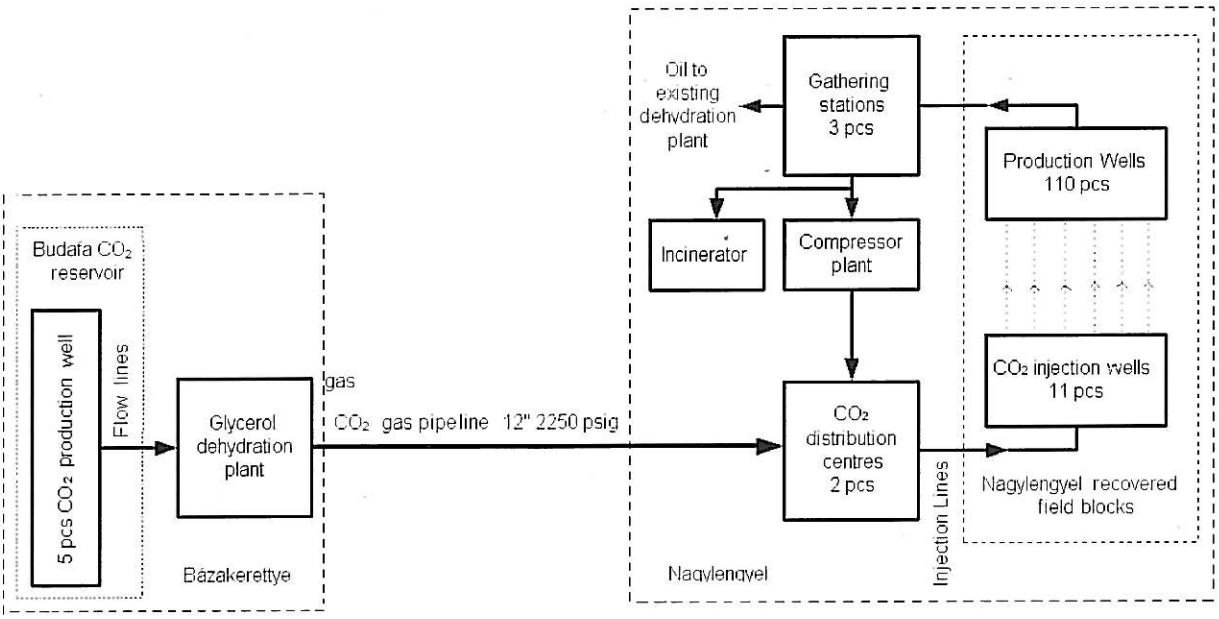


Fig. 9. Schematic of surface system of CO_2 recovery in Nagylengyel field.

Water Injection

In Budafa and Lovászi fields, the CO_2 injection was followed by water injection. Water was injected continuously or alternately (WAG). Formation water was mixed with fresh water. Following sedimentation, filtration and chemical treatment the water was injected with reciprocating pumps. The same injection lines used for CO_2 injection were used for water injection.

Surface Production Facilities

In Budafa and Lovászi fields, sucker rod pumping was used for mechanical production. Separation of the gas from the oil and water occurred in conventional metering stations. Oil was separated and treated in the central tank farm. Because of economic reasons the associated gas was vented into the atmosphere.

In Nagylengyel field initially radial gathering system with tank stations was built, but in the 2nd phase, due to economic reasons, a gathering header system was developed. Oil is treated in the central gathering station. The associated gas is reinjected and circulated to other blocks. On the gathering side also, significant advancement occurred. The associated gas with high CO_2 content was gathered, compressed and reinjected into a subsequent block of the reservoir. In case of compressor failure the low pressure associated gas was incinerated to convert the toxic H_2S content into less dangerous SO_2. During the blow-down phase in Nagylengyel reservoir an interesting method was used.

Between the block designated to blow-down and the subsequent block designated to gas injection, a gravitational stream (without any artificial pressure increase) is usable due to the special behavior of CO_2.

Certainly this gravitational stream can only take place in such a strongly fractured reservoir like Nagylengyel, in which there is, practically, no bottom-hole pressure drop/increase either in the blowing down or in the injection wells. In the Nagylengyel field, the dynamic flowing well head pressure can be higher than the static one in case of high CO_2 content gas mixture. If the surface system, especially the buried pipe system assures some temperature loss between the gas production and the gas injection well, the well head pressure on the injection well head is sufficient to inject the desired gas stream.

As for the emergency blow-down system, a further special phenomena was observed: the emergency blow-down system which consists of pressure vessels and pressure piping containing natural gas with high CO_2 content in the different sections of the system, CO_2 water hydrate, CO_2 liquid ice water and solid CO_2 can be formed due to the very low temperature during blow-down.

To prevent the consequences of this very dangerous situation, in case of a quick emergency, blow-down the initial method was to design a multi-step heating-expansion system. If it is desired to blow-down significant gas stream quickly, then huge heat exchangers and huge sources of heat were required for a short working time.

Based on our experience, if the route of the gas to be blown down is designed without sacks or sharp corners, all the multi-phased stream can be blow-down and solid particles can be swept without plugging the system. No separator, slug catcher *etc.* are built in. In case of sophisticated elaboration of the blow-down system, the high capacity of heat exchangers and heat supply system can be spared. Special steels are used to work in the low temperature environment.

CORROSION

Corrosion mitigation was a key issue throughout the recovery. The following measures were taken to reduce and solve the problem of corrosion:

- corrosion monitoring (coupons, wall thickness measurements, water analysis)
- failure analysis
- inhibition
- proper gas treatment (eliminate free water)
- reduce flow stream velocity (pipe diameter)
- select corrosion resistant materials in critical technologies (*e.g.* glycerol gas treatment)
- select proper materials for downhole equipment
- planned replacement of components of the technology, based on expected life and measurements, or visual checking
- plastic inner coating (e.g.: tanks).

Continuous corrosion monitoring is very important from the point of view of safety and smooth operations.

ENVIRONMENT PROTECTION

At the beginning of the seventies, the environment policy was not as strict as it is nowadays. Since then,

the protection of the environment has become a very sensitive subject. Both the associated and the cap gas have to be gathered and reinjected. Emergency blow-down into the air can be radically reduced by dividing the system into smaller volume sections by ESD devices which simultaneously and automatically close the gas source.

The development of process engineering, instrumentation and automation gives a lot of possibilities into the hand of the engineers to reduce or eliminate the emission of hazardous gases into the environment. The cost of these investments has to be taken into consideration during the economic evaluation of future projects.

CONCLUSION

CO_2 gas flooding is an effective process to increase oil recovery in sandstone and karst type limestone reservoirs. Analysis of downhole and surface conditions and requirements are essential to design downhole completions and surface facilities suitable for CO_2 injection and production. Continuous improvement is required based on operational experiences.

REFERENCES

[1] Szittár, A., Biró,Z, 1983 (March). Carbon dioxide injection in south-west Hungary. CO_2 EOR Symp. Budapest.

[2] Biró,Z., Szittár,A., 1989. CO_2 gas cap field test in karst type reservoir of Nagylengyel field. 5th European Symposium on IOR, Budapest.

[3] Biró,Z., Gerecs,L., Udvardi,G., Pógyor,K, 1994 (June). A new heavy oil recovery technique for Nagylengyel field in Hungary. THERMIE European Symposium, Berlin.

[4] Biró,Z., Udvardi,G., 1997. CO_2 gas cap recovery for Nagylengyel field in Hungary. THERMIE EOR in Albania Symposium.

[5] Cziczlavicz,L., 1991 (Jan.). A másodlagos-harmadlagos mûvelés kútkiképzéseinek tapasztalatai (Experiences gained in connection with the well completion during the secondary–tertiary exploitation) Kõolaj és Földgáz 24. (124.)

[6] Cziczlavicz,L., Szittár,A., Udvardi,G., 1989 (April). CO_2 EOR facilities in Hungary. Fifth European Symposium on Improved Recovery. Budapest.

Petroleum Res. J. Vol. 18 (2005); P. 69-80, 12 Figs.

Naturally Fractured Reservoirs – Modeling and Simulation Methods

Leonhard Ganzer* and Diethard Kratzer**

مكامن متشققة طبيعيا ـ طرق نمذجية ومحاكاة

ليونارد قانزير، ديثارد كراتزير

تلعب التشققات الطبيعية أو التي هي بسبب ما، دوراً حاسما في عدة مكامن نفطية، وبالرغم من أن نسبة صغيرة من النماذج تصف اليوم التشققات أو شبكات التشققات، فإنه يمكن لفرد أن يدعى أن معظم المكامن متشققة عمليا. وبالنظر إلى أهميتها التجارية، رغم تعقيداتها، فقد كانت المكامن المتشققة موضوع دراسات متعددة في العقود الأخيرة.

ستحاول هذه الورقة تقويم الوضع الحالي وتقويم طريقة نمذجة مكامن نفطية متشققة وسيتم التركيز وبصورة رئيسية على تطورات حديثة في مجال نمذجة ساكنة ونمذجة مناسبة ومتحركة لمكامن متشققة، وأثر آخر تقدم في نمذجة قدرات منظومة ساكنة في سير العمل التاريخي القديم وأدخلت تطورات جديدة في مجال محاكاة المكمن.

ومنذ بداية التطور التاريخي لنماذج محاكاة المكمن المزدوج والمفصل تمت إعادة النظر لعدة طرق محاكاة مكامن هيدروكربونية متشققة.

سيتم مناقشة عدة طرق تبدأ من مراجعة صيغ مألوفة ثم تنتقل إلى نموذج المسامية المزدوجة التقليدي ثم إلى نماذج شبكة مفصولة متشققة. وتتمتع كل الصيغ بمميزات ولكن لديها عجز عند وضعها بعضا من خصوصيات المكامن المتشققة.

حاولت صناعة النفط حديثا دمج المعلومات من كل المصادر المتاحة لكي تخلق نماذج شبكة متشققة ونماذج محاكاة مزدوجة ومتصلة، ونال حديثا دمج المعلومات السيزمية ضمن نماذج محاكاة ديناميكية اهتماما كبيرا. وأنعشت التطورات الأخيرة في تقنية التشبيك أمالا يمكن بواسطتها التعامل مع جميع شاذات النفاذية في القريب العاجل.

توجد الشقوق في مناطق محدودة من مكامن متشققة طبيعيا ينعت لها بـ "البقع الحلوة" فقط وتباعا لذلك فإن كل أجزاء نماذج المكمن لا تحتاج معالجة تشقق محددة لنماذج متصلة ومزدوجة.

سمحت أحد الطرق التي تم تقديمها في هذه المقالة بتوليد تلقائي لقطاعات شبكة مستمرة مزدوجة عندما تقترح ميزات النموذج الجيولوجي بهذا العمل. ويطلق على هذا الافتراض نموذج مستمر مزدوج ومكيف حيث أن نتائجه في نماذج المحاكاة المحتوية على قطاعات تشبه الوضع الجيولوجي.

Abstract: *Natural or induced fractures play a crucial role in many petroleum reservoirs. Even though only a small percentage of today's reservoir models explicitly describe the fractures or the fracture networks, one may claim that practically most petroleum reservoirs are fractured. Due to their complexity, but also due to their commercial significance, naturally fractured reservoirs have been the subject to extensive studies during the past decades.*

This paper will try to assess the current situation and methodology for modeling fractured reservoirs. Its main focus will be on recent developments in static and dynamic flow modeling of fractured reservoirs. Especially the latest

* Now with SMT Alps
** HOT Engineering GmbH

evolution in static modeling software capabilities significantly affected past, historical workflows and initiated new developments in the reservoir simulation area.

Starting from the historical evolution of dual continuum reservoir simulation models, a review is given on various simulation approaches for fractured hydrocarbon reservoirs. Several methods will be discussed, starting from conventional formulations to the traditional dual porosity model, to discrete fracture network models. All formulations have their own advantages, but have deficiencies in describing some other specifics of fractured reservoirs.

Recently, the petroleum industry tries to integrate information from all possible sources to generate fracture network models and dual continuum simulation models. Most recently, the integration of seismic data into dynamic simulation models has received a great deal of attention. Also, latest developments in the gridding technology raised hopes to be able to cope with full permeability tensors in the near future.

In many naturally fractured reservoirs, the fractures are found in limited zones, so called "sweet spots" only. Consequently, not all parts of the reservoir models will typically require explicit fracture treatment with dual continuum models.

One of the methods presented in this paper allows automatic generation of dual continuum grid blocks wherever the attributes of the geological model suggests to do so. This approach is called adaptive dual continuum model and it results in simulation models that contain grids that resemble the real geological situation very closely.

INTRODUCTION

Many petroleum reservoirs are fractured or at least partially fractured. Hence, one of the first questions to be raised is whether or not existing fractures are important for the reservoir behavior under producing conditions. In other words, what is the contribution of the flow in fractures to the overall fluid flow?

Posing this question to a petrophysicist, to a geologist or to an engineer, one can expect different views and answers. As far as the reservoir engineer is concerned, only fractures and fracture networks that affect fluid transportation to and from the wells are of significance. Only when there are fractures with sufficient length of penetration through the reservoir rock, fractures that are interconnected and with sufficient density or spacing, their effects can be observed and measured under dynamic flow conditions.

To assess fracture contributions accurately, a wide range of geological, petrophysical and engineering methods are applied. These methods apply to a large variety of different scales.

The paper will give a brief introduction to multi-continua approaches for modeling fluid flow in porous media. Then, a brief discussion of modeling approaches for naturally fractured reservoirs in static models is given, followed by an overview of available simulation and modeling approaches for fluid flow simulation. This will lead to the definition of a new and flexible method, referred to as the adaptive dual continuum method.

The adaptive dual continuum method can be applied to a large variety of cases. As will be shown in the paper, the approach is especially advantageous if the reservoir appears to be partially fractured, *i.e.* not all areas and regions of the reservoir (different lithologies, facies, aquifer region, *etc.*) contain active fracture networks.

THE MULTI-CONTINUA APPROACH

In the context of this paper, the void space in a fractured porous media is composed of two parts: (1) a network of fractures and (2) blocks of porous medium (called matrix). In principle, the mathematical model that describes the fluid flow through this void space of the porous medium can be stated for every point in the domain. This model would represent a description at the microscopic level, which we cannot solve directly, due to missing information at this detailed level. Therefore, a complete description of the fluid transport problem at the microscopic level is not possible.

We have to transform the problem from the microscopic level to a macroscopic level at which the problem is formulated in terms of averages. The average values are measurable quantities. This is referred to as the continuum approach.

In the continuum approach, the physical domain is replaced by a model in which each component (or phase) acts as a continuum that fills up the entire domain. For every point, average values of component and phase properties are taken over an

elementary volume. Those averages represent the macroscopic values of the considered variables. By moving the elementary volume throughout the entire porous medium domain, we obtain averaged values for all variables that are differentiable functions of time and space.

In the case of porous matrix and fractures, it is possible to classify the various problems related to the scale [3]:

Zone 1: The very near field. Interest is focused on fluid flow and contaminant transport within a single, well-defined fracture.

Zone 2: The near field. Flow is considered in a small domain, which contains a small number of fractures. The location and shape of the individual fractures must be known. However, the definition of the fractures may be statistical.

Zone 3: The far field. Here transport may be visualized as taking place simultaneously, in two overlapping continua. One composed of the fluid within the network of fractures, and the other involving the fluid within the porous blocks. Mass may be exchanged between the two continua.

Zone 4: The very far field. The fluid in the entire fractured porous medium may be regarded as a single continuum.

Local problems such as transport near sources and sinks or a single fracture intersecting a well are represented as a problem of the very near field (Zone 1). A reservoir simulation model could use a single continuum method with very fine grids to explicitly model the fracture. Note that a very detailed knowledge about the fracture is required (length, aperture, orientation). No specialized reservoir simulation models exist to simulate this very near field of naturally fractured reservoirs. Of course, very fine gridded models may be used to accomplish this level of detail.

If the domain of interest is larger (but insufficient for the application of the continuum method), we can construct a near field model (Zone 2) that requires information on every individual fracture. In most cases, information on the fractures is only available in the form of statistics (aperture, length, orientation, spacing, *etc.*) and we can construct different realizations of the domain and study their behavior. In the simulation context, the discrete fracture network (DFN) models [6, 10] consider this approach. The method is based on explicit modeling of fractures that are represented as planes or disks. It requires very detailed descriptions of the network and uses single-phase models to simulate the behavior under fluid flow. However, these statistically based models are not practical when considering fluid flow over large domains and fracture networks, as the inclusion of the total number of fractures in field-scale demands large amounts of input data and computer storage. In addition, the flow simulation on those models is generally performed under single-phase conditions and those models also lack comprehensive description of matrix-fracture fluid transfer. Large, field-scale domains are usually better handled by the far and very far field models described below.

For larger scale problems, the dual continua approach for the far field (Zone 3) may be used. The original concept as proposed by Barenblatt and Zheltov[11] and Barenblatt *et al*[12] is also known as the dual porosity model. In this conceptual model two co-located, but interacting, media represent the porous and fractured medium:

(I) The fractured network and

(II) The porous matrix.

Each is represented by a grid system covering the entire domain. Interaction between the two systems is accomplished by a transfer term that defines the fluid transport between fracture and matrix rock. This type of approach is commonly applied for the simulation of multi-phase fluid flow in naturally fractured reservoirs (Fig. 1).

The interconnected fracture network is represented by a grid system that is co-located with another grid system that represents the intergranular pore space (matrix). Usually, the matrix provides the majority of pore space and storage capacity, but only very limited conductivity. In the idealized dual porosity models, the matrix blocks are treated as sources (or sinks) to the fractures. The network of fractures represented by the fracture grid system provides the major fluid flow conduit and limited storage capacity.

If very large distances (and travel times) are involved, we can use the very far field model (Zone 4) in which we regard the entire domain as a single

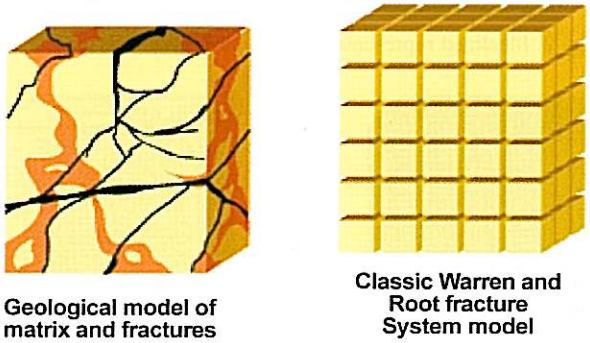


Fig. 1. Idealized grid block representation of naturally fractured rock by a dual porosity model (from Warren and Root, 1963)

continuum. This kind of model is applicable in cases where the system allows sufficient interaction between the fluids in the fractures and in the matrix such that there exists a local equilibrium at every point.

CLASSIFICATION OF NATURALLY FRACTURED RESERVOIRS

For the purpose of reservoir simulation, the classification of naturally fractured reservoirs after Nelson [13,14] or modifications of it[9,18] are used most commonly.

This classification defines the following types of fractured reservoirs:

Type 1: Fractures provide the essential porosity and permeability (Fig. 2)

Type 2: Fractures provide the essential permeability (Fig. 3)

Type 3: Fractures provide permeability assistance to an already producing reservoir (Fig. 3)

In the first case of fractured reservoirs (Type 1), all producible hydrocarbon fluid volumes reside within the fractures. Therefore, this type of fractured reservoirs requires the accurate calculation of fracture porosity, fracture width and fracture spacing. The estimation of these properties will predict whether initial flow rates can be maintained or will drop rapidly within short time after production starts. For this reservoir type, the definition of the fracture network is the decisive factor, whereas the definition of the rock matrix plays a minor role and the application of a dual porosity approach must be questioned.

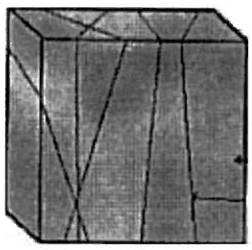


Fig. 2. Idealized representation of type 1 reservoirs.

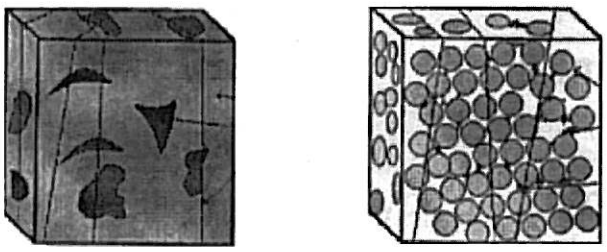


Fig. 3. Idealized representation of type 2 (left) and type 3 (right) reservoirs.

For fractured reservoirs of Types 2 and 3, where the main storage volume resides within the matrix rock volume, early knowledge of matrix-fracture interaction is extremely important. It will determine how efficiently the matrix can be drained by the fracture system. The accurate determination of the fracture porosity will be of less significance in those cases. Usually, a conventional modeling approach will fail for these types of fractured reservoirs, because it is impossible to generate average properties that represent the combined effects of fracture and matrix fluid flow. In most cases, those reservoirs will require explicit modeling of the two continua, matrix and fractures, with distinct property sets.

For all fractured reservoir types, the investigation of fracture orientation will be important in order to capture preferred flow directions. Fracturing may be caused from many possible reasons, but in the end will always represent the stress field of the reservoir and some rock failure associated to this stress.

SPATIAL DISTRIBUTION OF FRACTURES

Since, in most environments, the rock properties vary with location, we should expect the fracturing to do the same. Therefore, the majority of naturally fractured reservoirs will show areas with high fracture intensity just as there will exist areas that indicate no fracturing at all.

It is very likely that the static reservoir model (geological model) can account for the spatial distribution of the fractures and can identify areas with high and low fracture density. Most software packages in this context can relate fracturing to structural elements, lithology or facies types due to the amount and type of data input.

Unfortunately, most dynamic models (simulation models) do not account for the spatial distribution of fractures explicitly. Instead, the dual porosity mode in practically all reservoir simulators operates like a general switch that can be turned on or off. The main problem is that the implementation of dual porosity (or dual permeability) models into reservoir simulators was not appropriately done as true function of location, but as general switch acting globally on the simulation model. This is in conflict with the fracture intensity that most likely appears to be a function of location.

SIMULATION APPROACHES FOR FRACTURED RESERVOIRS

The section will discuss various approaches for the simulation of fluid flow in naturally fractured reservoirs. All methods have their advantages, but have deficiencies in some other specific areas of describing the physics of fluid flow in fractured reservoirs.

The last method presented in this paper allows automatic generation of dual continuum grid blocks wherever the attributes of the geological model suggest doing so. This approach is called adaptive dual continuum model and it results in simulation models that contain grids that resemble the real geological situation very closely.

DISCRETE FRACTURE NETWORK (DFN) MODELS

Discrete fracture network (DFN) models were developed to describe primarily the fracture networks. They are among the models developed most recently. Their focus is on fracture properties and not so much on the description of the rocks' matrix properties. Discrete fracture networks model the fractures as discrete features represented by planes or disks as shown in Figure 4. Contrary to other methods described in this paper, the DFN models require accurate descriptions of the fracture set and its properties. This makes them not very attractive for full field simulation.

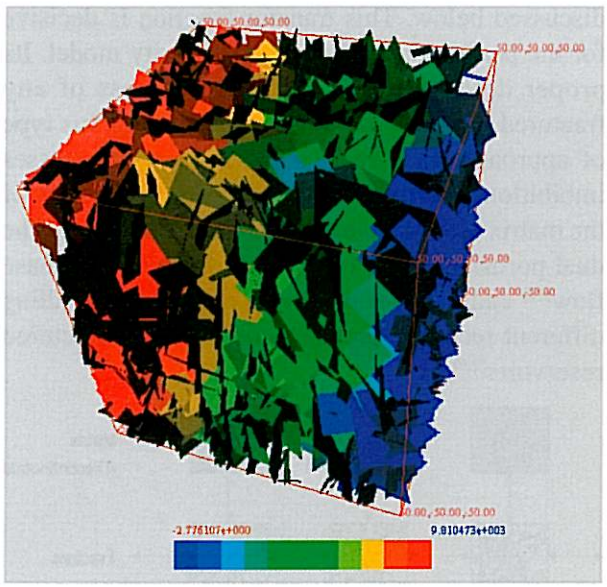


Fig. 4. Discrete fracture network model[15].

The DFN method can be considered a method of the near field or Zone 2. See the discussion on near field models (or Zone 2 models) above. In addition, these models typically perform single-phase calculations and are instructive to obtain fracture properties[6,10] One field of application of these DFN models is the pre-processing or upscaling of fracture information for dual continuum simulation[5].

However, DFN models are very powerful for visualizing the fracture networks. Generally, the DFN approach could be the preferred method for the simulation of fractured reservoirs that are classified as Type 1 according to Nelson[13], whereas their application is limited for reservoirs of Types 2 and 3.

The remainder of this paper describes another group of models that includes the traditional reservoir simulation approaches, where the reservoir is discretized into one rock continuum (single porosity) or two continua (dual porosity/dual permeability models) as first described by Barenblatt, Zheltov and Kochina[2].

SINGLE POROSITY MODELS

Of course, the 'conventional' single continuum simulation approach can be used for modeling fractured reservoirs under certain circumstances.

For example, single porosity methods are frequently used to generate fine grid models in order to investigate matrix-fracture communication on small scale. These high-resolution models are useful for developing generalized matrix-fracture transfer functions that can later on be applied to the field-scale reservoir model. In general, however, they cannot be used for the simulation of the entire reservoir.

One exception may be the fractured reservoirs of Type 1 following the classification by R. Nelson[13], where the fractures provide the main porosity and permeability for the reservoir (*i.e.* they provide the storage volume and the flow paths). In those cases, the single porosity approach may be sufficient to capture the flow behavior of the fracture network.

However, it may be difficult to capture the preferred flow directions, especially when the permeability field (tensor) changes with location and when k_{min} and k_{max} cannot be aligned with the principal co-ordinate directions.

The kPEBI grid proposed by Heinemann *et al.*[11] may be more flexible and powerful to capture those preferential flow directions. However, there are some

limitations with respect to the properties of the permeability tensor that must be considered when constructing a kPEBI grid in the 2D domain (Fig. 5).

An alternative modeling approach that uses a single porosity model is discussed by Saidi[16,17] In his model, the entire reservoir domain is divided into sectors. Those sectors represent also fractures with infinite transmissibility. The sectors are connected with each other. Each sector may contain several rock types that are represented by cylindrical matrix blocks. The fracture pressure and the fluid phase contacts provide the boundary conditions. This model can be considered a special case of the sub domain method of dual porosity models, but does not rely on the concept of shape factors. Saidi claims that this method allows proper handling of block-to-block interaction and re-imbibition processes.

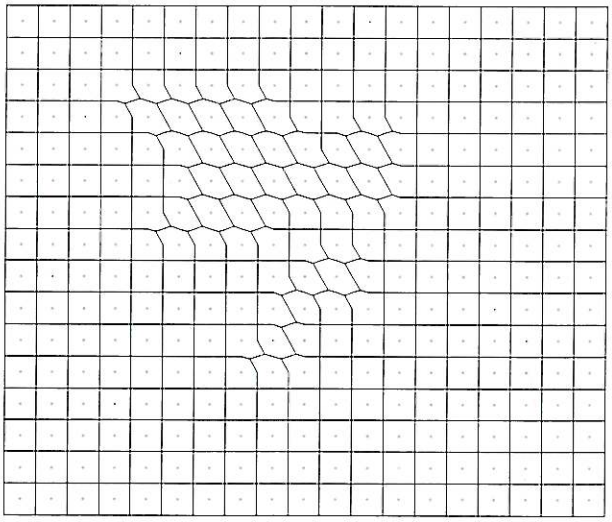


Fig. 5. kPEBI grid for single porosity modeling of fractured reservoirs.

DUAL POROSITY/DUAL PERMEABILITY MODELS

This class of simulation models describes the dual media models that have been introduced by Barenblatt and Zheltov[2] in 1960 and by Warren and Root[19].

In the original publication, the calculation of matrix block pressures assumed no flow between matrix blocks by neglecting matrix permeability. The matrix permeability was only considered in the fluid flow calculation between matrix and fractures. This model is usually named a dual porosity model. It contains a continuous primary medium, the fracture grid system that provides the main flow paths with high permeabilities, but typically low storage volume. The second medium is the matrix rock that is considered non-continuous and acts as a source term for the adjacent fractures. Figure 6 shows an idealized representation of the connections of two grid systems. Only for conceptual purposes, the two grid systems are shown at different locations. In fact, they are co-located.

In other words, the fractures are the boundaries of the matrix blocks. The fracture grid system is truly continuous (indicated by the black arrows between neighboring fracture grid blocks). The matrix grid system in a dual porosity approach has only connections into the fracture system (indicated by the red arrows). Therefore, the matrix grid system is considered discontinuous. Hence, the number of neighbors of the matrix grid block is always one, which is the fracture grid block that surrounds the matrix block. The total number of neighbors for the fracture grid block in a dual porosity model is equal to the total number of fracture neighbors defined by the geometry plus one block, which represents the matrix grid block that is in communication with the fracture grid block (Fig. 6).

Furthermore, the rock matrix in each grid block is idealized as a system of regularly shaped blocks (sugar cubes, see Fig. 1) that are not discretized individually. Instead, all matrix blocks in a grid block are represented by a single grid node, which holds some average value for the variables (pressure, saturations, etc.) of all matrix blocks.

The connection between matrix and fracture continuum that is indicated by the red arrows in Figure 6 is defined by a matrix-fracture transfer term that is discussed below. This transfer function is decisive for the performance of the dual porosity model. Its proper definition is vital to the success of any fractured reservoir simulation study using this type of approach. In particular the recovery processes imbibition, gravity drainage and capillary effects of the matrix blocks have received much attention. The dual porosity concept was extended to multi-phase flow[12] and later refined to be capable of handling different recovery processes occurring in fractured reservoirs[7,9]

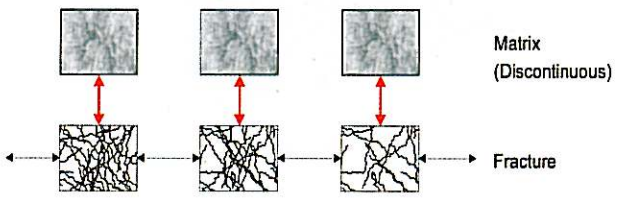


Fig. 6. Grid block connections in a dual porosity model.

When the discontinuous matrix grid system of the dual porosity model is transferred into a continuous grid system by adding the matrix-to-matrix connections, the model is referred to as dual permeability system (Fig. 7). In this case, two co-located media exist and both are continuous. The matrix blocks are no longer isolated, and contribute to the overall fluid flow.

The matrix-to-matrix grid block connections introduce capillary continuity through connected matrix blocks. This may have a significant impact on the recovery for a stack of matrix blocks. It appears that the dual permeability model captures this natural behavior better than the dual porosity model.

However, the dual permeability model comes with additional cost in terms of computation efforts. In a dual porosity model it is possible to pre-eliminate all matrix unknowns from the equation system, thus reducing the size of the Jacobian matrix equal to the size resulting from a model in a conventional single porosity formulation. This pre-elimination step is not possible for dual permeability models, resulting in equation systems that are twice as large in size compared to the size of the linear equation system resulting from an equivalent dual porosity model.

BALANCE EQUATIONS IN DUAL POROSITY AND DUAL PERMEABILITY MODELS

The fluid flow equations discussed in the following are based on a general purpose, compositional formulation, and can be applied to flow processes ranging from single-phase to three phases black-oil cases, or compositional cases using a cubic equation of state with n components.

The formulation of the mass balance equations follows the classical dual porosity/dual permeability approaches with a matrix-fracture transfer term q_{cmf}^{n+1} that is dependent on c , referred to as the shape factor.

First, let us look at a grid block in a conventional (single porosity) model. Then, the molar balance

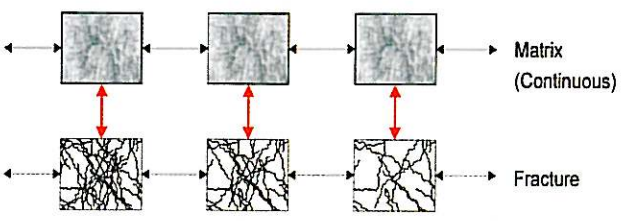


Fig. 7. Grid block connections in a dual permeability model.

equation for a component c in a grid block i is given by Eq. 1.

$$\sum_{j=1}^{N}\tau_{ij}\left[\sum_{p=1}^{P}\left(x_{pc}\lambda_p D_p\right)_{ij}^{n+1}\left(\Phi_{pj}-\Phi_{pi}\right)^{n+1}\right]+\sum_{p=1}^{P}\left(q_p D_p x_{pc}\right)_i^{n+1}=\frac{V_i}{\Delta t}\Delta_t\left[\phi\sum_{p=1}^{P}\left(S_p D_p x_{pc}\right)\right]_i \quad (1)$$

Where

N is the number of neighbors
τ_{ij} is the inter-block transmissibility between i and j
x_{pc} is the mole fraction of component c in phase p
λ_p is the phase mobility
D_p is the specific phase mole density
Φ_p is the phase potential
q_p is the phase production or injection rate
V_i is the block volume of grid block i
Δt is the time step length
ϕ is the porosity
S_p is the phase saturation

This equation is valid as long as the grid is orthogonal, i.e. the line connecting grid blocks i and j is perpendicular to the communicating surfaces between those two grid blocks.

One equation of this type is defined for each component in the reservoir fluid model. Together with other constraints, functions and equations these molar balance equations will yield the linear equation system. The linear equation system is then solved with IMPES, fully implicit or adaptive implicit mode.

In the simulation of fractured reservoirs by dual continuum models (dual porosity or dual permeability) one assumes the existence of two co-located continua, namely matrix and fractures. Eq. 2 defines the molar balance equation for a component c in a fracture block.

$$\sum_{j=1}^{Nf}\tau_{ij}\left[\sum_{p=1}^{P}\left(x_{pc}\lambda_p D_p\right)_{ij}^{n+1}\left(\Phi_{pj}-\Phi_{pi}\right)^{n+1}\right]+\sum_{p=1}^{P}\left(q_p D_p x_{pc}\right)_i^{n+1}+q_{cmf}^{n+1}=\frac{V_{if}}{\Delta t}\Delta_t\left[\phi\sum_{p=1}^{P}\left(S_p D_p x_{pc}\right)\right]_{if} \quad (2)$$

It is worth noting that the sum over the neighbors for the flow term is only over all neighbors in the fracture grid system. The neighborhood connection to the second continuum (the matrix neighbor) is treated in a special transfer term q_{cmf}^{n+1} defined below.

Similarly, for a component c in a matrix block, the balance equation is given by

$$\sum_{j=1}^{Nm}\tau_{ij}\left[\sum_{p=1}^{P}\left(x_{pc}\lambda_p D_p\right)_{ij}^{n+1}\left(\Phi_{pj}-\Phi_{pi}\right)^{n+1}\right]+\sum_{p=1}^{P}\left(q_p D_p x_{pc}\right)_i^{n+1}-q_{cmf}^{n+1}=\frac{V_{im}}{\Delta t}\Delta_t\left[\phi\sum_{p=1}^{P}\left(S_p D_p x_{pc}\right)\right]_{im} \quad (3)$$

The only difference between Eqs. 2 and 3 when compared to the molar balance equation of a single porosity block (Eq. 1) is the additional matrix-fracture

transfer term q^{n+1}_{cmf}. The matrix-fracture transfer term is (by convention) added to the fracture system (Eq. 2) and subtracted from the matrix system (Eq. 3).

The formulae above are valid, if both grid systems are continuous. This is the case for a dual permeability model, but not in the case of the dual porosity model. In the dual porosity model the matrix blocks act as source terms to the fracture system, but have no matrix-matrix connections (compare Fig. 6).

In a dual porosity model, the matrix grid block has no neighbors in the matrix grid system (it is a discontinuous system) and hence the entire flow term within the matrix grid can be disregarded.

If this is the case, then the equation for the matrix blocks (Eq. 3) simplifies (assuming that no well is perforated in the non-continuous matrix grid system) to

$$-q^{n+1}_{cmf} = \frac{V_{im}}{\Delta t}\Delta_t \left[\phi \sum_{p=1}^{P} \left(S_p D_p x_{pc}\right)\right]_{im} \tag{4}$$

because and . Eq. 4 shows why it is possible to eliminate all matrix unknowns from the equation system in a dual porosity system, thus reducing the size of the Jacobian matrix basically to the size of a conventional single porosity model. Of course, this is not possible for dual permeability models, which result in fully coupled and large sized coefficient matrices. Additional CPU time is required to solve those linear systems that stem from dual permeability simulation models when compared to their dual porosity equivalents.

The matrix fracture transfer term is based on the formulation proposed by Kazemi[1,2], following Darcys law. Thus, the total matrix-fracture transfer term (including the molecular diffusion rate) for a component c is given by

$$q^{n+1}_{cmf} = \tau_{mf} \sum_{p=1}^{P} \left(x_{pc} \lambda_p D_p\right)^{n+1}_{mf} \left(\Phi_{pm} - \Phi_{pf}\right)^{n+1} + q^{n+1}_{Dcmf} \tag{5}$$

Here, the matrix-fracture transmissibility is defined to be

$$\tau_{mf} = V_f k c \tag{6}$$

where it is not very obvious what the value for the permeability in this equation should be.

Many attempts have been made in the past to define the shape factor, the classical formula still being

$$\sigma = C \cdot \left(\frac{1}{l_x^2} + \frac{1}{l_y^2} + \frac{1}{l_z^2}\right), \tag{7}$$

where C is a constant and varies widely (see for example Table 1 in Boubiaux *et al.*[5]), but typically is between 4 and 12 and l_x, l_y and l_z are the matrix block dimensions.

Usually, the shape factor is multiplied by permeability and volume of the matrix grid block to yield the matrix-fracture transmissibility (Eq. 6).

This approach fails, however, when the permeability in the three co-ordinate directions is different. For this reason, we suggest the inclusion of the permeability, k, into the shape factor and use

$$\sigma = C \cdot \left(\frac{k_x}{l_x^2} + \frac{k_y}{l_y^2} + \frac{k_z}{l_z^2}\right), \tag{8}$$

if l_x, l_y and l_z are the matrix block dimentions.

Using Eq. 8 allows the application of Eq. 9 to calculate the matrix-fracture transmissibility. Then, the matrix-fracture transmissibility must be calculated from

$$\tau_{mf} = V_f c \tag{9}$$

which can be considered superior to Eq. 6. Experience shows that during history matching the transmissibility defined in Eqs. 6 or 9 needs to be modified. Hence, the following equation is used:

$$\tau_{mf} = F \cdot V_f c \tag{10}$$

Where F is a history matching parameter.

Nomenclature

D_p	=	Phase molar density
k	=	Permeability
l	=	Matrix element dimensions
S_p	=	Phase saturation
V_i	=	Block volume
x_{pc}	=	Molar fraction of component c in phase p
τ_{ij}	=	Inter-block transmissibility between block i and j
λ_p	=	Phase mobility
Φ_p	=	Phase potential
Δ_t	=	Time step length
ϕ	=	Porosity
σ	=	Shape factor

ADAPTIVE DUAL CONTINUUM METHOD

Not all parts of a fractured reservoir will typically require dual porosity/dual permeability treatment. Let us assume that the spatial distribution of the fractures is given by Figure 8. The different colors indicate different fracture intensity. Blue indicates no fracturing, green intermediate fracture intensity and red indicates high fracture intensity.

The adaptive dual continuum method takes this aspect into consideration[8]. It allows creating dual porosity/dual permeability cells adapted to user-defined conditions, grid block properties are based

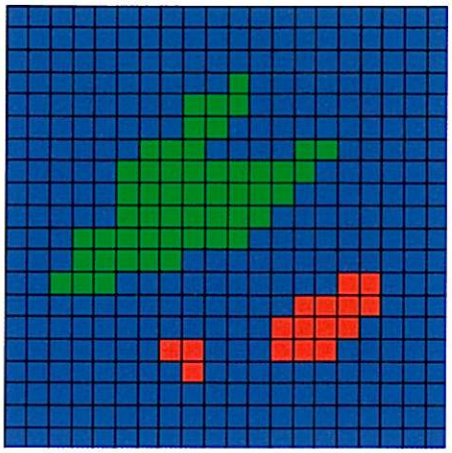


Fig. 8. Spatial distribution of fractures indicated by fracture intensity.

on geological attributes (facies, rock type, fracture intensity, etc.). Dual continuum cells are created only at locations, where those conditions are fulfilled, elsewhere – the unfractured part of the reservoir model – the grid blocks remain conventional single porosity cells. Hence the name adaptive dual continuum method.

Symbolically, the matrix grid blocks are shown in the center, surrounded by the fracture grid blocks. Note, that in fact, both grid systems (matrix and fracture system) are co-located, i.e. at the same location. (Fig. 9).

The standard dual continuum method (dual porosity/dual permeability models) generates dual continuum cells in the entire domain, as shown in left hand side of Figure 9. This means that dual porosity cells are created, even if there should be no fractures in a large portion of the reservoir volume. At times, this will create an excessive amount of additional grid blocks that should not exist in the simulation model. Those grid cells will waste resources of CPU time and computer storage. They may also lead to erroneous simulation results or stability problems during the solution process.

The simulator SURE[21, 22] using the adaptive dual continuum method, is able to generate dual porosity blocks where the fracture intensity is larger than a given threshold value and will convert the single porosity grid block accordingly into a matrix-fracture grid block pair. This is shown at the right hand side in Figure 9.

The dual continuum blocks are generated automatically, if the fracture indicator is available in the simulation model. After this gridding step has been completed, the model contains matrix-fracture grid block pairs only, where the geological model indicates fracturing.

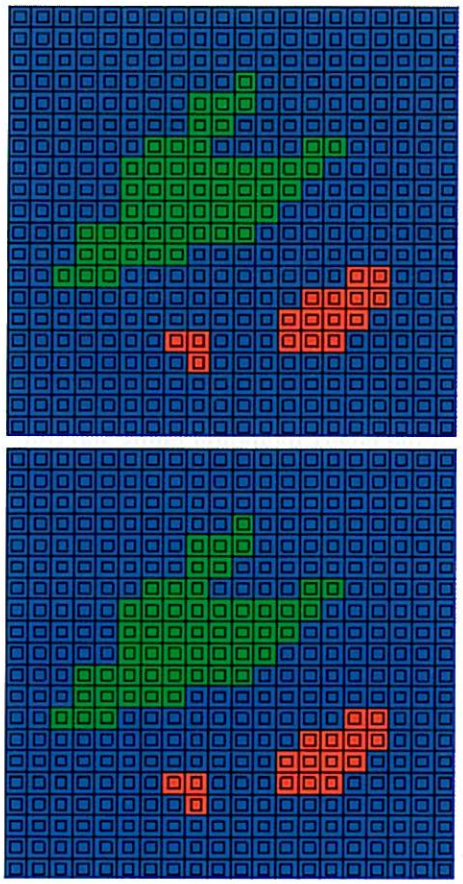


Fig. 9. Modeling naturally fractured reservoirs by standard dual continuum (left) and adaptive dual continuum method (right).

Any block in the simulation model can be set to dual porosity/permeability mode automatically or interactively, if necessary. There are no limitations with regards to any of the other modeling capabilities (like fault modeling or local grid refinement) as a result of those gridding steps. All properties are stored on a cell-by-cell basis and can be modified, correlated or assigned interactively. The shape factors are typically loaded directly from the 3D geological model and assigned to each individual matrix block. However, if requested, it is also possible to correlate shape factors based on matrixblock dimensions l_x, l_y and l_z. Those matrixblock dimensions can be loaded and assigned from maps or geological models and are stored also on block-by-block basis.

The advantages of the adaptive dual continuum method are the following:

- The simulation grid can resemble the geological situation more closely.
- The user flexibility and modeling capabilities are maximized through the advanced gridding processing.
- All fracture properties are stored on a cell-by-cell basis (including the matrix-fracture exchange parameter, "shape-factor").

- The CPU-time and memory requirements for the simulation run are minimized.

Application of Adaptive Dual Continuum Method

The methodology described above has been applied successfully to simulation models running in two-phase gas-water mode, three-phase black-oil mode and ° API models.

Figures 10 and 11 shows a typical application of the adaptive dual continuum method. Figure 10 displays one of the layers including faults and some local grid refinements located at the center of the model. Figure 11 displays a cross section through the model and the different fracturing in the various layers can be observed easily. Layers 2 and 3 are vertically refined in some parts and also the local grid refinement can be seen.

The example shown is the adaptive dual porosity model of a faulted and fractured undersaturated oil reservoir. Note that the fracturing varies with facies and rock types, therefore, a large number of blocks in the model are not fractured and modeled as single porosity blocks.

The fractured areas of the model are using the dual porosity formulation. The total model contains 18368 grid blocks in seven layers, from which 5978 are single porosity blocks, 6195 blocks are fracture, and 6195 are matrix blocks.

Unlike the application shown above, the following example shows how to model a reservoir, where the fracturing is associated with faulting. Figure 12 shows a model with slanted faults, where the fractures are only modeled if the grid blocks are close to a fault. The grid construction follows the PEBI grid construction principles and is fully automated.

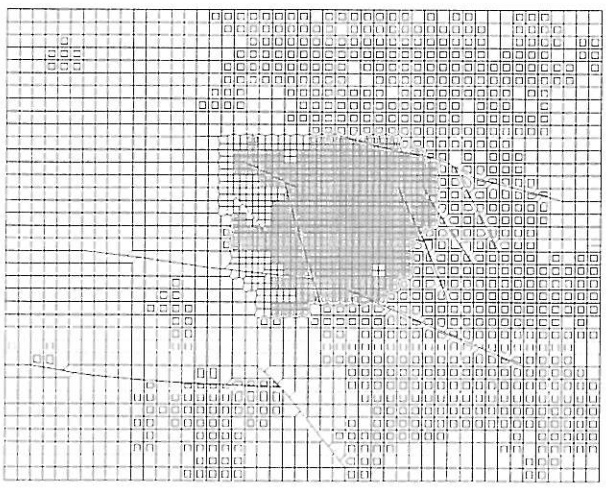


Fig. 10. 2D view of adaptive dual continuum simulation model.

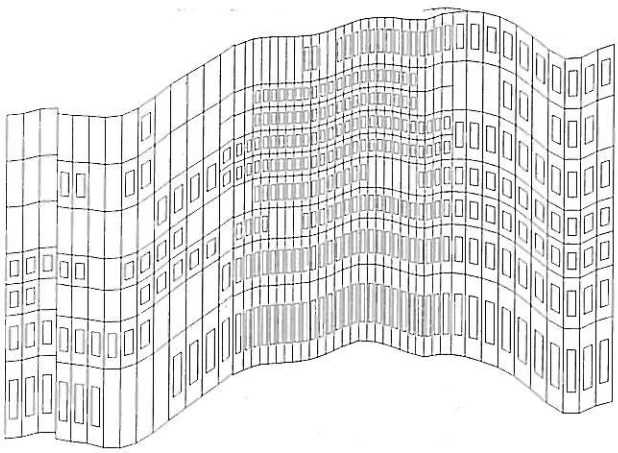


Fig. 11. Cross section through adaptive dual continuum reservoir model.

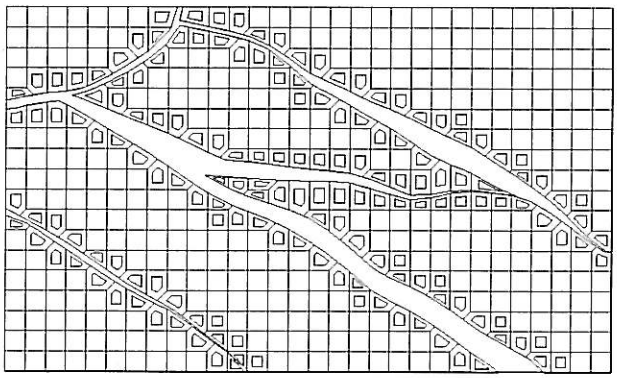


Fig. 12. Adaptive dual continuum model created from distance to fault parameter.

SUMMARY

This paper discusses the current situation and methodology for modeling and fluid flow simulation of naturally fractured reservoirs. Starting from the multi-continua approach different methods for different scales of models are discussed.

Natural fractures are not distributed evenly throughout the reservoir domain. Static models are very well suited to capture those spatial distributions.

Among the simulation models, the application of discrete fracture networks is discussed first. The strength of DFN models lies in the description of the connected fracture networks. Unfortunately, those models require very accurate descriptions of the fracture set and its properties. This makes them not very attractive for full field simulation. However, DFN models are very powerful for visualizing the fracture networks. One field of application of these DFN models is the pre-processing or upscaling of fracture information for dual continuum simulation.

Secondly, the application of single porosity and dual continuum methods is discussed. Single porosity models can be applied to fractured reservoirs under certain circumstances. A new gridding method, referred to as kPEBI grid, may also improve the potential application of single porosity models to special types of fractured reservoirs.

Dual porosity and dual permeability models are commonly applied to simulate the fluid flow in naturally fractured reservoirs. The differences between the dual porosity and the dual permeability models are discussed and the balance equations outlined.

In many naturally fractured reservoirs, the fractures are found in limited zones, so called "sweet spots" only. Consequently not all parts of the reservoir models will typically require explicit fracture treatment with dual continuum models. The last method presented in this paper allows automatic generation of dual continuum grid blocks wherever the attributes of the geological model suggest doing so. This approach is referred to as adaptive dual continuum model. The adaptive dual continuum method results in simulation models that contain grids that resemble the real geological situation very closely. Just like the static fracture characterization methods, the adaptive dual continuum method generates simulation models that represent the spatial distribution of fractures.

The adaptive dual continuum method was implemented in the reservoir simulator SURE. Experience shows that performance and flexibility of this approach are clearly superior to all other methods discussed in the literature. The method is especially powerful when the simulation model is based on a 3D geological model for fracture characterization.

REFERENCES

[1] Barenblatt, G.I, and Zheltov, I.P., 1960. Fundamental equations of filtration of homogeneous liquids in fissured rocks, *Soviet Dokl. Akad. Nauk. (USSR)*, **13**, No. 2, 545-548.

[2] Barenblatt, G.I, Zheltov, I.P., and Kochina, I.N., 1960. Basic concepts in the theory of seepage of homogeneous liquids in fissured rocks, *J. Appl. Math. Mech. (USSR)*, **24**, No. 5, 852-864.

[3] Bear, J., 1993. Modeling flow and contaminant transport in fractured rocks, In *Flow and Contaminant Transport in Fractured Rock*, Academic Press, 1-37

[4] Bear, J., 1972. *Dynamics of Fluids in Porous Media*, American Elsevier Publishing Company.

[5] Bourbiaux, B., Granet, S., Landereau, P., Noetinger, B., Sarda, S., and Sabathier, J.C., 1999 (October). Scaling up matrix-fracture transfer in dual-porosity models: theory and applications, *SPE* 56557 presented at the SPE Annual Technical Conference and Exhibition, Houston.

[6] Cacas, M., Ledoux, E., de Marsily, G., and Tillie, B., 1990. Modeling fracture flow with a stochastic discrete fracture network: calibration and validation, *Water Resources*, **26**(3), 479-489.

[7] Coats, K.H., 1989 (February). Implicit compositional simulation of single-porosity and dual-porosity reservoirs, *SPE* 18427 presented at the SPE Symposium on Reservoir Simulation, Houston.

[8] Ganzer, L.J., 2002 (April). Simulating fractured reservoirs using adaptive dual continuum, *SPE* 75233 presented at the SPE/DOE Thirteenth Symposium on Improved Oil Recovery, Tulsa, OK.

[9] Gilman, J.R., Kazemi, H., 1987 (February). Improved calculations for viscous and gravity displacement in matrix blocks in dual porosity simulators, *SPE* 16010 presented at the SPE Symposium on Reservoir Simulation, San Antonio, Texas.

[10] Granet, S., Fabrie, P., Lemonnier, P., and Quintard, M., 1998 (September). A single-phase low simulation of fractured reservoirs using a discrete representation of fractures. Paper presented at the Sixth European Conference on the Mathematics of Oil Recovery (ECMOR VI), Peebles, Scotland.

[11] Heinemann, G.F., and Heinemann, Z.E., 2001 (September). Gridding concept for third generation reservoir simulators. Paper presented at the Sixth International Forum on Reservoir Simulation, Hof/ Salzburg.

[12] Kazemi, H., 1983 (November). Numerical simulation of water-oil flow in naturally fractured reservoirs. *SPE* 5719 presented at the SPE Symposium on Reservoir Simulation, Los Angeles.

[13] Nelson, R.A., 1979. Natural fracture systems: description and classification. *Bull. Am. Assoc. Petrol. Geol.*, **63** (12), 2214-2221.

[14] Nelson, R.A., 1982 (September). An approach to evaluating fractured reservoirs. *SPE J. Petrol. Tech.*, 2167-2170.

[15] Ouenes, A. and Hartley, L.J., 2000 (October). Integrated fractured reservoir modeling using both discrete and continuum approaches, *SPE* 62939 presented at the 2000 SPE Annual Technical Conference and Exhibition in Dallas, Texas.

[16] Saidi, A.M., 1983 (November). Simulation of naturally fractured reservoirs, *SPE* 12270 presented at the 1983 SPE Reservoir Simulation Symposium, San Francisco, CA.

[17] Saidi, A.M., 1987. *Reservoir Engineering of Fractured Reservoirs*, Total Press.

[18] Stearns, D.W. and Friedman, M., 1972. Reservoirs in fractured rock, *Mem. Am. Assoc. Petrol. Geol.*, 82-106.

[19] Warren, J.E., and Root, P.J., 1963 (September). The behavior of naturally fractured reservoirs, *SPE Journal*, 245-255, *Trans. AIME*, 228.

[20] Wong, P.M., and Boerner, S., 2003 (June). Ranking geological drivers for mapping fracture intensity at the pinedale anticline. Presented at the 65th EAGE Conference and Exhibition, Stavanger, Norway.

[21] HOT Engineering GmbH: *SUREGrid* User Manual, 2003.

[22] HOT Engineering GmbH: *SURESim* User Manual, 2003.

Petroleum Res. J. Vol. 18 (2005); P. 81–90, 8 Figs.

New Parallelized Adaptive Implicit Methods for Large Compositional Reservoir Simulations

Y. Caillabet, J.F. Magras and O. Ricois*

أساليب ضمنية تكييفية متوازية لمحاكاة المكمن كبير التركيب

ي. كيلابيت، ج. ف. ماقراص وأ. ريكواس

لا تزال محاكاة نماذج تركيبات المكامن الكبيرة والمقبولة لتوقيت وحدة المعالجة المركزية المفتاح لأي منظومة محاكاة مكمنية. وهكذا فإن النمذجة المتوازية مطلوبة لزيادة سرعة المحاكاة وكذلك نحتاج إلى تطبيق الحلول العددية القوية لضمان نتائج دقيقة خاصة عند محاكاة مركبات معقدة الطبيعة. في هذا السياق الأنظمة الضمنية الكلية التقليدية غالبا ما تكون غير مستعملة لسبب الذاكرة ومتطلبات وحدة المعالجة المركزية.

نحن نقترح أساليب جديدة حكيمة والتي تمزج الدقة والاستقرار للأساليب الضمنية الكاملة وأداءات وحدة المعالجة المركزية واستهلاك قليل للذاكرة للمجموعة الواضحة. بحدود هذه الطرق نظام ضمني كامل يطبق بأجزاء من المكمن ذو الاختلالات في الخواص الطبيعية العالية. وأسلوب واضح يستخدم في المجموعة الأخرى. الأسباب الواضحة تحدد باستقرار ظروف CFL الخلايا الواضحة ذو الافتلاتات الكبيرة من غير المعروفة تفتح ديناميكيا للأخريات الضمنيات لتحسين أداءات وحدة المعالجة المركزية المحاكاة العالمية. هذه الحالات للحسابات وضعت أساسا على معايير أما مبدئية أو طيفية. إقفال الشبكة الضمنية ربما تحكم باستعمال أنظمة ضمنية كاملة أو أنظمة شبه ضمنية اعتمادا على اختلافات مركبات المائع.

هذه الأنظمة المختلفة تم موازاتها وتكاملها بمنظومة محاكاة صناعية متعددة الأغراض. معايير CFL تم مناقشتها واختبارها بحالات أكاديمية وبعدها تم مقارنة الأساليب المتوفرة والتي تم عرضها لدراسات حالات حقلية حقيقية لمركبات كبيرة على منصات معدنية متوازية ومختلفة.

Abstract: *Simulation of large compositional reservoir models in an acceptable CPU time still remains a key issue for any reservoir simulation software. Parallel computing is thus required to speed up the simulations and robust numerical solutions need to be implemented to insure accurate results especially for simulations of complex compositional physics. In that context, classical fully implicit schemes are often not practical or, even unusable, due to memory and CPU restrictions. We propose new time discretization methods which mix the accuracy and stability of the fully implicit methods and CPU performances and low memory consumption of the explicit ones. Within these approaches, a fully implicit scheme is applied in parts of the reservoir with highest physical property variations, and an explicit method is used in the other ones. Explicit schemes are delimited by a stability CFL condition. Explicit cells with large variations on the unknown are switched dynamically to implicit ones to improve global simulation CPU performances. These status computations are based on either threshold or spectral criteria. Implicit grid blocks may also be discretized using fully*

*Institut Français du Pétrole, France.

implicit or quasi-implicit schemes depending on the fluid composition variations.

These different schemes have been parallelized and integrated in a multi-purpose industrial reservoir simulator. The CFL criteria are discussed and tested on academic reference cases and then, comparisons of the available methods are presented for large compositional real case studies run on different parallel hardware platforms.

INTRODUCTION

High performance computing has always been used in the petroleum industry for the simulation at fine scale of large full field reservoirs. With the emergence of low-price multiprocessor hardware platforms, such as PC clusters or clusters of symmetric multiprocessing (SMP) architectures, commercial simulator software have been adapted to always give the best performance. Given these increased capacities, the reservoir engineers now require a more detailed characterization of the reservoir structure resulting in mega-cell discretized reservoir models. Moreover, gas condensate or volatile-oil reservoir modeling requires a large number of hydrocarbon components to insure better description of oil and gas compositions.

Due to these requirements, the traditional fully implicit models are not adapted to treat these problems within acceptable computing time and/or memory requirements. On the other hand, simulations of complex compositional recovery processes in a heterogeneous or largely faulted reservoir is not viable with IMPES conventional approaches[1] due to the low level of implicitness used and due to the well-known stability criterion which requires reducing the time step length to impractical values. Improved formulations with reduced time and memory requirements have to be defined to solve these large problems.

In this paper, some hybrid formulations of the equations addressed in reservoir simulation are exposed and discussed. All these formulations define regions where more robust and, thus, more expensive schemes are needed and others where simpler schemes are sufficient. Criteria are defined to automatically switch status of the reservoir cells from one region to another. Different criteria have been tested and their advantages and drawbacks are discussed.

Moreover, all these formulations have been optimized through a parallel algorithm to achieve good performances for large compositional reservoir models run on multiprocessor hardware.

Some applications of these techniques are displayed on a large compositional model with more than one million active cells and a 9-component oil representation.

MODEL DESCRIPTION

General Considerations

The main equations to be solved in reservoir simulation are mass conservation equations for each component.

Mass conservation for the water component,

$$\frac{\partial}{\partial t}(\rho_w S_w \phi) + div(\rho_w v_w) = f_w \quad (1)$$

Mass conservation for a hydrocarbon component i,

$$\frac{\partial}{\partial t}(\rho_o S_o X_i \phi + \rho_g S_g Y_i \phi) + div(\rho_o X_i v_o + \rho_g Y_i v_g) = f_i \quad (2)$$

In reservoir simulation, these equations are solved using a Newton method and the transport term may be written using either an explicit[2] or implicit[3] formulation. The implicit formulation is unconditionally stable and allows large time steps. It is commonly used in reservoir simulations, however, for large compositional cases it is limited both in terms of memory and CPU time. The explicit formulation has a CFL condition, which limits the time step extension. However, this method is cheaper in terms of memory and Newton resolution time.

Adaptive Implicit Method (AIM)

Work has already been carried out to adequately mix these two formulations[4,5,7,10]. The main idea is to have an unconditionally stable formulation for cells with the greatest variations on variables (typically near the wells or near a saturation front where the CFL condition is most critical) and to use an explicit and cheaper formulation for the cells where the CFL condition is less constraining. This method is called Adaptive Implicit or AIM and should take advantage of the two above methods with large time steps and small memory and CPU costs. The main difficulty is to adequately define a way to switch cells from an explicit status to an implicit one.

In our work, two different criteria have been tested. The first one is based on an approach already

presented by Russell[10], which uses a CFL condition on the pressure only, and threshold criterion on both the saturation and composition variations.

The second criterion is based on a more complex approach and intends to define the CFL condition for both pressure and saturation variations. Some approaches have also been proposed in other papers[5] which take into account the composition variations. But, in our study, we have found that the calculations of this more general CFL to be quite expensive and we have chosen a practical approach mixing quick CFL calculations and threshold conditions.

Moreover, the CFL calculations proposed for compositional model[4,5], in general, do not take into account the capillary pressure effects and the EOS equilibrium between the different phases. So in this paper, we only focus on the transport phenomenon and a CFL criterion is built for transport between independent phases. The capillary effects are not taken into account by the criterion and both the phase apparition and composition variations due to EOS equilibrium are treated by saturation and composition thresholds.

Using these assumptions, the mass conservation equations may be simplified. The resulting equations for a non-perforated reservoir cell can be written as follows:

$$\frac{\partial}{\partial t}(\rho_w S_w \phi) + div(\rho_w v_w) = 0 \tag{3}$$

$$\frac{\partial}{\partial t}(\rho_o S_o \phi) + div(\rho_o v_o) = 0 \tag{4}$$

$$\frac{\partial}{\partial t}(\rho_g S_g \phi) + div(\rho_g v_g) = 0 \tag{5}$$

where,

$$S_w - S_o - S_g - 1 = 0 \tag{6}$$

Using Darcy's law, the phase velocity is related to the pressure gradient,

$$v_w = -\frac{TK_{rw}}{\mu_w}\nabla(P - \rho_w g z + P_{cw}) \tag{7}$$

a first order system, a new variable q is defined by the following equation,

$$\nabla P - q = 0 \tag{8}$$

Here, it should be noted that this system of equations ((3) to (8)) only gives some information on the approximate local CFL, and the mass conservation equations are otherwise solved using a Newton's method. So, the CFL calculations aim at addressing the cell status based on a flux criterion.

For simplicity sake, the problem is first written in 1D. For each reservoir cell, fluxes between neighboring cells are computed separately and a CFL is defined for each cell. The gradient term in the above equations may then be computed in a given direction (hereafter called x), and the system of equations gives,

$$\frac{\partial P}{\partial x} - q = 0 \tag{9}$$

$$S_w + S_o + S_g - 1 = 0 \tag{10}$$

$$\frac{\partial}{\partial t}(\rho_w S_w \phi) - \frac{\partial}{\partial x}(TM_w(q - \overline{\rho_w} g z)) = 0 \tag{11}$$

$$\frac{\partial}{\partial t}(\rho_o S_o \phi) - \frac{\partial}{\partial x}(TM_o(q - \overline{\rho_o} g z)) = 0 \tag{12}$$

$$\frac{\partial}{\partial t}(\rho_g S_g \phi) - \frac{\partial}{\partial x}(TM_g(q - \overline{\rho_g} g z)) = 0 \tag{13}$$

where, $M = \rho Kr / \mu$ is the phase mobility.

The system is written using a quasi-linear first order form.

$$A(P,q,S,x)R_x + B(P,q,S,x)R_t + C(P,q,S,x) = 0 \tag{14}$$

R is the unknown vector (P, q, Sw ,So ,Sg). The parameters constituting the matrices A and B are arranged as follows:

$$A = \begin{bmatrix} 1 & 0 & 0 & 0 & 0 \\ 0 & 0 & 1 & 1 & 1 \\ X & -TM_w & -Tq\frac{\partial M_w}{\partial S_w} & -Tq\frac{\partial M_w}{\partial S_o} & -Tq\frac{\partial M_w}{\partial S_g} \\ X & -TM_o & -Tq\frac{\partial M_o}{\partial S_w} & -Tq\frac{\partial M_o}{\partial S_o} & -Tq\frac{\partial M_o}{\partial S_g} \\ X & -TM_g & -Tq\frac{\partial M_g}{\partial S_g} & -Tq\frac{\partial M_g}{\partial S_g} & -Tq\frac{\partial M_g}{\partial S_g} \end{bmatrix}$$

$$B = \begin{bmatrix} 0 & 0 & 0 & 0 & 0 \\ 0 & 0 & 0 & 0 & 0 \\ X & 0 & \rho_w\phi & 0 & 0 \\ X & 0 & 0 & \rho_o\phi & 0 \\ X & 0 & 0 & 0 & \rho_g\phi \end{bmatrix}$$

The terms X contain the derivatives of the system with respect to P which are later eliminated. The stability of the system may be seen as an eigen-value problem,

$$\det(B - \mu A) = 0 \tag{15}$$

And the CFL is respected if the following relation is true,

$$\Delta t \le \Delta x . \min_{i=1,5}|\mu_i| \tag{16}$$

The system has zero eigen-values corresponding to the pressure variable. As the pressure is always an implicit variable, these zeros may be discarded and we only focus on the non-zero eigen-values for the stability study. Moreover, the size of the system may be reduced if the pressure is eliminated and if we note $\lambda=1/\mu$,

$$\det(B-\mu A)=\mu_1 A_{11}.\det(F-\lambda G)=0 \qquad (17)$$

The CFL criterion becomes $\Delta t \le \Delta x.\max_{i=1,4}|\lambda_i|$ and F and G have the following expressions,

$$F=\begin{bmatrix} 0 & -1 & -1 & -1 \\ TM_w & Tq\frac{\partial M_w}{\partial S_w} & -Tq\frac{\partial M_w}{\partial S_w} & -Tq\frac{\partial M_w}{\partial S_g} \\ TM_o & -Tq\frac{\partial M_o}{\partial S_w} & -Tq\frac{\partial M_o}{\partial S_o} & -Tq\frac{\partial M_o}{\partial S_g} \\ TM_g & -Tq\frac{\partial M_g}{\partial S_w} & -Tq\frac{\partial M_g}{\partial S_o} & -Tq\frac{\partial M_g}{\partial S_g} \end{bmatrix}$$

$$G=\begin{bmatrix} 0 & 0 & 0 & 0 \\ 0 & -\rho_w\phi & 0 & 0 \\ 0 & 0 & -\rho_g\phi & 0 \\ 0 & 0 & 0 & -\rho_g\phi \end{bmatrix}$$

This small system is solved using direct methods and the eigen-values are determined along the x direction (1-D problem) of each reservoir cell.

In 3-D reservoir geometries, The CFL for each reservoir cell may be written as in 1D for a given direction. For a unit vector n, the CFL condition for the stability of an explicit discretization of a reservoir cell i has the following expression,

$$\lambda(n)\Delta t^{n+1}.\left(\max\left(|n_x|\Delta x_i,|n_y|\Delta y_i,|n_z|\Delta z_i\right)\right)^{-1} \le 1 \qquad (18)$$

The global CFL is then the maximum of the above expression for all vectors n. This relation is too restrictive for reservoir simulations and more cells than needed are switched to implicit. So, we use a CFL using total fluid velocity[5], which requires that the domain of dependence of the system of equations remains within a rectangular prism on the neighboring cells. The CFL on a cell is calculated for a unit vector n parallel to the total fluid velocity v. So, we can write, $n = v/\|v\|$, with $v=v_w+v_o+v_g$.

$$\lambda_{\max}.\Delta t^{n+1}\max\left(\frac{|v_x|}{\Delta x_i},\frac{|v_y|}{\Delta y_i},\frac{|v_z|}{\Delta z_i}\right)/\|v\| \le 1 \qquad (19)$$

This last condition assured good stability in our tests and is quite cheap to evaluate.

Implicit Explicit Method (IMPEX)

Another solution has already been proposed to mix advantages of explicit and implicit treatment of the flow terms in the transport equations. Quandalle and Savary[6] presented in 1989 a method, implicit in pressure and saturations and explicit in compositions for compositional models. More recently, robustness and efficiency of this method have been verified on synthetic compositional models[7]. In this approach, the full Jacobian matrix, reduced to a 3 x 3 - block matrix by elimination of selected equations is used to solve the implicit P, Sw, and Sg unknowns. The variations of oil and gas compositions are next calculated easily from these implicit unknowns. Behind this method is the assumption that pressure and saturation unknowns are strongly coupled by mobility and relative capillary pressure terms, while component mole fractions are less strongly coupled from grid block to neighboring ones. This is often the case even with compositional models unless the diffusion/dispersion fluxes are modeled.

Advantages of this approach are numerous. It is easy to implement in a multipurpose reservoir simulator, and benefits from optimized and efficient Black-oil implicit linear solvers. The parallelization of the method should give better speed-up than AIM because problems of load balancing between implicit and explicit regions of the reservoir could be avoided and it can be used without constraint on the time step length by any CFL condition.

Hybrid AIM-IMPEX Method (AIMPEX)

This scheme is a further optimization of the AIM scheme. It mixes both AIM and IMPEX approaches and three different statuses may be addressed to the reservoir cells. A fully implicit formulation is used for the cells with the greatest variations. An IMPEX formulation is applied for the cells with important pressure and saturation variations and weak mole fraction variations, an explicit formulation is used for the remaining cells.

High Performance Computing Aspects

The parallel version of the IFP Group multipurpose reservoir simulator is designed for parallel shared memory platform (SMP nodes) and used the

OpenMP paradigm[11] for the management of the parallelism. A hybrid version is under development and will mix MPI (Message Passing Interface)[12] for high level communications and OpenMP for low level parallelism. This version will work on clusters of SMP nodes, the inter-nodes communications will be handled by MPI and the intra-nodes parallelism will be managed either by MPI and or by OpenMP.

This paper only concerns the development and the results obtained with the OpenMP version of the software but the hybrid version to come will have the same features.

The conventional implicit (SOLSS) and explicit (IMPEM) formulations implemented in the software have already been parallelized in former works[8]. The new models AIM, IMPEX and AIMPEX described here before, which mix implicit and explicit models, mainly use the SOLSS and IMPEM parts of the program but some specific optimizations have been performed to take advantage of the particular structure and reduced number of unknowns of the matrix of the linear system.

As the ratio between implicit and explicit cells changes during the simulation in the AIM and AIMPEX models, we designed dynamic data structures for the linear solver which are updated when status of cells changes.

With these structures, we reduced significantly the memory requirements. For instance, the memory used by the AIM model for the one million grid blocks test is 40% less than the memory required to run the simulation with the fully implicit scheme.

The critical part of the program is the parallel linear solver. The software uses the Bi-Conjugate Gradient Stabilized (Bi-CGSTAB)[9] algorithm preconditioned with the Incomplete LU Factorization of degree zero either on the pressure unknowns (P-ILU0P) or on the full Jacobian matrix.(P-ILU0). The Bi-CGSTAB implementation is mainly made of two calculation units, a matrix/vector product and the pre-conditioner.

The test cases described hereafter in this paper are very interesting because of the conductive fault and the injector wells which introduce heterogeneities on the distribution of implicit cells inside the reservoir. As a same calculation for an implicit cell is much more CPU time-consuming than an explicit one, these heterogeneities create bad load balancing on the processors and slow down the code running on a parallel computer.

Typically, matrix/vector products in the linear solver are very sensitive to this and a dynamic and optimized load balancing for parallel calculations was developed. This algorithm automatically computes at each time step the best way to distribute the calculations above the processors. As the load balancing was very bad without this algorithm, the speedup of this part of the code was limited to a value lower than half times of the number of processors. Now, with this algorithm, even if the load balancing still remains not perfect because the number of treated elements is never exactly the same and some cache memory effects have important impacts, we recorded on the treated cases a speedup of 8 for the matrix/vector products on 8 processors.

As explained before, two parallel pre-conditioners P-ILU0P and P-ILU0 are implemented in the software. For the simulations, we used the P-ILU0P method. This pre-conditioner is not affected by the distribution of the implicit cells because only pressure unknowns are considered as for explicit formulations. The parallelization of the P-ILU0/P-ILU0P pre-conditioners is based on a partitioning of the matrix graph of the linear system. An in-house graph partitioner has been developed, based on matrix graph and selected grid properties. The parallel algorithm of the P-ILU0/P-ILU0P pre-conditioners alternates calculations on domains and inter-domain zones[8].

If the distribution of the implicit cells has no impact on the performances of P-ILU0P, it is not the case for P-ILU0. Optimization of this algorithm still has to be done and the idea is to build a better partitioning by adding constraints on the nodes of the matrix graph as inputs of the partitioner. These added constraints should be for example the number of implicit unknowns of the cells represented by a node. The dynamic aspect of the AIM and AIMPEX models makes more difficult the use of this method because the graph partitioning should be updated when the status of the cells changes. Such update should be very expensive in CPU time. A solution could come from the grid partitioning algorithm such as ParMETIS[13] which allows re-partitioning with lower calculation costs.

RESULTS AND DISCUSSION

These different methods have been implemented in a commercial release of the IFP Group multipurpose reservoir simulator and have been tested on a compositional field case study. Two grids have been build, one with roughly 180,000 active cells (later referred as 180k case), and the other with one

million active cells (later referred as 1M case). The reservoir has an area of 3.75 km*10.2 km, and the 180k case has a 75*204*12 grid with 50m*50m cell dimensions (Fig. 1). The 1M case uses a 150*408*17 discretization grid with 25m*25m cell dimensions. The reservoir is slightly slanted from west to east and an aquifer is located on the eastern flank. The porosity varies from 0.01 to 0.2 and is better on the reservoir crest and in its northern part. Horizontal permeabilities are about 20 mD and vertical permeabilities are ten times lower. Moreover, there is a conductive fault in the southern part of the reservoir. This fault is oriented from east to west (from the aquifer to the crest) and extends for 3 km. Its permeability is about 1.5D and is modeled using the conductive fault model integrated in the simulator[13].

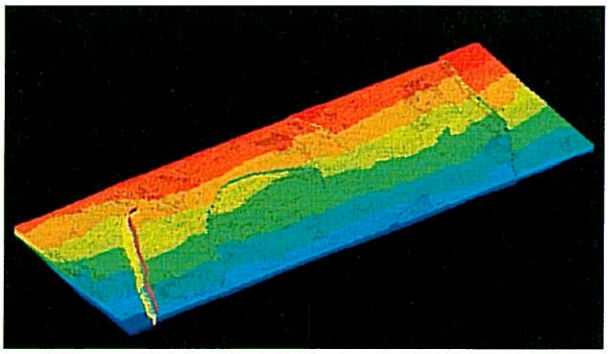


Fig. 1. Reservoir grid.

The oil is modeled by a compositional model with 9 components (C1, N2, C2-COH, C3-C4, C5-C6, C7-C9, C10-C13, HCO1, and HCO2). The initial oil in place is 191 Mm^3 at standard conditions and initial pressure is 450 bars at a depth of 3500 m (the reservoir is located between 3100 and 3800m) and the initial water-oil contact is located at 3800m depth.

Eight (8) oil producers are situated in the crest and 6 water injectors are located on the flank near the aquifer. The surface oil rate of each producer is set constant at 2500 m3/d and the surface water injection of each injector is 4000 m3/d. The injection is automatically calculated by the simulator such that the total reservoir injection rate equals its total voidage production rate. The wellhead pressure of the producers is controlled and limited to 17 bars. The bottom-hole pressure of the injectors is limited to 600 bars. The reservoir is produced for 20 years.

The presence of the conductive fault disables the use of explicit scheme because of the water invasion at its vicinity. The simulation runs using the AIM, the IMPEX and the AIMPEX formulations were made on parallel computers. The test cases presented in this paper were run on different parallel SMP platforms:

-a Dell Precision 530, bi-processor Pentium4 Xeon @2,4GHz with 2GB DDRAM,

-a SGI O2000, 20 processors R10K @195MHz, 10GB memory,

-an IBM p690 Turbo, 32 processors Power4 @1,3GHz, 64GB memory.

180k Case Study

At the end of the simulation, the injected water has invaded large areas of the reservoir and oil has been displaced to the producers. Using AIM schemes, correlation may be found between implicit cells and water invaded cells (Figs. 2 and 3). During the simulation, important saturation variations occurred in these cells and those have been switched from explicit to implicit by the simulator. During the simulation 82,813 cells (45 %) have switched to an implicit status.

The mixed formulation of the equations (AIM or IMPEX) allows great reduction in the simulation time. The results are displayed in Table-1 and Figure-7 for different machines for the 180k compositional case.

Table 1. Comparisons on a Linux computer.

	Step	Newton it.	Solveur it.	CPU time
AIM	278	278	13559	24315
AIMPEX	278	278	13177	22250
IMPEX	278	278	13870	20194
SOLSS	278	278	14813	73169

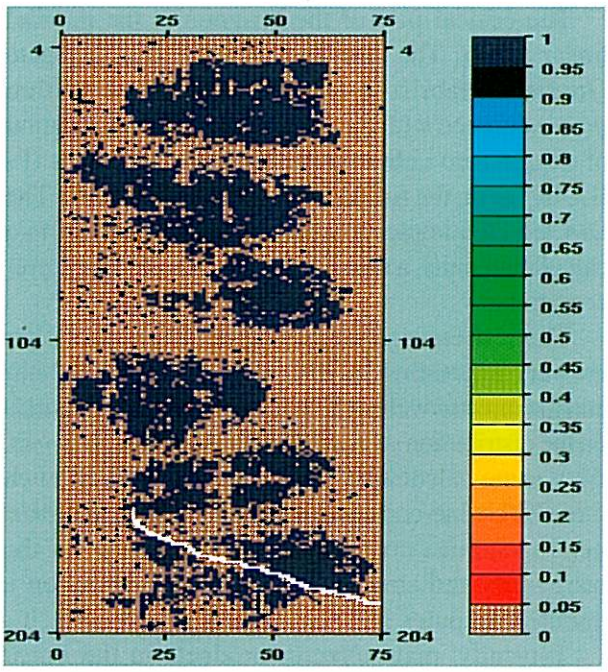


Fig. 2. Implication map in the most invaded layer.

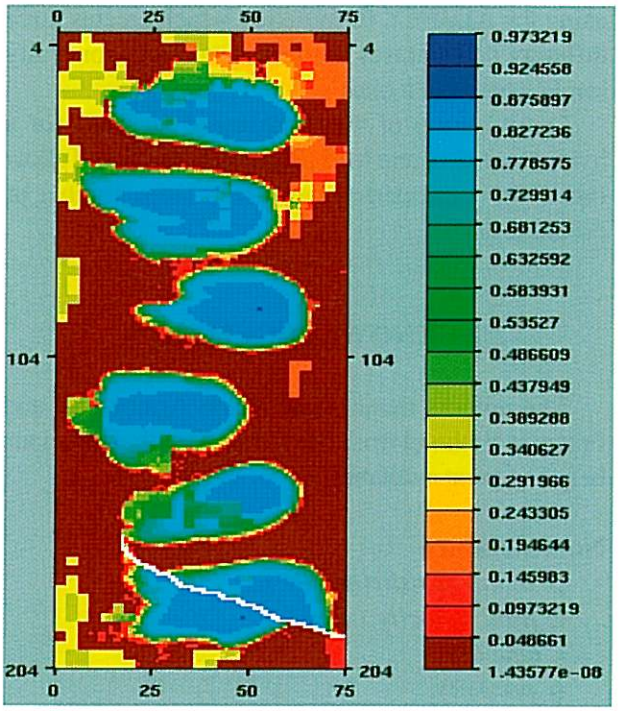


Fig. 3. Water saturation map in the most invaded layer.

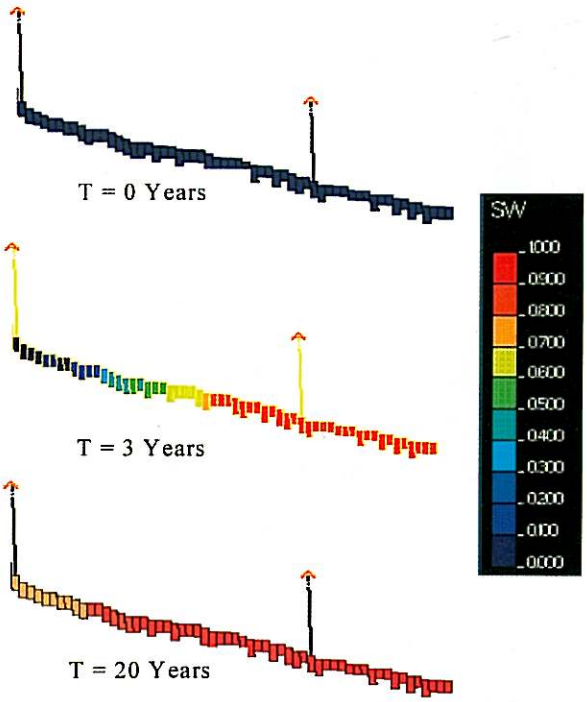


Fig. 4. Water invasion in the conductive fault.

The adaptive implicit method switches from explicit to implicit the most varying cells given our proposed CFL based criteria. The physical results are very similar to the fully implicit ones which is to say that the criterion adequately takes into account the saturation fronts and switch to implicit the cells located near the fronts (Figs. 5 and 6). The conductive fault is also quickly invaded by the water coming from the injectors and the water cut of the producing well located near the fault increases rapidly (Figs. 4 and 6). The fault-cells are treated implicitly due to their strong variations during the time steps. Moreover, the required memory is also decreased from more than 2Gb to less than 1Gb (55% gain).

Furthermore, hybrid formulations (AIM or AIMPEX) allow to reduce both time and memory requirements and ensure good physical results.

1M Case Study

The full production history has been run on 8 processors of the IBM P690 machine using the AIMPEX formulation. Partial simulations were carried out on 1, 4 and 8 processors in order to evaluate speedups for the other formulations. The obtained results are displayed on Figure 8. AIMPEX runs three times faster than the fully implicit model and makes feasible a large compositional simulation overnight. The IMPEX simulation is faster than the AIM. This is explained by the high number of implicit

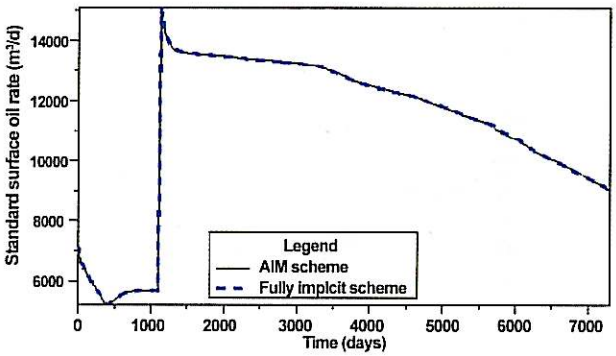


Fig. 5. Total oil rate comparison.

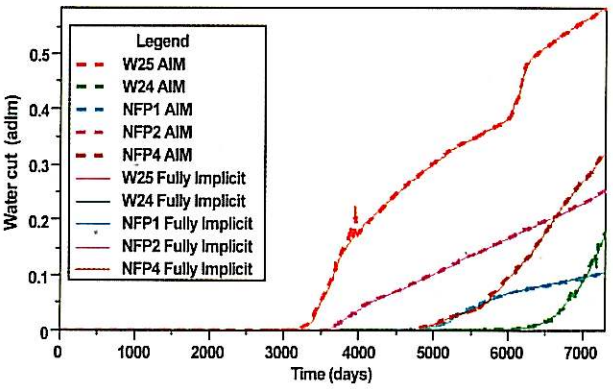


Fig. 6. Water cut comparison.

cells imposed by saturation variations. Nevertheless, it has been observed that for simulations with high oil or gas composition variations, AIM becomes faster than IMPEX. The field performance for this case is the same as for the 180k case.

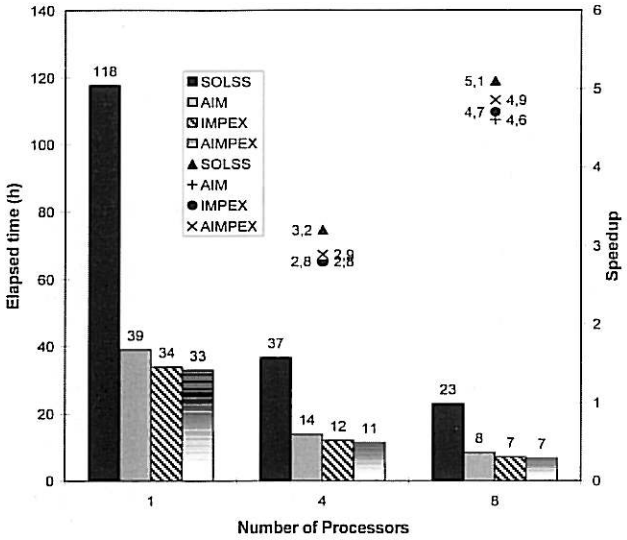


Fig. 7. Elapsed times and speedups for 180k case on SGI O2000.

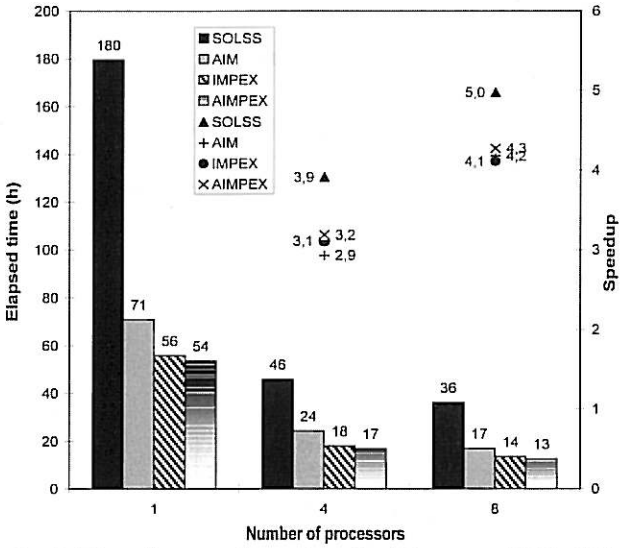


Fig. 8. Elapsed time and speedups for 1M case on IBM p690 Turbo.

The SOLSS fully implicit simulation requires 20 Gb whereas, the AIM, AIMPEX and IMPEX schemes only need less than 7Gb memory.

Our parallelized hybrid algorithms perform large compositional simulations where classical fully implicit methods, even parallelized, exceed computer capabilities in terms of memory and CPU time.

CONCLUSIONS

We propose integrated parallelized numerical schemes to perform large compositional reservoir simulations. In the presented results, the global simulation time is greatly reduced by using hybrid formulations. Best performances in terms of simulation time and physical results were obtained using the AIMPEX formulation which creates three different cell statuses in the grid varying from fully implicit to explicit ones.

Optimization of these advanced methods for a hybrid OpenMP and MPI parallelization should allow obtaining better performance on a large number of processors.

ACKNOWLEDGEMENTS

The authors thank Anne-Marie Armbruster and François Bothorel from IBM France for their precious help and great availability.

Nomenclature

ρ, *molar density*($mol.m^{-3}$).
v, *fluid velocity* ($m.s^{-1}$).
t, *time* (s).
ϕ, *porosity*.
T, *transmissivity* (m^3).
M, *mobility* ($Pa^{-1}.s^{-1}$).
S, *saturation*.
P, *pressure* (Pa).
w, *water phase*.
o, *oil phase*.
g, *gas phase*.
X, *molar fraction in oil phase*.
Y, *molar fraction in gas phase*.

REFERENCES

[1] Coats, K.H., 2001 (February). IMPES stability: the stable step. Paper SPE 69225, proceedings of the 16th SPE Symposium on Reservoir Simulation, Houston, TX.

[2] Coats, K.H, Nielson, R.L., Therhune, M.H. and Weber, A.G., 1959. Simulation of three-dimensional, two-phase flow in oil and gas reservoirs. *Trans. AIME*, **216**, 290-96.

[3] Coats, K.H., 1980 (December). An equation of state model. *Soc. Pet. Eng. J.*, 363-76.

[4] Fung L.S.-K., Collins D.A., and Nghiem L.X., 1989 (February). An adaptive-implicit switching criterion based on numerical stability analysis. *SPE Res. Eng.*, 45-52.

[5] Grabenstetter J, Li Y.K., Collins D.A. and Nghiem L.X., 1991. Stability-based switching criterion for adaptive-implicit compositional reservoir simulation. *SPE* 21225, 11th SPE Symposium on Reservoir Simulation, Anahaim, CA.

[6] Quandalle, P. and Savary, D., 1989 (February). An implicit in pressure and saturations approach to fully

compositional simulation. Paper *SPE* 18423, presented at the 1989 Symposium on Reservoir Simulation, Houston, TX.

[7] Hui Cao and Aziz K., 2002 (November). Performance of IMPSAT-AIM models in compositional simulation. Paper *SPE* 77720, presented at the SPE Annual Technical Conference, San Antonio, TX.

[8] Magras J-F, Quandalle P., 2001. High-performance reservoir simulation with parallel ATHOS. Paper *SPE* 66342, presented at the 2001 Reservoir Simulation Symposium, Houston, TX.

[9] Saad, Y., 2000. *Iterative Methods of Sparse Linear Systems*. Second Edition.

[10] Russel T.F., 1989. Stability analysis and switching criteria for adaptive implicit methods based on the CFL condition. *SPE* 18416 presented at the SPE Symposium on Reservoir Simulation, Houston.

[11] OpenMP web page: http://www.openmp.org

[12] MPI web page: http://www.mpi-forum.org

[13] ParMETIS link: http://www.cs.umn.edu/~metis.

[14] Henn N., Bourbiaux B., Quintard M., Sakrhikumar S., 2000. Modeling fluid flow in reservoirs crossed by multiscale fractures – a new approach. EAGE, 7th European Conference on Mathematics of Oil Recovery, Baveno, Italy.

Petroleum Res. J. Vol. 18 (2005); P. 91–104, 11 Figs.

Could WAG be the Right EOR Process for Libyan Carbonate Reservoirs?

Rafa Labedi, Omar Abdulkarim, Karlo Krizmanic and Saleh El-Fakhri*

هل تعاقب الماء بالغاز عملية إسترداد صحية بمكامن الصخور الكلسية بليبيا؟

رافع اللبيدي، عمر عبد الكريم، كارلو كريزمانيك وصالح الفاخري

كميات كبيرة من النفط الخام ستبقى غير مستخلصة من مكمن الصخور الكلسية المنتجة بطريقة الغمر بالماء من وحدة النافورة – أوجلة أحد الحقول العملاقة التابعة لشركة الخليج العربي للنفط، نقدم في هذه الورقة أهمية الدراسات المعملية ومعرفة البحث التقني كجزء رئيسي من إنجاز دراسات المحاكاة المتكاملة لتقييم المسترد الإضافي من الناحية التقنية والجدوى الاقتصادية والتخطيط. تعتبر نتائج تحاليل اللب المتقدمة أحد الأدوات القوية لمعايرة النماذج المكمنية، ومن أجل تشريق خواص المائع وخاصة الابتلالية ونهاية نقاط التشبع، تجري التجارب عند ظروف المكمن الحقيقية.

دلت تجارب كثافة الاستنفاذ لثاني أكسيد الكربون على الاختراق المبكر لثاني أكسيد الكربون وانخفاض في كفاءة الإزاحة بينما نتج عن اختبارات الإزاحة بطريقة تعاقب الماء بالغاز غير الممتزج استخلاص زيت عالي، وكما هو الحال في الأنبوب الرفيع عند الضغط الأدنى للإمتزاجية.

إذا طريقة تعاقب الماء بالغاز غير الممتزج بمقدرتها العمل أفضل عند أي عملية حقن للغاز غير الممتزج باستخدام الغاز الهيدروكربوني والنيتروجين أو غازات الاحتراق عند ضغوطات منخفضة للغاية بدلا من الضغط الأدنى للإمتزاجية بمكامن جيرية ذات بيئات ترسيب متشابهة وتغير في نشأة النسيج وانتقائية في الإذابة.

Abstract: *In Nafoora Augila Unit (NAU), one of the giant oil fields of AGOCO, an appreciable amount of oil will remain unrecoverable in the prolific carbonate layers after waterflooding. In this paper, we present the importance of experimental studies and knowledge (technological research) as a major part of achieving integrated simulation studies for evaluating the EOR technical and economical feasibility, and planning.The special core analysis (SCAL) results are one of the most powerful tools to calibrate reservoir models. The laboratory experiments are performed at actual reservoir conditions to honor fluid properties, the wettability and saturation end-points. CO_2 gravity drainage experiments resulted in an early CO_2 breakthrough and low displacement efficiency, while immiscible water alternating gas (IWAG) displacement tests resulted in an oil recovery as high as in case of slim tube, at the minimum miscibility pressure (MMP). Therefore, IWAG could potentially work well for any other immiscible gas injection process using hydrocarbon gas, nitrogen, or fuel gases, and at significantly lower pressures than the MMP in carbonate reservoirs of similar depositional environment and diagenetic fabric selective dissolution.*

INTRODUCTION

The common classification of WAG processes is to distinguish between miscible, MWAG, and

* Arabian Gulf Oil Company (AGOCO), Benghazi, Libya.

immiscible, IMWAG displacements. Because of failure to maintain sufficient pressure, real field cases may oscillate between MWAG and IMWAG during the implementation of the WAG process. Important technical factors affecting WAG performance have been identified: heterogeneity, wettability, fluid properties, miscibility conditions, injection techniques, WAG parameters, and physical dispersion and flow geometry.

The oil recovery can be described by three contributions: microscopic displacement efficiency, horizontal and vertical sweep efficiencies. Our concern is to highlight aspects of microscopic displacement efficiency in IWAG process by integrations of previous SCAL studies and technological research.

When performing a miscible gas displacement, the residual oil saturation will tend to go toward zero in the flooded area. A problem in MWAG process is that injected water blocks contacts between injected gas and remaining oil. This reduces microscopic displacement efficiency, resulting in higher residual oil saturation. This effect has been found to be a strong function of rock wettability and oil recovery is adversely affected by the presence of mobile water in water-wet cases, but the effect of mobile water is almost negligible in mixed-wet and preferentially oil-wet reservoirs[1,2,3].

With IWAG process the residual oil saturation after gas-flooding is lower than after water-flooding, meaning that gas has a better microscopic displacement efficiency than water. In water swept zones, the residual oil saturation to water-flooding is reduced through the gas entrapment process. The degree of oil saturation reduction and corresponding trapped gas saturation depend on initial gas saturation and wettability. The experiments demonstrate the need to measured the IWAG microscopic displacement efficiency and trapped gas saturation on preserved or wettability restored cores[4,5,6].

Gas saturation is divided into two contributors, trapped and mobile gas saturations. Trapped gas can be only become remobilized by dissolving in the oil, and the only contributor to gas flow is the free gas saturation. Reduced residual oil saturation increases the oil mobility. For given oil saturation the water saturation is less in WAG injection by the amount of reservoir volume occupied by the trapped gas. As a result the water mobility and therefore water cut must be less for given oil saturation. Reduced permeability of the gas phase can be achieved by alternate injection of gas and water. Therefore improved microscopic sweep efficiency in three-phase zones of the reservoirs could add benefit from reduction of mobility in IWAG processes.

The displacement mechanism in IWAG process occurs in a three-phase regime, where the cycling nature of the process creates a combination of imbibitions and drainage. Conventional two-phase relative permeability hysteresis models were unable to describe MWAG and IWAG flows in cores and field trials, where gas and water saturations will increase and decrease alternating. This gives special demands for relative permeability for oil, gas and water phases. Recent approach has been designed for WAG injection using cycle dependant oil, water and gas relative permeabilities[7,8,9].

Therefore the optimum WAG design is different for each reservoir and needs to be determined for specific reservoir and fine tuned for particular area within reservoir[10,11].

Microscopic displacement efficiency by WAG processes has to be determined from laboratory experiments.

SCAL PROGRAM

Minimum Miscibility Pressure Requirements

Slim tube tests showed that MMP is 270 barg, and that displacement efficiency does not fall sharply below MMP. A significant amount of oil could be recovered at pressures substantially below slim-tube MMP[11,12,13].

Keeping in mind with principle of economy we have investigated that possibilities incorporating our best knowledge of the state of art technology.

Petrophysical Classes and Pore Space Classification

Reservoir rock is relatively clean bioclastic limestone. The depositional texture is skeletal grainstone and packstone/wackstone. Early consolidation preserved much of primary porosity. Selective dissolution of skeletal debris in the undersaturated zones of the meteoric phreatic environment provided moldic and pinpoint vuggy porosity. Mesovuggy porosity is the main pore type with additional interparticle and variable microporosity[14,15]. Figure 1 shows CT-SCAN investigations of the internal structure of the whole

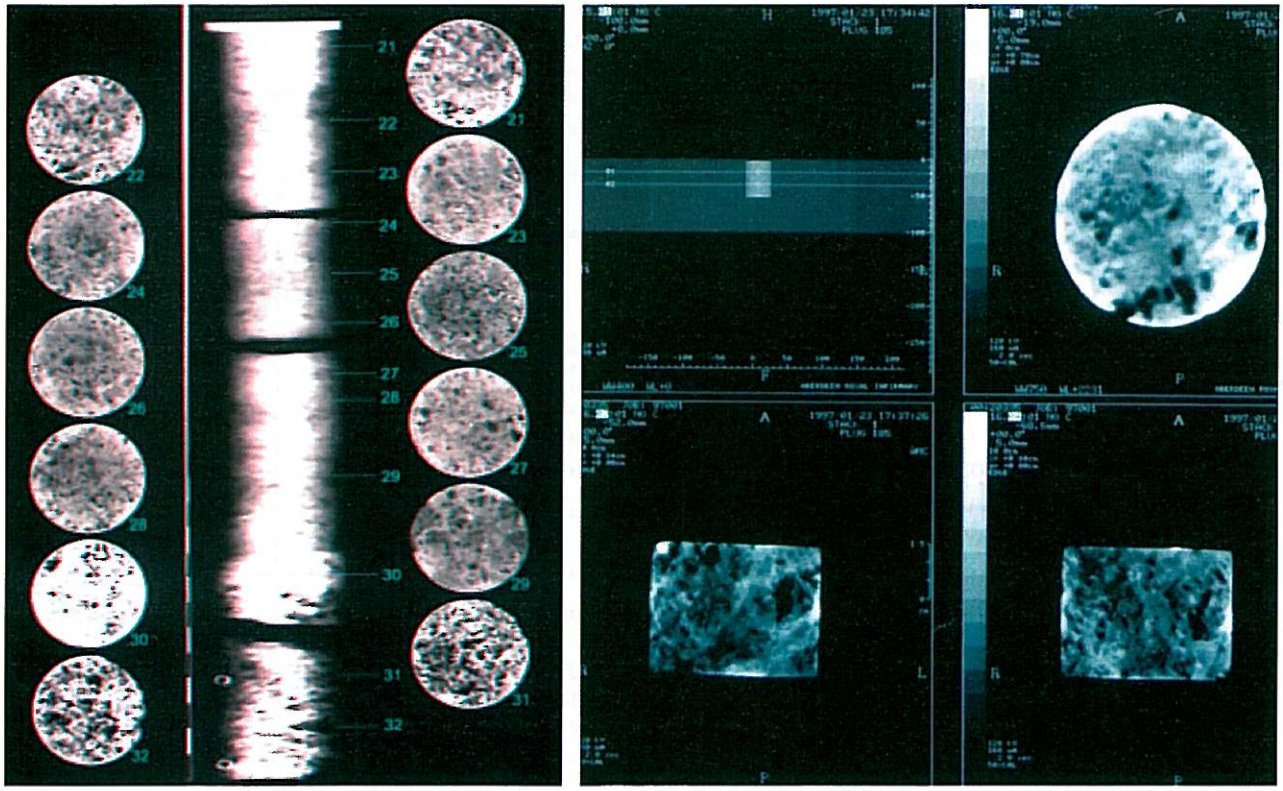


Fig. 1. CT-SCAN images showing pore structure.

core samples. In particular the macroporosity is well visible on most slices.

Rock fabrics has been grouped into four rock-fabric petrophysical classes:

1. clean coquina limestone dominated by large skeletal grains.
2. skeletal bioclastic grainstone
3. grain dominated packstone/wackstone
4. mud (micritic) dominated limestone

Principal pore types and pore interconnections are grouped into:

1. intergranular, macro in rock-fabric class 1, good connected in rock-fabric classes 1 and 2, variably occupied by micritic matrix in rock-fabric classes 2 and 3.
2. secondary dissolution, moldic and vuggy
3. good microporosity within micrit materials composed of loosely arranged small calcite crystals (rock-fabric classes 2 and 3).

Pore interconnections in secondary dissolution pore space

1. abundant and interconnected touching vuggy porosity and channel like from skeletal and micitic matrix leaching (dominant on 1" and 1.5" small plug scale)
2. discrete, separate vuggy porosity (dominant on full diameter and well log scale).

Wettability

The capillary imbibition curves are typical of oil-wet samples. The Amott/USBM wettability tests show the reservoir wettability ranges from weak-to-strong oil-wetness[14,15]. The vuggy system connected by the largest thresholds pore entry radii is strongly oil-wet. The spontaneous imbibitions of water at 80°C for three weeks resulted in the increase of water saturation in the range 8.3% to 9.5%. This is an indication that the majority of intergranular/ intercrystalline pore system, variably occupied by micritic matrix, could be less oil wet due to pore structure. Therefore wettability question in intergranular/intercrystalline pore system may be the matter of some concern.

Resistivity Measurements and Interpretation

A.) *Use of Maxwell-Garnett Model to Interpret Formation Factor, FF, Measurements.*

In heterogeneous carbonate reservoirs the porosity exponent, m, is a major factor of uncertainty in the calculation of fluid saturation. Complex electrical behavior may result from the way in which vuggs are related to each other, and to the intergranular pore space.

FF's were measured on core plugs from two carbonate reservoirs at net overburden pressure, NOB, by simulated formation brine, and reservoir oil[14,15]. CT-SCAN images of core samples were used to characterize pore types and interconnections in secondary dissolution pore space. The Maxwell-Garnett, M-G, model:

$$F_t = \frac{1}{\Phi_i^m}\left[\frac{1-\Phi_v\left(\frac{1-\Phi_i^m}{1-2\Phi_i^m}\right)}{1+2\Phi_v\left(\frac{1-\Phi_i^m}{1+2\Phi_i^m}\right)}\right] \quad (1)$$

allows for better interpretation of FF if both, the intergranular, Φi, and vuggy porosity, Φv, vary independently and simultaneously, resulting in a range of FF for a single total porosity, Φt[16,17].

Eq. (2) and Eq. (3) are the results of M-G model for abundant, interconnected touching and channel like vuggy poro system, and for discrete and separate vuggy pore system, respectively[18,19].

$$F = 2.3217\Phi^{-1.1619} \qquad r^2 = 0.8332 \quad (3)$$

$$F = 0.4469\Phi^{-2.549} \qquad r^2 = 0.8511 \quad (2)$$

Intercept a, known as tortuosity parameter, could be related to depositional environments and diagenetic fabric-selective dissolution process. Figures 2 a and b are the application of M-G model to interpretation of FF-Φrelationships, and division of total porosity into matrix and vuggy[18,19].

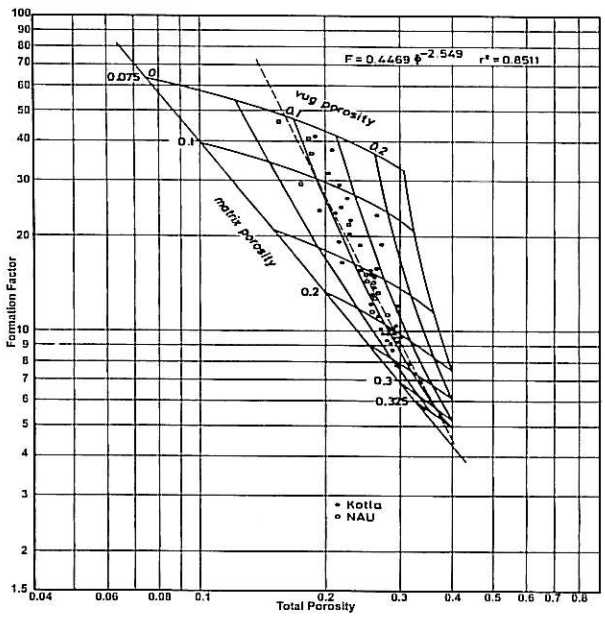


Fig. 2(a). Application of Maxwell-Garnett model to abundant interconnected touching and channel like vuggy porosity from skeletal and micritic matrix leaching, dominant on 1" and 1.5" small plug scale.

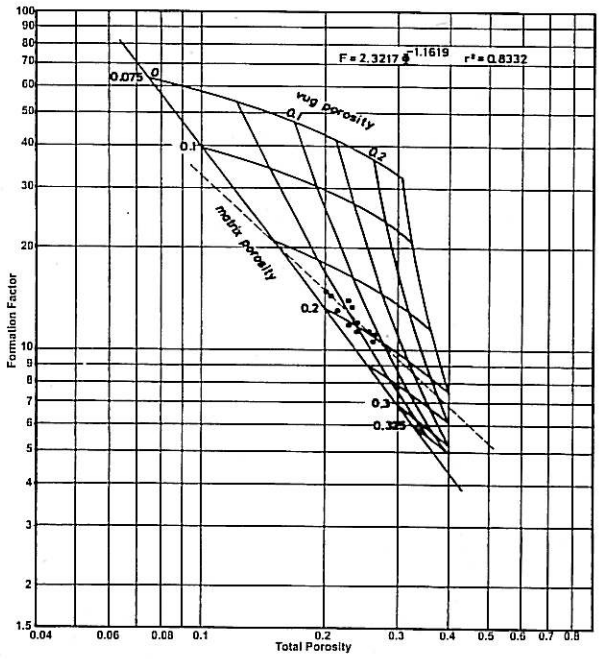


Fig. 2(b). Application of Maxwell-Garnett model to discrete, separate vuggy porosity, dominant on 1.5", full diameter and well log scale. Model allows division of total porosity into matrix and vuggy porosity components (from El-Ashahab, Krizmanic, Gherryo)[18,19].

For a elatively clean carbonate rock with a high salinity environment FF does not appear to be affected by surface conductance of clay component.

B.) *Use of Maxwell-Garnet Model to Separate Total Porosity into Intergranular and Vuggy Pore Space.*

Vuggy porosity is difficult to calculate from wireline logs, and requires detailed core-log calibration to give reasonable results. We separate total porosity into intergranular and vuggy porosity components, applying the M-G model [18,19]. The relations are:

$$\Phi_v = 0.8139\Phi_t - 0.1353 \qquad r^2 = 0.7495 \quad (4)$$

discrete vuggy system

$$\Phi_i = 0.0263e^{6.9401\Phi_t} \qquad r^2 = 0.7847 \quad (5)$$

abundant vuggy system

Thin-section image analysis provides a good approach of the effective vuggy porosity in carbonate rocks. Figure 3 shows comparison between vuggy versus total porosity from the M-G model, and from thin-section description of core material[20].

The M-G model is efficient in separating total porosity into intergranular and secondary dissolution.

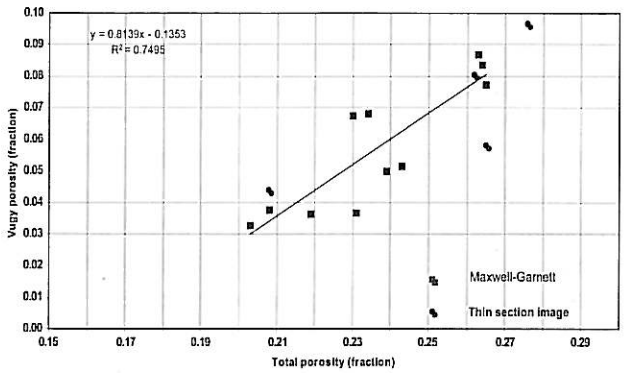


Fig. 3. Good agreement of vuggy vs. total porosity from thin-section analysis and from the Maxwell-Garnett model indicates usefulness of the model (from Krizmanic, Labedi, Abdulkarim, Gherryo) [18,19,20].

C.) *Resistivity Index.*

Laboratory resistivity measurements of FF and resistivity index, I_R, are acquired on rock samples to increase consistency of the log data interpretation. The evaluation of the amount and distribution of oil in place depend heavily on the model applied to describe links between FF, I_R and water saturation.

The resistivity index measurements were performed in conjunction with porous-plate, oil/brine capillary pressure. Sufficient time is allowed at each point for wattability restoration and equilibrium saturation to be achieved. A 4-electrode setting was used to avoid contact resistance and end effects[14]. Table 1 shows the properties of sample used and formation brine.

Figure 4 shows resistivity index curves versus saturation. Mercury capillary pressure curves interpreted in terms of pore throat size distribution show uni-modal pore size distribution within intergranular pore space. Low saturation exponent (n), and departure of I_R versus S_w from ideal Archie's law recently have been paid attention, and have been experimentally documented and theoretically explained 21 through 26.

Table 1. Core sample petrophysical parameters, properties of formation brine and tests condition.

Ambient condition air permeability, mD	15.5
NOB condition porosity, fraction	0.262
Saturation exponent (n)	1.65
Net overburden (NOB) pressure	3000
Temperature, ^{0}F, (^{0}C)	150, (66)
Brine salinity, mg/l TDS	189 991
Resistivity of brine, Ohm-m at 77^{0}F	0.054

Two slopes could explain I_r versus S_w relation. The first shows the invading of the vuggy pore space by oil. Vuggy rock surface is rendered to be strongly oil wet. The second describes subsequent invasion of the intergranular pore space[20]. Best fit of the second straight-line segment is:

$$I_r = 2.6731 S_w^{-1.09} \qquad r^2 = 0.9961 \qquad (6)$$

The relation is valid in saturation range $0.78 < S_w > 0.099$. The change in the value of n at S_w = 0.78 provides the vuggy porosity component of

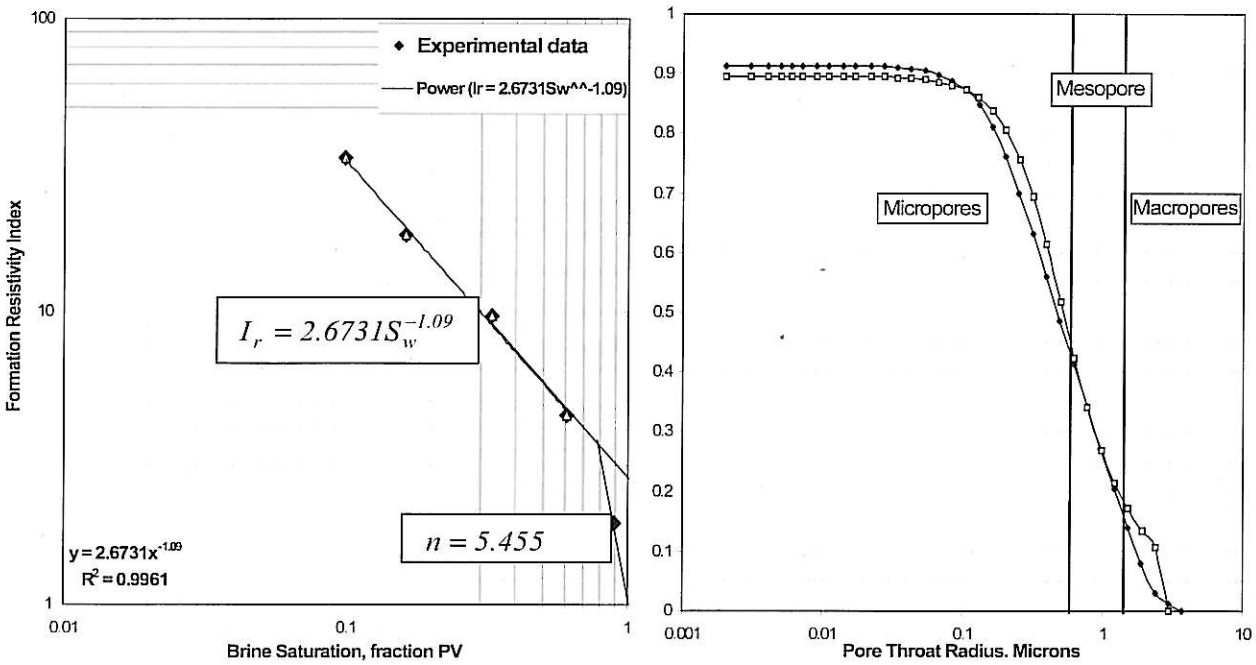


Fig. 4. Two straight-line segments of I_r vs. S_w: desaturation of vuggy pore space resulted in n = 5.455 and desaturation of unimodal interganular pore space resulted in $I_r = 2.673 IS_w^{1.09}$. Microporosity is linked to the presence of micrite crystals (from Gherryo Krizmanic, Labedi, Abdulkarim) [20].

Φvug = 0.058, for the total sample porosity Φtot = 0.262. The oil content in vuggy pore space is S_{ov} = 0.22. The M-G model (4) provides vuggy porosity component of Φvug = 0.078, and S_{ov} = 0.292.

The second straight-line implies:

a) Unimodal pore size distribution of the intergranular pore space, as indicated by the mercury injection data and

b) There is no wettability induced change in electrical properties within intergranular pore space.

The wettability question in intergranular pore system may be the matter of some concern.

D) *Water Saturation Model.*

Use of coreflood test data to provides arguments for the choice of adequate saturation models. Checking the validity of different models, and calibration of the parameters remain a frequent problem in log interpretation[23,25 through 29]. We modified Archie's model. The modified Archie's model is[20]:

$$S_w = \left[\left(\frac{R_w}{R_t}\right)\frac{a}{b}\Phi^{-m}\right]^{1/n} \qquad (7)$$

where b comes from : $S_w = bI_r^{-n}$

The model: $I_r = 2.6731 S_w^{-1.09}$ provides model parameters $b = 2.6731$ and $n = -1.09$. Eq. (3) provides model parameters $a = 2.3217$ and $m = -1.1619$, while Eq. (4) provides model for separation of total porosity into discrete vuggy porosity component in total. These model parameters, coupled with gas-flood tests data, provide arguments that the selected saturation model is adequate.

For considered carbonate formations, Figure 5 shows vuggy oil saturation as a function of initial oil saturation, porosity and formation resistivity range.

Tables 2 and 3 show secondary CO_2 gravity drainage experimental data. Breakthrough, BT, of CO_2 occurred at 38.2% PVI, resulting in oil saturation reduction of ΔS_o = 0.271. The M-G model provides vuggy oil saturation S_{ov} = 0.292. Evidently oil contained in intergranular pore space is not efficiently accessible to CO_2 with IFT = 2.7 mN/m.

Figure 6 shows comparison of vuggy porosity and oil content in vuggy pore space evaluated by: M-G models, resistivity index and displacement experimental tests. The Archie's water saturation model, conditioning to gas core-flood tests data, exhibits high consistency of all data.

Fig. 6. shows the comparison of vuggy porosity and vuggy oil saturation from M-G model, resistivity index, and displacement tests. Resitivity and coreflood tests provide arguments for the choice of adequate

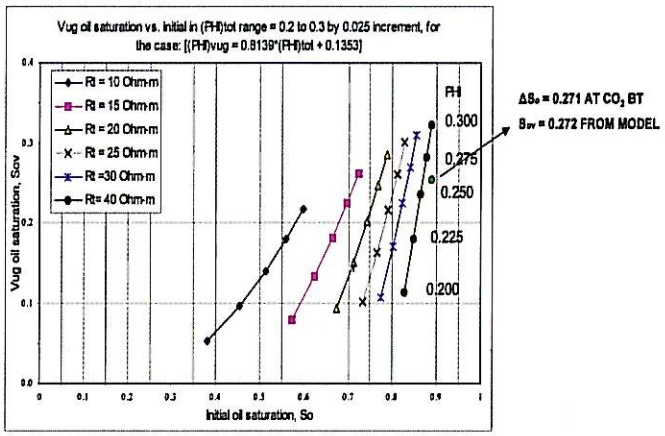


Fig. 5. Vuggy oil saturation versus initial saturation. Integration of I_R measurements with displacement test provide arguments for the choice of adequate saturation model.

Table 2. Long stacked core properties

Test	L (cm)	D (cm)	V (m/d)	Swi	Kw (mD)	Ko(Swi) (mD)	Φ
Gravity stable	150	4.5	0.146	0.079	28		0.264
WAG	147	4.5	0.150	0.251	37	17	0.255

Table 3. Statistics of gravity stable and WAG secondary displacement tests.

	@ water breakthrough					@ gas breakthrough			
	PVI (%)	R (%OOIP)	S_{oi}	S_o@BT	S_{oi}-S_oBT	PVI(%)	R(%OOIP)	S_o@BT	S_{oi}-S_oBT
Gr. Dr.			0.921			38.1	26.3	0.65	0.271
WAG	62.66	63.46	0.749	0.272	0.477	88.16	73.8	0.202	0.547

	@ the end of continuous gas injection					
	PVI (%)	Rfinal (%OOIP)	S_{oi}	S_{or}	S_{oi} - S or	S_{gfinal}
Gr. St	191.2	51.4	0.921	0.514	0.407	0.407
WAG	109.4	90.72	0.749	0.0769	0.6795	0.6721

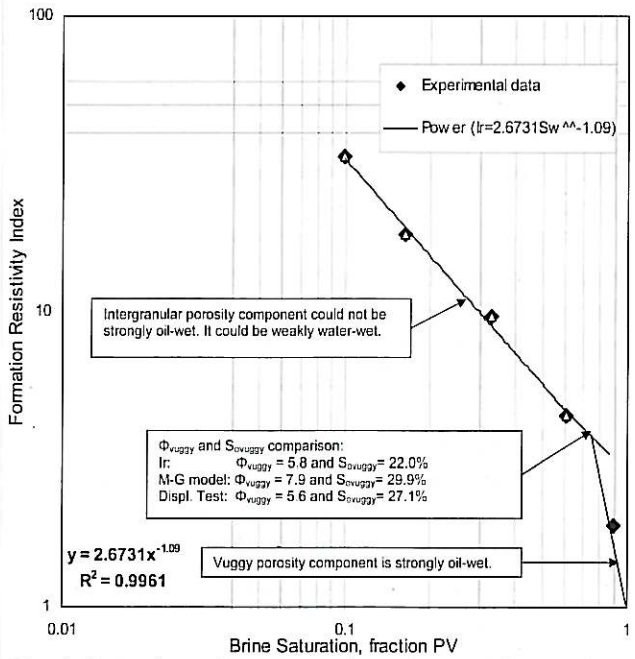


Fig. 6. Comparison of vuggy porosity and vuggy oil saturation from M-G model, resistivity index, and displacement tests. Resitivity and coreflood tests provide arguments for the choice of adequate interpretation model. (from Gherryo, Krizmanic, Labedi, Abdulkarim) [20].

interpretation model. (From Gherryo, Krizmanic, Labedi, Abdulkarim[20]).

The model provides higher values for oil in place contained in mesopores and micropores of intergranular pore space, target for EOR technologies. It provides good estimates of both the vuggy porosity component in total and the oil content in vuggs.

CORE-FLOOD DISPLACEMENT TESTS

Petrophysical Characterization on Small Core Plugs.

The petrophysical characterization on small core plugs is essential for considering interpretation of the IWAG and gravity drainage experiments on long composite cores. The tests include:

a) Mercury injection and pore throat size distribution analysis,

b) Centrifuge oil/water drainage/imbibitions and gas/oil/connate water drainage capillary pressure curves - the average saturations are corrected to obtain the saturations at inlet face of the plugs,

c) Oil/water imbibitions relative permeability curves and gas/oil/connate water drainage relative perms and

d) IFT measurements on CO_2 swollen fluids.

The tests were performed on wettability restored 1.5 inches in diameter, and 2.5 to 3 inches in length plugs. The resulting two-phase relative permeability will be used to help interpretation of IWAG and gravity stable drainage displacement tests on long,stacked cores.

Research shows that the centrifuge method is a fast and reliable method for obtaining oil desaturation curve as a function of trapping number, NT, in regions of low oil relative permeability, and in reservoirs where gravity drainage controls the recovery process[11,30 through 34].

$$N_T = \frac{\left|K\left(\nabla P + g\Delta\rho\nabla D\right)\right|}{\sigma} \qquad (8)$$

Figure 7 shows oil desaturation curves for two-phase oil/water, and three-phase oil/gas/connate water systems. The advantage over displacement tests is evident.

Reservoir simulation requires a realistic spatial distribution of capillary pressure and relative permeability. Drainage capillary pressure curves are used to predict initial water saturation, while imbibitions capillary pressure curves significantly impacts overall displacement efficiency. Figures 8 a and b show oil/water and gas/oil/ connate water centrifuge capillary pressure curves.

Unsteady-state water-flood and gas-flood tests were carried out on restored state cores. Capillary pressure curves were used as an input for numerical calculation – which means that the residual oil

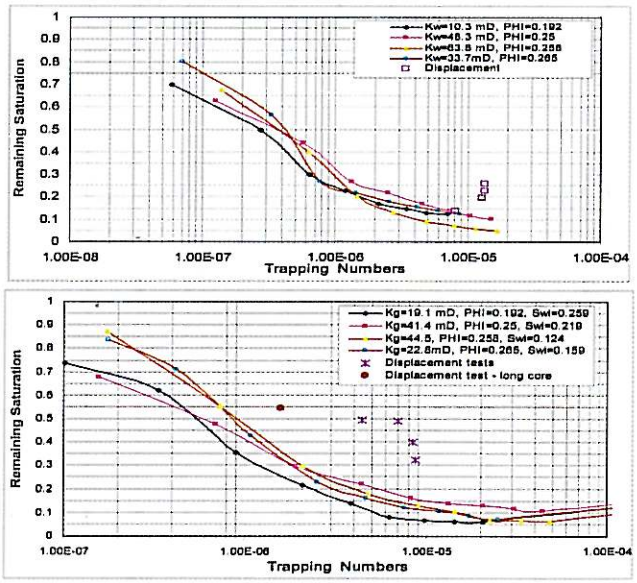


Fig. 7. Remaining oil saturation, S_{or}, achieved in displacement tests in comparison with oil de-saturation centrifuge capillary pressure curves: oil/water and oil/gas/connate water systems. Low S_{or} values are result of continuous oil film drainage.

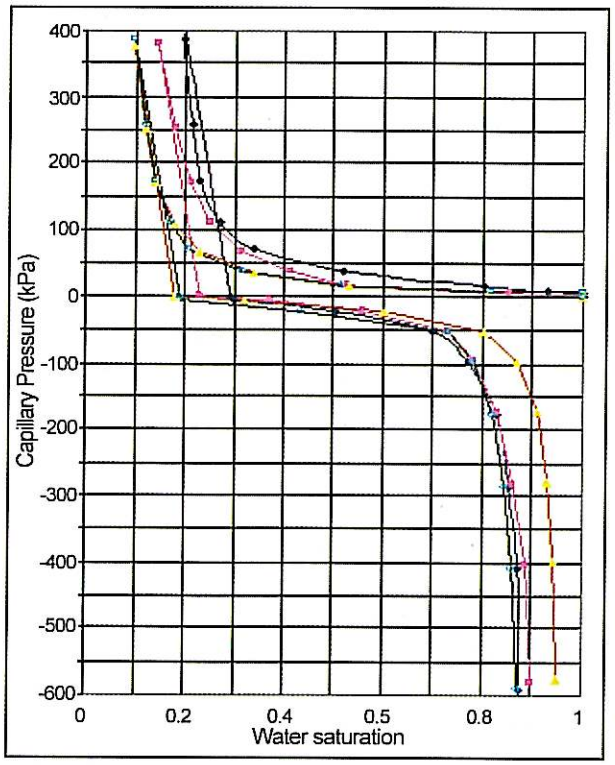


Fig. 8(a). Capillary pressure oil/water drainage/imbibitions curves – negative branches of Pc curves show that displacement efficiency could be deteriorated by strong capillary retention forces.

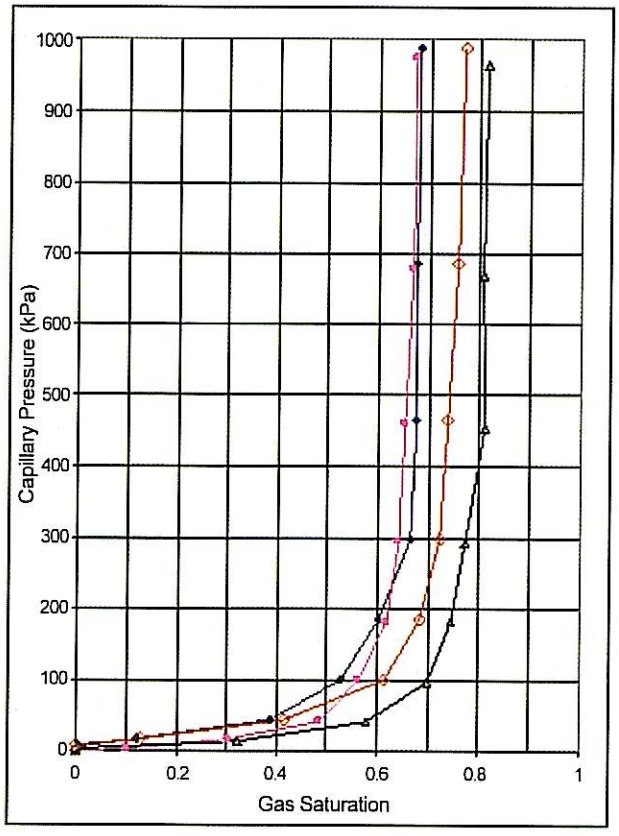


Fig. 8(b). Drainage gas/oil/connate water Pc's. capillary pressure curves were input in core-flood simulator.

saturations are supposed to be equal for displacement and centrifuge experiments. Therefore the relative permeability curves, obtained by history matching of production data with numerical coreflood simulator, take into account of viscous, capillary and gravity forces.

Figures 8 c and d show oil/water and gas/oil relative permeability curves. Although the oil could be displaced by oil-wetting layers to very low S_{or} values, the efficiency would be deteriorated by low

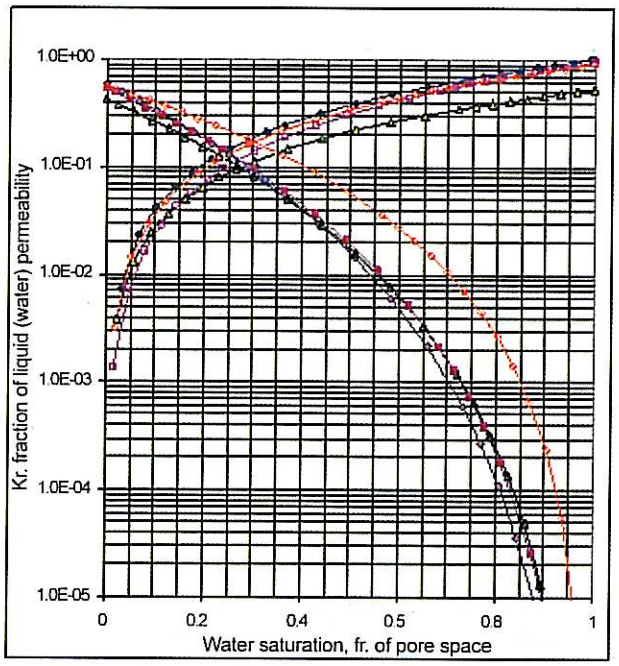


Fig. 8(c). Relative permeability curves oil/water.

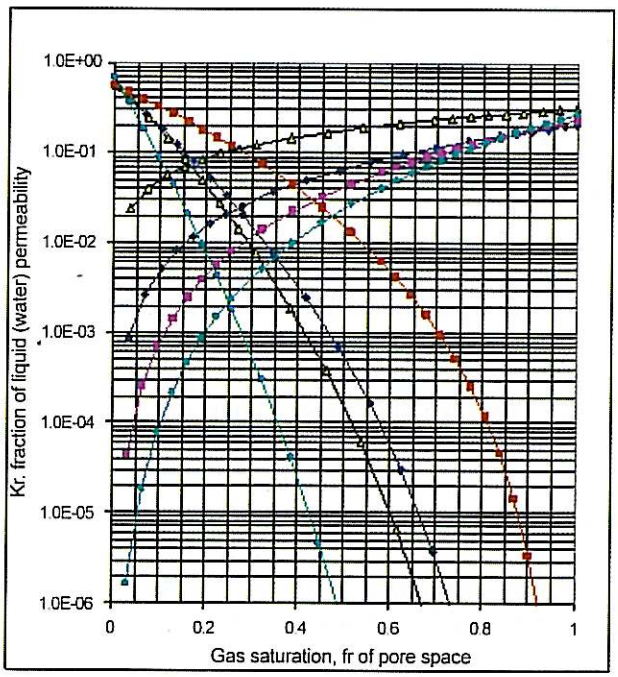


Fig. 8(d). Gas/oil relative permeability curves correctly account for viscous, capillary and gravity effects.

rates because relative permeability is also low in the range from 1E-3 up to 1E-5 and lower. Large scatter of oil/gas relative permeability curves is related to heterogeneity of small core-plugs.

Petrophysical characterization on small core plugs is an indispensable step for interpretation of displacement tests on long stacked cores.

Statistics of Secondary CO_2 Gravity Drainage and WAG Experiments on Long Stacked Cores.

Tests were performed at pressure of 193 barg. (MMP = 270 barg). Table 2 lists basic rock properties of long stacked cores. Dual energy x-ray detection allows assessing oil, water, and gas saturation profiles along the core.

Secondary CO_2 Gravity Drainage Experiment.

Table 3 shows statistics of the secondary gravity drainage and IWAG displacement tests. Final oil recovery R = 41.4% of OOIP, left behind residual oil saturation S_{org} = 0.544. CO_2 BT occurred at 38.2% PVI, when oil recovery at gas BT is 26.3 % of OOIP. Oil saturation reduction of $\Delta S_o = 0.271$ is exactly the swept volume of oil contained in vuggy porosity space (The M-G model provides $S_{ovug} = 0.292$). Evidently oil contained in intergranular pore space is not efficiently accessible to CO_2 with IFT = 2.7 mN/m. To access the oil contained in this pore space, a high reduction in IFT is needed. The reservoir pressure should be maintained at a level in excess of P_r = 270 bar.

The test was interpreted by numerical calculation to provide oil/gas relative permeability as an input for correct description of IWAG process on core scale.

Secondary IWAG Displacement Test was carried out with CO_2 injected first, followed by water. The slug sizes were approximately 8.4% PV. The IWAG injection resulted in final oil recovery, R_f= 90.7% of the OOIP with left behind residual oil saturation, S_{or}= 0.0769. Water broke through first resulting in oil recovery, R_{wbt} = 63.5% of OOIP, followed by gas BT with an oil recovery of R_{gbt} = 73.8% of OOIP.

The IWAG process is more efficient than secondary gravity drainage. From core scale point of view the IWAG technology could be the right technology for carbonate reservoirs of identical depositional environment and fabric-selective dissolution process. The process is immiscible and it could potentially: a) recover the same amount of oil as the miscible process with CO_2, but at a significantly lower pressure, b) work well using the other gases, and c) work well at even lower reservoir pressures.

Pore scale and core scale displacement scenario. In vuggy porosity space, oil is a strongly wetted phase retaining continuity even at low oil saturation based on SCAL tests results. Water is a non-wetted phase. Gas is a wetting phase relative to water. Neither gas in presence of water, nor water in presence of gas, could spread on oil forming continuous gas or water films.

The first gas injection cycle.

Gas displaced oil from the largest oil-wet vuggy pore space by piston like displacement, and through continuous oil film drainage.

The first water injection cycle.

Water displaced gas and oil from the largest oil-wet vuggy pore space by double displacement. Gas had been displaced by piston-like and, oil through continuous wetting oil film flow. Due to adverse mobility ratio, gas had channeled through the oil occupied pores forming an oil bank ahead of water. As a result of capillary competition between gas and oil and gas and water, snap-off of gas and trapping could occur only by oil in the gas occupied pores.

Gas snap-off by water and gas trapping could not be possible in water invading zone. However in this zone, gas could be bypassed in larger oil-wet pores.

In intergranular pore space, wettability was randomly distributed to a degree of $COS\Theta_{ow}$ for each pore size. Larger pores preferentially oil wet, were surrounded by smaller preferentially water-wet pores. Water had invaded the smallest weakly-water to weakly-oil wet pores by capillary diffusion. From this pore network, oil could be displaced by a corner filaments flow and by a piston like displacement depending upon wettability and water/oil contact angle hysteresis[5,33,34].

As a consequence of this capillary dominated flow, feeding and thickening of oil films in larger oil-wet pores of vuggy pore space occurred. Oil bank ahead water-front increased in size through oil film flow, and more gas was trapped by snap-off and bypassing. Trapped and bypassed gas reduced mobility of advancing water-front and formed oil bank, which resulted in a steady increase of water injection pressure.

Increase of water injection pressure favored a capillary controlled water flow into the smallest pore network and forced (viscous) controlled into the largest pore network of intergranular pore space. Viscous flow of water from vuggy to intergranular pore space has been initiated when the water pressure in vuggy pore space, P_w, exceeded oil pressure in integranular, P_o by capillary entry pressure given by $(s_{ow}\, cos\Theta_{ow})/r$. For largest preferentially oil-wet intergranular pores, $-1 \le cos\Theta_{ow} \le 0$. Oil which squeezed into vuggy pore space supported flow of continuous oil films, and made oil bank increased in size trapping more gas.

Trapped gas could be remobilized by dissolving in water and oil and by compression. At some threshold pressure, compressed trapped gas globules collapsed and/or were squeezed ahead, forming a small gas bank of free gas saturation within oil bank. Compression/decompression of trapped gas added to increased/decreased oscillations of injection pressure. Figure 9 shows oscillations of injection pressure for the first and second water injection cycles.

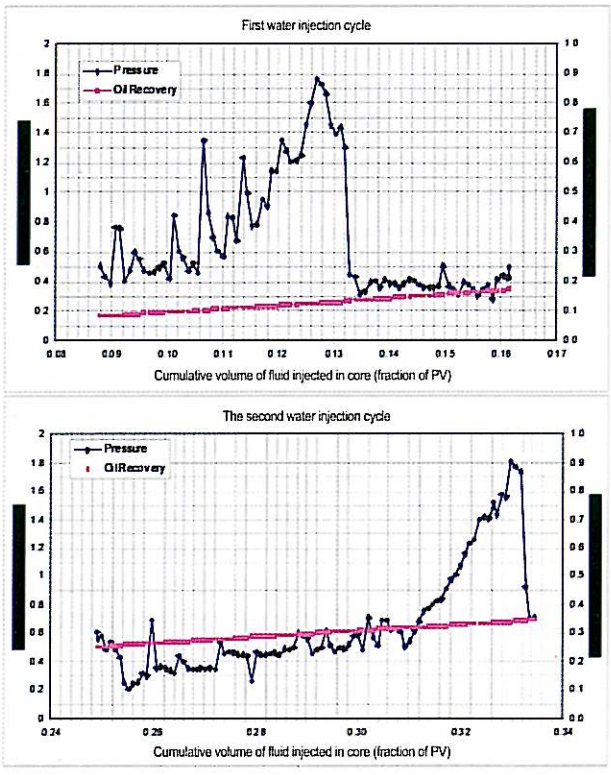


Fig. 9. Bypassed and trapped gas in vuggy pore space caused increase of water injectivity. Pressure increase favored spontaneous and forced imbibitions of water from vuggy into intergranular pore space and countercurrent flow of oil into vuggy pore space. More gas was trapped in formed oil bank. Collapse of trapped gas resulted in a sudden decrease of injection pressure and forming free gas bank ahead of formed oil bank.

Subsequent gas injection cycles.

Since for strongly oil-wet vuggy pore network, $-1 \le cos\Theta_{gw} \le 0$ and $0 < cos\Theta_{go} \le 1$, or $(\sigma_{go} cos\Theta_{go}) \ge (\sigma_{gw} cos\Theta_{gw})$ gas preferred to enter the water filled pores of strongly oil-wet vuggy pore network. In the first injection cycle, injection pressure was higher when gas displaced oil and injection pressure became almost zero, or even small minus when gas displaced water from pores previously occupied by oil. This indicates that gas was a wetting phase relative to water in the strongly oil-wet vuggy pore space.

Water has been displaced by a piston-like displacement, and oil by a continuous oil films drainage. This means that water could become disconnected phase.

Due to the reduced mobility of water-front and oil bank, gas injection pressure had increased. Gas was forced to penetrate from vuggy into intergranular pore space. Gas could be either wetting or non-wetting phase relative to water, depending upon randomly distributed wettability for each pore size and non-wetting relative to oil. Gas occupancy preference of pore space is given by the relations between wettability, IFT, and pore size: $(\sigma_{go} cos\Theta_{go})$/r, and $(\sigma_{gw} cos\Theta_{gw})$/r. Gas preferred to occupy the largest pores filled by water from previous water injection cycle. Then, when faced with pores of equal radius, gas preferred to enter pores filled with oil, as the IFT between gas and oil was lower than between gas and water.

The process caused feeding the vuggy pore space by oil and redistribution of oil, gas and water in the intergranular pore space. Due to the redistribution of fluids and gas compression, the gas cycles were inefficient in oil recovery. Figure 10 shows that these features are common in gas injection cycles.

Subsequent water injection cycles.

Water invaded the smallest water-wet pores by capillary diffusion and displaced gas and oil from previously gas filled pores by double displacement process because of wetting and spreading conditions. Oil expelled from intergarnular pore space has increased thickness of continuous oil films in oil-wet vugyy pore network, which had been efficiently drained to the formed oil bank ahead waterfront.

As a result of multiple displacements gas had been squeezed from the largest to the next to largest, oil saturated pores. Therefore gas could be trapped since

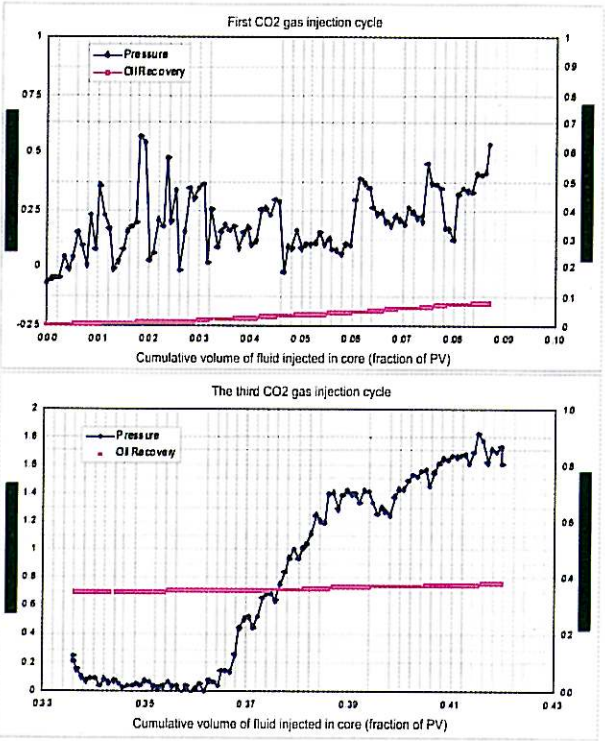


Fig. 10. Gas displaced water and oil from the largest vuggy pore space. Mobility increase in water-front and oil banks in vuggy pore space increase gas injectivity. Gas was forced to occupy the largest water and oil filled pores, squeezing oil into vuggy pore space. Gas was trapped in intergranular pore space by redistribution of phases in randomly distributed wettability for each pore size.

water became wetting to gas in the more weakly oil-wet pores. It is also expected that gas could be bypassed in relatively larger pores as these pores were surrounded by smaller, water wetting pore throats, from which water could not be displaced by gas.

Obviously continuity of oil wetting films in both pore networks made this process extremely efficient in oil recovery on scales of pores and core scale.

Cycling of gas and water injection resulted in an increasing-decreasing oscillation in the injection pressure. Therefore within leading oil bank, gas saturation consisted of trapped gas and formed slugs of free gas saturation. The gas production profiles in Figure 11 show that the slugs of free gas were produced before and after water breakthrough. Oil expelled from intergranular pore space was efficiently drained through the increased thickness of continuous oil films.

Additional 10% of oil was produced between water breakthrough and followed gas breakthrough. Large quantity of gas had been retained efficiently in intergranular pore network of randomly distributed wettability for each pore size.

Water saturation model provides higher values for oil in place contained in mesopores and micropores of

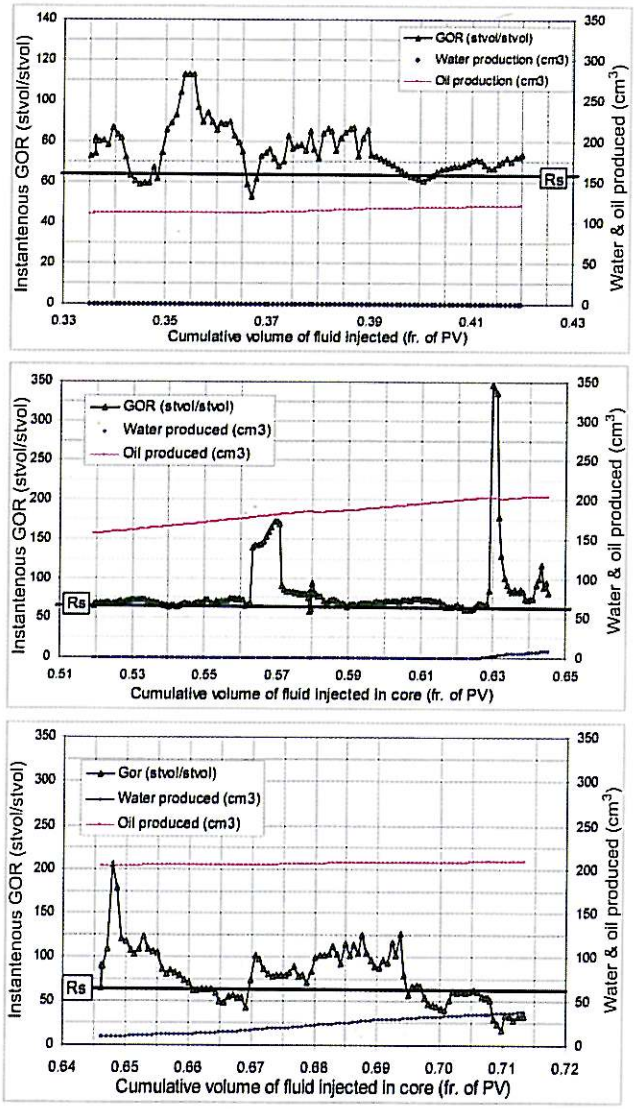


Fig. 11. Banks of free gas produced ahead of gas breakthrough suggested efficient oil expelling from intergranular pore space into vuggy by water and gas invasion. 10% of oil recovered between water and gas breakthroughs suggested efficient oil film flow in vuggy and intrgranular pore space and efficient gas trapping and blockages in intergranular pore network of randomly distributed wettability for each pore size.

intergranular pore space target for EOR technologies. From this point of view, IWAG process could be economically attractive. However the question is: could IWAG efficiently recover oil contained in intergranular pore space on large field scale application?

CAN WE EXPECT IWAG INJECTIVITY ABNORMALITIES AND EXTEND THREE-PHASE IWAG PHENOMENA THROUGHOUT RESERVOIR IN THE FIELD APPLICATION?

Well-documented three-phase phenomena can

lead to abnormal injectivity losses in IWAG processes. Substantial loss in water and gas injectivity observed on core scale could potentially increase the injection pressure, adding additional injection wells in the field application. Reduction of water and gas relative permeabilities from a situation when only water and oil phases flow, to the situation where flows of water, oil and gas are present, is important to consider for the IWAG injectivity abnormalities, pressure profiles within reservoir, and breakthrough of water. IWAG efficiency could be restricted in the reservoir volume around injection wells, where most of three-phase phenomena would occur, potentially reducing benefit of IWAG efficiency on the scale of field.

Therefore to predict IWAG behavior in the reservoir from experimental displacement results, a numerical simulation with an effective hysteresis description of three phase (oil, water and gas) relative permeability should be developed.

CONCLUSIONS

1. The technological research, experimental and simulation studies are prerequisites for selecting the right technologies for IOR. The integration of SCAL and core-flood tests results supports implementation of IWAG technology in a number of carbonate reservoirs of identical depositional environment and selective fabric-dissolution process. The process is immiscible and it could potentially work well with any other immiscible gases, at a significantly lower pressure than required MMP.

2. Further theoretical, experimental and simulation studies are required to provide technological and economical feasibility such as: selecting the right technology for the reservoirs, the amount of increased hydrocarbon reserves on field scale and reduction in unit production costs and initial developments of maturing oil fields.

3. To achieve these goals, the reservoir must be characterized from a variety of viewpoints with a large number of parameters and with remarkable degree of accuracy and consistency. All information should be gathered and integrated to reduce uncertainty, improve efficiency and help to select the right technology for selected reservoirs.

4. Tree-phase phenomena could lead to abnormal high injectivity losses in WAG process. Increasing the injection pressure, adding additional injection wells, and IWAG efficiency restriction in the reservoir volume around injection wells, where most of three-phase phenomena would occur, would potentially add difficulties to apply IWAG successfully in fields. Therefore a development of realistic cycle-dependent three-phase relative permeability model from coreflood tests by numerical simulation should be performed.

5. Design of IWAG process by simulation should include three-phase flow description through development of an effective hysteresis description of three-phase, cycle-dependent oil, water and gas relative permeability.

REFERENCES

[1] Green,D.W., Willhite, G.P., 1998. Enhanced Oil Recovery. SPE Textbook Series **6**, Richardson, TX.

[2] Huang, E.T.S., and Holm, L.W., 1988 (Feb.). Effect of WAG injection and rock wettability on oil recovery during CO_2 flooding. SPERE.

[3] Lin.E.C., and Huang, E.T.S., 1990 (May). The effect of rock wettability on water blocking during miscible displacement. SPERE..

[4] Schneider, F.N., Owens, W.W., 1976 (Feb.). Relative permeability studies of gas-water flow following solvent injection in carbonate rocks. *SPEJ.*

[5] Kralik, J.G., Manak, L.J., Jerauld, G.R., and Spence, A.P., 2000 (Oct.). Effect of trapped gas on relative permeability and residual oil saturation in an oil-wet sandstone. SPE 62997 presented at the 2000 SPE ATCE, Dallas, TX.

[6] Krizmanic, K. El-Ashahab, B., Abdelkarim, O. and El-Fakhri, S., 2001 (Nov.) Trapped gas saturation – interpretation of experimental data for considering immiscible and miscible WAG injection." Nafta (Zagrb-Croatia).

[7] Skague, A., 1996 (Sept.). Influence of wettability on trapped nonwetting phase saturation in three-phase flow. Procedings 4th International Symposium on Wettability and its' Effect on Oil Recovery, Montpelier, France.

[8] Larsen,J.A., Skague, A., 1998 (June). Methodology for Numerical Simulation With cyclic-Dependent Relative Permeabilities. *SPE Journal.*

[9] Larsen, J.,A., Skague, A., 2000 (Oct.). Simulation of the immiscible WAG process using cycle-dependent three-phase relative permeabilities. SPE 56475 presented at the 1999 SPE ATCE, Houston, TX.

[10] Christie, M.A., Muggeridge, A.H., Barley, J.J., 1993 (Feb.). 3D simulation of viscous fingering and WAG schemes. SPE Reservoir Evaluation.

[11] Abdelkarim, O., Krizmanic, K., El-Ashahab, B., El-Fakhri, S. and Nesmari, N, 2001 (June). Some aspects of CO_2 flood for Sirte Basin reservoirs (Libya). OAPEC_IFP Joint Seminar, Paris, France.

[12] Abdelkarim, O., El-Fakhri, S. Krizmanic, K., and Nesmari, N., 1999 (Nov.). An overview of CO_2 flood projects in the Arabian Gulf Oil Company. The 6th Mediterranean Petroleum Conference and Exhibition, Tripoli, Libya.

[13] Krizmanic, K., Abdelkarim, O., El-Fakhri, S. and Nesmari, N., and El-Ashahab, B., 2000 (July). CO_2 flood projects of clastic and carbonate reservoirs in The Arabian Gulf Oil Company - Libya. Nafta (Zagrb-Croatia).

[14] Core Laboratories: Advanced Rock Properties Study for the AGOCO. March 1998 through July, 2002.

[15] TOTAL, 1998 (Oct.). Nafoora Augila field – long composite cores and reservoir fluid characterization.

[16] Maxwell-Garnett, J.C., *Transaction of the Royal Society, London*, **203**, 385.

[17] Herrick, D.C., and Kennedy, W.D., 1995 (June). Formation resistivity factor and permeability relationships in rocks characterized by secondary solution porosity. Paper QQQ presented at SPWLA 36th Annual Logging Symp., Paris.

[18] Krizmanic, K., El-Ashahab, B.M., and Gherryo, J., 2000 (Aug.). Kotla and Nafoora Augila Unit – Formation Resistivity Factor Analysis. AGOCO internal documentation.

[19] El-Ashahab, B.M., Krizmanic, K., and Gherryo, J., 2002 (July). Formation resistivity factor for carbonate reservoirs – Sirte Basin, Libya. Nafta.

[20] Gherryo, J.S, Krizmanic,K., Labedi, R., Abdulkarim,O., 2004 (Jan.). Integration resistivity, pore size distribution and core-flood displacement tests provides arguments for the choice of adequate saturation model in rock characterized by solution porosity. Paper presented the 8th Mediterranean Petroleum Conference & Exhibition, Tripoli, Libya.

[21] Swanson, B.F., 1985 (June). Microporosity in reservoir rocks. its measurement and influence on electrical resistivity. Paper F presented at the 1985 SPWLA Annual Logging Symposium, Dallas.

[22] Wortington, P.F., Pallat, N., and Toussaint-Jackson, J.E., 1989 (June). Influence of microporosity on the evaluation of hydrocarbon saturation. SPE Formation Evaluation.

[23] Argaud, M., Giouse, H., Starley, C., Tomanic, J., and Winkler, K., 1989 (Oct.). Salinity and saturation effects on shaly sandstone conductivity. Paper SPE 19577 presented at 1989 SPE ATCE, San Antonio, TX.

[24] Wortington, P.F., and Pallat, N., 1992 (June). Effect of variable saturation exponent on the evaluation of hydrocarbon saturation. SPE Formation Evaluation.

[25] Krizmanic, K., Mesmari, N., Obeida, T.A., and El-Ashahab, B.M., 1997 (July). The effect of variable saturation exponent on original oil in place evaluation –Sarir sandstone case, Libya. Nafta, **48**.

[26] Claudine, C., Brosee, E., and Cerepi, A., 2001 (June). Effect of pore-lining chlorite on petrophysical properties of low-resistivity sandstone reservoirs. SPE Reservoir Evaluation & Engineering.

[27] Waxman, M.H., and Smiths, L.J.M., 1968 (June). Electrical conductivities in oil-bearing shaly sands. *SPEJ.*

[28] Waxman, M.H., and Thomas, E.C., 1974 (Feb.). Electrical conductivities in shaly sands -I. The temperature coefficient of electrical conductivity. *JPT.*

[29] Clavier, C., Coates, G., and Dumanoir, J., 1977 (Oct.). The theoretical and experimental bases for 'dual water' model for the interpretation of shaly sands. Paper SPE 6859 presented at 1977 SPE ATCE, Denver, Colorado.

[30] Hirasaki, G.J., 1995 (Oct.). Dependence of waterflood remaining oil saturation on relative permeability, capillary pressure and reservoir parameters in mixed-wet, turbidite sands. Paper SPE 30076 presented at 1995 SPE ATCE, Dallas, TX.

[31] Sharma, M.M., and Filoco, P.R., 2000 (Sept.). Effect of brine salinity and crude-oil properties on oil recovery and residual saturations. *SPE Journal.*

[32] Jain, V., Chattopadhyay, S., and Sharma, M.M., 2002 (April). Effect of capillary pressure, salinity, and aging on wettability alteration in sandstones and limestones. Paper SPE 75189 presented at the 2002 SPE/DOE IOR Symp., Tulsa, OK.

[33] Sohrabi, M., Henderson, G. D., Tehrani, D.H., Danesh, A., 2000 (Oct.). Visualisation of oil recovery by water alternating gas (WAG) injection using high pressure micromodels – water-wet system. Paper SPE 63000 presented at 2000 SPE Annual Technical Conference and Exhibition, Dallas, TX.

[34] van Dijke, M.I.J., Sorbi, K.S., Sohrabi, M., Tehrani, D.H., Danesh, A., 2002 (April). Three-phase flow in WAG process in mixed-wet porous media: pore-scale network simulations and comparison with micromodel experiments. Paper SPE 75192 presented at the 2002 SPE/DOE Improved Oil Recovery Symposium, Tulsa, OK.

Petroleum Res. J. Vol. 18 (2005); P. 105–114, 4 Figs.

Application of Downhole Oil-Water Separation: A Feasibility Study

Mohamed A. Alhoni*

تطبيق فصل الماء عن الزيت بقاع البئر

محمد الهوني

تم إجراء دراسة جدوى هندسية على حقل نفطي رئيسي يدار بواسطة شركة الواحة للنفط وذلك لتحديد جدوى تطبيق تقنية فصل الماء عن الزيت بقاع البئر، وتحديد الآبار المناسبة بهذا الحقل لتطبيق هذه التقنية. إن استراتيجية الاستنزاف الحالية (أو أي تطويرات مستقبلية) للمكمن GE تؤدي إلى أن إنتاجية الاحتياطي النفطي المتبقي سيتم بزيادة مضطردة لنسبة المياه في الزيت، لذلك فإن فصل الماء عن الزيت في قاع البئر والتخلص من المياه المفصولة تمثل وسيلة هامة لتحسين أداء الحقول الحالية والمستقبلية.

لقد تم تطوير معيّرة لمراجعة خصائص المكمن والبئر أكثر تفصيلا ولتحديد الآبار المرشحة لاحتمال تطبيق هذه التقنية (فصل الماء عن الزيت بقاع البئر). كما تم تحديد المخاطر والمحاذير الموجودة في الآبار المرشحة حيث أظهرت ثمانية عشرة بئراً من أصل أربعة وعشرون بئرا خصائص مميزة للمكمن والبئر وتوافقت مع الشروط الأولية لتطبيق هذه التقنية. إن المعيّرة المستعملة ربما تستعمل لتقييم حقول أخرى بهدف تطبيق هذه التقنية (فصل الماء عن الزيت بقاع البئر). سيتم في هذه الورقة استعراض تصميم أولي لتطبيق طريقة فصل الماء عن الزيت في قاع البئر على ثلاثة آبار.

Abstract: *An engineering feasibility study has been conducted on a major oil field operated by Waha Oil Company to determine the feasibility of applying downhole oil-water separation technology (DHOWS) and to rank the candidate wells within this field on the basis of their suitability for a DHOWS installation. With the current depletion strategy (or any future developments), the nature of the GE reservoir is such that, the remaining oil reserves will have to be produced at high and constantly increasing watercuts. Downhole separation and disposal of produced water present a material opportunity to improve the current and future field performance.*

A screening template was developed to review the reservoir and well characteristics in more detail and to identify a list of candidate wells for the possible implementation of DHOWS technology. Several operational risks and concerns that exist in respect of the candidate wells were identified. Eighteen wells out of twenty four wells demonstrated favorable reservoir and well characteristics and met the initial DHOWS screening criteria. The screening template may be used to evaluate other fields for potential conventional DHOWS applications. A preliminary design of a DHOWS application for three wells is presented in this paper.

INTRODUCTION

It is widely known that the continuous increase in the water-oil ratio hinders the oil production rate, contributes to high operating cost and is a major source of environmental concern to the oil companies. In the past, the response of operators to increasing water production rates was to go up to the top section of

* Waha Oil Company, Libya.

the reservoir in an oil well away from the rising water, while trying to slow down the advance of water with squeeze cement and cement plug techniques. The oil industry experiences with these techniques have shown mixed results. Meanwhile, if water cannot be stopped and the cost of handling the water and additional other costs exceed the revenue the operator has to abandon the well despite the fact that significant volumes of oil can still be produced.

The Centre for Engineering Research Inc. initiated a feasibility study in 1991 to test a new technique to reduce water-handling costs by reducing the volume of water produced at the surface. This work produced the idea of combining separation and pumping systems downhole and simultaneous injection of the produced water in the same wellbore. Matthews *et al.*[1] presented a novel system for downhole separation and re-injection of produced water in the same well. The technique was applied to two wells in the Alliance field and the results indicated an increase in oil rates. Peachey *et al.*[2] presented a brief summary of field trials completed and the key results achieved, including oil production increases, water reduction, predicted increases in reserves recovery and main factors affecting a successful DHOWS application. Shaw *et al.*[3] indicated that The DHOWS technology could be applied successfully in low risk wells. They defined the risk as a function of workover cost and deferred production; high risk therefore being a prolific well with high workover costs. Scaramuzza *et al.*[4] described the separation system implemented in Grey, Red and Green sands of Barrancas formation, the candidate wells selected, and the results of pilot field trials. Li *et al.*[5] conducted indoor dynamic simulation experiments to test downhole separation and injection technique for a rod pumping well. Jokhio *et al.*[6] reviewed in some detail the economic parameters that affect DHOWS and summarized the characteristics of a waterflood operation that can benefit economically from this technology.

The aim of this feasibility study is to determine the technical and economical justification to use the downhole oil-water separation system in the GE reservoir, to rank candidate wells within this field on the basis of their suitability for a DHOWS installation, and to develop a screening template that can be used in the evaluation process of oil fields for potential DHOWS applications.

RESERVOIR CHARACTERISTICS

The suitability of the GE reservoir for DHOWS application was studied in terms of the observed/ demonstrated reservoir behavior. The GE reservoir has been under primary recovery operations since 1964. The succeeding sections individually examine each of the following reservoir characteristics: reservoir description, drive mechanism, production history, and water disposal/injection zone potential.

Reservoir Description: The GE reservoir is located in the upper part of the G limestone, a formation present in most areas of the Sirt Basin. The formation lithology/depositional environment can be classified as a nummulitic-shallow shelf carbonate sequence with an aggregate formation thickness of 1500 to 1700 ft in the highs and over 2000 ft in the troughs. The reservoir interval is comprised of a shoaling upward sequence defined by 4 main reservoir units. Table 1 presents reservoir

Table 1. GE reservoir – reservoir unit facies/lithologic descriptions.

Name	Dominant facies	Dominant texture	Vugs
Shoal 1	Wackestone w/ whole numulites	Mud-dominated packstone (45 %) + Grainstone (20 %)	15 % Touching 35 % Separated
Shoal 2	Nummulitic wackestone + nummulitic packstone	Mud-dominated packstone (45 %) + Grain-dominated packstone (30 %)	20 % Touching 20 % Separated
Shoal 3	Nummulitic packstone	Grain-dominated packstone (60 %) + Mud-dominated packstone (25 %)	30 % Touching 15 % Separated
Shoal 4	Nummulitic packstone +bryozoan packstone	Grain-dominated packstone (50 %)	10 % Touching 15 % Separated
Lower 1	Bryozoan packstone	Grain-dominated packstone (65 %)	5 % Touching 30 % Separated
Lower 2	Bryozoan packstone	Grain-dominated packstone (65 %)	0 % Touching 10 % Separated
Lower 3	Nummulitic packstone	Grain-dominated packstone (50 %) + Grainstone (40 %)	10 % Touching 30 % Separated
Basal	Nummulitic packstone + packstone w/ Large Nummulites	Grainstone (85 %)	~0 % Touching ~0 % Separated
Sub-basal	Not defined	Not defined	

unit facies/lithologic descriptions. The GE reservoir is a highly undersaturated oil reservoir producing under the influence of a strong natural water drive. In spite of the strong natural water drive, there has been significant decline in reservoir pressure over the last 37 years. Also, available pressure data indicate that the pressure decline is not uniform over the entire reservoir volume. Historical and recent RFT data suggest that there are pressure differentials existing across some of the lower reservoir sub-units.

DHOWS Suitability: The reservoir drive mechanism is highly favorable for DHOWS applications. Presences of bottom water drive as well as edge water drive affecting reservoir performance suggest the following two potential DHOWS water disposal/injection options:

1. Into formerly oil producing sub-units that have watered out under the influence of the edge and bottom water drives;
2. Into the reservoir sub-units which comprises a portion of the connected water aquifer responsible for the water influx.

In either case, the water disposal/injection will, most probably, help to supplement the already strong natural water influx and the reservoir pressure.

Production History: Initial production from the field began in 1964. Production peaked at 250 MB/D of oil and immediately went on decline. This is coincident with the first observation of significant water production in the field during 1966. During the early 1980's a program of well shut-ins/cutbacks was executed, reducing produced liquid volumes to ~140 MB/D. In the late 1980's early 1990's, reservoir liquid withdrawal rates were increased to ~300 MB/D and maintained to the present day. After 36+ years on production, at steadily increasing watercuts (which have been in excess of 75 % since the late 1970's), some 250 MB/D of water from the reservoir is being produced to surface for separation, treatment, and eventual disposal. Given the vintage of the producing wells, there are some concerns regarding the mechanical integrity of the wellbores. The producing field water cut and the large absolute volumes of produced water brought to surface are both clear indications that the GE reservoir warrants further consideration as a potential DHOWS application candidate. Reservoir and fluid properties of GE reservoir are presented in Table 2.

Oil Reserves. With a recovery factor of 40+ % of OOIP realized to date, it is important to consider what amounts of incremental oil recovery are still available to the existing primary recovery operation. Under existing primary recovery operations, and even in the case of numerous possible developments for incremental recovery, a considerable amount of the reserves is still left to be recovered for the next 30 years (to 2030); all of these results confirm that a more thorough assessment of potential DHOWS applications in the GE reservoir is warranted.

Table 2. Reservoir and fluid properties of GE reservoir.

Reservoir properties		
Top GE	2670-2770	ft kb
Initial pressure (datum)	1176	psig @ 2410 ft ss
average pressure (datum)	764	psig
Reservoir Temperature	131	^{0}F
Field average free water level	2610	ft ss
Structural dip	0.5	^{0}
Closure (main)	2342	ft ss
Reservoir productive area	5660	acres
Oil properties		
Reservoir oil density	0.81	g/cc (at 1176 psig, 131 ^{0}F)
Stock tank oil density	0.83	g/cc
Oil viscosity	2.59	cp (at Pi)
B_{oi} (flash separation)	1.038	RB/STB
B_{ob}	1.046	RB/STB
Solution GOR	41.2	SCF/STB
Separator gas gravity	1.046	(air=1)
Oil compressibility	6.75	10^{-6} psi^{-1}
Bubble point pressure	140.3	psig (131^{0}F)
Initial formation water Properties		
Chlorinity	6134-9800	ppm
Salinity	15000-19440	ppm
Resistivity	0.466-0.381	Ohm.m (at 68^{0}F/20^{0}C)
Density	1.01	g/cc (68^{0}F/20^{0}C)
Viscosity	1.052	cp (68^{0}F)

Water Disposal/Injection Zone Potential: Several proximal but unproven water disposal/ injection zones have been identified that require further evaluation before they can be considered acceptable for DHOWS applications.

WELL CANDIDATE CATEGORIES

The following sections evaluate the suitability/ applicability of DHOWS with respect to the well characteristics under consideration. It is important

to remember that in assessing a well's suitability for DHOWS applications, its characteristics must be assessed several times, and a suitable candidate well must be shown to meet or exceed the minimum acceptance criteria for each of the well characteristics that are considered. The GE reservoir wells are divided into 9 different categories as presented in Table 3.

Table 3. DHOWS candidate well group descriptions.

Category	# Wells	Description
A	54	currently producing from the GE
B1	16	previously produced from the GE currently not on production
B2	6	previously produced from the GE have been recompleted in a reservoir above the GE currently not on production
B3	5	previously produced from the GE have been recompleted in a reservoir above the GE currently on production
B4	11	previously produced from the GE plugged and abandoned
C1	23	penetrates, but has never produced from the GE currently not on production
C2	44	penetrates, but has never produced from the GE producing from a reservoir above the GE
C3	27	penetrates, but has never produced from the GE producing from a reservoir below the GE
C4	17	penetrates, but has never produced from the GE plugged and abandoned
Total	203	

Well Characteristics. This part of the evaluation is more quantitative than the evaluation of the reservoir characteristics, and if done thoroughly, and supported by sufficient data, will identify almost all of the inputs required for the evaluation of potential DHOWS.

The well characteristics that have been addressed in this part of the evaluation are as follows: current water cut, offset distance, water disposal/injection zone potential, wellbore size and geometry, well history, wellbore isolation, inflow potential, and artificial lift performance.

DHOWS Watercut Threshold: The physical limitations of the liquid-liquid hydro-cyclone separation process determine the minimum producing watercut required for efficient separation of the produced oil-water stream. By setting a minimum of 75% threshold watercut for consideration of DHOWS applications (single stage separation) in candidate wells producing from the GE reservoir, Figure 1 shows water cut cumulative frequency.

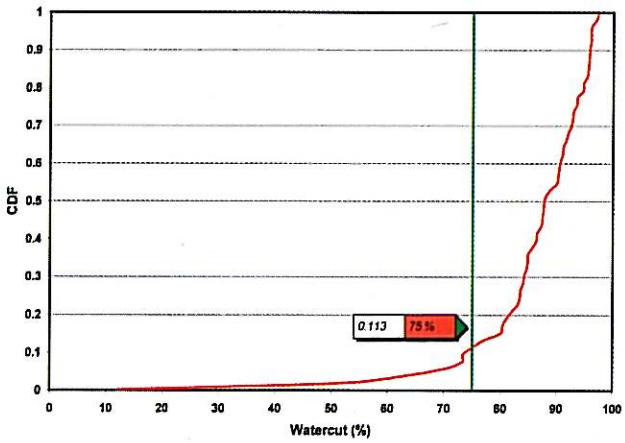


Fig. 1. Watercut cumulative frequency.

Production Zone and Water Disposal/Injection Zone Offset: The consideration of offset distance is more of assessing operational risk to which a candidate DHOWS application might be subjected, as opposed to determining whether or not a candidate DHOWS application is possible (unlike for current watercut, wellbore size, and water injection zone potential). Within individual candidate wells, as was the case for the candidate reservoir as a whole, a larger offset distance is preferred as it tends to mitigate/lessen the operational risks associated with: 1. cooling of downhole motors in the specific case of GE producers which are configured with ESP's and whose DHOWS applications under evaluation would maintain the current method of artificial lift – this can be "shrouded" away, but may reduce the maximum amount of horsepower and flow capacity of the gallery of bypass tubes that are available for a candidate DHOWS.

2. re-circulation of disposed/injected water into the production zone in the near wellbore region. Figure 2 shows offset distance cumulative frequency for GE reservoir.

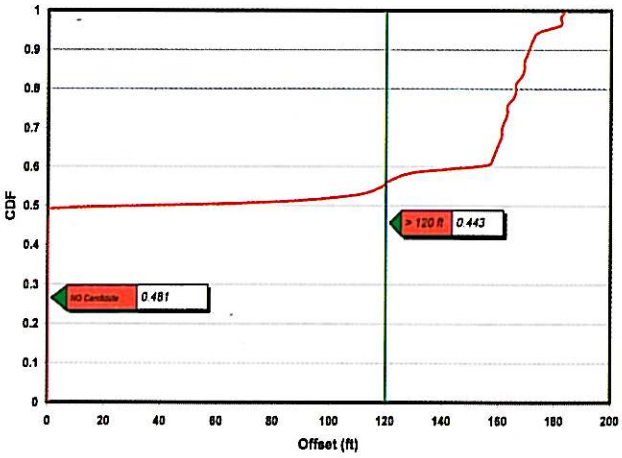


Fig. 2. Offset distance cumulative frequency.

Water Disposal/Injection Zone Potential: The assessment of water disposal/injection zone performance addressed two important considerations:

(1) design constraint(s) for potential DHOWS applications in respect of the candidate water disposal/injection zone.

(2) characterization of the relationship(s) which govern the water disposal/injection rate accepted by the candidate zone.

The candidate water disposal/injection zone performance has the largest impact on the specifications for DHOWS equipment designs, most notable of which are:

(1) It determines the number of injection and (if necessary) production pump stages.

(2) It establishes minimum horsepower requirement.

(3) It influences overall equipment length and determines the required offset distance between producing and disposal zones which is required to avoid the necessity for equipment designs with shrouded motor sections.

Zone Characterization: The uncertainty regarding the characterization of the candidate water disposal/injection zones identified at the reservoir level is confirmed from an examination of the DHOWS candidate well data.

Wellbore Size and Geometry: The wellbore size and geometry are important considerations governing the engineering design of potential DHOWS applications. The production casing sizes and setting depths and their relationship with the production and water disposal/injection zones have a direct impact on DHOWS equipment rated capacity. Having completed a review of the well size and geometry of the DHOWS candidate wells, the results can be summarized as follows:

(1) 31 % of the candidate wells lack production casing over the target production zone and as such are no longer considered to be high graded DHOWS candidate wells at this time (potential exists to deepen and install cemented liners in place for the 9 5/8 inch cased wells);

(2) of the remaining candidate wells, 35 % are completed with 9 5/8 inch, 18 % with 7 inch, and 11% with 5 inch casing over the target production zone (the wells completed with 5 inch production casing over the target production zone are not considered to be DHOWS candidates at this time);

(3) the DHOWS candidate wellbores are vertical wells which exhibit little deviations.

Well Workover History: As a part of the screening of an individual well, it is important to review the candidate well's workover/completion history. By identifying problematic wells or wellbore conditions, the likelihood of the long-term success of a DHOWS application can be increased. The cement bond also should be checked as part of casing leakage evaluation.

Wellbore Isolation: The utilization of two or more zones (in most applications) for the production and disposal/injection of reservoir fluids increases the requirement for hydraulic isolation, in the vicinity of the wellbore, between the production casing and surrounding reservoir units.

Inflow Potential: An examination of the candidate well's inflow performance behavior was addressed utilizing several complementary viewpoints. In respect of a final DHOWS evaluation design, a candidate well's inflow performance (IPR) is an integral portion of the nodal analysis that is the basis of any DHOWS design. In this case, the IPR serves to quantify the dynamic behavior of the sole fluid source for a candidate well.

Artificial Lift Performance: ESP systems are the sole artificial lift application present in all of the DHOWS candidate wells. Figure 3 shows ESP run life in the GE reservoir. The installed ESP system

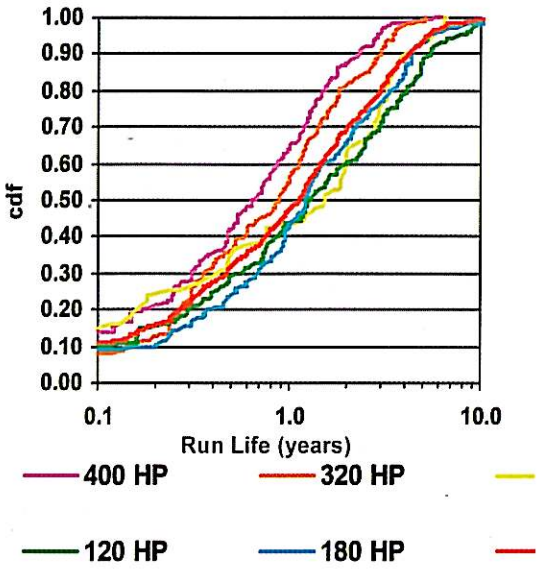


Fig. 3. ESP run life in the GE reservoir.

design, subsequent operation, and logistics in respect of any associated infrastructure will have some effect on the operational reliability of a potential DHOWS application. A DHOWS application equipped with ESP artificial lift system behaves very much like a conventional ESP application except for: (1) the direction of flow out of the pump, (2) the attached hydro-cyclone liners, (3) the extra plumbing to direct the hydro-cyclone overflow to surface.

EQUIPMENT DESIGN AND INSTALLATION

A significant number of operational risks and uncertainties have been identified as part of the evaluation of reservoir and well characteristics (primarily the uncertainty of the disposal/injection zone quality) for the DHOWS candidate wells. To prepare templates for DHOWS equipment designs and installation procedures would be the most appropriate once a water disposal/injection test has been completed on one or more of the candidate wells. To illustrate the impact of key design parameters and their associated inputs/constraints, several preliminary DHOWS equipment designs for a candidate DHOWS well are presented. The analysis has been summarized in the following sections: candidate well ranking, design inputs and constraints, DHOWS designs.

Candidate Well Ranking: The well ranking scheme utilized at this stage of the evaluation was at best only partially quantitative. Ranking characteristics and weights are presented in Table 4. The ranking system was implemented as follows:

Table 4. Category "A" wells – candidate ranking scheme.

Ranking characteristics	Weight (%)
Current watercut	10.0
Wellbore size and geometry	25.0
Water injection zone potential	15.0
Inflow potential	20.0
Offset distance	15.0
Oil reserves	7.5
Well history	7.5

1. Only the well characteristics were addressed by the ranking scheme.

2. For each well and sub-well characteristic (some wells had more than one quantitative characteristic included), as many as 7 possible designations were assigned (NC = no candidate, this well characteristic is of such a state that the well cannot be considered as a candidate without considerable/costly well construction/intervention; blank = no data available, the well can still be considered as candidate based on the other characteristics; 5 to as low as 1 (best to worst) = a numerical ranking approximately ordering the candidate wells with available data for that characteristic into 5 groups where possible).

3. With the aim of maximizing the liquid and associated oil throughput from a DHOWS application, a weighting scheme to combine these rankings into a total score with the largest total score indicative of the "best" DHOWS candidates. (The blanks having been treated as zeroes in the linear combination of the characteristic ranks)

4. The data have been rank ordered according to this total score (as opposed to by well name) to highlight at this preliminary stage of the feasibility study which wells are expected to exhibit the best overall combination of well characteristics when applying DHOWS.

Of the original 54 DHOWS candidate wells, 36 of the wells are believed to exhibit well characteristics that would require to relegate them from immediate consideration. Again, it is the evaluation team's belief that these NC characteristics would require that these candidate wells undergo significant well construction/ modification before the NC was upgraded to a relative ranking. Because of this, they have been dropped from further consideration for this study. Table 5 presents Ranked Candidates. Rather than isolate the top 5 DHOWS candidate wells for further examination, it is decided to select 3 more wells from the remaining inventory of 18 that to some extent were representative of the range of circumstances/well characteristics present in the entire well inventory. The wells selected are as follows: E-001, E-038, E-095.

Design Parameters and Constraints: Before undertaking a DHOWS design, it is somewhat beneficial to document at the first place the relevant design inputs and, where necessary, identify any constraints that might apply in respect of an actual design that must be worked up prior to actually preparing the design. In addition to the well constraints (watercut, wellbore size/geometry, drawdown, fracture pressure, and operational risks

Table 5. Ranked candidates.

Well	Water cut rank	Wellbore. size & G rank	Well history rank	Inflow potential rank	Offset distance rank	Injection zone potential rank	Remaining reserves rank	Total score
E-001	4	5	5	5	5	4	5	4.35
E-033	4	5	3	5	3	4	5	4
E-035	4	3	5	5	3	5	5	3.9
E-038	4	5	5	4	1	4	4	3.675
E-094	1	5	5	1	5	4	1	3.65
E-278	2	5	5	3	4	2	3	3.45
E-037	1	5	3	4	4	3		3.325
E-095	2	3	5	5	2	5	4	3.275
E-275	1	5	5	2	2	4		3.225
E-036	2	5	3		3	4	5	3.2
E-072	3	3	5		4	5	4	3.175
E-025	1	5	3	3	3	3	2	3.125
E-031	2	5	5		1	5	4	3.125
E-299	1	5	5	2	3	2	1	3.05
E-040	1	5	3		5	2	2	2.875
E-092	2	3	5		2	5	2	2.625
E-054	3	3	3	1	1	3	1	2.55
E-066	1	3	5	1	1	3	1	2.3

– wellbore isolation, wellbore integrity, and artificial lift run life), there are other DHOWS equipment related constraints that must be addressed these are: motor horsepower and bypass tube velocity. Table 6 presents the motor horsepower limitations. It is essential that the relevant constraints be identified and quantified before the design is made in order to ensure that a design that is produced is consistent with the constraints and good engineering practice.

DHOWS Designs: The preparation of a DHOWS design, like most downhole equipment designs, requires a considerable amount of data and oversight in order to ensure that an internally consistent, reliable, and operable equipment specification is the final result. The DHOWS designs completed in the course of preparing this report were developed as follows:

1. The required design data were collected in a summary input data sheet;

Table 6. Motor horsepower limitations.

Equipment series	Max single motor HP @ 60 hz	Single motor length (ft)	Max total combined HP @ 60 hz	Max # of motors combined	Minimum Casing Size (")
456	150	30.7	450	3	5.5, 7 shrouded
540	250	30.4	750	3	7
562	450	34.9	900	2	9.625, 9.625 shrouded

2. The input data sheets were vetted and the inputs for each data element were compared with data for the DHOWS candidate well population, after which the relevant design constraints applicable to each of the candidate wells were searched and documented;

3. In the absence of accurate injectivity indexes, all designs were created using an estimated value calculated from the medium permeability estimates for the Lower 3 and Basal reservoir intervals;

4. The individual designs were created to maximise the production, within the bounds of the design constraints.

Table 7 summarizes the DHOWS design for this candidate well in relation to the 5 dominant system constraints (CAPsep – hydro-cyclone capacity, HP – motor horsepower, VELbp – bypass tube velocity, DD – drawdown, Pfrac – formation fracture pressure). Figure 4 shows DHOWS Diagram. Having prepared a series of concept proof equipment designs for DHOWS candidate wells, the following summarizes the findings:

Table 7. DHOWS design inputs.

Description	Value	Units
General information		
Casing size	9.625	inch
Casing weight	40 (est.)	lb/ft
Casing condition/impairment/doglegs	uncertain	
PBTD/TOC	2779	ft KB
Liner and interval	NA	ft KB
Tubing size (OD)	3.5	inch
Tubing weight	9.3 (est.)	lb/ft
Tubing landing depth	To be determined	ft KB
Current method of artificial lift	ESP	
Power	To be determined	hp
Voltage available		V
Frequency	50 (est.)	Hz
Producing data		
Formation and type (e.g. carbonate, sandstone, etc.)	Shoal 1 and 2 (carbonate)	
Production perforation interval(s) – MD (1967)	2710-2730	ft KB
Production perforation interval(s) – TVD	2710-2730	ft KB
Anticipated production rate		
Oil rate	1200	BBLD
Water rate	18800	BBLD
Total fluid rate	20000	BBLD
Wellhead pressure (for the casing)	~100	psi
GOR	20	SCF/BBL
Bubble point pressure	140.3	psi
Stock oil density	0.83	g/cc
Reservoir oil density @ 1176 psig, 131 deg. F	0.81	g/cc
Oil viscosity @ 1176 psig, 131 deg. F	2.59	cp
Water density @ 68 deg. F	1.01	g/cc
Bottomhole temperature	131	F
Producing bottomhole pressure @ mpp	487	psi
Producing fluid level from surface (mD)	To be determined	ft KB
Static bottomhole pressure @ mpp	790	psi
Producing wellhead (for the tubing) pressure	~100	psi
Liquid productivity index (estimated)	66.208	BBLD/psi
Abrasives, Scale, CO_2, H_2S, asphaltenes, waxes	H_2S = 5.22% ; CO_2 = 30 %	
Chlorides and concentrations	19 100	ppm
Anticipated water injection zone data		
Formation and type (e.g. carbonate, sandstone, etc.)	Lower 3 and basal – carbonate	
Injection perforation interval(s) – mD	2904-3022	ft KB
Static injection zone pressure @ mpp	895	psi
Sandface injection pressure	To be determined	psi
Estimated fracture gradient	0.65	psi/ft
Injectivity index (estimated)	40.0	BBLD/psi
Notes: Injectivity index based on mid k of 88md skin –4. Cement will have to be drilled out to access the Lower 3 + Basal zones.		

1. Of 54 Category "A" DHOWS candidate wells, only 18 were deemed to exhibit sufficiently robust wellbore characteristics to be considered for further evaluation at this stage of the examination of potential DHOWS applications;

2. Of the 18 remaining DHOWS candidate wells, only 3 were selected for preparation of detailed proof of concept DHOWS equipment designs;

3. With the exception of well E-038, the remaining DHOWS candidate wells have an equipment related

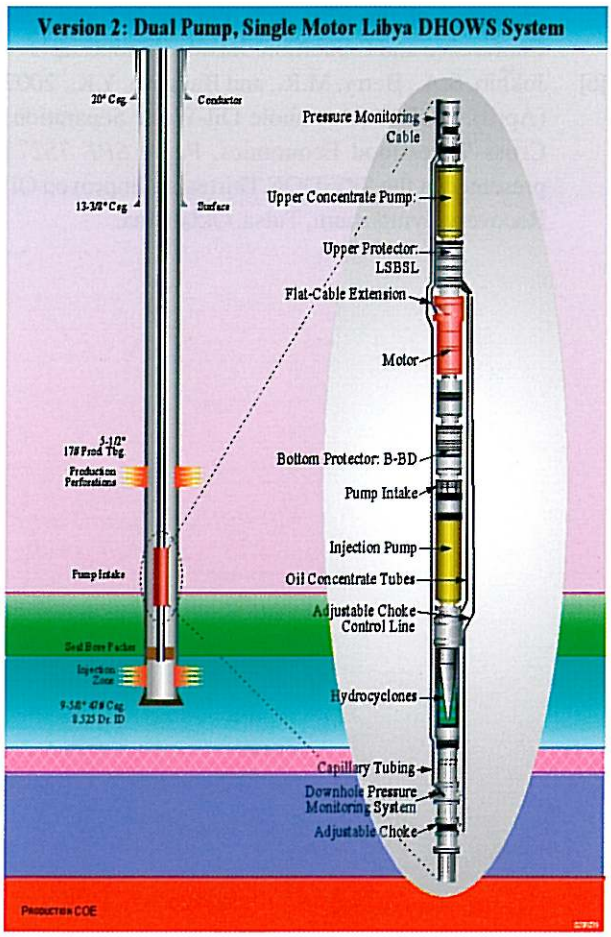


Fig. 4. DHOWS diagram.

limiting design constraint (hydro-cyclone separator capacity);

4. The drawdown limiting design constraint evidenced in well E-038 is not unexpected in the case of DHOWS candidate wells with low PI's;

5. The separator capacity limiting design constraint evidenced in wells E-001 and E-095 is not unexpected in wells with large PI's – especially for small diameter wellbores, (however, not unexpected in large diameter wellbores as well);

6. The design for the well E-095 appears to be extremely robust with minimal anticipated mechanical strain; therefore, a long run life would be anticipated.

CONCLUSIONS

1. Based solely on the DHOWS watercut threshold of >= 75% , some 88.7% of the candidate wells are identified as potential DHOWS candidates;

2. The injection indices, a critical parameter in specification of DHOWS designs, of the candidate wells are not adequately defined by the existing data set, and can only be better defined by undertaking one or more properly designed and executed injection/ disposal tests;

3. 31 % of the candidate wells lack production casing over the production zone and, therefore, are not considered as high quality DHOWS candidates – 35 % of the candidate wells are completed with 9.625 inch and 18 % with 7 inch casings, potentially permitting the installation of 20 and 10 MB/D capacity DHOWS systems respectively;

4. The majority of the candidates have some type of downhole obstruction (TOC or bridge plugs) that give rise to some form of operational risk in gaining access to the targeted disposal/injection zone(s);

5. Casing leaks are a persistent and recurring problem and represent an operational risk to the potential DHOWS candidates, these leaks appear to be increasing in frequency with time.

6. Of the 54 candidate wells, 18 demonstrate favourable reservoir and well characteristics and meet the initial DHOWS screening criteria, and have been rank ordered accordingly. The remaining 36 wells exhibited some unfavourable well characteristics which required the evaluation team to remove them from immediate consideration.

ACKNOWLEDGEMENT

I thank the Management of Waha Oil Co. for permission to publish this work.

REFERENCES

[1] Matthews, C. M., Chachula, R., Peachey, B. R., and Solanki, S. C., 1996 (June). Application of downhole oil-water systems in the Alliance field. Paper *SPE* 35817 presented at the third International Conference on Health, Safety and Envirnment in the Oil & Gas Exploration and Production, New Orleans.

[2] Peachey, B. R., Solanki, S. C., Zahaacy, T. A., and Piers, K., 1998 (July). Downhole oil/water separation moves into high gear, *J. Canad. Petrol Technology*, **37** (7) 34-40.

[3] Shaw, C., and Fox, M., 1998 (Oct). Economics of downhole oil-water separation: A case history and implications for the North Sea. *SPE* 50618 presented at the 1998 European Petroleum Conference, The Haige, the Netherlands.

[4] Scaramuzza, J. L., Fischetti, H., Strappa, L., and Figliuolo, S., 2001 (March). Downhole oil-water

separation system-field pilot-secondary recovery application project. Paper *SPE* 69408 presented at the SPE Latin America and Caribbean Petroleum Engineering Conference, Buenos Aires, Argentina.

[5] Li, X., Song, K., Cao, X., Xu, W., and Zhu, Y., 2002 (April). Research of downhole separation and injection technique for rod pumping well. *SPE* 68719 presented at the SPE Asia Pacific Oil and Gas Conference and Exhibition, Jakarta, Indonesia.

[6] Jokhio, S.A., Berry, M.R., and Bangash, Y.K., 2002 (April). DOWS (Downhole Oil-Water Separation) Cross-Waterflood Economics. Paper *SPE* 75273 presented at the SPE/DOE Thirteenth Improved Oil Recovery Symposium, Tulsa, Oklahoma.

Petroleum Res. J. Vol. 18 (2005): P. 115–122, 9 Figs.

Water Shutoff Polymer/Gel Treatments for Oil or Gas Production Wells

A. Zaitoun, R. Tabary and N. Kohler*

المعالجة باستخدام Polymer/gel لمنع دخول الماء للآبار المنتجة للزيت والغاز

أ. زيتون، ر. تباري ون. كوهلر

يعتمد المعهد الفرنسي للبترول طريقة منع دخول الماء على استخدام تقنية تقليل النفاذية غير المتكافئ (DPRs) على سبيل المثال المواد الهلامية الضعيفة والبوليمرات تقلل بانتقاء النفاذية النسبية للماء بالنسبة للنفاذية النسبية للزيت أو الغاز وهذه المنتجات تضخ لكل المنطقة المفتوحة بدون عزل وهو اختيار جذاب مقارنة بالهلاميات المستخدمة للغلق والمقترحة من قبل الشركات.

إن منتجات المعهد الفرنسي للبترول من DPRs وهي بوليمرات قابلة للذوبان في الماء والتي هي عادة ما تنتفخ أو ضعيفة الارتباط لزيادة انخفاض النفاذية للماء دون إفساد أو إتلاف لنفاذية الزيت أو الغاز وهذه الكيماويات اختيرت لكي تكون ذات ضرر قليل جدا على البيئة ويغطي كل مزيج أو خلطة مجالا محدودا من الحرارة والملوحة.

تم تطبيق عمليات منع دخول الماء من قبل المعهد الفرنسي للبترول في مدى واسع من ظروف الآبار والمكامن وهو ما سيشهد تطورات مستقبلية عالية الاحتمال.

تصميم المعالجة يجب أن يهيأ لكل حالة خاصة حيث أنها تحتاج إلى شغل معملي لتحسين تركيبة الهلام ومحاكاة مكمنية باستخدام نموذج WSO الداخلي للتحكم في حجم الهلام وقوته. مجموعة من الحالات الحقلية الناجحة تم وصفها فيما يتعلق بآبار الغاز وآبار الزيت الثقيل الأفقية وآبار الغمر بالماء متعددة الطبقات.

Abstract: *IFP water shutoff technology is based on the use of Disproportionate Permeability Reducers (DPRs), i.e. polymers or weak gels that reduce selectively the relative permeability to water with respect to the relative permeability to oil or to gas. The products are usually injected into the whole open interval, without zonal isolation, which is a very attractive option compared to plugging gels proposed by service companies. IFP DPR products are water-soluble polymers, which are either swelled or weakly cross-linked in-situ to increase permeability reduction to water, without impairing oil or gas permeability. The chemicals have been chosen to have minimal environmental impact. Each combination covers a specific domain of temperature and salinity.*

IFP water shutoff processes have been applied in a broad range of well and reservoir conditions, thus showing a high potential for future developments. Treatment design has to be adapted to each specific case. It requires both laboratory work to optimize gel formulation, and reservoir simulations with an in-house WSO model, to size up gel slug and gel strength. Several successful field cases are described, including gas wells, heavy-oil horizontal wells, and multi-layer water-flooded wells.

* Institut Français du Pétrole (IFP), France.

INTRODUCTION

Excessive water production is often due to water channeling in the part of the reservoir surrounding the well-bore, making oil production inefficient and sometimes uneconomical. Figure 1 shows a typical case, *i.e.* a two-layer reservoir well with a strong permeability contrast (for example 1 to 10), and a horizontal barrier which prevents cross-flow. Since the high-permeability layer is swept first by water, it has a tendency to overtake the oil production from the low-permeability layer. This situation calls for a treatment which intends to decrease water influx from the high-permeability layer, thus favoring low-permeability layer production.

When the different layers are clearly separated and workover costs are acceptable, the sealing of the watered-out layer with packer, cement or strong gels, placed with mechanical tools, is the best option. Nevertheless, in practice, the operator has to face several problems like poor identification of water zones, multilayered production, unfavorable completion (gravel pack, slotted liners, *etc.*) or excessive workover costs (offshore wells, marginal wells). All these issues, plus the recent development of horizontal, multilateral, sub sea wells (where mechanical intervention is costly and risky) call for more bullhead treatments in the future. One viable technique, confirmed by numerous field successes, is the use of "Relative Permeability Modifiers" (RPMs), *i.e.*, high-molecular-weight water-soluble polymers or weak gels, which reduce selectively the relative permeability to water with respect to the relative permeability to oil or to gas (Fig. 2)[1]. These products are generally bullheaded into the existing completion without zonal isolation, which makes their use very attractive.

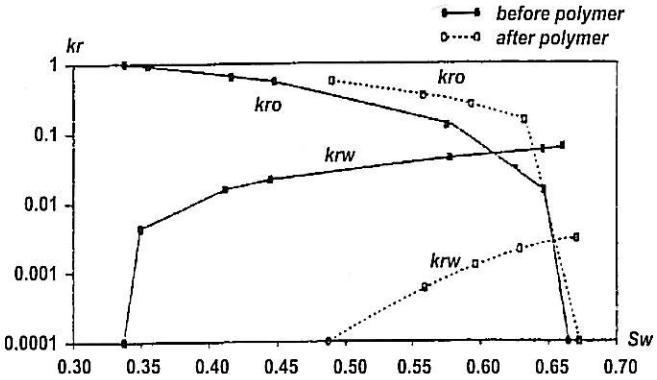


Fig. 2. Modification of relative permeability after polymer adsorption in water-wet sandstone.

Since 1980, more than 100 well treatments have been performed worldwide with IFP RPM processes. This paper describes these processes and reviews some field applications.

IFP PROCESSES

IFP processes use non-toxic high-molecular-weight water-soluble-polymers which can be either swollen or weakly cross linked *in-situ*. Each process covers a certain domain of temperature and salinity (Fig. 3).

Process A

Applicable in low-salinity, low-temperature matricial reservoirs, the process consists of injection of hydrolyzed polyacrylamide dissolved in a high-salinity make-up brine. After production release, low-salinity formation water replaces progressively

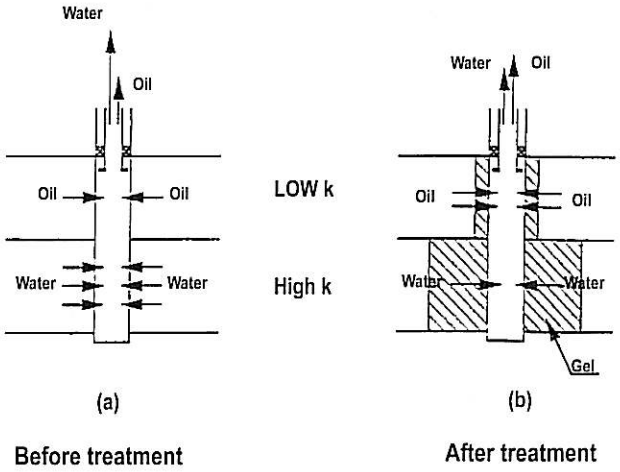


Fig. 1. Principle of RPM treatment.

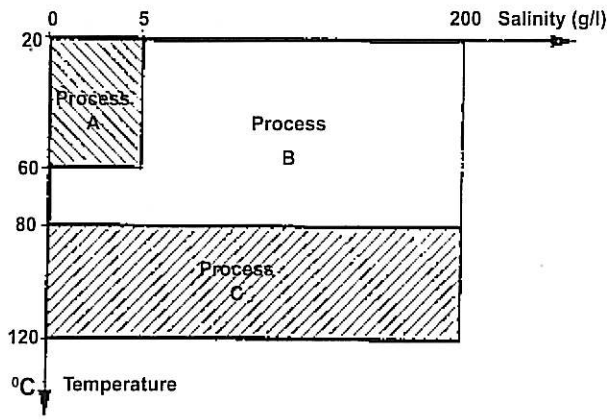


Fig. 3. Domains of application of IFP processes.

injection brine and swells the polymer adsorbed on pore walls. Advantages of this process are a low viscosity during injection, a high level of polymer adsorption on reservoir rock and a high permeability reduction to water. Moreover, the use of single polymer instead of gel reduces the risk of well impairment. For more details the reader is referred to Zaitoun, *et al.*, 1991[2].

Process B

It consists of nonionic polyacrylamide injection with either a caustic swelling agent (that hydrolyzes the polymer *in-situ*) or an organic cross-linker. For higher temperatures, acrylamide copolymers can be cross linked by zirconium lactate. A process description with different options is given.[2,3]

Process C

Applicable in high-temperature matricial reservoirs, the process uses scleroglucan, a polysaccharide with strong shear-thinning rheology and excellent thermal stability. Polymer swelling can be simply obtained by the release of shear forces between high injection rate and low production rate. The polymer can be weakly cross linked by zirconium lactate. Process description is given. [4,5]

METHODOLOGY

The preparation of a RPM water shutoff treatment requires a laboratory study and numerical simulations (for example with the specific reservoir software designed by IFP, namely, ATHOS).

The laboratory study aims at (1) optimizing chemical formulations, and (2) determining input data for the simulations (polymer adsorption and end point relative permeabilities before and after polymer treatment).

Numerical simulations are run in three phases, *i.e.* (1) establishment of a history match of candidate well fluid production with a simplified near-wellbore reservoir description, (2) simulation of polymer or polymer/cross-linker injection, (3) post-treatment production forecasts. Numerical simulations aim at sizing treatment slug volume, optimizing polymer characteristics and (or) gel strength, and evaluating after treatment expected performances.

FIELD CASES

Different field cases are discussed here below.

1) Gas Storage Wells: Treatments of Sandstone and Limestone Reservoirs (France)

Several water shut-off treatments on gas storage wells in sandstone reservoirs have been performed. Well treatments based on RPM technology have proven to be effective in most cases.[2,6]

For example the treatment of well VA 48 of the Cerville-Velaine Gaz-de-France gas storage reservoir by Process A reduced the water/gas ratio for at least 3 years. The main characteristics of the well treatment are shown in Table 1. The treatment is documented.[2]

Another Gaz-de-France candidate well from Saint-Clair-sur-Epte gas storage limestone reservoir was proposed for a polymer treatment. The formation consists of a superposition of alternating high-permeability grainstone layers ($k = 0.7\ \mu m^2$) and low-permeability packstone layers ($k = 0.01\ \mu m^2$) (Table 1). Due to the higher formation brine salinity, Process B was chosen, combining polyacrylamide (polymer) and KOH (activator). It was concluded from numerical simulations and laboratory tests that the optimal RPM slug volume was 200 m^3 and that injection had to be done in the zone below a formation packer located in the middle of the pay-zone.

Unexpected compatibility problems between the bactericide and the swelling agent induced a premature cross-linking of a part of the polymer in both surface installations and in the wellbore. Polymer

Table 1. Treatments of gas storage wells.

Characteristics	Sandstone reservoir VA 48	Limestone reservoir VN 21
Reservoir parameters		
Lithology	Massive sandstone	Layered limestone
Thickness (m)	60	28
Permeability (μm^2)	0.1-1 (top 55 m) ≥ 5 (bottom 5 m)	grainstones: 0.7 packstones: 0.01
Brine salinity (g/L TDS)	0.972	14
Temperature (°C)	30	36
Treatment		
RPM process	Process A (HPAM + salinity gradient)	Process B (PAM + KOH)
Polymer concentration (ppm)	3000	2000
Brine salinity (g/L TDS)	8.2	river water
Injected volume (m^3)	700	200
Results	Water/gas ratio ↓ Water production strongly reduced Gas injection/production unchanged	Gas productivity improved Water production rate divided by 3

injection was nevertheless continued without swelling agent but with a reduced injection rate and followed by fresh water post flush.

After two years, where no significant reduction of water production was observed, the well started to behave much better and maintained these good performances for more than ten years (Fig. 4). Today, water annual production is 1/3 of the value before treatment, and, concerning gas productivity, the well, which was one of the worst in the storage, became one of the best. The delay in well response to the treatment is not well understood yet. It may be due to make-up water back up production.[7]

2) Horizontal Wells: Treatments in Pelican Lake and South Winter Fields (Western Canada)

Four heavy-oil horizontal wells from Pelican Lake field, namely wells 11-15A, 11-15B, 14-10A and 14-10B, were treated by Process B (Table 2).[8] Although the same injection procedure was applied, *i.e.* bullheading the chemicals into the

Table 2. Horizontal well treatments in Pelican Lake and South Winter.

Characteristics	*Pelican Lake*	*South Winter*
Reservoir Parameters		
Horizontal length (m)	500	800
Lithology	Wabiskaw sand	Dina sand
Permeability range (μm^2)	> 1	3 – 5
Aquifer	very weak	very strong
Oil viscosity (mPa·s)	1000	3000
Brine salinity (g/L TDS)	10	52
Treatment		
RPM process	Process B (PAM + KOH)	Process B (PAM + Glyoxal)
Injected volume (m^3)	60 – 110	400
Injected viscosity at 9.5 s^{-1} (mPa·s)	50	15
Results		
Water cut (%)	85-90 → 50-70 (2 years)	95 → 80 (2 months)

slotted liner drainhole, only well 11-15A gave a good response. After treatment, the water cut dropped immediately from 85 to 50% and remained low afterwards (Fig. 5). For this well both an increase in oil production and a decrease in water production were observed for two years following the treatment (Fig. 6).

For the three other wells, the response to the treatment was much weaker, although positive. A possible explanation for this difference in behavior, could be the less favorable placement of the polymer.

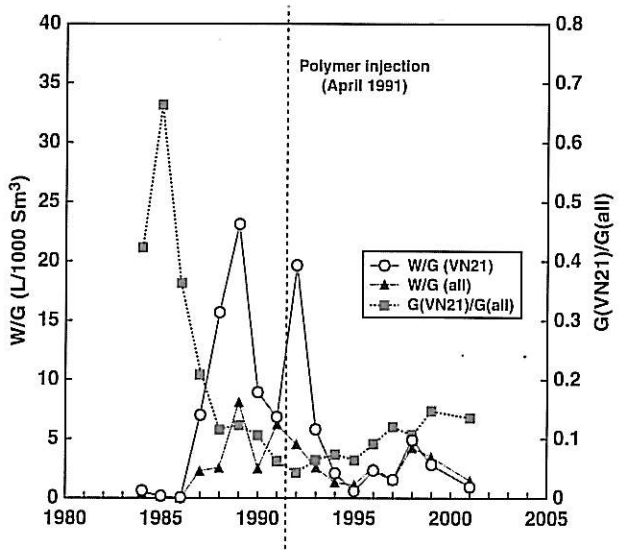


Fig. 4. Effect of polymer treatment on gas well VN-21 (Gaz-de-France, France).

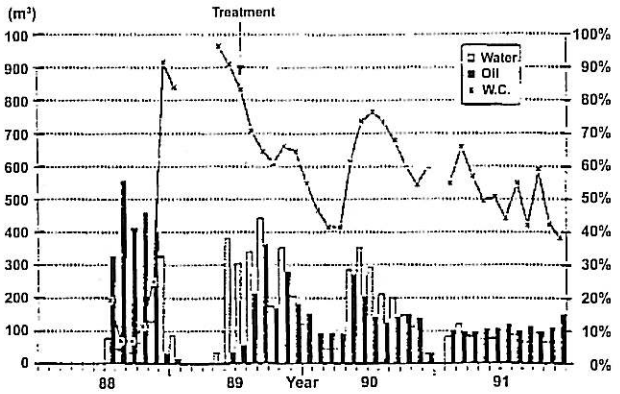


Fig. 5. Pelican Lake well 11-15A production history (CS resources, Canada).

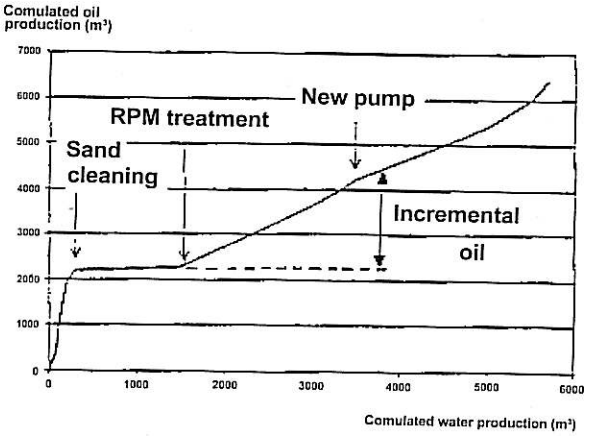


Fig 6. Pelican Lake well 11-15A cum. oil *vs.* cum. water curve (CS resources, Canada).

Indeed, horizontal well profiles (Fig. 7) show that the lowest points of the drainhole (corresponding to higher water saturation) are at the heel for well 11-15A and further away for the other wells. Probably, for these wells, an appreciable amount of polymer invaded oil

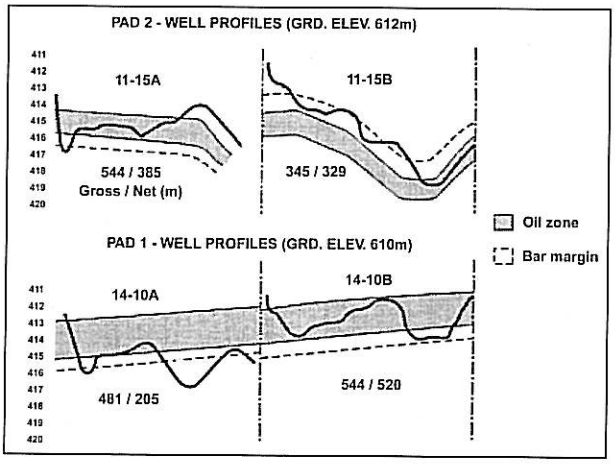


Fig 7. Pelican Lake well trajectories (CS resources, Canada).

productive zones before reaching water zones, thus making the treatment less efficient.

Another horizontal well, B 4-10 from the South Winter field, was treated by Process B. This well was producing heavy oil from a high-permeability sand reservoir lying above a very active bottom aquifer. Bottom water coning was responsible for the high water cut, rendering the production uneconomic. It was decided to perform the treatment in two steps, bullheading the first half of the injected polymer volume through a tubing placed at the heel of the horizontal slotted liner and the second half at the toe. Due to the high oil/water mobility ratio, it was estimated that the polymer would invade the water zones preferentially.

After treatment, the water cut decreased from 95 to 80% for 2 months and then slowly increased again to reach the economic productivity limit. It was concluded that polymer diversion to water zones was well achieved. However, the treatment effect did not last due to the presence of a strong bottom aquifer and a too weak gel formulation.

Table 2 summarizes the treatments of the horizontal wells in both fields.

3) Multilayer Water Flooded Wells: (A) Treatments in the Chagirtsk Field/Sandstone Reservoir (Russia)

A number of wells from the Chagirtsk field were treated by Process B. Candidate wells were selected on the basis of the existence of layering and permeability anisotropy. In this extensively water flooded field, Bobrick 2 (Bb 2) is the main oil producing interval. All wells are usually perforated over the total height of the sandstone reservoir. Nevertheless, some of the wells are also producing from the upper Tula 2b (Tl 2b) and Bobrick 1a (Bb 1a) intervals. Prior to polymer treatment, a water injectivity logging test was performed on each candidate well. For all wells except two, the injected water entered the Bb 2 reservoir. The exceptions were wells C 325 and C 1160, where brine injection affected respectively the top of reservoir Bb 1a and the total height of the reservoir Tl 2b (Table 3).

Process B was usually implemented in two sequences: first, a single polymer treatment aiming at diverting the gelant, then, the gelant itself, which is assumed to enter preferentially the more permeable water-bearing layers.

The size of each sequence is deduced from data such as reservoir thickness, injection rate, wellhead pressure during water injectivity test and production prior to the treatment.

Table 3 shows that for both wells C 325 and C 1160 the volume of the second sequence was much larger than for the other wells. This was done in order to reduce

Table 3. Main characteristics of well treatments in Chagirtsk.

Well	Perforated interval (m)				Water injectivity test			Treatment (m^3)	
	Layer								
	Tl 2b	Bb 1a	Bb 2	Total	Rate (m^3/day)	Pressure (kPa)	Intake interval	Polymer alone	Polymer + X-linker
C 2131	-	-	10	10	116	11 000	Bottom Bb 2	50	42
C 336	-	-	11	11	286	10 000	Total Bb 2	50	33
C 1143	-	-	9	9	208	8000	Bottom Bb2	44	42
C 1177	3	7	8	18	132	11 000	Bottom Bb 2	48	36
C 325	5.2	6.6	7.8	19.6	192	9000	Top Bb 1a	36	66
C 1160	5	-	16	21	150	13 500	Total Tl 2b	25	67.5

water productivity from reservoirs Bb 1a or Tl 2b and favor production from reservoir Bb 2. Table 4 shows that this choice seemed to be erroneous for well C 325 and right for well C 1160. For well C 325 the water cut was found to increase after the treatment leading to an estimated loss of about 3,400 tons of oil over a 13-month period of time. For well C 1160, the water cut decreased drastically during the first 4 months after treatment and increased again to values close to 100%. Presumably for both wells it would have been preferable to force the treatment to enter the lower Bb 2 reservoir.

As can be seen in Table 4, the water cut in all the other wells was reduced, leading to appreciable amounts of incremental oil.

Table 4. Main results of well treatments in Chagirtsk.

Well	Production data before treatment		Production data 4 months after treatment		Incremental oil (tons in [x] months)
	Rate (m^3/day)	Water cut (%)	Rate (m^3/day)	Water cut (%)	
C 2131*	120	90	150	80	2149 [4]
C 336	35	80	35	50	3054 [13]
C 1143	150	85	160	75	4988 [13]
C 1177	130	90	145	80	5464 [13]
C 325	160	90	190	100	- 3399 [13]
C 1160**	110	85	110	45	3534 [4]

* Well C2131 was shut in after 4 months due to pump failure
** The water cut of well C1160 increased strongly to near 100 % after 4 months

4) Multilayer Waterflooded Wells: (B) Treatments in the Kudryachevo Field/ Limestone Reservoir (Russia)

Process B was also implemented on three wells in the Kudryachevo field producing from the Tournaisien formation (limestone reservoir). This formation is characterized by a superposition of three to seven oil producing layers more or less clearly differentiated. According to the operator the existence of large fractures in this reservoir is not proven. The formation has thus to be considered as essentially matricial with production characteristics quite similar for the three candidates.

A water injectivity logging test on these wells showed a reasonable injectivity, equally distributed over the entire height of the perforated intervals. Wellhead pressure during this test was nevertheless much lower for wells K 2 and K 9, indicating the presence of micro-fissures or high permeability streaks (Table 5). Consequently, the slug size of the polymer/cross-linker sequence for these wells was chosen to be larger than for well K 3. Actual wellhead pressure during treatments remained quite similar for all the wells (5,000 to 10,000 kPa).

Table 5. Main characteristics of well treatments in Kudryachevo.

Well	Perforated interval (m)	Water injectivity test		Treatment (m^3)	
		Rate (m^3/day)	Pressure (kPa)	Polymer alone	Polymer + X-linker
K2	13	775	3000	25	59
K3	24.5	680	8000	30	41
K9	20	750	1000	20	67.9

Table 6 gives main treatment results. Both wells K 2 and K 9 maintained their overall productivity after treatment and had a strong reduction in water cut. On the contrary, well K 3 showed a loss in average production rate over 9 months resulting from an initial mechanical failure of the pumping equipment and an irreversible damage of formation productivity. Although the treatment of wells K 2 and K 9 produced the same amount of incremental oil, their post-treatment behavior was quite different (Figs. 8, 9). For both wells, the production rate took about 3 months to reach the level before treatment. Well K 9 showed an improvement in oil productivity during this period while the water cut of well K 2 remained high. After 3 months the opposite was observed: the water cut of well K 2 dropped sharply and remained low, while, for well K 9, it increased to pre-treatment level. The reason for this difference in behavior cannot be clearly explained.

Table 6. Main results of well treatments in Kudryachevo.

Well	Production data before treatment		Production data 6 months after treatment		Incremental oil (tons in 9 months)
	Rate (m^3/day)	Water cut (%)	Rate (m^3/day)	Water cut (%)	
K2	110	90	110	50	6272
K3	115	95	60	95	not evaluated
K9	120	90	120	60	4772

TREATMENT EVALUATION

For most operators, a successful treatment should induce both a significant reduction in water production

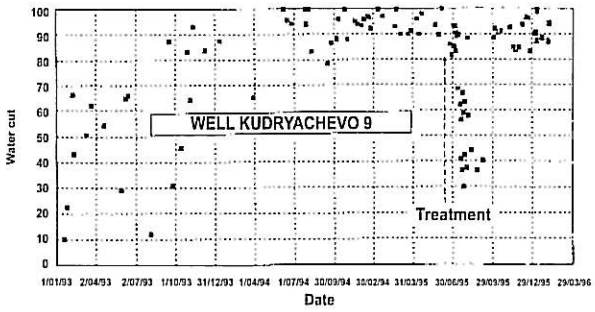


Fig 8. Water cut history of Kudryachevo well 2 (Russia).

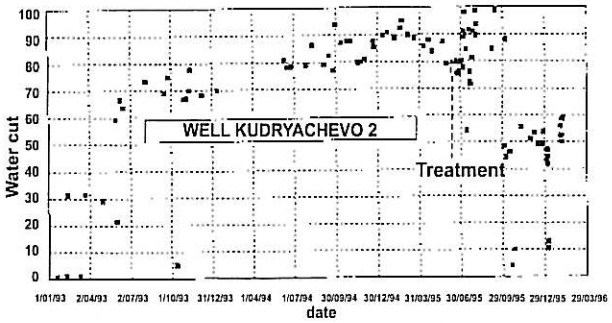


Fig 9. Water cut history of Kudryachevo well 9 (Russia).

and an increase in oil production. From the examples given above, it follows that the effect of a RPM treatment can last for several months up to several years.

A convenient tool to evaluate incremental oil production is given by plots of cumulative oil *vs.* cumulative water (Fig. 6). A successful water shutoff treatment induces a break in the plot, with a strong increase in the slope. Incremental oil can be estimated then by the difference between the actual cumulative oil curve and the extrapolated values from pre-treatment slope.[9] However, this plot does not indicate the production rate evolution, which has to be checked also to evaluate treatment success. In general, the treatment success can be measured by the pay out time, POT, and the cumulative returns vs. exceed treatment costs, PIR. In our best cases, (for example Well 11-15A in Pelican Lake), the pay-out was obtained in a couple of weeks and the return was more than ten times the treatment cost.

CONCLUSIONS

IFP has designed several RPM water shutoff processes in order to treat various types of reservoir characteristics. They are based on adsorption of high-molecular-weight water-soluble polymers, which can be either swollen, or weakly gelled by cross-linkers. Their application domains in terms of temperature and salinity are quite complementary. IFP processes can be applied at various salinities and temperatures up to 120°C. Since the treatment can be bullheaded into the whole open interval, without need for costly workover, its economy is very attractive.

The processes have been used in quite different field situations such as (1) gas storage wells, (2)heavy-oil horizontal wells and (3) multilayer waterflooded wells both in sandstone and in limestone reservoirs. In favorable cases, the duration of a successful treatment can exceed several years.

ACKNOWLEDGEMENTS

The authors wish to acknowledge the managements of Gaz-de-France, CS Resources and Permneft for their cooperation.

REFERENCES

[1] Zaitoun, A., Bertin, H. and Lasseux, D., 1998 (April). Two-phase flow property modifications by polymer adsorption. *SPE* 39631 presented at the 1998 SPE/DOE IOR Symposium, Tulsa, OK.

[2] Zaitoun, A., Kohler, N. and Guerrini, Y., 1991 (July). Improved polyacrylamide treatments for water control in producing wells. *J.Pet.Techn.* 862-867.

[3] Zaitoun, A., Rahbari, R. and Kohler, N., 1991 (October). Thin polyacrylamide gels for water control in high-permeability production wells. *SPE* 22785, 66th SPE Annual Fall Meeting, Dallas TX.

[4] Kohler, N. and Zaitoun, A., 1991 (February). Polymer treatment for water control in high-temperature production wells. *SPE* 21000, SPE International Symposium on Oilfield Chemistry, Anaheim.

[5] Kohler, N., Rahbari, R., Han, M. and Zaitoun, A., 1993 (March). Weak gel formulations for selective control of water production in high-permeability *and high-temperature production Wells*, *SPE* 25225, SPE International Symposium on Oilfield Chemistry, New Orleans, LA.

[6] Pusch, G., Kohler, N. and Kretzschmar, H.J., 1995 (May). Practical experience with water control in gas wells by polymer treatments, *8th European IOR Symposium,* Proceedings **2**, 48-56, Vienna.

[7] Zaitoun, A. and Pichery, T., 2001 (September). A successful polymer treatment for water coning

abatement in gas storage reservoir. *SPE* 71525 presented at the 2001 SPE Annual Technical Conference and Exhibition, New Orleans.

[8] Zaitoun, A., Kohler, N. and Montemurro, M.A., 1992 (October). Control of water influx in heavy-oil horizontal wells by polymer treatment. Paper *SPE* 24661 presented at the 1992 SPE Annual Technical Conference and Exhibition, Washington, DC.

[9] Kohler, N., Lessi, J. and Tabary, R.., 1995. Successful application cases of water control treatments in Russia. *Rev. Instit. Fr. Pétrole,* **50** (3), 381-390.

Petroleum Res. J. Vol. 18 (2005); P. 123–132, 8 Figs.

Field Applications of a Productivity Tool for Improved Oil Recovery (IOR)

M. B. Amish*, M. B. Oyeneyin* and M. H. Hodder**

تطبيقات حقلية لأداء الإنتاجية لتحسين المسترد النفطي

م. عميش، م. عوينين، م. هودر

أظهرت الصناعة النفطية في الآونة الأخيرة زيادة في الوعي نحو المحافظة على إنتاجية أفضل للبئر من خلال تصميم أفضل لسوائل الحفر والاستكمال عند ضغط عال ودرجة حرارة عالية. وعلاوة على ذلك فإن آلية ترشيح سوائل الحفر وتأثيرها على آداء الإنتاج غير مفهوم عند ظروف قاع البئر.

وعند الانتهاء من البئر فإن فواقد الإنتاج حرجة لأن التلف الذي يحدث قرب فتحة البئر لا يمكن تخطيه بواسطة التثقيب، كذلك فإن أي نموذج مقبول لتطبيقات حقلية تحاكي الضرر قرب فتحة البئر من حيث أداء انسياب البئر المأخوذ من تحاليل لب البئر المعملية لا تتوفر حاليا.

تزود نتائج معطيات تجريبية معمقة مصحوبة بتحاليل بيانات نماذج ترشيح ساكنة ومتحركة قاعدة بيانات لنماذج آلية شبه تجريبية تم تطويرها.

تم ضم هذه النماذج ودمجها نحو أدوات تصميم وتقويم وأداة الإنتاجية وذلك للتنبؤ بتأثير ترشيح سائل الحفر ذو الضغط العالي ودرجة الحرارة العالية على إنتاجية التكوين من حيث ضرر التكوين بالآبار العمودية.

نقدم في هذه الورقة تطبيقات أداة الإنتاج باستخدام بيانات حقلية من حقول نفط بشمال أفريقيا (WBM and OBM)، تم اختيار السوائل لأنها تتناسب مع الضغط العالي ودرجة الحرارة العالية. وتظهر أداة الإنتاج توافقا جيدا مع القياسات الحقلية.

Abstract: *In recent times, the oil industry has shown increasing awareness towards maintaining optimum well productivity through better high pressure, high temperature (HP-HT) drilling/completion fluids design. However, the mechanisms of drilling fluid filtration and impact on productivity performance are not well understood under downhole conditions.*

In open hole completions, the productivity losses are critical because the near-wellbore damage is not by-passed by perforations. Furthermore, a satisfactory model for field applications to simulate the near-wellbore damage in terms of well flow performance from laboratory core test analysis still is not available.

The results of in-depth experimental data combined with data analysis of static and dynamic filtration models provides the database for the semi-empirical mechanistic models that were developed. These models have been combined and incorporated into a design and evaluation tool - the productivity tool (PRT), for predicting the effect of HP-HT drilling fluid filtration on formation productivity in terms of formation damage in vertical wells.

In this paper, we present applications of the PRT using field data from North African oilfields with both water-based and oil-based muds (WBM

* Robert Gordon University, UK
** M-I L.L.C.

and OBM), both selected as suitable for HP-HT wells. The PRT shows good agreement with the field measurements.

INTRODUCTION

The most common source of formation damage has proved to be drilling operations[1]. Permeability is a characteristic of the formation, and can be altered by solids and mud filtrate invasion during drilling operations. Drilling fluids are used to facilitate various drilling processes. Drilling mud filtrate will invade the formation to a greater depth than drilling mud particles. A decrease of the permeability (formation damage), results in a decrease of the well productivity[2,3]. The formation damage depends upon many parameters such as formation characteristics, type, composition, filtration and rheological characteristics of drilling fluid and operating conditions (overbalance pressure, time, *etc.*).

A key parameter in quantifying formation damage is the skin factor[4]. The skin factor estimated from well test data is used in the inflow equations to estimate the production rate in wells that are affected by formation damage.

Generally, when rating performance of various drill-in fluid formulations, the permeability damage evaluation is quantified through oil return permeability measurements and flow-initiation pressures performed on core samples damaged during mud filtration tests[5,6].

Extensive laboratory studies of formation damage and several modeling efforts for prediction of formation damage have been reported in the literature. Most of the previous studies have focused on formation damage from drilling fluid filtration of water-based mud (WBM) and incompressible fluids in low-pressure, low temperature (LP-LT) applications.

Few attempts have been made to transfer these laboratory data into a near-wellbore model to evaluate the permeability damage. Liu *et al.*[7] simulated formation damage by fluid injection and mud filtration while Scott Lane[8] and Semmelbeck, *et al.*[9] simulated filtrate invasion for improving log interpretation, but their impact on well performance was not investigated. Some workers[10,11] studied well performance using representative formation damage, but laboratory tests were not integrated in their studies.

The economic impacts of wellbore formation damage justify a thorough study of this problem in order to find ways to minimize its effect on well performance.

This paper presents applications of the productivity tool using field data for screening different HP-HT drilling fluids (WBM and OBM), which specify the invaded zone skin as well as the depth of invasion, and evaluates the damage factor of a given fluid in terms of inflow performance.

FUNCTION OF THE PRODUCTIVITY TOOL

The productivity tool was constructed to provide a design and analysis package, which can be used to perform the following key functions:

1. To analyze wellbore pressure distribution.
2. To analyze the response of the fluid to static and dynamic filtration in an HP-HT environment.
3. To characterize the rheology and filtration of the selected fluids in an HP-HT environment.
4. Quantify the level and depth of damage and determine the best operating conditions.
5. Determine the impact of the selected fluid on formation productivity.
6. Screen appropriate HP-HT fluids desired for achieving minimum formation impairment.

In order to perform these functions, the productivity tool incorporates a number of mechanistic models, which have been developed as part of the initial project study, which include:

- Rheology prediction models.
- Static and dynamic filtration prediction models.
- Filter cake build-up on sand face evaluation models.
- Prediction models for filtration pressure drop across sand face and filter cake.
- Formation morphological characteristics.
- Prediction models for depth of solids and filtrate invasion.
- Prediction models for skin factor and flow efficiency.

The models are semi-empirical, which have been developed from the input of selected data generated from extensive experimental studies into filtration and formation damage[12,13] phenomena. All the analyses carried out on laboratory core tests were conducted under linear flow conditions, and upscaled into radial flow conditions, to simulate near-wellbore damage caused by particulate and filtrate invasion.

PRODUCTIVITY TOOL FORMULATION

Drilling Fluid Rheology. The rheological behavior of the drilling fluid has a major impact on pressure distribution in the wellbore and, hence, affects drilling overbalance pressure and fluid filtration. Therefore, to adequately predict downhole filtration, it is also necessary to predict downhole rheology.

Several studies of the HP-HT rheology of WBM and OBM have been presented in earlier papers[14,15]. Some of these studies which include many mathematical expressions are subjective. Politte[14] presented a multi-term equation with 13 numerical constants to model the viscosity of diesel oil. Houwen *et al.*[15] presented several equations to model rheological parameters. An API Bulletin[16] presented two equations to calculate pressure and temperature constants.

In this study, a different procedure has been adopted. Shear stress has been multiplied by a correction factor that depends on pressure and temperature. Then the rheological behavior and rheological parameters can be calculated from shear stress prediction at the pressure and temperature of interest. Two prediction models have been developed for WBM and OBM.

The models follow the general equation:

$$\tau_i = \tau_s[A_C \exp(AP - BT)] \quad (1)$$

Where τ_i is the shear stress at depth of interest and τ_s the shear stress at standard conditions. The difference between the models is in respect of the empirical constants (A_C, A and B). Data used to evaluate the empirical constants have been obtained from selective HP-HT Fann-70 viscometer measurements.

The models often used to describe the behavior of the two fluids are Bingham Plastic[17], Power Law[18] and Herschel Bulkley models[19]. However, in this study the WBM and OBM rheological data are best described by the Herschel Bulkley model.

The main difference between OBM and WBM are the effects of pressure, which are more pronounced for OBM than WBM. For WBM the effect of pressure is very small, but is highly affected by an increase in temperature.

Temperature and pressure affect behavior and interactions of water or oil, clay, polymers and solids in mud. The effect of increasing the temperature of a liquid is to reduce the cohesive forces while simultaneously increasing the rate of molecular interchange. The former effect tends to cause a decrease of shear stress, while the latter causes an increase. The net result is that liquids show a reduction in viscosity with increasing temperature. The effect of increased pressure on OBM is to increase the cohesive forces, which tends to increase the viscosity.

Drilling Fluid Filtration. One of the major functions of a drilling fluid is the control of formation pressure. In order to prevent formation fluids from flowing into the borehole, the hydrostatic pressure of the mud column is usually made to exceed the formation pressure.

Wellbore differential pressure can cause excessive loss of liquid and associated drilling mud solids leading to potential permeability impairment of the formation, and contribute to borehole instability[20,21] and formation damage[22], especially in the HP-HT environment. The differential pressure depends on mud weight, fluid rheology and formation pressure.

As a result of overbalance pressure, the filter cake may form on sand face, through which only filtrate can pass, depending on the relationship between mud particle size distribution and formation pore size.

The process of drilling a well results in alternating periods, of varying duration, of dynamic and static filtration (sequential filtration). Dynamic filtration occurs when the mud is circulated; the cake thickness is the difference between the rate of deposition by filtration and the rate of erosion by circulating mud. The erosion rate of particles is proportional to the shear stress exerted by the circulating mud on the cake surface[23].

Static filtration occurs when the mud is not circulated, and the cake thickness increases as filtration continues.

The existing static and dynamic filtration[23,24] equations can be modified for downhole pressure and temperature conditions.

(i). *Static Filtration:*

Two prediction models have been developed for WBM and OBM. The models follow the general format:

$$t = Y_1 V + Y_2 V^2 \exp.\ (AP + BT) \quad (2)$$

Where t is time and V the volume of filtrate. The difference between the models is in respect of the empirical constants (Y_1, Y_2, A and B).

(ii). *Dynamic Filtration:*

Two prediction models have been developed for WBM and OBM. The models follow the general format:

$$t = X_1 V - X_2(1 - e^{-X_3 V}) \exp.(AP + BT) \quad (3)$$

Equation (3) also can be used to predict dynamic from static filtration data. Since the modified filtration Equations (2) and (3) can predict the filtration coefficients (Y_1, Y_2, X_1, X_2 and X_3) therefore the filter cake characteristics such as cake resistance, permeability, porosity, etc. can be computed.

Filtration Pressure Drops. At the start of filtration, the pressure drop, ΔP_T, is across the sand face, but as the filter cake builds up more of the pressure drop is dissipated across the filter cake, P_C, and less across the sand face, P_f, thus.

$$\Delta P_T = \Delta P_f + \Delta P_C \quad (4)$$

Damage from Drilling Fluid. Formation damage mechanisms were studied extensively[25, 26]. However, formation damage from drilling fluid can be characterized by the thickness of filter cake, depth of solids and filtrate invasion and permeability reduction.

The two main damaging mechanisms which have been studied are particulate invasion during initial filtration period, and filtrate invasion through filter cake.

A. Filter Cake Build up

Filter cake thickness is given by:

$$\frac{dh_C}{dt} = \frac{\rho_f s V - K_\tau \tau}{(1 - ms)} \quad (5)$$

The shear stress should be calculated from rheological behavior of the mud Equation (1).

If the mud is not circulated then the shear stress τ is zero and the filter cake becomes thicker as static filtration continues.

B. Depth of Solids Invasion

Solids invasion occurs during initial filtration period. It is primarily a function of mud particle size distribution and the pore throat diameter of the formation. Semi-empirical equations have been developed for predicting the depth of solids invasion. These models are based on pressure drop in pipes and, therefore, involve the rheological behavior of the drilling fluid.

For Herschel Bulkley and Power Law fluids the model has been computed as:

$$L_S = \frac{C_1 \Delta P_f D_P^{(1+n)}}{K V_P^n (C_2 \frac{3n+1}{n})^n} \quad (6)$$

For Bingham Plastic fluid the equation is:

$$L_S = C_3 \Delta P_f \frac{D_P^2}{(C_4 \mu_P V_P + C_5 \tau_y D_P)} \quad (7)$$

These equations assume that the rheological properties of the fluid moving through the pore are the same as that of the bulk fluid. This assumption becomes increasingly invalid as the pore throat diameter decreases and mud components that affect the viscosity are screened out. In the limiting case, the viscosity is that of the filtrate.

As it can be observed from the above models, the depth of solids invasion requires the knowledge of the formation morphological characteristics such as permeability, porosity, tortuosity, *etc.*

Tortuosity (η) is the actual flow path and can be computed in laboratory from formation resistivity factor (F_R) and porosity thus:

$$F_R = a / \phi^b \quad (8)$$

$$\eta = \phi F_R \quad (9)$$

Then the mean pore throat diameter can then be calculated as:

$$D_p = 4.08 (\eta K / \phi)^{0.5} \quad (10)$$

C. Depth of Filtrate Invasion

The radius of filtrate invasion can be determined from filtration volume as:

Invasion in static condition:

$$r_f = \sqrt{r_w^2 + \frac{2r_w}{\phi}\left(\frac{-Y_1 t}{2Y_2} + \frac{(Y_1^2 + 4Y_2 t)^{1.5}}{12Y_2} - \frac{Y_1^3}{12Y_2}\right)} \quad (11)$$

Invasion in dynamic condition:

$$r_f = \sqrt{r_w^2 + \frac{2r_w t(1 - ms)K_\tau \tau}{\phi \rho_f s}} \quad (12)$$

All the parameters in equation (11&12) can be computed from sequential filtration experiments and Equations (2&3).

D. Permeability Damage

The initial formation permeability damaged in the zone occupied by particulate and filtrate is characterized by permeability reduction (damage) as a function of core length or distance from the wellbore in radial well flow conditions. The permeability damage factor can be described as:

$$C_F = k_d / k_f \quad (13)$$

The permeability alteration (k_d) can be computed from the knowledge of overall average permeability and total depth of invasion.

Productivity Evaluation

Well performance is reduced when near-wellbore formation is damaged. Key parameters in quantifying the formation damage or the reduction of the well productivity will be the skin factor or by the flow efficiency.

The skin factor s_d, defined as:

$$s_d = (1 - k_f / k_d) \ln (r_w/r_f) \quad (14)$$

Using a well productivity index (PI) usually represents well performance. Therefore, well flow efficiency due to near wellbore damage can be calculated as:

$$FE = PI_{actual} / PI_{ideal} \quad (15)$$

Then the damage factor can be computed from the reciprocal of the well flow efficiency.

$$DF = 1 / FE \quad (16)$$

PRODUCTIVITY TOOL STRUCTURE

In order to simulate the impact of drilling fluid filtration on well performance in terms of formation damage, a computer package with the models developed above is required. The structure of calculation is described as follows:

1. Input the data required for the models: wellbore parameters (hole geometry, casing size, *etc*), operating parameters (overbalance pressure, pump rate, *etc*), drill-in fluid parameters (mud type, rheology, *etc*) and formation parameters (permeability, porosity, *etc*).
2. Compute the rheological behavior at standard conditions and depth of interest.
3. Compute the rheological parameters and calculate the wellbore pressure distribution.
4. Compute the static and dynamic filtration and calculate filter cake properties.
5. Calculate the pressure drop across filter cake and sand face.
6. Quantify level of resultant damage by computing depth of solids and filtrate invasion, average permeability and permeability damage.
7. Evaluate the results of well performance by computing skin factor, ideal and actual productivity index, flow efficiency and damage factor.

APPLICATION OF THE PRODUCTIVITY TOOL

Specific case studies to illustrate the interpretation and practical usefulness of the productivity tool have been carried out using actual field data. The data are collected from four oil companies in North Africa (Table 1) and can be summarized as follows:

Table 1. Well summary.

Co.	Field	Well No.	TVD (ft)	Temp. (^{0}F)	Fluid type	Hole section (inch)	Completion
1	A	A1	14580	330	Oil based	8.50&6	cased
		A2	14500	322	Lignosulphonate	6	cased
2	B	B1	13528	320	Oil based	5.875	Openhole
		B2	13390	314	Lignosulphonate	8.50&5.875	Openhole
		B3	12245	280	Lignosulphonate	5.875	Openhole
3	C	C1	12370	290	Potassium chloride	8.50	cased
4	D	D1	10045	240	Dispersed polymer	8.50	cased

1. Seven wells with the total well depth ranging from 10045 ft to 14580 ft.
2. Reservoir sections drilled in 5.87, 6 and 8.50 inch holes.
3. Open hole and cased hole completions.
4. Wellbore pressure ranging from 5000 psi to 12800 psi.
5. Bottom hole temperature ranging from 240 ^{0}F to 330 ^{0}F.
6. Reservoir permeability ranging from 50 md to 400 md.
7. Oil-based and water-based drill-in fluids types (dispersed polymer mud, potassium chloride mud and lignosulphonate mud).

The application of the productivity tool has been used in two ways:

1. Evaluation Stage: The PRT simulated results have been evaluated against field data (post drilling):
   a) Predicted total wellbore pressure distribution versus field data (pump pressure).
   b) Predicted well performance in terms of formation damage against field measurements (depth of invasion from logging and skin factor from well test data).
2. Planning stage: The PRT has been used for fluid optimization and selection against different operating parameters, such as fluid type, rheology, pressure, *etc.*

Evaluation Stage. Table 2 illustrates the predicted total wellbore pressure distribution versus field data

Table 2. Predicted pump pressure versus field data (pump pressure).

Pump Pressure (psi)

Well number	Total depth (ft)	Hole section (inch)	BHtemp (^{0}F)	Field data (Psi)	PRT prediction (Psi)
A1	13790	8.50	315	2575	2466
	14580	6	330	1780	1670
A2	14500	6	322	1700	1695
B1	13528	5.875	320	2000	2032
B2	12175	8.50	305	2600	2820
	13390	5.875	314	2000	2083
B3	12245	5.875	280	1500	1566
C1	12370	8.50	290	2850	3000
D1	10045	8.50	240	1950	2092

(pump pressure). The prediction shows agreement with field data. Table 3 shows predicted (depth of invasion and skin factor) against field measurements. The field measurement from well test data gives the total skin and the PRT predicts the drilling skin. However, stochastic analyses have been carried out based on

Table 3. Formation damage predicted against field measurement.

				Depth of Invasion (inches)		Skin	
Well No.	TVD (ft)	Hole (inch)	BHT (^{0}F)	Field data	PRT predic-tion	Field data total skin	PRT prediction drilling skin
A1	14580	6	330	40	34.79	9.00	4.11
A2	14500	6	322	60	77.73	12.0	5.24
B1	13528	5.875	320	60	45.43	10.0	4.00
B2	13390	5.875	314	70	92.73	10.0	5.87
B3	12245	5.875	280	70	90.81	10.0	5.63
C1	12370	8.50	290	60	77.63	9.00	4.48
D1	10045	8.50	240	40	48.69	8.00	3.62

standard assumptions to calculate both the partial completion skin and perforation skin and add them to the drilling skin predicted from the PRT, in order to enable comparison with field test data. Table 4 shows agreement between the PRT predicted skin and field measurement.

Table 4. Formation damage predicted against field measurement.

Well No.	TVD	Mud type	Field data Total skin	PRT prediction Sd	Sc+Sp	Total Skin
A1	14580	OBM	9.00	4.11	3.10	7.21
A2	14500	CL/CLS	12.00	5.24	3.32	8.56
C1	12370	KCl	9.00	4.48	2.84	7.32
D1	10045	PWBM	8.00	3.62	2.61	6.23

Planning Stage. The input data are from well number (A1) for a 6 inch hole section and the

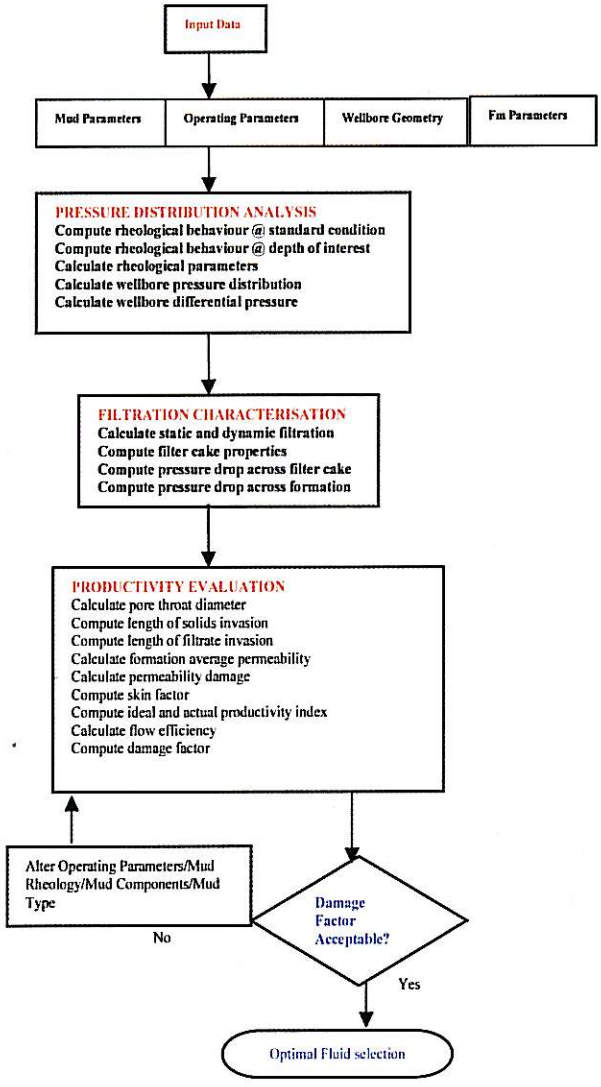


Fig. 1. Shows a flow chart on which the productivity tool has been developed.

assumption was made to select the best HP-HT drilling fluid to drill this well with minimum formation damage. The types of the drilling fluids that have been used for evaluation are oil-based and water-based muds (dispersed polymer mud, potassium chloride mud and lignosulphonate mud). The fluid rheology and mud composition data for these types of mud have been used from field data of six wells drilled by various oil companies.

Figures 2 to 8 illustrate the effects of different parameters such as rheological behavior, drilling time, temperature, and overbalance pressure on flow efficiency comparing different types of WBM and OBM drill-in fluids. Three different rheological properties for both OBM and WBM have been used for fluid selection of this particular well (A1).

OPTIMIZATION PROCESS

Effect of Rheological Parameters. Figures 2 and 3 show that an increase in rheological parameters (yield stress and consistency index) results in an increase in depth of filtrate invasion and, hence, an increase in damage factor.

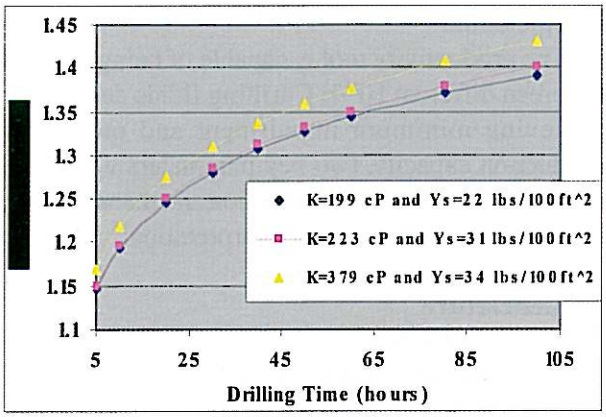


Fig. 2. Effect of rheology on formation damage for OBM.

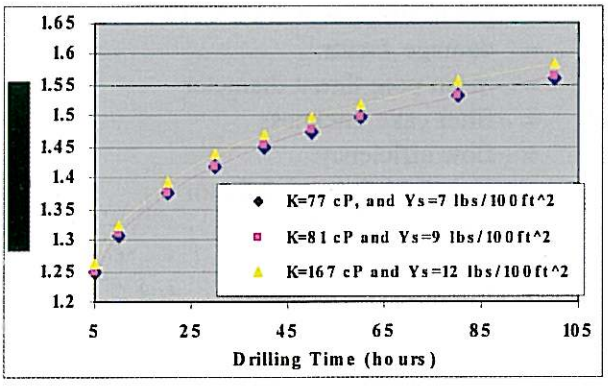


Fig. 3. Effect of rheology on formation damage for WBM.

Effect of Rheological Characterisation. Figure 4 shows the depth of invasion profile for WBM and OBM. The figure also shows the accurate description of the rheological behavior of the drill-in fluid required to accurately predict the depth of invasion.

Figure 4 illustrates effect of rheological behavior on formation damage characterization. A comparison has been made between the actual fluid rheological behavior models, i.e. Herschel-Bulkley, Power Law and Bingham Plastic models. The figure shows that the Bingham model predicts

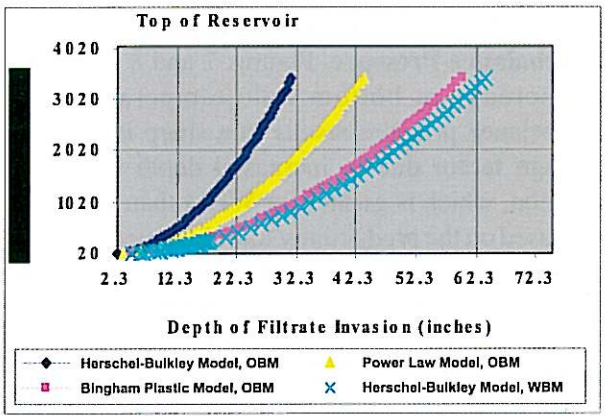


Fig. 4. Effect of rheology characterisation on depth of invasion.

higher formation damage than the actual model. The Herschel-Bulkley model best represents actual fluid rheology. The depth of invasion was found to be greater for WBM than OBM. Figure 5 shows damage profile using OBM.

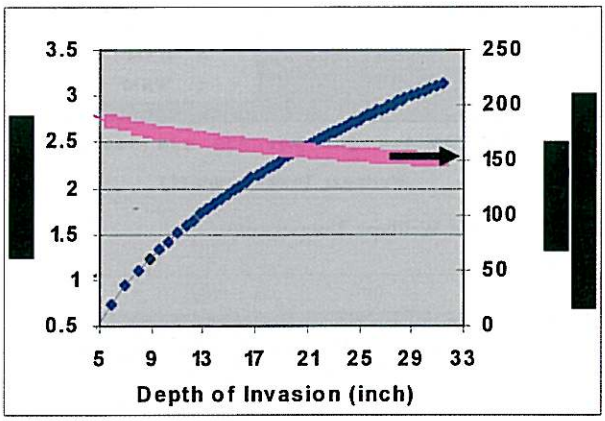


Fig. 5. Damage profile using OBM.

Effect of Drilling Time. Figure 6 shows an increase in drilling operational time results in an increase in depth of filtrate invasion and, hence, an increase in damage factor, which is greater for WBM than OBM.

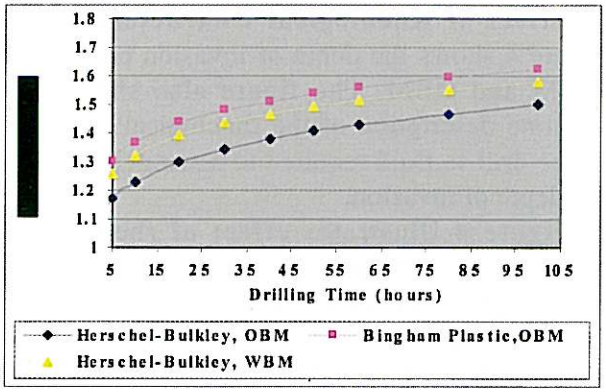


Fig. 6. Effect of Drilling Time.

Effect of Wellbore Temperature and Overbalance Pressure. Figures 7 and 8 show that an increase in bottom hole temperature and overbalance pressure results in a sharp increase in damage factor due to increased depth of filtrate invasion, which is greater for WBM than OBM.

Based on the productivity tool simulated analysis, the selection of OBM with rheological parameters [n= 0.66, K= 199 cp and Ys=22 lb/100ft^2] to drill this particular well (A1) gives more advantages for well flow performance than for WBM.

However, it is necessary during the fluid design stage to screen different HP-HT fluids also based on a higher percentage of the return permeability test. This is because the depth of invasion is inversely proportional with percentage of the return permeability test[27].

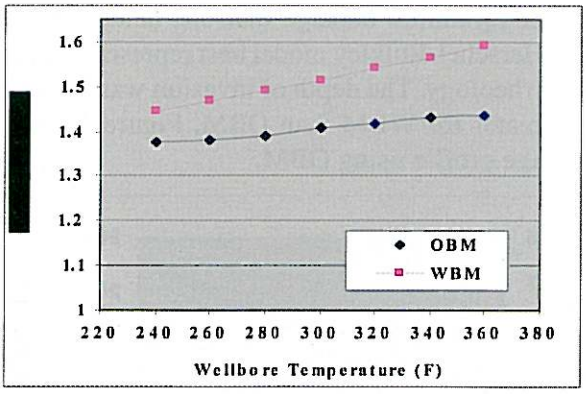


Fig. 7 - Effect of Wellbore Temperature.

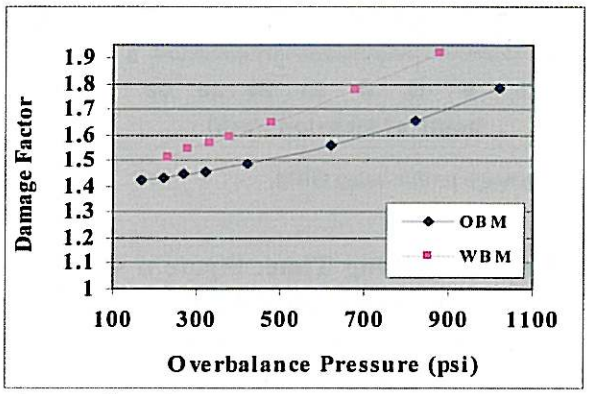


Fig. 8 - Effect of Overbalance Pressure.

CONCLUSIONS

The field application of the productivity tool is presented to simulate impact of drilling fluid filtration on formation productivity in an HP-HT environment. The productivity tool can be used for predicting formation damage mechanisms caused by particulate and filtrate invasion.

The tool can evaluate formation damage in laboratory as linear-flow core tests and can be converted to radial-flow scale for oil field applications.

Input requirements include parameters such as hole geometry, BHA configuration, mud type, composition, rheology data and formation characteristics.

The productivity tool can be used to investigate the influence of many parameters on the well flow performance.

The tool can be used before drilling as a design (planning) tool, and during drilling and post drilling as evaluation and comparison tool with well test data interpretation.

The productivity tool is capable of being utilized to screen different HP-HT drilling fluids desired for achieving minimum impairment and maximum production capacity, two key parameters which are relevant to optimum fluid selection and management, in addition to well test data interpretation.

Nomenclature

a, b = coefficients
A, B = pressure and temperature coefficients
A_c = constant
C1, C2, C3, C4, C5 = constants
C_F = permeability reduction factor
DF = damage factor
D_p = mean pore throat diameter
dh_c = filter cake thickness
FE = flow efficiency
F_R = resistivity formation factor
k = consistency index
k_τ = erodability coefficient
k_i = formation permeability
k_d = permeability damage
L_S = depth of solids invasion
m = ratio of wet to dry cake

n = Power law index
P = applied pressure
PI_{actual} = productivity index after formation damage
PI_{ideal} = productivity index before formation damage
ΔP_T = total differential pressure
ΔP_f = pressure across formation
ΔP_c = pressure across filter cake
r_f = radius of filtrate invasion
r_w = wellbore radius
s = solids concentration
s_c = partial completion skin
s_d = drilling skin factor
s_p = perforation skin
t = time
T = temperature
V = filtrate volume
V_p = velocity in porous medium filtration coefficients
Ys = yield stress

Greek Symbols

η = tortuosity
μ_p = plastic viscosity
τ_y = yield point
τ_s = shear stress at standard condition
τ_i = shear stress at depth of interest
ϕ = porosity of formation
ρ_f = density of filtrate

Acronyms

BHA = bottom hole assembly
BHT = bottom hole temperature
Cl/Cls = lignosulphonate mud
KCl = potassium chloride mud
PWBM = dispersed polymer mud
LP-LT = low pressure-low temperature
HP-HT = high pressure-high temperature
OBM = oil-based mud
md = millidarcy
TVD = total vertical depth
WBM = water-based mud

REFERENCES

[1] Michael J. Economides, A. Daniel Hill, and Christine Ehlig- Economides, 1994. Petroleum production systems.

[2] Krueger, R. F., 1986 (Feb.). An Overview of Formation Damage and Well Productivity in Oilfield Operation. *JPT*, 131-152.

[3] Dearing, H. L and Ali, S, A., 1996 (Jan). Drill-in fluid selection crucial to well productivity. *Petroleum Engineer. International*, 21-25.

[4] Van Everdingen, A, F., and Hurst, W. The Application of the Laplace Transformation to Flow Problems in Reservoirs. *TRANS. AIME*, 1949, 186, 305-324.

[5] Fraser, L. J., Ried, P., Williamson, D., and Enriquez, F., 1995 (October) . Mechanistic investigation of the formation damaging characteristics of mixed metal hydroxide drill-in fluids and comparison with polymer-base fluids. SPE 30501 presented at the SPE Annual Technical Conference and Exhibition held in Dallas, U.S.A.

[6] Davison, J.M., Jones, M., Shuchart, C. E., and Gerard, C., 2000 (Feb.). Oil-based muds reservoir: their performance and cleanup characteristics. SPE 58798 presented at the 2000 SPE International Symposium on Formation Damage Held in Lafayette, Louisiana.

[7] Liu. X. and Civan. F., 1994 (Feb.). Formation damage and skin factor due to filter cake formation and fines migration in the near-wellbore region. SPE 27364 presented at the SPE Int. Symposium on Formation Damage Control, Lafayette, LA.

[8] Scott Lane, H., 1993 (June). Numerical simulation of mud filtrate invasion and dissipation. SPWLA 34th Annual Logging Symposium.

[9] Semmelbeck, M.E., Dewan, J.T. and Holditch, S.A.,1995 (Oct.). Invasion based method estimating permeability from logs. SPE 30581 presented at the SPE ATC&E, Dallas.

[10] Permadi, P. and Wibowo, W., 2001 (May). Effects of non-uniform skin distribution on horizontal well inflow performance. SPE 68952 presented at the SPE European Formation Damage Conf. The Hague, The Netherlands.

[11] Menour, H., Al-Majed, A. and Hassan, S., 2000 (April). Effect of formation damage, length and reservoir thickness on the inflow performance of horizontal wells. SPE 59356 presented at the 2000 SPE/ DOE Improved Oil Recovery Symp. Tulsa OK.

[12] M. B. Amish and M. B. Oyeneyin (The Robert Gordon University) and M. H. Hodder (M-I L.L.C.), in progress. Characterisation of drilling fluid filtration under downhole conditions.

[13] M. B. Amish and M. B. Oyeneyin (The Robert Gordon University) and M. H. Hodder (M-I L.L.C.), in progress. Characterisation mechanisms of formation damage.

[14] Politte, M. D., 1985. Invert oil mud rheology as a function of temperature and pressure. SPE/IADC 13458, New Orleans, U.S.A..

[15] Houwen, O. H., and Geehan, T., 1986. Rheology of oil-base muds. SPE 15416, New Orleans, U.S.A.

[16] API Bulletin 13B, 1995. *Recommended Practice on*

the Rheology and Hydraulics of Oil-Well Drilling Fluids, API BUL 13D, Third Edition.

[17] Bingham, E. C., 1922. *Fluidity and Plasticity*. McGraw-Hill Book Co., New York.

[18] Govier, G. W. and Aziz, K., 1972. *The Flow of Complex Mixtures in Pipes*. Van Nostrand Reinhold, New York..

[19] Herschel, W. H. and Bulkley, R., 1926. Measurement of consistency as applied to rubber-benzene solutions. *Proceedings of the American Society of Testing Materials*, **26**, 621-633.

[20] Chenevert, M.E., 1970 (Oct.). Shale control with balanced-activity oil continuous muds. *JPT*, 1309.

[21] Bushnell, Y.M, and Panesar, S. S., 1991 (Oct). Differential sticking laboratory Tests can improve mud design. SPE 22549 presented at the 66th Annual Technical Conference and Exhibition of the SPE, Dallas, TX.

[22] Ali Ghalambor.and M. J. Economides, 2000 (Feb.) Formation damage abatement: a quarter-century perspective. SPE no. 58744.

[23] Shuang Jiu Peng, and Peden, J. M., 1992 (Feb.). Prediction of filtration under dynamic conditions. SPE 23824 presented at the SPE Ind. Symposium on Formation Damage Control held in Lafayette, Louisiana..

[24] Arthur, K. G. and Peden, J. M., 1988. The evaluation of drilling fluid filter cake properties and their influence on fluid loss. SPE 17617.

[25] Yan Bingo, M. B. Oyeneyin, and J. M. Peden, 1994. Investigation of pore blocking mechanism in gravel packs in the management and control of fines migration. SPE 27342.

[26] Oyeneyin, M. B., Peden, J. M., Ali Hosseini, and Ren, G., 1995. Factors to consider in the effective management and control of fines in high permeability sands. SPE 30112.

[27] M. B. Amish, in progress. A productivity tool for impact of filtration on well performance in an HP-HT.

Petroleum Res. J. Vol. 18 (2005): P. 133–136, 3 Figs.

Depressurization as an Effective IOR Strategy

M. Babs Oyeneyin*

التقليل من الضغط كإستراتيجية مؤثرة للاسترداد الإضافي

م. بابس أوينين

يتم الآن ضمن عمليات الاسترداد الإضافي تبني طريقة تخفيض ضغط المكمن كأفضل تقنية من المنظور الاقتصادي بعدة مكامن فتاتية.

حددت أعمال سابقة على تحليل الإجهاد بالمكمن بوضوح العلاقة المعقدة بين خواص انسياب المكمن وإجهاد المكمن المؤثر والسائد.

تقدم هذه الورقة نتائج دراسات استهلت بجامعة روبرت جوردون في الأعوام القليلة الماضية وأكدت هذه الدراسة نتائج دراسات سابقة عديدة تنص على وجود علاقة معقدة بين خصائص انسياب المكمن والإجهاد السائد المؤثر. وأكدت النتائج أيضا وبقوة أن كفاءة فاعلية انسياب المكمن ومعامل الاسترداد هما دالة نفاذية المكمن الأولية، ومعامل جودة الخزان ومسار الإجهاد.

لقد بينت دراسات النفاذية حتى الآن أن تأثير مسار الإجهاد على فاعلية الانسياب ومعامل الاسترداد يعتمد على معامل جودة الخزان وعلى ما يسمى بمؤشر جودة الخزان والذي تم تعريفه بأنه المعامل الوحيد الذي يشمل المزايا الجيولوجية للنسيج والمحتوى المعدني في تمييز سحنات الفراغات الهندسية والتي تعرف بالوحدات الهيدروليكية.

يمثل مسار الإجهاد تباين شدة الإجهاد بالمكمن، وتم إجراء بعض التحاليل باستعمال مجموعة من المعلومات الحقلية التي يمكن استعمال نتائجها في تطوير وأخذ قرار يخص اختيار المكمن الأمثل وظروف العمل المناسبة وبما يضمن تحسن في الاسترداد الإضافي.

Abstract: *Reservoir depressurization is now being adopted as the most economic improved oil recovery (IOR) technique in many clastic reservoirs. Early work on reservoir stress analysis has clearly identified a complex relationship between the reservoir flow properties and the prevailing reservoir effective stress.*

This paper presents the results of studies initiated at The Robert Gordon University over the last few years. These results have confirmed a number of previous studies that there is a complex relationship between reservoir flow properties and the prevailing effective stress. The results have confirmed that the reservoir flow efficiency and the recovery factor are both strongly a function of the initial reservoir permeability, Reservoir Quality Index (RQI) and the stress path.

Preliminary studies to date have indicated that the effect of the stress path on flow efficiency and recovery factor depend on the RQI and the so-called Flow Zone Indicator (FZI) defined to be a unique parameter that incorporates the geological attributes of texture and mineralogy in the discrimination of pore geometrical facies known as hydraulic units. The Stress Path represents the

* The Robert Gordon University, UK.

magnitude of stress anisotropy in a reservoir. Stochastic analysis have been carried out using a variety of field data the results of which can be used to develop a decision for optimum reservoir candidate selection and operating condition required to guarantee improved oil recovery.

INTRODUCTION

Depressurization has long been identified as one of the strategies for enhanced oil recovery especially in mature, depleted reservoirs.

Generally during depressurization, the reservoir pressure drops to release solution gas and mobilize trapped or by-passed oil. The flowing bottom hole pressure can also be reduced to create the necessary drawdown for improved inflow efficiency.

Depressurization itself can generally be achieved by withdrawing large volumes of liquid and free gas from the reservoir. This technique includes[1,2]:

1. Use of gas lift, for example, in mid-flank oil wells to maximize off take.
2. Depressurization of aquifer via ESP water off-take to maintain required pressure depletion rate
3. Under balanced drilling

Irrespective of the technique used, it is believed that during depressurization the reduction in the pore pressure profile will alter the effective stress in the rock matrix the magnitude of which will depend on the type of reservoir. For an HP-HT reservoir in offshore environment, this reduction may be drastic in the initial transient stage[5]. This will induce changes in pore structure and pore volume thereby causing permeability changes. Early work on reservoir stress analysis has clearly identified a complex relationship between the reservoir flow properties and the prevailing reservoir effective stress. The effective reservoir stress is here defined as the difference between the externally applied overburden stress and the internal stress created by the pore fluid pressure. The level of depressurization will no doubt affect the rate of pore pressure decline.

Recent studies initiated at The Robert Gordon University over the last few years [6] on the effect of depressurization on unconsolidated reservoirs has confirmed a number of previous studies by Amaefule *et al* [7], Ottesen *et al* [8] among others [9-11], that there is a complex relationship between reservoir flow properties and the prevailing effective stress. The results have confirmed that the reservoir flow efficiency and recovery factor are strongly a function of the initial reservoir permeability, Reservoir Quality Index (RQI) and the stress path.

A parallel work on UBD indicated that the productivity improvement in UBD-drilled wells is more complex than just mere reduction in formation damage/skin. The studies have indicated that the productivity improvement mechanism in UBD might be akin to ''transient'' or rapid depressurization mechanism[12].

EFFECT OF STRESS

Preliminary studies to date have indicated that the effect of the stress path on flow efficiency and recovery factor depend on the RQI and the so-called Flow Zone Indicator [FZI] defined by Amaefule *et al.* [7] to be a unique parameter that incorporates the geological attributes of texture and mineralogy in the discrimination of pore geometrical facies known as hydraulic units. The early work by Amaefule has indicated that the FZI for the Niger Delta ranged between 0.3 to 11. This may need to be confirmed for the deep offshore where the overburden stress will be a lot higher.

The Stress Path represents the magnitude of stress anisotropy in a reservoir. It is defined as the ratio of the changes in effective horizontal stress and the changes in effective overburden stress.

The stress path K_{sp} is defined mathematically as:

$$K_{sp} = \frac{\Delta\sigma_H}{\Delta\sigma_{OB}} \quad (1)$$

$\Delta\ \sigma_H$ = Change in effective horizontal stress

$\Delta\ \sigma_{OB}$ = Change in effective overburden stress

The model for predicting the vertical stress for Offshore Niger Delta was derived by Ottesen *et al* [8] as:

$$\sigma_{OB} = 0.374D^{1.0984} - 10.7 \quad (2)$$

$[\sigma_{OB}]$ = psi

D = True vertical depth, ft

Likewise, the horizontal stresses can be derived as:

$$\sigma_{H\,max} = 0.1807D^{1.1650}$$
$$\sigma_{H\,min} = 0.1779D^{1.15865} \quad (3)$$

The Reservoir Quality Index is a unique property of any reservoir that takes into account the impact of the effective stress on reservoir flow properties [Porosity and permeability]. It can be obtained mathematically as [7-9]:

$$RQI = 0.0314\sqrt{\frac{k}{\phi}} \quad (4)$$

The FZI can be computed from a log-log plot of RQI vs. normalized porosity index (φ_z)

$$\varphi_z = \frac{\phi}{1-\phi} \quad (5)$$

In order to define the relationship between the reservoir flow properties and effective stress, attempts have been made to develop a semi-empirical correlation using a combination of database from Niger Delta and offshore locations in the North Sea and Dulang Field[9] in Malaysia. The resulting correlation is given as:

$$\frac{k}{k_i} = A + [B * \sigma] - [C * \sigma * K_{sp}] + [D * \sigma * FZI] \quad (6)$$

A, B, C, and D = Empirical constants
σ ?= Effective stress, psi
k_i = initial permeability, mD
k = effective permeability, mD
K_{sp} = Stress path
FZI = Flow zone indicator, mD

EFFECT ON RECOVERY FACTOR

Some basic equations for recovery factor [RF] are as follows[13]:

1. Recovery Factor for Gas Drive Reservoir

$$RF = 0.41815\left[\frac{\varphi(1-S_W)}{\mu_{OB}}\right]^{0.1611} * \left[\frac{10^{-3}k}{\mu_{OB}}\right]^{0.0979} * [S_W]^{0.3722} * \left[\frac{P_b}{P_a}\right]^{0.1741} \quad (7)$$

2. Recovery Factor for Water Drive Reservoirs

$$RF = 0.549\left[\frac{\varphi(1-S_W)}{B_{Oi}}\right]^{0.0422} * \left[\frac{10^{-3}k\mu_{wi}}{\mu_{Oi}}\right]^{0.0979} * [S_W]^{-0.1903} * \left[\frac{P_i}{P_a}\right]^{-0.2159} \quad (8)$$

Where:

φ = Porosity;
k = Effective permeability
$k\mu_{wi}$ = connate water viscosity at irreducible water saturation level
μ_{OB} = Fluid viscosity at bubble point condition
B_{oi} = Formation volume factor at initial reservoir pressure P_i
S_w = Connate water saturation
P_b = Bubble point pressure
P_a = Ambient pressure

As can be observed from equations 7 and 8, any increase in permeability can be said to normally lead to a corresponding increase in recovery factor. Therefore for situations where the increase in effective stress leads to a corresponding increase in permeability, there will be an increase in productivity and recovery.

RESULTS

Figures 1, 2 and 3 show that whilst some reservoirs, appear to indicate an increase in reservoir flow efficiency and RF, others indicate no change and sometime outright decrease in recovery factor.

Figure 1 indicates clearly that for FZI greater than 5 the flow efficiency appears to increase with increase in the effective stress. This also leads, as expected, to a corresponding increase in recovery factor for the same FZI range, (Fig 2). This increase in RF however appears to be more pronounced in the low permeability sands than in the high permeability ones, as shown in Figure 3. On the other hand, the recovery factor appears to increase with decrease in stress path especially for stress paths less than 0.5.

These results appear to indicate therefore that the level of effective stress or drawdown and therefore the stress path will have an effect on reservoir performance depending on the type of reservoir. Therefore for sustainable improvement in

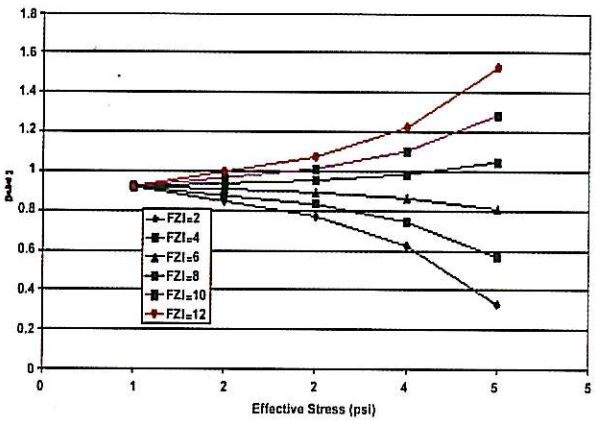


Fig. 1. Effect of stress on permeability.

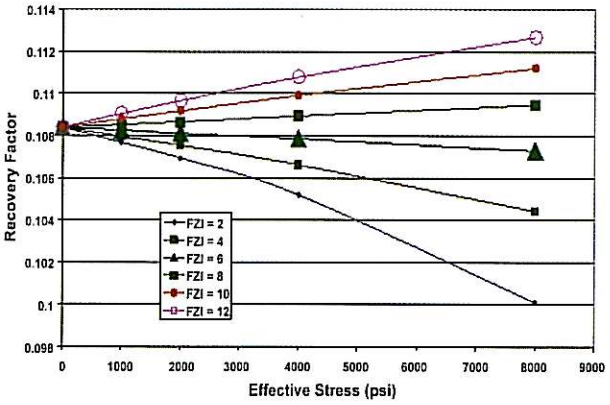


Fig. 2. Recovery factor as a function of effective stress.

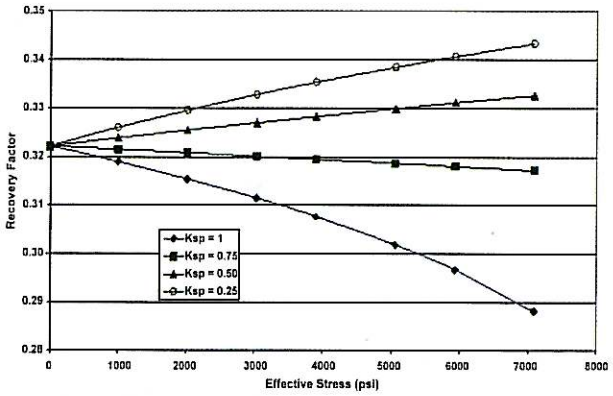


Fig. 3. Effect of stress path on recovery factor.

productivity, it may be logical to say that there must be an optimum level of effective stress or drawdown if productivity improvement is to be sustained over a long period. The same can also be said for under-balanced drilling condition where transient depressurization appears to be taking place during drilling[12]. The studies on UBD are still in their preliminary stages and more extensive studies are required to develop a comprehensive strategy for under-balanced drilling.

CONCLUSIONS

In this paper attempts have been made to present the effect of depressurization and corresponding change in effective stress on recovery factor. The main conclusions are:

1. Depressurization and therefore change in effective stress has a mixed effect on recovery factor depending on the RQI [and thus the type of reservoir], the initial reservoir permeability, type of completion and stress path.

2. Increase in effective stress leads to a higher RF in low permeability reservoirs than it does in higher permeability sands.

3. The increase in RF is limited to FZI greater than 5 and stress path less than 0.5.

4. For lower FZI and stress path higher than 0.5, the RF appears to decrease.

5. Effective reservoir characterization studies are essential to a successful depressurization as an effective IOR strategy

REFERENCES

[1] Braithwaite, C.I.M, 1994. A review of IOR/EOR opportunities for the Brent field: depressurisation, the way forward, *SPE/DOE* Paper No. 27766.

[2] Braithwaite, C.I.M and W.M.Schulte. Transforming the future of the v.

[3] Brent Field: Depressurisation-The next development phase. *SPE* Paper No. 25026, 1992

[4] Oyeneyin, M. B., 2003. Challenges of underbalanced drilling for West Africa. *SPE* Paper No. 85662.

[5] Lage, A.C.V.M, Rommetvet, R and R.W.Time. Study for improved understanding of transient phenomena in UBD operations. *SPE* Paper No. 52829.

[6] Omeroglu, Isa, 2000. *Analysis of the Effect of Depressurisation on the Inflow Performance of Unconsolidated Reservoirs*. M.Sc Project Thesis, The Robert Gordon University.

[7] Amaefule, Jude O, Altunbay, Mehmet, Kersey, David G. and Keelan, Dare, 1993. Enhanced reservoir description using cores and log data to identify hydraulic flow units and predict permeability in uncored intervals/wells. *SPE* Paper No. 26436.

[8] Ottesen, S and Lowrey, J.P., 1995 (March). An assessment of the mechanical stability of wells offshore Nigeria. *SPE* Drilling & Completions.

[9] Zarool Hassan An Tajul Amar Mehmet Altumbay and Duncan Barr, 1994. Stress sensitivity in the Dulang Field - how it is related to productivity. *SPE* Paper No. 30092.

[10] Rhett, D.W and Teufel, L.W., 1992. Effect of reservoir stress path on compressibility and permeability of sandstones. *SPE* Paper No. 24756.

[11] Gray, D.H, Fatt, I. and Bergamini, G., 1963. The effect of stress on permeability of sandstone cores. *SPE* 531.

[12] Oyeneyin, M.B., 2003. Challenges of underbalanced drilling for West Africa", *SPE* Paper 85662.

[13] Reuven Hollo, Holmes, M and Pais, V. 1983. *Reservoir Economics and Engineering Manual*. Gulf Publishing Company, Texas.

Petroleum Res. J. Vol. 18 (2005); P. 137–148, 10 Figs.

Evaluation and Ranking of Scenarios for Redeveloping Mature Fields: A Need for Improved Methodologies

François Kalaydjian, Isabelle Zabalza-Mezghani, Emmanuel Manceau, Mathieu Feraille and Paul van Lingen*

تقييم وتصنيف سيناريوهات لإعادة تطوير الحقول المعمرة: الحاجة إلى تحسين المنهجيات

فرانسوا كالايديجان، إيزابيل زابالزا-مزغاني، إيمانويل ماسو، ماثيوفيراي وبول فان لينجين

تتعلق هذه الورقة بمنهجيات ووسائل جديدة تبدو ضرورية لتحسين إنتاجية الحقول المعمرة، وذلك بتصميم طرق كفاءة لإعادة هندسة تلك الحقول، ومن ثم يمكن زيادة إنتاجيتها والوصول إلى الحد الأقصى لتلك الإنتاجية.

لقد تم تأسيس تلك المنهجيات على تقنية COUGR التي تم تطويرها بمعهد النفط الفرنسي، للتعامل مع الغموض المصاحب لوضع استراتيجية لتطوير الحقل. كما توفر هذه التقنية زيادة التعرف على المكمن بأقل تكلفة وتقترح طرقا للكشف عن نقاط الغموض متعددة المصادر، ومن ثم وضع استراتيجية متطورة لبلوغ الحد الأقصى اقتصاديا في بيئة محفوفة بالمخاطر.

وتقدم هذه المنهجيات، جنبا مع جنب المعرفة المعمقة لهندسة عمليات الاسترداد الإضافي ومنهجيات معالجة البئر، طريقة كفؤة لتحسين الاسترداد الإضافي لمكامن النفط والغاز في الحقول المعمرة.

Abstract: *This paper deals with new methodologies and tools which appear necessary to improve the evaluation of the potentials of mature fields. By designing efficient ways for reengineering, it becomes possible to increase their recovery factor and thus maximize their value.*

Those methodologies are based on the COUGAR™ technology developed at the IFP for dealing with uncertainties associated with field development strategy. This technology allows enhancing the knowledge of a given reservoir at the lowest cost, propose ways to minimize the uncertainties of various origins, and thus improve the sweeping strategy in order to maximize the economics in a risk-prone environment. Principles and applications of this technology to actual field cases are presented in this paper.

These methodologies, along with a deep understanding of the design of recovery processes and well treatment strategies, offer new and efficient ways of improving the oil and gas recoveries from mature fields.

INTRODUCTION

According to the reference scenario retained by the WETO European Commission (World Energy, Technology and Climate Policy, Outlook 2030), the world demand for energy should reach 17 Gtep in 2030 and possibly 30 Gtep in 2050 whereas today it is only equal to 10 Gtep. In 2030, approximately two-thirds of the energy demand will be provided by the hydrocarbons. Still in 2050 and beyond, hydrocarbons will constitute the main and easiest access to energy for humanity.

* Institut Français du Pétrole (IFP).

To sustain this rapid growth in demand (approximately 1.8% per year), the hydrocarbon reserves renewal through exploration alone will not be sufficient. Another key source has to be "the improvement in recovery factor" from mature fields.

In a recent paper[1], the concept of Integrated Reservoir Management (IRM) as a key issue to enhance the production of existing reservoirs was addressed. IRM consists not only of EOR techniques such as chemical or gas flooding as was the case in the seventies and early eighties. It includes, as well, strategies of field redevelopment using field surveillance and monitoring to locate by-passed oil zones, complex well architectures to target those zones, well productivity and injectivity enhancement.

Combination of all those methodologies and techniques allows to optimize the development of the fields, lower the cost of that development, extend the life of the existing fields, and, hence, increase the recovery factor and the value of those fields.

Discriminating among the different possible scenarios, performing sensitivity analysis by accounting for various technical and economic constraints is, as quoted in reference 2 (Zekri and Jerbi, 2002), "the ultimate goal of reservoir engineering management".

To reach that goal, compare and rank different development strategies, the reservoir engineer has to be provided with specific methodologies and tools.

This paper is addressing those issues in two sections.

- The first section will present the COUGAR™ methodology, fully detailed in reference 3 (Zabalza-Mezghani and *et al.*) which allows quantifying uncertainties and provides a way to optimize the economics in a risk prone environment. A field application is presented.
- In the second section of this paper, the question of ranking between several development strategies is addressed. A field application is presented.

THE COUGAR METHODOLOGY

The Problematic

Information acquired while evaluating and exploiting hydrocarbon reservoirs has increased and improved during the last decade. Thanks to high technology data acquisition programs, it is nowadays possible to calibrate complex numerical models that integrate all this information for generating detailed geological and fluid flow modeling and optimizing these models for maximizing oil recovery and economics. Unfortunately, all these data are generally associated with significant errors and uncertainties. The main consequence is that the output of the modeling workflow, such as the production profiles, final oil recovery and economic evaluation, will be uncertain as well.

Uncertainties may be present at any stage of a reservoir modeling workflow. They include:

- ***The Static Modeling***: based on the main structural and sedimentary geological features. A lot of data are generally combined to build this static model, starting from surface geology, outcrops, regional studies, core and fluid properties, to well log analysis and seismic acquisition. This means acquiring and combining data from very different scales.
- ***The Scale-up***: To limit the computation time, up-scaling consists in converting a static model fine grid to a coarser one. This can cause very significant uncertainties, especially for highly heterogeneous media.
- ***The Fluid Flow Modeling***: uncertainties concern physical parameters, such as up-scaled Kr-Pc curves, well architecture and productivity, as well as other uncertainties such as the PVT modeling itself or the numerical solver chosen for the simulations.
- ***The Integration of Production data***: which can be efficiently used to better inform the reservoir model, though presenting uncertainties due to acquisition errors or surface reallocation problems. On top of that the history matching process itself presents uncertainties because of the non uniqueness of the solution, or the mathematically ill-posed problem to be solved.
- ***The Production Scheme Development and the Economic Evaluation***: The maximization of the net present value requires making choices regarding the field production scheme based on technical and economic criteria. This may include a decision on the number of production wells, their location and architecture, injection schemes, as well as surface facilities.

The Experimental Design Methodology

Due to the variety of uncertainties occurring all along the modeling workflow, an exhaustive sensitivity analysis is excluded as it would require a too large

number of numerical simulations. Moreover, if the sensitivity analysis is conducted without any support it will be hardly possible to evaluate the coupling effects of various parameters as each parameter will be varied successively. The COUGAR methodology was developed at IFP to perform a comprehensive sensitivity analysis at the lowest cost, both in terms of CPU simulation time and result interpretation.

It consists in using an experimental design technique[4,5] to compute an approximation - or a "proxy" model - of each output of the modeling workflow. The experimental design technique enables one to select, for a given cost, the minimum set of numerical simulations required to accurately calibrate these "proxy" models.

Any output of the modeling workflow (including for instance volumes of fluid in place, production profiles, additional recovery factor or field net present value) can hence be linked to the influential uncertainties through a specific "proxy" model. These models running quasi instantaneously can then be used for further analytical purposes, such as the computation of probabilistic reserves or the optimization of a redevelopment scheme scenario.

Engineers specify any output of the modeling workflow, called response (cumulative oil production, net present value, ...) and some input uncertain parameters X_1, X_2, ..., X_n called factors, that may influence the response (petrophysics, field structural map, well locations, redevelopment scenarios, ...). The COUGAR™ methodology provides tools for identifying the factors that are influential on the response, and for building a proxy model linking the response to the influential factors, such as illustrated below:

$$\begin{aligned}\text{Response} = {} & a_0 + a_1X_1 + a_2X_2 + \ldots + a_nX_n \\ & + a_{12}X_1X_2 + \ldots + a_{n-1,n}X_{n-1}X_n \\ & + a_{11}X_1^2 + a_{22}X_2^2 + \ldots + a_{nn}X_n^2\end{aligned} \quad (1)$$

where a_0, a_1 ,..., a_{nn} are constant coefficients obtained by fitting a set of numerical simulations.

The main advantage of this proxy model is its negligible cost to estimate new values of the response compared to full reservoir simulations. This regression model can then be used to make safe predictions of the process over the uncertain domain, to generate probabilistic distribution of the response using Monte-Carlo sampling technique and to optimize controllable factors (such as development scenario parameters on well location, well horizontal length and orientation,...) to maximize the response.

The standard method described above applies for deterministic uncertainties which are assumed to vary continuously between a minimum and a maximum value. Porosity and permeability mean facies values, PVT data and well locations, are examples of such parameters. The method has to be extended to tackle the following uncertainties:

- ***"Discrete" Uncertainties*** which correspond to a parameter that can take only a finite number of discrete values, such as the depositional scenario, the boolean behaviour of a fault which is conductive or not, or the optimal number of new production infill wells to be implemented. To take these parameters into account, the COUGAR methodology proposes to combine specific discrete experimental designs[6] with decision tree capability.
- ***"Stochastic" Uncertainties*** which do not present a smooth behavior on production responses (for instance a small increment of the parameter value may lead to drastically different results in terms of production profiles) or uncertainty that can take an infinity of equi-probable discrete values (for instance infinity of equi-probable structural maps, fracture maps, geostatistical realizations, history-matched models). To take into account these kind of uncertainties, the COUGAR™ methodology suggests to use the Joint Modeling method[7,8,9] which consists in computing two statistical proxy models:
  - One for the production response as a function of deterministic uncertainty
  - One for the variance of the production response to represent the effect of the stochastic uncertainty.

RISK ASSESSMENT OBJECTIVES

Once the uncertainties relative to a specific field case have been identified, risk assessment may consist of various objectives:

- Assessing the relative impact of each uncertainty on the production and determining the influential ones.
- Quantifying the risk on field production associated with those influential uncertainties.
- Optimizing all "controllable" uncertainties (such as well locations).
- Reducing risk by integrating any dynamic data when available.

These risk assessment objectives can be tackled using the experimental design methodology[10-14] and further detailed below.

Assessing the Uncertainty Impact

For such an objective, a linear model (equation 1 is a first order polynomial function) is generally sufficient. It involves a limited number of reservoir simulations for a large number of uncertain parameters.

The relative contribution of each uncertain parameter on the response is then calculated and illustrated using the so-called Pareto plot. Uncertainties are ranked and a threshold below which uncertainties are reputed negligible is defined.

Quantifying the Risk on Field Value

Having identified the influential uncertain parameters, reservoir engineers would like to know the resulting risk on the reservoir modeling workflow outputs, for instance on incremental oil productions, oil recovery factor or field net present value.

This resulting risk on field value is obtained using a sampling method, such as Monte-Carlo technique, using the fast proxy-model. The final result is a probabilistic distribution and corresponding percentiles of any reservoir modeling workflow outputs are derived from probabilistic input parameters.

APPLICATION TO MATURE FIELDS

Due to their long history, mature fields have a large amount of dynamic data. Reservoir engineers systematically integrate these data to better calibrate the reservoir model and, therefore, to reduce the uncertainty range on each modeling workflow input, hence on field production forecasts. This history match process is, however, recognized as a challenging issue, and in practice it is difficult to derive a reservoir model that perfectly fits all the dynamic data.

Many reservoir simulation models, which properly match the dynamic data, can hence be obtained by using either manual history-matching techniques or assisted history matching with optimization methods. All these reservoir models are equi-probable. The main concern is to select the "right" matched model for performing further production forecasts and further production scheme optimization. To achieve that purpose, the Joint-Modeling method, as stated above, is used assuming that all the matched models are considered as a unique stochastic uncertainty. Using this method, it is then possible to quantify the risk associated with the history-matching process uncertainty itself (which actually can be very high) and/or to optimize the future production scheme while taking into account the dynamic data available. This methodology has been fully validated on a synthetic case[15] as well as on the PBR case[16] as summarized here below.

Risk Assessment on a Mature Field Case - The PBR field

We present here the JM method applied to a real field located offshore Brazil (PBR field)[16]. The objective was to maximize the incremental production of the reservoir through a redevelopment plan while taking into account the uncertainty in history-matching induced by the existence of infinite number of equi-probable matched models. The study employed the following two steps:

- ***History-matching***: The geostatistical and flow models were constrained to the production data. Several equi-probable matches were obtained.
- ***Redevelopment Production Scheme Optimization***: The goal was to quantify the added value of history-matching in terms of uncertainty reduction on production forecast and the optimization of new well location and rates taking into account the remaining uncertainty after matching.

PBR Field Modeling Workflow

The PBR reservoir is developed with 34 oil production wells and 13 water injection wells, such as illustrated in Figure 1. The production started June 1979. During the first five years, the field was produced by primary depletion. Water injection started April 1984 for pressure maintenance.

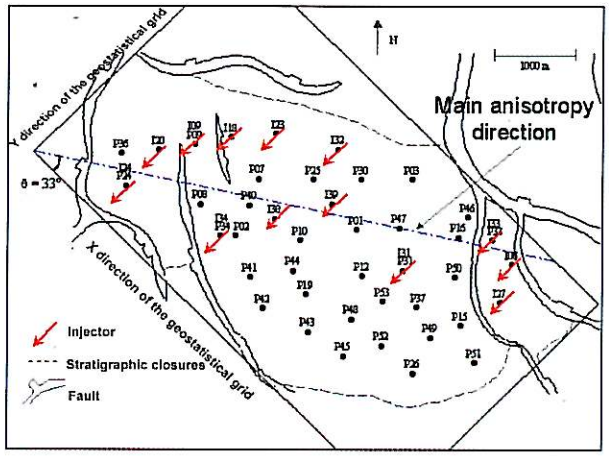


Fig. 1. Well location map of the PBR field.

Four facies were identified in the reservoir: sandstone LT-1 and LT-2 facies have good reservoir properties, whereas LT-3 and LT-4 (actually non-reservoir zones) include clays and marls. The workflow of the PBR reservoir model has been fully integrated in the same simulation process, from the construction of the geostatistical lithofacies model to the fluid flow simulation.

History-matching Process

A main objective was the definition for the entire simulation workflow to measure the mismatch between the observed data (d_i^{obs}) and the simulated data (d_i^{sim}) using the weighted least square

$$OF = \frac{1}{2}\sum_{i=1}^{n} w_i (d_i^{obs} - d_i^{sim})^2$$

formulation: where w_i are the weighting factors.

The production data available for the PBR field were the oil flow rates at surface conditions, the water cuts and the static pressures for all producers.

A preliminary sensitivity study was performed, using the experimental design technique to select the most influential inversion parameters among the deterministic uncertain parameters of the simulation workflow. In addition to these 8 deterministic inversion parameters, the geostatistical realization itself was considered unknown in the inversion process. The spatial distribution of the facies model was parameterized using the Gradual Deformation Method[17,18].

The history-matching process was performed 5 times with different sets of initial deterministic parameters and with different initial geostatistical realizations. The initial sets were chosen within the predefined uncertainty domain. These five matched models led to the same quality of match (same order of magnitude for the resulting objective function), which was considered as satisfactory except in the south-east region where some major geological assumptions may have to be reviewed.

Re-development Scheme Optimisation

The objective was to maximize the reservoir cumulative oil production after an additional period of production of 10 years (COS-10y) by including two new producers. A technical issue concerned the choice of the matched model which was to be used for this optimization process. In fact, the 5 history-matched models were used through a unique stochastic uncertainty on the matching process. The production parameters to optimize were the locations and production rates of the two infill production wells (NW1, NW2). A preliminary sensitivity study has shown that the Y locations of the wells were not significantly influential on the production forecasts. Finally, the JM method was used to model the COS_10y response with respect to the following production parameters: the X locations (X1, X2) and the oil production rates (Q1, Q2) of the two infill production wells (NW1, NW2). Dispersion induced by the history match uncertainty was considered through the variance model.

The joint models obtained were used to optimize the production scheme by maximizing the mean model. This gave the optimal values for X1, X2, Q1 and Q2 parameters and the corresponding mean and variance values of COS_10y response forecast, summarized in Table 1. A 95% prediction interval due to the uncertainty on the history match process was deduced: from 53.68 MMm^3 to 56.97 MMm^3 in terms of final cumulative oil production.

Table 1. Optimisation of the production parameters using the JM method.

	Optimal	Unit
X1	38	cell #
X2	47	cell #
Q1	852	m3/d
Q2	1500	m3/d
Mean COS_10y	55.32	MMm3
Variance	0.71	$(MMm3)^2$
Standard deviation	0.84	MMm3
Min of 95% conf. Interval	53.68	MMm3
Max of 95% conf. Interval	56.97	MMm3

In Figure 2, the cumulative oil production profile intervals since the beginning of field production without history match and after history match are displayed. As expected, the history matching

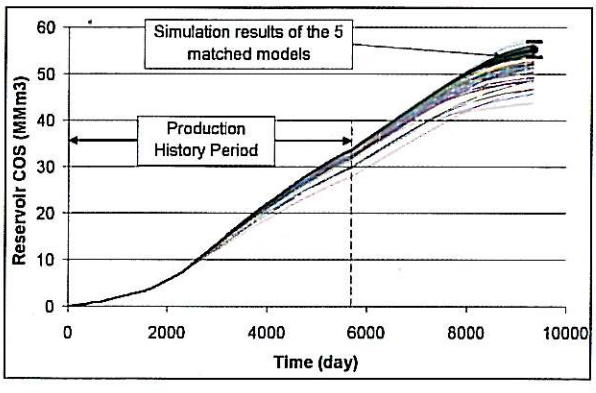


Fig. 2. Uncertainty on the cumulative oil production.

significantly reduces the uncertainty on prediction, by 75%.

However, even when using very high technology history match process such as constraining both the geostatistical realizations and the dynamic parameters as matching parameters, 25% of uncertainty remains acceptable due to the history match process. The Joint Modeling method has enabled a successful quantification of the impact of the history match process on further production forecast, and consequently, redevelopment plan has been optimized taking into account the associated risk.

CONCLUSIONS ON THE COUGAR™ METHODOLOGY

The COUGAR™ methodology was developed within a Joint Industry Project (JIP) named COUGAR, which was launched by IFP in March 2001 for two years and which is currently open to new oil industry partners for a 3-year extension work program. The main objective of this JIP is to develop a prototype software based on statistical approaches, such as experimental design methodology validated through real field case studies provided by the partners. All kind of uncertainties may be simultaneously or separately investigated, from the static model including the main geological assumptions (structural, stratigraphic, ...), the geostatistical parameters (seed, correlation length, variograms, petrophysical properties, ...), the scale-up model assumptions, the fluid flow simulation model parameters (relative permeabilities, fluid properties, well location and productivity, ...), up to the surface facilities scenarios and economic uncertain parameters (oil price, OPEX, CAPEX, ...). Any outputs of the modeling workflow, including, for instance, volume of fluids in place, production profiles per well, field net present value, etc., can be computed as a specific "proxy" model which represents the impact of the main uncertainties on this output. These proxy models can then be used to optimize for instance a redevelopment plan (infill well location and architecture, injection rates, plateau duration,...) while taking into account all the inherent risk in the reservoir.

Using COUGAR™, petroleum engineers will be able to propagate an uncertainty within their own modeling workflow and to compare the uncertainty impact on any output of the field evaluation, whether technical or economic. Decisions at each phase of the field life, from exploration, appraisal, development, to final recovery, can hence be taken while quantifying the risk associated with all the technical and economic uncertainties that may affect this decision.

Ranking of Development Strategies

The advent of new techniques for better evaluating reserves and developing continuously improving field surveillance and monitoring strategies, leads the oil industry to build evermore detailed static and dynamic reservoir models.

As seen in the previous section, the COUGAR™ technology is designed to help in the decision making process in all phases of field life starting from exploration to late IOR development strategies.

To simplify even more the duty of the reservoir engineers and assess a limited number of pre-select development scenarios it can be worth considering additional ingredients such as the combination of "light" calculations and analysis techniques for screening and optimization with computationally intensive full physics simulation.

Figure 3 illustrates this workflow. The rectangular boxes on the top indicate the elements of a conventional reservoir modeling study. The rounded boxes on the bottom represent new tools that would need to be developed in order to assist the engineer to (1) take coherent modeling decisions and (2) pre-select potential redevelopment scenarios which will be analyzed and ranked using our COUGAR™ technology.

This workflow consists of three different themes: Data Analysis, IOR Screening and Drainage Pattern Optimization. These themes are detailed in the next sections.

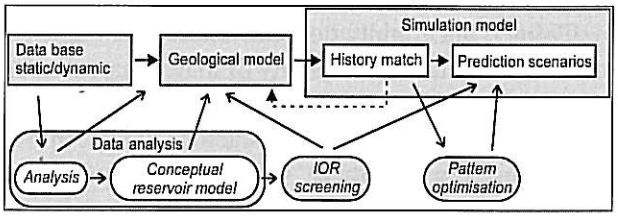


Fig. 3. Work flow combining "light" analysis techniques with detailed geological modelling and full physics simulation.

Data Analysis

Analysis

Besides elaborate static or dynamic reservoir modeling, it is important to obtain the best possible understanding of the reservoir architecture and the

performance of the present recovery processes. This understanding can be obtained from review of previous reservoir studies (with risk of prejudice), as well as from direct analysis of the field data. Analysis of the production history serves to identify potential alternative strategies to target remaining oil, as well as possible inefficiencies in the current recovery strategy (cross flow behind casing, scale formation, gas cusping, thief zones). Analysis of the production history can also help detail the appropriate reservoir modeling approach: point out the key geological features and flow processes that need to be captured in the models.

Analysis of the production history of mature reservoirs generally involves handling of large volumes of data of varying quality. There may be hundreds of wells, a long production history, a large number of workovers, a multitude of SCAL data as well as several subsequent recovery strategies (natural depletion, water injection, gas injection, infill drilling). Construction of a well-organized data base (as complete and accurate as possible) is an essential first step for efficient analysis of the recovery history.

Data analysis can include material balance, statistical analysis routines for production data and assessment of main displacement characteristics (gravity dominated, viscous dominated, thief zones). A key element of the analysis is also the visualization of the data; bubble plots of production, composite plots showing production, static pressure, PLT and RFT data, as well as perforation history. To this end, the reservoir data base should be linked to a flexible user interface allowing composite visualization of all data, as well as the execution of (user defined) analysis scripts and software (material balance). Development of this type of flexible software is currently being contemplated by the IFP.

The Conceptual Reservoir Model

Based on above analysis, a conceptual reservoir model can be elaborated. This conceptual reservoir model is a simplified description of the reservoir which is representative of a volume fraction of the total reservoir.

Depending on the process of interest (for example well inflow performance modeling or sweep efficiency analysis) a conceptual model can be a 2D cross section, a single well in a radial geometry, a symmetry element of a pattern (quarter five spot) or a pattern with a limited number of wells. The conceptual model should contain the key reservoir heterogeneities. Although an exact history match is not required, the model should capture the global dynamic reservoir behavior. The model can have a geostatistical basis, being constructed of rock types with certain correlation lengths. The conceptual model should be simple enough so that it can be changed easily, and the turnaround time should be low (< 1 hour per run) so that many sensitivities can be evaluated in a relatively short timeframe. If required, several conceptual models can be constructed, each of which being representative for a specific part of the total reservoir volume.

In the analysis phase of the study, COUGAR™ type studies as presented in part-1 can be run on the conceptual model to assess, in more detail, the effects of different reservoir characteristics (heterogeneity, vertical permeability, fluid properties, *etc*) on reservoir performance under the current recovery mechanisms. This work provides additional insight into the reservoir performance, helps in defining an appropriate modeling approach, helps to identify an history matching strategy, and can also serve to identify and evaluate IOR strategies.

IOR Screening

Screening for IOR redevelopment scenarios is performed on different levels. A first step consists of the use of basic screening parameters. For example, many chemical processes can not be applied at high reservoir temperature and salinity due to their rapid degradation. In a second step, the additional recovery of the pre-selected processes can be assessed using either analytical models, or by running the pre-selected processes on the conceptual reservoir model. Again, the COUGAR™ approach can be applied to quantify the uncertainties associated with the proposed IOR processes (*e.g.* water shutoff, EOR, productivity/ injectivity enhancement).

IOR screening should take proper account of the facilities aspects, and the present state of the wells and completions. The IOR project should be considered as an integrated project in which geologists, production engineers and reservoir engineers make their contribution.

Field example of Analysis and IOR Screening

A field example of the above IOR screening process is an offshore carbonate reservoir located in the Gulf of Oman. The reservoir is a multi layer formation which has been on commingled injection

and production for about 25 years. Characteristic of the displacement process is the rapid water breakthrough in thief zones. As a result of high water cycling, pressure maintenance has not been fully achieved, and the reservoir is below the bubble point pressure. Analysis of the water flooding data indicated four "types" of remaining oil (Fig. 4): (1) Oil remaining in low permeability layers, (2) bypassed oil in layers with a thief zone, (3) traditional residual oil, and (4) remaining oil associated with areal sweep (due to well pattern and sub-seismic faults).

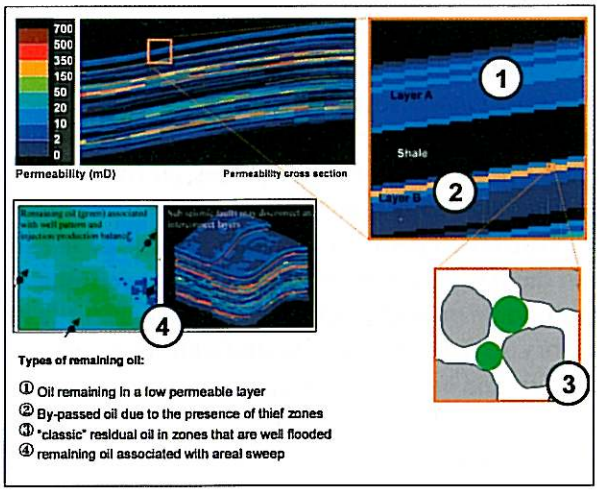


Fig. 4. Drainage pattern optimisation, workflow.

Preliminary screening revealed that specific reservoir conditions (P, T, water chemistry, heterogeneity) make it difficult to apply most conventional EOR processes like chemical floods, miscible or immiscible gas flooding gas flooding.

After reviewing the options, water alternating gas injection (WAG) was identified to potentially target "type" (2) and (3) remaining oil, while intelligent completions were proposed for better distribution of the injection water over the reservoir layers, targeting type (1) remaining oil.

Conceptual reservoir models were constructed in the form of high resolution cross section models to quantify the EOR potential of WAG. Special emphasis was put on the three-phase relative permeability and capillary pressure description. COUGAR™ based sensitivity analysis, focusing on the reservoir heterogeneity and uncertainty in three-phase petrophysical data, indicated a disappointing incremental oil recovery of WAG of the order of 3%. This incremental recovery was insufficient to justify the required surface facilities modifications for WAG injection in this mature offshore field. However, review of existing surface facilities, showed that there was a possibility to apply the existing gas lift system for a SWAG (simultaneous water and gas injection) scheme. Further simulation studies indicated that the expected additional recovery of SWAG was of the same order of magnitude as WAG. Economic analysis of the SWAG process showed that this process, due to its low cost, would be of significant economic value as a breakeven additional recovery of less than 0.3% was required.

Drainage Pattern Optimization

The third theme of the workflow presented at the beginning of this section consists of drainage pattern optimization (Fig. 5). Evaluation and optimization of drainage pattern is a problem that can involve a large number of variables: well positions, well architecture, balance of injectors and producers, intelligent completion technology, stimulation. Optimization of all these options on the full field model would require a two-stage approach starting with a simplified model.

The approach proposed would be to run the development optimization studies on a simplified model, which runs very rapidly. The optimization is not performed on the actual parameter of interest (recovery, Net Present Value), but on a parameter which is equivalent to this parameter of interest. The result of the optimization is validated in the full physics reservoir simulator.

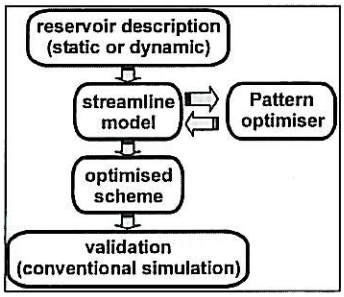


Fig. 5. Drainage pattern optimization, workflow.

For the optimization, a streamline code would be used. These optimization runs are performed in incompressible mode. Therefore, there are no pressure transients (which can present some limits for certain cases), only one pressure calculation is required to obtain the "steady state" plateau rate for a given scenario. This allows very efficient comparison of different competing strategies to maximize production rate, like horizontal well length, reduction of well spacing, stimulation, gas lift, ESP.

For the optimization of the volumetric sweep efficiency, the Time of Flight (TOF) data (weighted

by the mobile oil) and the drainage area data from the simulator are used. The basic idea is illustrated in Figure 6. The TOF approach allows rapid optimization of the well locations to equilibrate the TOF of the mobile oil from its present location to the production well. Note that the optimizations of well type, number of wells (injectors and producers) and well location are performed simultaneously for all the wells in the model.

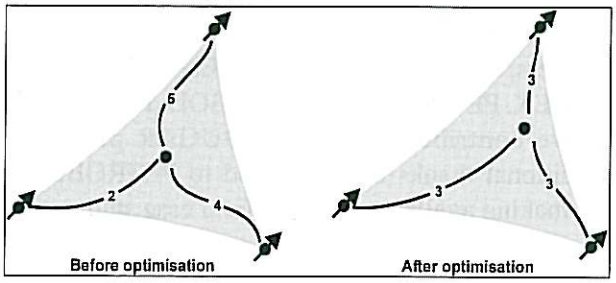


Fig. 6. Illustration of the optimization of well location using Time of Flight (TOF) information.

Field Example, Pattern Optimization Studies

The development studies on a giant field located in Middle East form an illustration of the use of streamline simulation to optimize drain length, drain orientation and well architecture of the horizontal development wells.

This field is divided into three increments (Fig. 7). Increment 2 was recently put on production, and is the subject of this field example.

The increments are characterized by three main features: the matrix, which has a good permeability of up to 200 mD, thin super-K layers, with a typical permeability of 2+ D, and high permeable fracture swarms. Data analysis and simulation studies indicated that fracture swarm is a main cause of early water production.

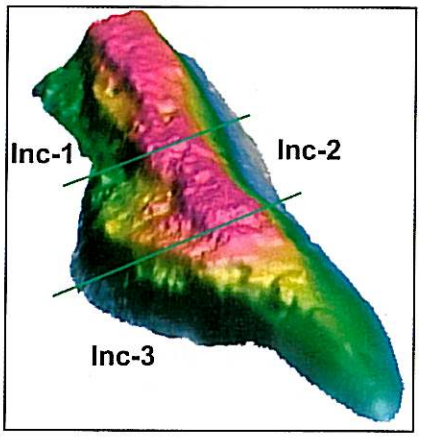


Fig. 7. Structure map.

Figure 8 shows a map of the fracture distribution in increment 2, as well as a contour pressure map generated by high resolution streamline simulation. TOF calculations corresponding to Figure 7 are shown in Figure 9.

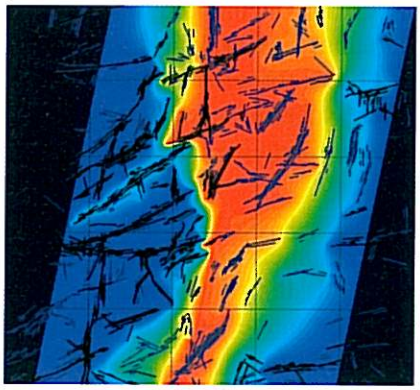


Fig. 8. Drainage pattern optimisation, workflow.

Based on the TOF plot in Figure 9, a Monte Carlo approach was applied to determine the performance of different well types (horizontal wells, multilateral wells), well lengths and well orientations.

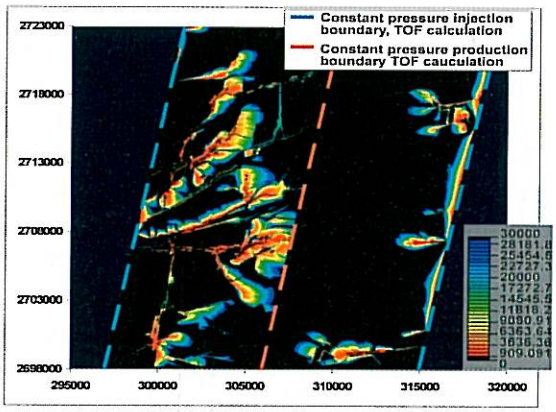


Fig. 9. TOF data for increment 2.

Figure 10 shows results, in terms of achieved PI per invested dollar, for the single drain horizontal wells, as a function of the well length and well orientation. The optimum configuration was subsequently validated in the finite difference simulation model. A statistical survey of existing horizontal wells in the area also confirmed the results of Figure 10.

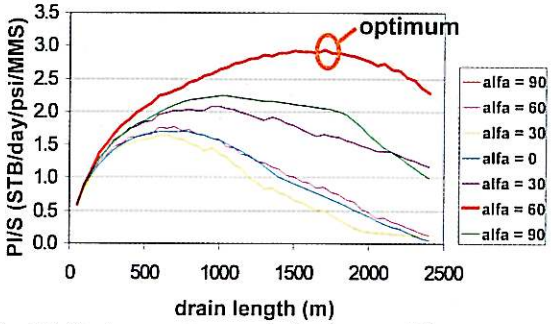


Fig. 10. Drainage pattern optimisation, workflow.

Combining Those Approaches: Towards Integrated Reservoir Studies for Optimal Development Scheme

We have clearly seen in the two previous sections concerning the COUGAR™ methodology developed for quantifying uncertainties and ranking development strategies that a fast but rigorous diagnosis of each possible development scheme has to be properly accounted for, and would require, sometimes, to be studied in a detailed way.

One concern is related to the fact that generally the outcome of a development strategy can still be uncertain. This demands the development of the experimental design technique so as to deal with specific decision tree where scenarios are of probabilistic nature.

This is the goal of the follow-up of the development of the IFP led COUGAR II joint industry funded project. Such an issue is vital to be able to optimize any petroleum production in the future.

CONCLUSIONS

Nowadays, due to the advent of the field surveillance and field monitoring strategies, a large amount of data is acquired and should allow the improvement of the understanding of the reservoirs and, hence, optimize their exploitation. This applies, as first priority, to mature field production which needs to be optimized to face the fast growing world energy demand for the next 30 to 50 years.

Taking advantage of this huge amount of data, and quantifying and reducing the uncertainties they create in the field development process, is a main objective of the comprehensive methodology based on the COUGAR™ technology presented in this paper. This methodology is employed to define a simplified model (the proxy model) which will behave as the true reservoir model but running much more rapidly. This proxy model, which can be coupled to some economic spread sheets can then be used to make production forecasts and optimize the recovery factor as well as the net present value.

In order to perform a preliminary screening analysis which can help to rapidly point out best candidates among possible (re)development strategies, the methodology can comprise specific items including use of simplified simulations.

Those methodologies and tools are already available as illustrated by the field cases presented in this paper and are subject to continued development and improvement at IFP. Those developments are conducted under the form of joint industry-funded projects and should contribute to constitute in the coming years important components of the new toolbox of the reservoir engineers.

ACKNOWLEDGMENT

The authors wish to thank the current COUGAR partners, namely BHP Billiton, ENI-AGIP, GDF, PEMEX, PETROBRAS and REPSOL-YPF for their active contribution to the COUGAR program. Additional thanks are addressed to PETROBRAS for making available the PBR field case study.

REFERENCES

[1] Kalaydjian, F. and Bourbiaux, B., 2002. Integrated reservoir management: a powerful method to add value to companies' assets. a modern view of the EOR techniques. *Oil Gas Sc. Tech. Rev.* IFP, **57**, 3, 251-258.

[2] Zekri, A.Y. and Jerbi, K.K., 2002. Economic evaluation of enhanced oil recovery. *Oil Gas Sc. Tech. Rev.* IFP, **57**, 3, 259-267.

[3] Zabalza-Mezghani, I., Manceau, E., Feraille, M. and Jourdan, A., 2003. Uncertainty management: from geological scenarios to production scheme optimization. submitted to the *J. Petrol. Sc. Eng.* A special edition on *Risk Analysis Applied to Petroleum Exploration and Production.*

[4] Box, G.-E.-P. and Draper, N.-R., 1987. *Empirical Model Building and Response Surfaces.* John Wiley.

[5] Box G.E.P, Wilson K.B., 1951. On the experimental attainment of optimum conditions. *J. R. Stat. Soc.* B13.

[6] Jourdan, A., Zabalza-Mezghani, I., 2003. Experimental design method for scenario management and uncertainty quantification in production. *Mathem. Geol.*

[7] Zabalza-Mezghani, I., 2000 (May). *Analyse Statistique et Planification d'expérience en Ingénierie de Reservoir.* IFP Thesis.

[8] Zabalza-Mezghani, I., Manceau, E., Roggero, F., 2001. A new approach for quantifying the impact of geostatistical uncertainty on production forecasts: the joint modelling method. Paper presented at the 2001 IAMG, Cancun.

[9] Zabalza , I., Mezghani, M., Blanc, G., 2001 (September). Constraining reservoir facies models to dynamic data - impact of spatial distribution uncertainty on production forecasts. Paper *SPE*

71335 presented at the 2001 SPE Annual Technical Conference & Exhibition, New Orleans.

[10] Corre, B., Thore, P., de Feraudy, V., Vincent, G., 2000 (October). Integrated uncertainty assessment for project evaluation and risk analysis. Paper *SPE* 65205 presented at the 2000 SPE European Petroleum Conference, Paris.

[11] Damsleth E., Hage A. And Volden R., 1991 (September). Maximum information at minimum cost: a North Sea field development study using experimental design. Paper *SPE* 23193 presented at the Offshore Europe Conference, Aberdeen.

[12] Dejean, J.P. and Blanc, G., 1999 (October). Managing uncertainties on production predictions using integrated statistical methods. *SPE* 56696, SPE Annual Technical Conference and Exhibition, Houston, USA.

[13] Manceau, E., Zabalza-Mezghani, I., and Roggero, F., 2001 (June). Use of experimental design to make decisions in an uncertain reservoir environment - from reservoir uncertainties to economic risk analysis. OAPEC seminar, Rueil-Malmaison, France.

[14] Zabalza, I., Dejean, J.P., Collombier, D., Blanc, G., 1998 (September). Prediction and density estimation of a horizontal well productivity index using generalized linear models. Paper B31 presented at the 1998 ECMOR VI, Peebles.

[15] Manceau, E., Mezghani, M., Zabalza-Mezghani, I. and Roggero, F., 2001 (September). Combination of experimental design and joint modeling methods for quantifying the risk associated with deterministic and stochastic uncertainties - an integrated test study. Paper *SPE* 71620 presented at the 2001 SPE Annual Technical Conference & Exhibition, New Orleans.

[16] Feraille, M., Manceau, E., Zabalza-Mezghani I., Roggero F.; Hu LY and Reis Leandro, 2003. Integration of dynamic data in a mature oil field reservoir model to reduce the uncertainty on production forecasting. AAPG, Salta Lake City.

[17] Hu, L.Y., 2000. Gradual deformation and iterative calibration of gaussian-related stochastic models. Math. Geology, **32**, 1.

[18] Hu, L.Y., 2003 (June). History matching of object-based stochastic reservoir models. *SPE* paper 81503, presented at the 13th Middle East Oil & Gas Show and Conference, Bahrain.

Petroleum Res. J. Vol. 18 (2005); P. 149–158, 13 Figs.

Consequences of Asphaltene Adsorption on Flow Phenomena in Porous Media

B. Rayes*, I. Lakatos** and J. Toth**

النتائج المترتبة من امتزاز الاسفلتين على ظاهرة الانسياب في الوسط الصخري

بشار الرايس، آي. لاكاتوس وج. توث

يمكن لأغلب معادن المكمن المبتلة بالماء أن تتغير بامتزاز المركبات القطبية أو نتيجة لترسبات عوامل عضوية أو أشياء أخرى موجودة أصلا بالنفط الخام.

ومن بين هذه العوامل العضوية النشطة من تألف الماء أو تطرده. وتمتز النهايات التي تألف الماء على السطح تاركة النهايات الطاردة للماء مكونة السلوك المبتل بالزيت.

وحيث أن قابلية الابتلال تعرف على أنها قابلية الأسطح للبلل بواسطة أحد الموائع المكونة للسوائل المكمنية، وعلى هذا الأساس تؤخذ قابلية الابتلال للصخور على أنها من أهم العوامل التي تساهم في تغيير الخواص البتروفيزيائية لصخور المكمن، حيث أنها تؤثر على سبيل المثال، على الضغط الناتج من الخاصية الشعرية ونسبة نفاذية الماء النسبية على نفاذية الزيت النسبية وتوزيع الموائع في الوسط الصخري وخواص النفاذية النسبية، ويترتب على هذا المستهدف من الإنتاج النفطي بطرق تطوير المسترد النفطي.

تهدف هذه الدراسة إلى وصف قابلية الابتلال لصخور حقل الشرارة وتطوير مركب كيميائي مبتكر لحماية وصيانة المكامن. تمت اختبارات تشبع ديناميكية بواسطة عمود زجاجي مجوف استخدم فيه صخر مفتت مأخوذ من حقل القوي المجري وذلك لاستقصاء عملية امتزاز الأسفلتين الذي تم فصلة من زيت ليبي خفيف جدا، وزيتان خفيف ومتوسط من حقل مجري. كما تمت دراسة تأثر قابلية امتزاز الصخر للاسفلتين. أظهرت النتائج الأولية عدم وجود اختلاف ملحوظ في امتزاز الاسفلتينيات التي تم استخدامها، كما تم الحصول على علاقة خطية واضحة تربط بين التركيب المعدني للصخور وفاقد الامتزاز النوعي عندما تمت معالجة الصخر بواسطة الكلسايت (كربونات الكلسيوم البلورية) والطين.

استقرارية الطبقة الرقيقة المجهرية للماء المنتشر في مسام السطح الصخري كانت من النتائج المتحصل عليها التي أظهرت علاقة خطية تشرح تأثير نسبة إشباع الصخر بالماء المتخلف مع امتزاز الاسفلتين.

تأثر امتزاز الأسفلتين على قابلية الابتلال الصخري أظهر نظام طارد للماء فعال على العينات التي تم استخدامها.

نتائج البرنامج البحثي تقترح أن المحاليل الاسفلتية وقطفات المنتجات الثقيلة وأيضا الزيت الخام التي تحتوي على نسبة عالية من الاسفلتين يمكن أن تستخدم كوسط معالج لطرد الماء في الوسط المسامي.

Abstract: *The original water wetting of most reservoir minerals can be altered by adsorption of polar compounds or deposition of organic agents or matter originally present in the crude oil. These organic active agents include both a polar (hydrophillic) and non-polar (hydrophobic) ends. The hydrophillic ends are adsorbed on the surface, exposing the hydrophobic ends leading to oil-wet behavior.*

Since wettability is defined as the tendency of surfaces to preferentially wet by one fluid

*Petroleum Research Centre, Libya.

** Research Institute of Applied Chemistry, University of Miskolc, Hungary.

phase; Altering the wettability is, therefore, considered to be a key factor in shifting the petrophysical properties of the reservoir rock (e.g. Pc, and krw/kro), the distribution of fluids within the porous medium, relative permeability characteristics, and consequently, the target of oil production by any improved oil recovery (IOR) process.

Primary aims of the present investigations were the wettability characterization of the Sharara field and development of an innovative chemical for protection and maintenance of reservoirs.

Column saturation dynamic tests were performed to investigate the adsorption of asphaltenes separated from light Libyan oil, medium and heavy Hungarian oils onto a crushed formation rock obtained from Algyö field. The effect of asphaltenes adsorption on wettability was also studied. Initial results revealed that there is no significant difference in the adsorption of different asphaltenes. A well-defined correlation was found between the mineral composition of the adsorbent and the specific adsorption loss when the rock was treated with a particular percentage of calcite and clay. Stability of microscopically thin layers of water distributed along the surfaces of the pores was also investigated. A correlation showing the effect of residual water saturation on asphaltene adsorption processes was presented.

The effect of asphaltene adsorption on wettability has shown an effective hydrophobization on all rock samples. The final conclusion of the research program suggests that a solution of asphaltenes, distillation heavy cuts and even crude oils with high asphaltene contents can, equally be used as a treating media for hydrophobization of porous media.

INTRODUCTION

Understanding the role of asphaltene in wettability reversal will help in planning more efficient oil recovery processes. In this context, this work has two objectives:

- The wettability characterization of the Sharara field (located in Libya)
- Development of an innovative chemical for protection and improvement of the recovery at the field scale.

The wettability characterization of the Sharara field was performed using water contact angle measurements as a function of time on carbonate rock having homogenous and heterogeneous surface. The reservoir wettability characteristics are often attributed to adsorption of asphaltenes onto the mineral surface of reservoir rock[1]. Therefore, the effect of asphaltene adsorption on wettability was evaluated by treating the rock plates with asphaltenes-toluene solution, stock tank

oil-toluene solution and just stock tank oil. For comparable conditions, three asphaltenes were precipitated from three different oils: light (Sharara), Medium (Algyö) and heavy (Nagylegyel).

Dynamic tests served for determination of specific adsorption of asphaltenes from the three types of oils were conducted. Reservoir rocks and natural adsorbents having different mineral compositions were used to compare the adsorbed amount under a fixed flow conditions.

An asphaltene adsorption study was started on asphaltene/rock system. This system consists of adsorbent as a toluene suspension packed in a glass column and a fixed stock asphaltene solution of 0.5g/l concentration was flowed continuously onto adsorbent.

All cumulative curves showed a definite maximum. The value of the maximum and the corresponding injected volume depend on both the asphaltene and the adsorbent type. Asphaltene/rock/water system was then investigated. Water is added in this system to account for the effect of residual water saturation on asphaltene adsorption processes.

The flow measurements were focused on the effect of asphaltene adsorption on absolute, effective, relative and normalized relative permeability of natural formation cores in gas/water system. Similarly, the impact of asphaltene treatment on capillary pressure curves and J functions were determined by centrifugal method using the same formation (sandstone) cores.

Literature Survey

Even though the main cause of asphaltene deposition has not been well understood yet, and this topic is far from being concluded[3], many research papers agreed on the fact that the efficiency of recovery processes was affected by the amount of asphaltene adsorption onto rock surface and asphaltene deposition onto the production facilities.

Many factors like: the change in flow conditions,

temperature, pressure, composition of crude oil, brine chemistry, viscosity, capillary pressure, characteristics of reservoir rock and, the wetting degree of the rock, etc. were considered important in wettability alteration due to the presence of crude oils, consequently, the asphaltene adsorption on the rock surface. For instance, it had been proved that one of the main problems in miscible flooding processes was the asphaltene precipitation accrued due to the change of flow behaviour, phase equilibrium and rock characteristics during the injection of miscible gas. It is well known that a rich variety of wetting behaviours can be induced in rocks by treatment with crude oils. As with reservoir wettability, these changes are commonly ascribed to adsorption of asphaltenes[4]. It has also been confirmed that the physical adsorption of polar compounds/organic materials that were initially present in the reservoir crude oils has a great effect on shifting the wet conditions from a water-wet to oil-wet and vice versa. In this direction, Morrow *et al.*[5] screened several polar compounds present in the crude oil that may be responsible for the change in wettability. Ali *et al.*[6] studied the effect of asphaltene precipitation on carbonate rock permeability. That had been done when the effluent asphaltene concentration was compared to that at the inlet, asphaltene deposition was noted in the pore channels. They thought that two distinct mechanisms were identified, deposition and adsorption. Deposition could be explained in terms of trapping and mechanical plugging. They concluded also that most of the asphaltene deposition is likely to take place near the well bore.

The deposition was found to be a function of permeability, flow rate and concentration. On the other hand, experimental results showed that asphaltene deposition has an impact on reservoir permeability and end-point saturations. That was concluded by Kamath *et al.*[7] when a series of dynamic displacement tests were conducted to evaluate the effect of asphaltene deposition on water flooding in both consolidated and unconsolidated sand pack.

Glampietro *et al.*[8] accomplished a series of adsorption tests to determine the isotherms of asphaltene on sandstone rock. They noted that the asphaltene adsorption is a continuous phenomenon and does not reach saturation similar to conventional surface-active materials. Collins *et al.*[9], used in their work, an asphaltene sample recovered from a deposit on the tubing string of a producing well in Alberta, Canada, light oil reservoir to study the adsorption of asphaltenes and water on reservoir rock minerals. One of their conclusions was that adsorption of asphaltenes was reduced but not eliminated by the presence of water.

Dubey and Waxman[10] studied the asphaltene adsorption and desorption on clay minerals, silica and carbonates. The effect of adsorbed asphaltenes on water-wet sandstone rock resulted in a partially water-wet or neutral water-wet system. That was illustrated by the United States Bureau of Mines Method (USBM) wettability indices and oil saturation vs. capillary number curves.

The asphaltene fractions of oil generally consist of condensed aromatic and naphthenic molecules with molecular weight in the range of several hundred to several thousand grams per mole. "Heteroatoms in asphaltene such as nitrogen, sulfur and oxygen indicate the presence of polar groups. Such a molecular structure has properties similar to that of surfactant"[11]. Surfactant injections are considered to be one of the effective IOR methods.

Kim *et al.*[11] concluded that the role of asphaltenes seems to be substantial in altering the interfacial properties of water and oil systems. They also added that the instability of interfacial tension (IFT) is due to asphaltene characteristic of asphaltene particles.

Yu Liu and Buckley[12] conducted an experimental work in which they stated that adsorption of crude oil components on prewetted surface was strongly time dependent and followed a two stage pattern: initial fast adsorption followed by low rearrangement of adsorbate. They also concluded that desorption of crude oil components depends on both brine composition and temperature.

Buckley *et al.*[13] summarised that the extent to which wetting is altered in crude oil/brine/rock (COBR) systems by adsorption of crude oil asphaltic material, was affected by changes in oil solvent properties, even in a mixture in which the asphaltenes are stable with respect to precipitation.

Wettability of reservoir rock can cover a broad spectrum of wetting conditions that range from very strong water-wet (VSWW) to very strong oil-wet (VSOW). Within this range, complex mixed wettability conditions, given by combination of preferentially water wet and oil wet surface, have been identified. Consequently, wettability is considered to be a significant issue in multiphase flow problems ranging from oil migration from source rocks to enhanced oil recovery processes as alkaline flooding or alternate injection of CO_2 and water[2].

Laboratory displacement tests were used to evaluate the effect of wettability on oil recovery. Wettability of COBR systems is usually determined by the Amott test or the USBM methods. Results for (VSWW) conditions are commonly used as a reference state. Reported changes in recovery as systems become less water-wet range from being much lower to being much higher than those given by the originally VSWW conditions. Accordingly, the goal of wettability studies was to provide consistent explanation of these apparent inconsistencies and to identify most favourable conditions for oil recovery.

Chang *et al.*[14] studied the impact of wettability and core heterogeneities on relative permeability. Their numerical simulation runs on separately characterized lithologies to describe the flow mechanism in mixed-wet porous media showed that an increase in oil wettability increases the water relative permeability and decreases the oil relative permeability. They also concluded that a decrease of initial water saturation, produced an increase in relative permeability hysteresis. Baldwin[15] stated that the magnitude of the fluid surface interaction, as measured by wettability affects the movement of ultimate production of oil. He found that relative permeability vary with the surface permeability, and confirmed that relative oil permeability decreases as the strength of oil interactions with the rock surface (oil wettability) increased.

It is worth mentioning that relative permeability is not only a single function of fluid saturation and wettability of rock surface, but it is dependant on saturation history as well. The saturation history hysteresis is an outcome of the redistribution of two or more immiscible phase saturation during drainage and imbibition processes. That was confirmed by Jun-Zhi and Lile[16] in their study of the influence of wettability and saturation sequence on relative permeability hysteresis in unconsolidated porous media.

Desbrandes and Bassiouni[17] have conducted an experimental study to investigate the effect of wettability on formation pressure profile recorded at the oil water contact with residual oil present in the water zone. They observed that in a water-wet sand pack, the pressure gradient changes quickly from oil to water gradient at the movable oil level. This change was located above the free water level. However, in the oil-wet sand pack, the gradient also changes quickly at the movable water level, and this change was located below the free water level. Using the J-function concept, they related the contact angle to the water rise in the water-wet model or the oil fall in the oil-wet model. Dixit *et al.*[18] have developed a three dimensional (3D) network model to derive the capillary pressure curves from a non uniform, mixed and fractionally wet systems. Results indicated that oil recovery via water imbibition in weakly water-wet cores can often exceed that obtained from strongly water-wet samples. McDougall and Sorbie[19] used network modelling to examine the sensitivities of a given process to a variety of phenomena. They investigated the very important role played by wettability at the pore scale in both fractionally and mixed wet media in order to explain how wettability influences the resulting capillary pressure, relative permeability and water flood recovery efficiency. They found out that the simulated capillary pressure data have demonstrated that standard wettability tests (*e.g.*, Amott-Harvey and free imbibition) may give misleading results when the sample is fractionally wet in nature.

Basu and Sharma[20] used the Atomic Force Microscopic to record the force required to rupture thin brine films on quartz surfaces in order to follow the change in wetting properties of the reservoir rock. They concluded that the film breaks when the magnitude of capillary pressure exceeds the repulsive surface force in the thin film. These thin film forces are related in a complicated way to the brine chemistry, oil composition and surface morphology. They added that low values of critical capillary pressure imply that large section of reservoir rocks may be rendered mixed-wet as the brine film are unstable. On the other hand, high critical pressure values imply water-wet reservoir.

ADSORPTION STUDIES

In a recent paper[3], a detailed comparative study of asphaltenes adsorption on reservoir rocks was reported. The laboratory measurements were extended to different n-pentane asphaltenes precipitated from Hungarian and Libyan crude oils (Table 1). A crushed reservoir rock (Algyõ field, Hungary) in its original form and enriched then by

Table 1. Asphaltene content and viscosity of the tested crude oils.

Oil	Asphaltene content, %	Viscosity, mPa s (30 °C)
NL-119 (Hungarian)	19.04	380.00
Alg-541 (Hungarian)	2.21	4.27
A27 (Libyan)	0.56	3.14

montmorillonite and calcite were used as basic adsorbents. The adsorption tests were performed under static (batch type) and dynamic (column elution) conditions.

The amount of asphaltene adsorbed by the formation rock was calculated by the following equation:

$$\Gamma = (C_i - C_e)\frac{V}{W}$$

Where:

Γ = the adsorption (mg/g of adsorbent).
C_i = the initial concentration (mg/l).
C_e = the effluent concentration (mg/l).
V = volume of solution (ml).
W = weight of adsorbent (g of dry core).

In the static tests, the dependence of the adsorption loss on concentration was described by the Tóth's isotherm:

$$n^s = \frac{n^s_\infty \cdot c_e}{\left[1/k + c_e^t\right]^{1/t}}$$

$$n^s = n^s_\infty \text{ if } 1/k << c_e^t$$

Where:

n^s = Calculated adsorbed amount mg/g.
C_e = Concentration of asphaltene mg/cm^3.
t = Interaction parameter.
K = Constant.

It was concluded that there was no significant differences in the adsorption of n-pentane asphaltenes, but a well-defined correlation was found between the mineral composition of the adsorbent and the specific adsorption (retention) loss (Figs. 1 and 2).

The outermost layer of molecules dominates the wetting properties of a solid. The water thin film formed on the solid surface as result of spreading the water was investigated experimentally (column elution as well) to determine its effect on asphaltene

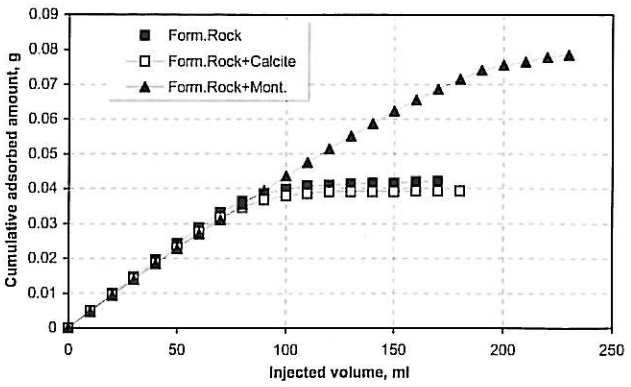


Fig. 1. Dynamic adsorption of A-27 asphaltene solution.

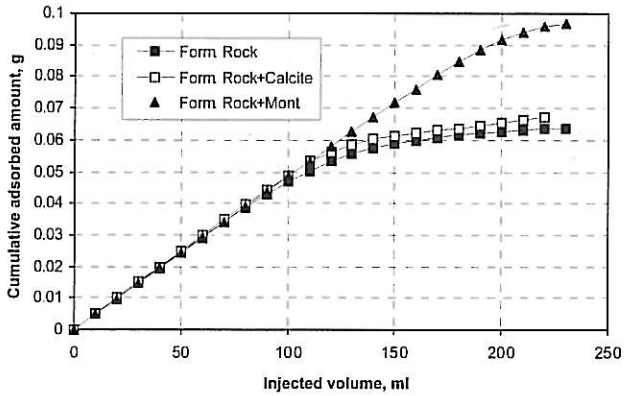


Fig. 2. Dynamic adsorption of NI-119 asphaltene solution.

adsorption. That was done when different volumes (0.1-1.0 ml.) of distillate water were added into the dry formation rock. The VIS spectrophotometry reading showed that there were no asphaltene adsorbed when the sand pack was fully saturated with water. The relation between the volumes of water utilized to saturate the adsorbent and the specific adsorption (retention) loss produced another well-defined correlation (Fig. 3).

WETTABILITY STUDIES

The wettability of a smooth carbonate rock having homogeneous and heterogeneous surface were used as a model material for evaluation of the asphaltene treatments. First, the contact angle of water on carefully cleaned rock plates was determined as a function of time. After this step, the same plates were immersed into asphaltene toluene solution for 24 hrs. The treated rock plates were then rinsed with solvent and dried at 80° C in vacuum oven. In a parallel test, the treatment was carried out with a solution that contained not asphaltene, but the original oil in the same concentration. In another test, the treatment was carried out with the original oil only. Equilibrium

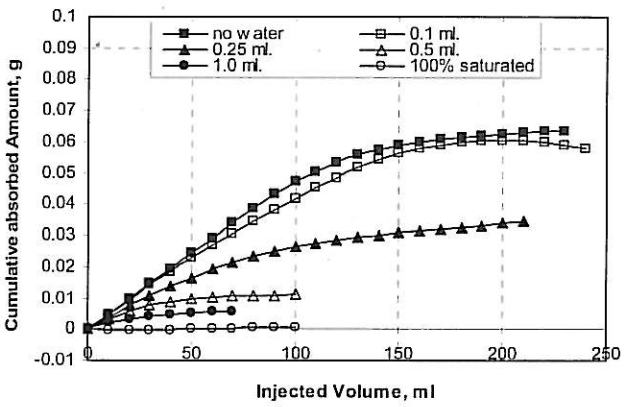


Fig. 3. Effect of water added on asphaltene adsorption.

contact angle was set after 10 min. in all the cases. Results of the wettability tests are shown in (Table 2). in which the contact angles measured on untreated

Table 2. Effect of asphaltene on wettability (contact angle).

Treatment	Homogenous	Heterogeneous
No-treatment	85	54
NL-119 asphaltene in toluene	124	115
A-27 asphaltene in toluene	121	120
NL-119 oil in toluene	120	110
A-27 oil in toluene	77	54
A-27 oil	107	113

surface serve as a basis of comparison. The presented results confirmed that the contact angle on homogeneous surfaces was always higher than those measured on heterogeneous surfaces, except in the case of treating with just original A-27 oil, the contact angles were almost equal. The results showed also that the asphaltenes from heavy and light oils were equally effective in wettability alteration. When the oil solution was used as a treating agent, only the heavy oil proved to be effective. The Libyan oil was also effective when it has been used alone as a treating agent.

EFFECT OF ASPHALTENE ADSORPTION ON FLOW PROPERTIES

Asphaltene Solution and Reservoir Rock

Standard procedure was used to precipitate the asphaltene by n-pentane. First, the light cut of the oils was removed by atmospheric distillation up to 210°C. The solvent-residue ratio was 10:1, namely 15 ml of the light cut-free oil was mixed with 150 ml solvent. After 24 hours, the mixture was filtered; the solid asphaltene washed carefully and dried in vacuum at 70°C. Diluted asphaltene solutions were used. First, a stock solution with 0.5 g/l concentration was prepared using toluene as a solvent. All tests were performed with this stock solution. The analytical (calibration) curve was practically linear in the mentioned concentration range. The RSD of the measurements was better than ±5 %. The formation rock sample was obtained from the Algyõ field (S-Hungary). The data of the mineralogical composition of the rock determined by X-ray diffraction were listed in recent paper[21]. Prior to flow studies, the cores were characterized by He and Hg porosimetry. The geometry and porosity of these cores before and after treatment with asphaltene solution are summarized in Tables 3 and 4. It can be seen that the effect of asphaltene treatment on porosity is negligible.

Table 3. Geometry, pore volume and porosity of formation cores.

Symbol	Length, cm	Cross-section, cm^2	Vp, cm^3	Φ_{He-b}, -	Φ_{w-b}, -
SB-1	6.961	4.691	6.422	0.2154	0.1956
SB-2	7.092	4.711	6.669	0.2147	0.1996
SB-3	7.137	4.707	7.286	0.2169	0.2046
SB-4	7.112	4.714	7.517	0.2242	0.2075

Table 4. Effect of asphaltene treatment on porosity of cores.

Symbol	Φ_{He-a}, -	Φ_{w-a}, -	Φ_{He-b}/Φ_{He-a}, -	Φ_{w-b}/Φ_{w-a}, -
SB-1	0.2212	0.1830	0.9738	1.0686
SB-2	0.2181	0.1909	0.9844	1.0454
SB-3	0.2201	0.1704	0.9855	1.0454
SB-4	0.2292	0.1777	0.9782	1.0454

Permeability Measurements and Water Saturation

The absolute, effective, relative and normalized relative permeability of cores were determined with the aim at characterizing the flow properties of water and gas in the original and the asphaltene treated cores. In the literature, numerous methods have been proposed for the determination of the relative permeability curves. The so-called "displacement" type procedure developed by Tóth *et al.*[22,23] was applied in this study. Four relatively similar cores were selected for this study. Absolute and effective permeability before treatment are listed in Table 5.

Table 5. Absolute and effective permeability of cores before asphaltene treatment.

Symbol	k_{a-b}, mD	b_b^*, -	k_{w-b}, mD
SB-1	37.36	0.2837	n.d.
SB-2	44.97	0.0731	25.34
SB-3	33.82	0.4312	19.08
SB-4	45.30	0.2128	25.12

b_b^* = Klinkenberg constant before treatment

The absolute permeability of cores was determined by nitrogen using the Klinkenberg's technique. The protocol and sequence of relative permeability measurements in gas/water system was described in detail in a previous paper[3]. Results of the permeability measurements are summarized in Table 6 and (Figs 4-7). The normalized curves are also presented in these figures. It can be seen that the absolute gas permeability of cores decreased after asphaltene treatments. Parallel with this change, the

Table 6. Absolute and effective permeability of cores after asphaltene treatment.

Symbol	k_{a-a}, mD	b_a^*, -	k_{w-a}, mD
SB-1	27.56	0.9591	23.28
SB-2	38.33	0.6493	29.66
SB-3	30.10	0.8452	16.01
SB-4	39.51	0.5677	36.64

b_a^* = Klinkenberg constant after treatment

Klinkenberg constant multiplied and became more uniform among the treated cores. On the basis of these experimental findings, it may be concluded that the smallest pores and capillaries were really blocked, and as a result, the tortuosity and the free flow cross-section decreased after asphaltene treatment. With regards to the effective water permeability, the impact of the asphaltene treatment was controversial and the number of experiments is not enough to draw statistically correct conclusion and unfortunately the

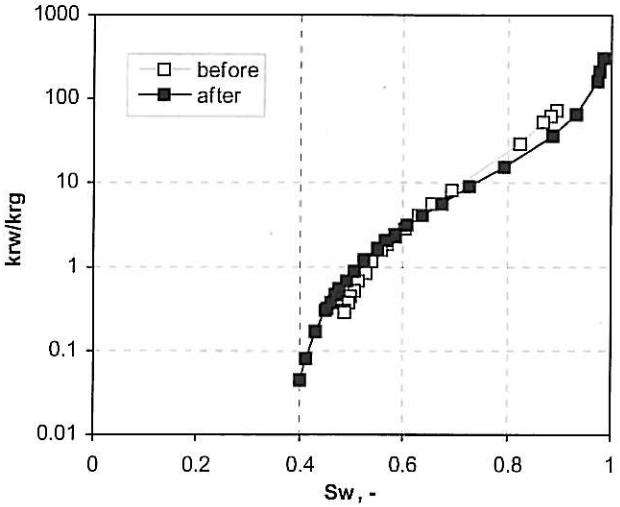


Fig. 4. Effect of asphaltene treatment on relative relative permeability (SB-1 core, drainage direction).

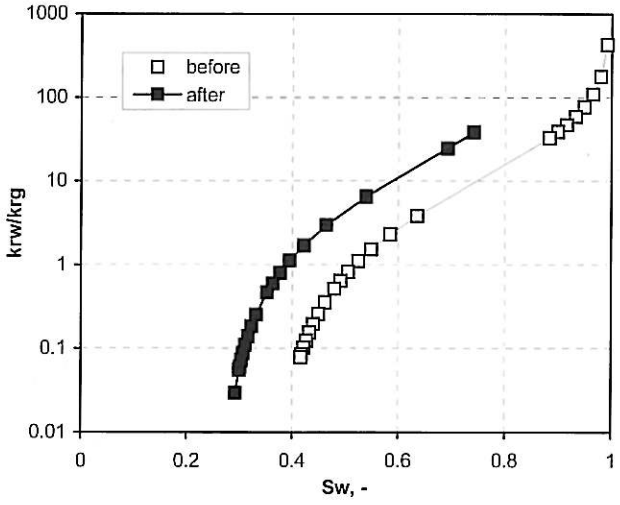


Fig. 5. Effect of asphaltene treatment on relative permeability (SB-2) core, drainage direction).

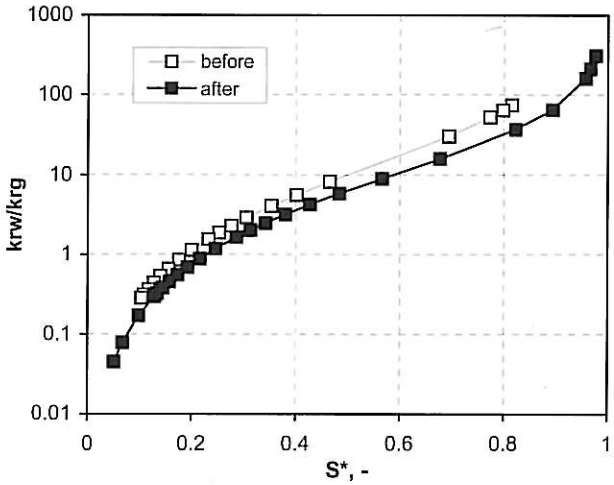


Fig. 6. Effect of asphaltene treatment on normalized relative permeability (SB-1 core, drainage direction).

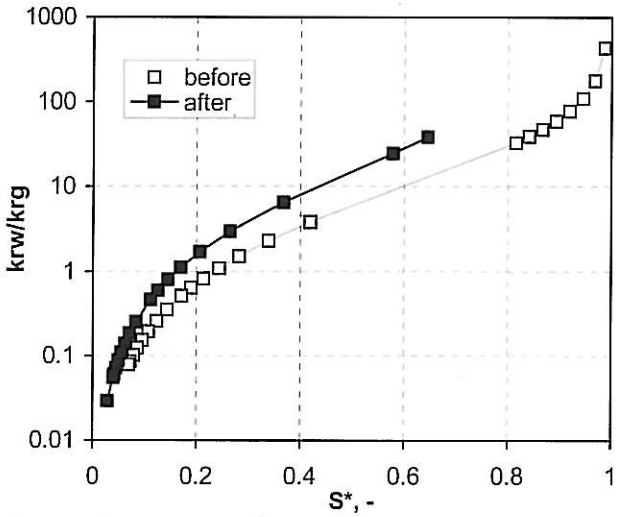


Fig. 7. Effect of asphaltene treatment on normalized relative permeability (SB-2 core, drainage direction).

data for core SB-1 was missing. Evaluation of water saturation data obtained before and after asphaltene treatments clearly indicated a hydrophobization effect in all cores (Table 7). In general, the residual saturation measured after gas injection decreased by 4-6 %, except in the case of core SB-4, the change is roughly 50 %. On the other hand, the residual gas saturation or maximal water saturation at the end of water injection increased a little. Thus, the asphaltene treatment may have both positive and negative effect

Table 7. Effect of asphaltene treatment on water saturation of cores.

Symbol	Before treatment		After treatment	
	S_{wmin-b}, -	S_{wmax-b}, -	S_{wmin-a}, -	S_{wmax-a}, -
SB-1	0.4252	0.9730	0.3676	0.9710
SB-2	0.3723	0.9830	0.3357	0.9857
SB-3	0.2121	0.9128	0.1797	0.9383
SB-4	0.2012	0.8973	0.1038	0.9134

on relative gas permeability depending on the core structure and fluid saturation. That can be seen in the relative permeability curves shown in Figures 4 and 5. The normalized relative permeability curves shown in (Figs. 6 and 7) proved a similar behavior as the original ones did. It has been noted that the curves were not coinciding, that is to say, that the actual flow path of gas and water in cores are different in the original and the treated cores. Once again, the reasons must be searched in the hydrophobization and its consequences in porosity, tortuosity, capillary forces, *etc.*

Capillary Pressure Measurements

Experimentally, both the diaphragm and the centrifugal methods were routinely used. Two of the serial measurements will be presented here which well demonstrate the effect of asphaltene treatment on capillary pressure curves. Basically, two methods are used for fitting of laboratory data to reservoir conditions. The so-called J-function uses the physical properties of rock and fluid as a correcting term and is expressed as:

$$J(S_w) = \frac{P_c}{\sigma}\left(\frac{k}{\Phi}\right)^{1/2}$$

Another proposed formula in literature is:

$$J(S_w) = \frac{P_c}{\sigma \cos\Theta}\left(\frac{k}{\Phi}\right)^{1/2}$$

$$W = \frac{J(S_w)_a}{J(S_w)_b}$$

Where:

σ = Interfacial tension (dyane/cm).

Pc = Capillary pressure (dyne/cm^2).

K = Permeability (cm^2).

Φ = porosity (%).

Θ = Contact angle (æ%).

Supposing that the hydrophobization slightly affects k, Φ and σ, the W value gives an indirect information for wettability alteration at constant P_c. Therefore, the second procedure was used in this research program. The primary obtained capillary pressure curves and the normalized J-functions as a function of water saturation are shown in Figures 8 to 11. Meanwhile the data for water saturation and threshold pressure are listed in Table 8.

Results reflected that both the normal and the normalized J-function curves run below the original ones after asphaltene treatment (Figs. 10-11). At low water saturation, the curves may intersect each other, however, they practically approach the same limiting residual values. Effective hydrophobization could not be predicted by the residual water saturation (Table 8) and this fact apparently contradicts to the conclusions, which might be drawn by the modification of capillary and threshold pressure data. The phenomena are explained by the small size and end effect of cores and the native properties of the centrifugal technique. After asphaltene treatment, the threshold pressure considerably decreased. These experimental results definitely indicate a strong

Table 8. Effect of asphaltene treatment on residual water saturation and threshold-pressure (P_c data).

Symbol	Before treatment		After treatment	
	S_{wmin-b}, -	P_{t-b}, bar	S_{wmin-a}, -	P_{t-a}, bar
SB-6	0.2352	0.1402	0.2491	0.1304
SB-6 (normalized)	-	0.0885	-	0.0673
SB-10	0.2395	0.1168	0.2414	0.0985
SB-10	-	0.1077	-	0.0763

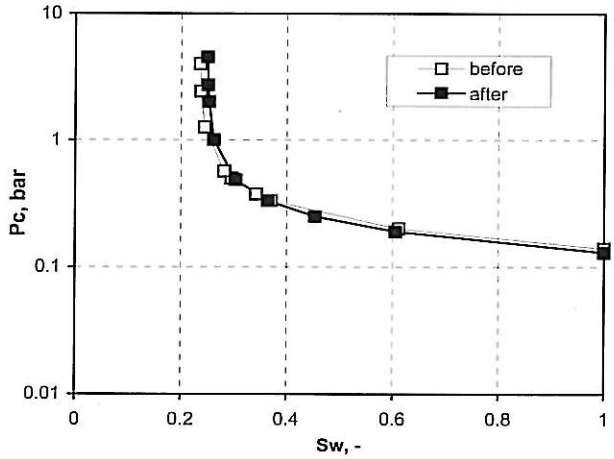


Fig. 8. Effect of asphaltene treatment on capillary pressure curve (SB-6 core, centrifugal technique).

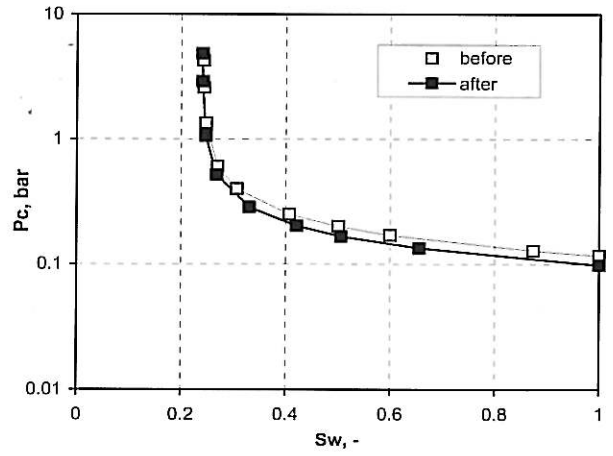


Fig. 9. Effect of asphaltene treatment on capillary pressure curve (SB-10 core, centrifugal technique).

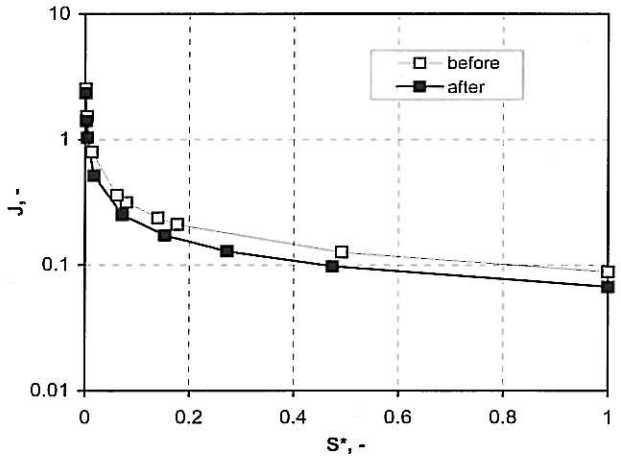


Fig. 10. Effect of asphaltene treatment on normalized capillary pressure curve (SB-6 core, centrifugal technique).

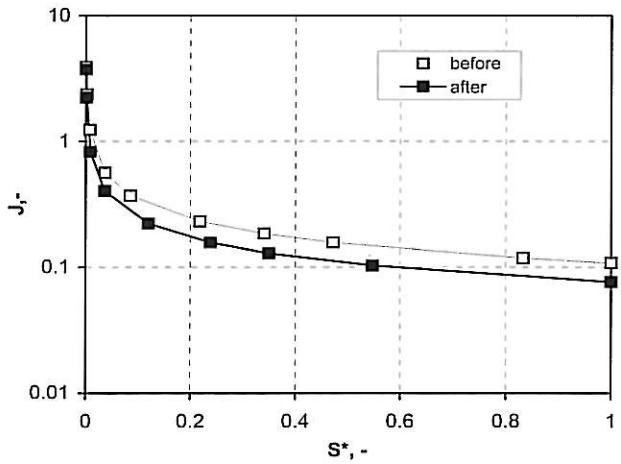


Fig. 11. Effect of asphaltene treatment on normalized capillary pressure curve (SB-10 core, centrifugal technique).

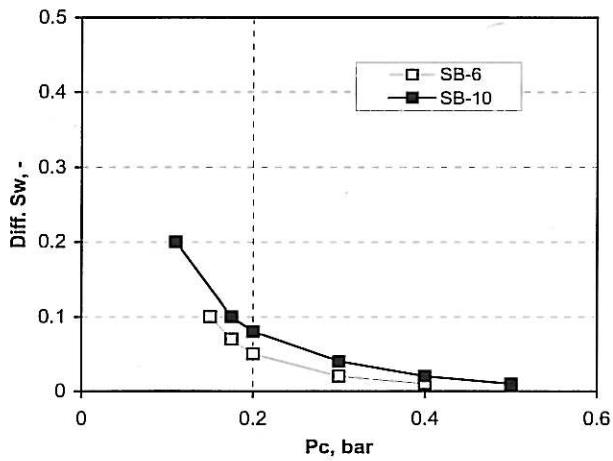


Fig. 12. Difference of water saturation at constant capillary pressure caused by asphaltene treatment.

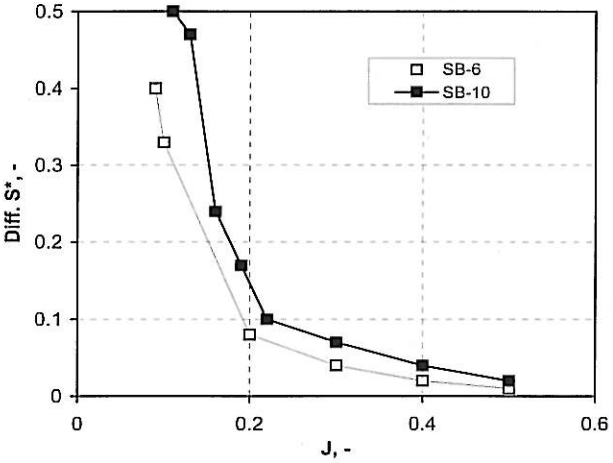


Fig. 13. Difference of normalized water saturation at constant J function caused by asphaltene treatment.

hydrophobization after treatment not only in the initial period of water drainage by gas, but through almost the whole process (down to 30 % water saturation which is close to the residual value). Although the curves in (Figs. 8-11) fall very close to each other, the difference of water saturation belonging to constant capillary pressure and J values are remarkable. As shown in Figures 12 and 13, that difference rapidly decreases with the capillary pressure and reaches zero as the drainage gets to the final stage. Anyhow, the asphaltene adsorption resulted in an accelerated water displacement in both cores, or in other words, identical water saturation could be obtained at lower capillary pressure after asphaltene treatment.

CONCLUSION

1. Langmuir and the Tóth isotherm were used to describe the static (batch or equilibrium type) adsorption tests. However, in high asphaltene concentration, particularly in clay rich system, these formulas cannot be applied for description of the sorption phenomena.

2. The measured and calculated adsorbed amounts of the static tests were in good agreement with the dynamic adsorption loss determined by the maximal values.

3. All asphaltenes (light, medium and heavy) significantly influenced the wettability of carbonate type formation rocks.

4. The Libyan oil, in its original form, caused nearly the same wettability alteration on carbonate rock surface as its asphaltenes in toluene solution did. This result suggests that the sandstone Sharara field, probably remained water-wet or intermediate after contact with oil, but the native wettability of the consolidating mineral components (carbonates, dolomites) was substantially modified and became oil-wet during the accumulation and entrapment process.

5. The effect of asphaltene adsorption on wettability influencing the accessible pore volume,

residual water saturation, threshold pressure, *etc.*, clearly shows an effective hydrophobization on all formation core samples.

6. Modification of the relative permeability and capillary pressure curves suggests that the spontaneous water imbibition might be drastically restricted by asphaltene treatment.

REFERENCES

[1] Anderson, W.G., 1986 (Oct.) Wettability literature survey-part 1: rock/oil/brine nteractions and the effects handling on wettability . Paper *SPE* 13932,JPT,1125-1144.

[2] Morrow, N.R.,1990 (Dec.). Wettability and its effect on oil recovery. Paper *SPE* 21621, JPT.

[3] Rays, B.H., Lakatos, I., Pernyesz, T., and Janos, T., 2003 (June). Adsorption of asphaltenes on formation rocks and its effect on wettability. *SPE* Paper 81470, presented at the 13th *SPE* Middle East Oil Show and Conference Bahrain.

[4] Yan, J., Plancher, H., and Morrow, N., 2001 (Feb.). Wettability changes induced by adsorption of asphaltenes. Paper *SPE* 37232, Presented at the *SPE* International Symposium on Oilfield Chemistry held in Houston, Texas.

[5] Morrow, N.R., Gram, P.J., and McCaffery, F.G., 1973 (Aug.). Displacement studies in dolomite with wettability control by octanic acid *Soc. Pet. Eng.J.*, 221-232.

[6] Ali, M.A. and Islam, M.R., 1997 (Oct.). The effect of asphaltene precipitation on carbonate rock permeability. Paper *SPE* 38856, presented at *SPE* Annual Technical Conference and Exhibition held in San Antonio, Texas, USA.

[7] Kamath, V.A., Yang, J., and Sharma, G.D., 1993 (May). Effect of asphaltene adsorption on dynamic displacement of oil by water, Paper *SPE* 26046, proc. *SPE* Western Regional Meeting, Anchorage, Alaska.

[8] Glampietro, P., Canonico, L.B., Galbariggi, G., Bertero, L. and Camianl, C., 1996 (Aug.). Asphaltene adsorption onto formation rock: an approach to asphaltene formation damage prevention *SPE* Production and Facilities, 156-160.

[9] Collins, S.H. and Melrose, J.C., 1983 (June). Adsorption of asphaltene and water on reservoir rock minerals. Paper *SPE* 11800, presented at the International Symposium on Oilfield and Geothermal Chemistry held in Denver, CO. USA.

[10] Dubey, S.T. and Waxman, M.J., 1991 (Aug.). Asphaltene adsorption and desorption from mineral surfaces. Paper *SPE* 18462, *SPE Reservoir Engineering*, 389-395.

[11] Kim, S.T., Boudh-Hir, M.E., and Mansoori, G.A., 1990 (Sep.). The role of asphalene in wettability reversal. Paper *SPE* 20700 presented at the 65th Annual Technical Conference and Exhibition of the SPE held in New Orleans, LA.

[12] LIU, Y. and Buckley, S., 1997 (March). Evolution of wetting alteration by adsorption from crude oil. Paper *SPE* 28970, *SPE Formation Evaluation*, 5-11.

[13] Buckley, S., Liu, Y., Xie, and Morrow, N., 1997 (June). Asphaltenes and crude oil wetting- The effect of oil composition. Paper *SPE* 35366, *SPE Journal*, 107-119.

[14] Chang, Y.C., Mohanty, K.K., Huang, D.D., and Honarpour, M.M., 1997. The impact of wettability and core-scale heterogeneities on relative permeability. *J. of Pet. Sc. and Eng.I*, **18**,1-19.

[15] Baldwin, B.A., 1988 (March). Water imbibition and characterization of North Sea chalk reservoir surface. Paper *SPE* 14108. SPE Formation Evaluation, 125-130.

[16] Jun-Zhi Wei and Ole B. Lile., 1992 (May). Influnce of Wettability and saturation sequence on relative permeability hysteresis in nconsolidated porous media. Paper *SPE* 25282.

[17] Desbrandes, R.,and Bassiouni, Z., 1990 (Oct.). In situ formation wettability determination in depleted zone. Paper *SPE* 21182, Presented at the SPE Latin American Petroleum Engineering Conference held in Rio de Janeiro.

[18] Dixit, A.B., McDougall, S.R., Sorbie,K.S., and Buckley, J.S., 1996 (April). Pore scale modelling of wettability effects and their influence on oil recovery. Paper SPE/DOE 35451, Presented at the 1996 *SPE/DOE* Tenth Symposium on Improved Oil Recovery held in Tulsa, OK.

[19] McDougall, S.R., and Sorbie,K.S., 1995 (Aug). The impact of wettability on water flooding: Pore-scale simulation. Paper *SPE* 25271, SPE Reservoir Engineering.

[20] Subhayu Basu and Mukul M. Sharma, 1996 (Oct.). Defining the wettability state of mixed wet reservoirs: measurement of critical capillary pressure for crude oils. Paper *SPE* 36679, Presented at the SPE 71st Annual Technical Conference and Exhibition held in Denver, Colorado, U.S.A.

[21] Rayes, B.H., Pernyeszi, T., Lakatos, I., Tóth, J. 2003 (Feb.). Comparative study of asphaltene adsorption on formation rocks under static and dynamic conditions. Paper *SPE* 80265, presented at the SPE International Symposium on Oilfield Chemistry held in Houston, TX, U.S.A.

[22] Tóth, J., Bódi, T., Szûcs, P. and Civan, F. 2000. Analytical Techniques for determination of relative permeability from displacement experiments. in lakatos, I. *Novelties in Enhanced Oil and Gas Recovery*, Progress in Mining and Oilfield Chemsity, 2:91, Akadémiai Kiadó Ltd., Budapest .

[23] Tóth, J., Bódi, T., Szucs, P. and Civan, F. 2002. Convenient formulae for determination of relative permeability from unsteady-state fluid displacement in core plugs. *J. Petroleum Geoscience and Engineering*, 35:33 .